# Use of additive manufacturing techniques for the production of customized implants with complex geometry : application to reparative hand surgery

Augustin Lerebours

Par **Augustin LEREBOURS**

# *Use of additive manufacturing techniques for the production of customized implants with complex geometry : application to reparative hand surgery*

Thèse présentée
pour l'obtention du grade
de Docteur de l'UTC

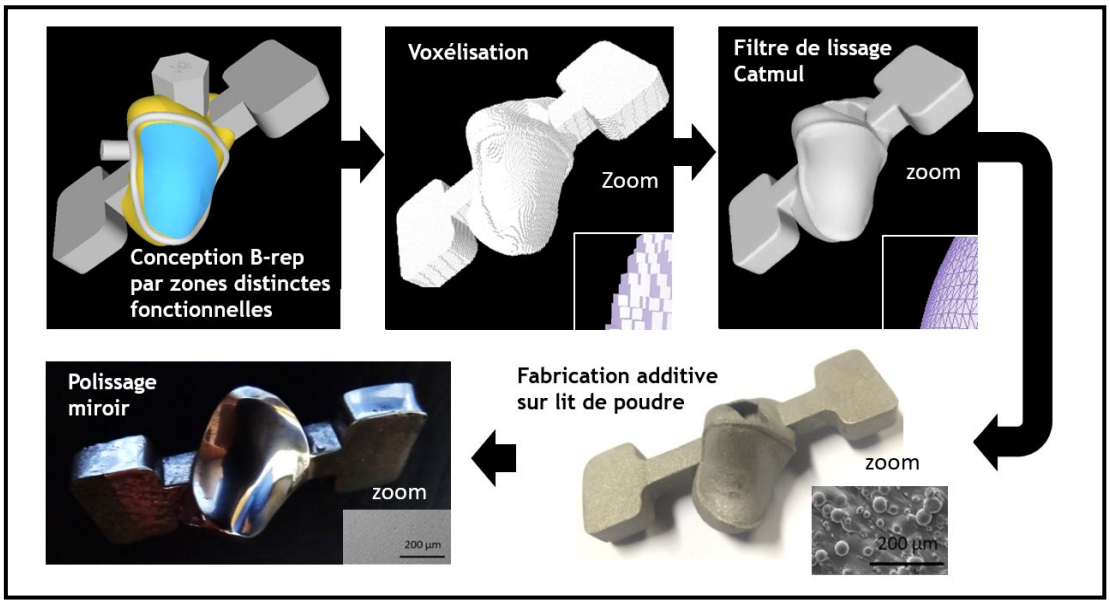


Soutenue le 2 décembre 2019
**Spécialité :** Mécanique et Matériaux et Biomécanique : Unité de recherche en Mécanique - Laboratoire Roberval (FRE UTC - CNRS 2012)
D2531

Ecole doctorale n° 71 : Sciences pour l'ingénieur

Laboratoire Roberval, CNRS FRE 2012

# USE OF ADDITIVE MANUFACTURING TECHNIQUES FOR THE PRODUCTION OF CUSTOMIZED IMPLANTS WITH COMPLEX GEOMETRY. APPLICATION TO REPARATIVE HAND SURGERY

Spécialité : Mécanique et Matériaux et Biomécanique

02/12/2019

---

PRESENTED BY: **Augustin Lerebours**

---

JURY REFEREES:

- Karine Anselme, CNRS Research director, IS2M- CNRS UMR7361, UHA
- Nabil Anwer, Professor, LURPA, ENS Cachan

OTHER JURY MEMBERS:

- Stephanie Dakpe, Maxillofacial surgeon and stomatologist, CHU Amiens
- Frédéric Marin, Professor, BMBI-CNRS UMR7338, UTC
- Pierre Feissel, Professor, Roberval-CNRS FRE2012, UTC
- Benyebka Bou-Saïd, Professeur, LaMCoS, INSA Lyon

THESIS SUPERVISORS:

- Alain Rassineux, Professor, Roberval-CNRS FRE2012, UTC
- Christophe Egles, Professor, BMBI-CNRS UMR7338, UTC

INVITED MEMBERS:

- Salima Bouvier, Professor, Roberval-CNRS-FRE-2012, UTC
- Maxence Bigerelle, Professor, LAMIH, UPHF
- Clémence Demangel, Engineer R&D, CRITT-MDTS

THESE PRESENTEE POUR L'OBTENTION DU GRADE DE DOCTEUR DE L'UNIVERSITE DE TECHNOLOGIE DE COMPIEGNE

# Remerciements

J'exprime ma sincère reconnaissance à l'ensemble des membres du jury pour avoir accepté d'évaluer mon travail. Je remercie notamment le professeur Nabil Anwer et la professeure Karine Anselme de l'honneur que vous me faites en en acceptant d'être rapporteurs de ma thèse ainsi que le président du jury. Je remercie Stéphanie Dakpé, chirurgienne maxillo-faciale et stomatologiste, le professeur Frédéric Marin, le professeur Pierre Feissel et le professeur Benyebka Bou-said de me faire l'honneur de participer à mon jury de thèse. Je remercie également la professeure Salima Bouvier, le professeur Maxence Bigerelle et Cléménce Démangel, Ingénieur R&D au Critt MDTS, d'être présent en tant qu'invités d'honneurs.

Je tiens tout à exprimer mes plus sincères remerciements au professeur Alain Rassineux, au professeur Christophe Egles et à la professeure Salima Bouvier de m'avoir encadré pendant ma thèse. Merci Alain de m'avoir fait confiance dans mes travaux, d'avoir pris le temps de travailler jusqu'à tard le soir pour moi et de m'avoir fait part de ta passion pour le violon. Merci Christophe, pour ta grande disponibilité, les discussions scientifiques, tes nombreux conseils et corrections durant la rédaction des articles scientifiques et du manuscrit de thèse. Je te suis reconnaissant de m'avoir permis d'aller à Boston afin de découvrir comment se fait la recherche dans des institutions prestigieuses comme le MIT, Northeastern University ou encore Tuft. Tu m'as transmis ta passion pour la recherche.
Merci Salima, tu as été ma directrice de thèse pendant un an, mais tu as toujours pris le temps jusqu'à la fin afin de m'aider au niveau de la valorisation, au niveau de l'organisation. J'ai particulièrement apprécié que tu m'aies fait confiance et de m'avoir appris à répondre à des appels à financement pour les besoins de ma thèse. Merci également au professeur Fréderic Marin pour avoir co-encadré ce travail de thèse. Je te remercie pour le temps consacré pour la mise au point des implants et la méthode d'implantation. J'exprime mes sincère remerciement au professeur Alain Charles Masquelet d'avoir pris une part importante dans l'élaboration des travaux de ma thèse et surtout de m'avoir invité à participer aux tests de performances chirurgicales sur des cadavres. Ces expériences furent enrichissantes et forte d'émotions. Je suis également reconnaissant d'avoir pu participer à des congrès qui m'ont beaucoup apporté comme WCB 2018 à Dublin, ou encore ITOW 2018 à Stanford.

Mes remerciements vont également à Maxence Bigerelle pour m'avoir fait part de ton expertise dans le domaine de la texturation de surface et de tes nombreux conseils pour ma carrière de jeune chercheur. Ce fut un plaisir de collaborer avec toi. J'aimerais témoigner ma reconnaissance à Clémence Démangel. Tu m'as donné l'opportunité de travailler dans un centre

d'expertise en biotribologie, ce fut une expérience enrichissante scientifiquement et techniquement, le tout dans le cadre agréable des Ardennes.

Ce travail n'aurait pas été possible sans l'institut IUIS pour avoir financé ce projet. Je remercie notamment Christine Boutet, Véronique Perdereau et Pierre Mozer.

Je tiens également à remercier les membres de l'organisme de valorisation, la Satt-Lutech, pour leur investissement dans le projet. Je tiens particulièrement à remercier Carine Asensio, Matthieu Vogt, Amandine Le Guennec. Je souhaite également remercier Emmanuelle Laude Duval pour la rédaction du 2ème brevet. Et enfin je souhaite remercier Damien Baratte pour m'avoir aidé dans l'ensemble des démarches de valorisation. Vous m'avez donné l'opportunité de participer activement à la valorisation de ma recherche et de rencontrer des entreprises.

J'aimerais témoigner ma reconnaissance à tous les membres du laboratoire Roberval, au laboratoire BMBI et à l'équipe R&D du CRITT-MDTS. Vous m'avez accueilli chaleureusement, j'ai vécu des précieux moments. Pascale Vigneron, merci pour ton aide dans les tests de culture cellulaire. Je retiendrais nos astuces rock n'roll pour visualiser les MC3T3 à l'epiflu, mais aussi nos rires et peurs de l'*escape game* des pharaons. Merci Vanessa pour avoir été là pour moi dès que j'en avais besoin. Merci Valérie pour ta bonne humeur quotidienne. Je retiendrais surtout la belle randonnée.

Vous les doctorants et post doc du labo Roberval et BMBI, j'ai partagé tant de bons moments avec vous, vous êtes supers. Liang, j'ai adoré nos parties de tennis, notre café matinal, les tennis avec Paul et surtout d'avoir pu partager ta culture chinoise. Notre amitié est à l'épreuve des distances. Blanche, merci d'avoir partagé mes moments de doutes, ma musique et mes blagues. Khalil, je suis fier de te connaitre, tu as le sens de l'amitié, du partage, de l'empathie. Tu as toujours été là pour me soutenir, pour discuter de science mais surtout pour s'échanger nos histoires. Corentin, mon ami « salade-tomate quinoa », tu as su intégrer le vin aux pratiques du vendredi soir. Sylvain, tu es le meilleur partenaire de vin mais aussi de billard. Je ne peux pas oublier le reste de la team billard : Xavier, Thibaut, Dorrick, Christophe. Vos jeux de mots vont me manquer, c'est sûr. Merci aussi, à mon autre colocataire de bureau, Elisa. Je te souhaite le meilleur pour ton mariage.
La team CBB crew, nous voilà. Delphine, tu es super ! Merci pour ton amitié solide, ton aide si précieuses, tes conseils de vie, et nos discussions jusqu'à 3h du mat'. Mattia, mon ami, « mi hermano », notre personnage de la telenovela « les PhD of love ». Merci pour avoir été un super coloc'. J'ai trouvé en toi, un véritable ami. Tu pourras toujours compter sur moi, s'il y a une guêpe qui t'embête. Nos sessions musiques à base de poinçonneur des Lilas et d'« it's begining to look a

lot like christmas » vont me manquer. Lilou, on a partagé de bon moment entre la sicile et « ma these 180s ». En tout cas, sache que « j'ai foie en toi ma puce » ! Tu as eu le courage de conduire en sicile après cette fameuse soirée, tu mérites la palme d'or du labo. Antoine, merci de nous avoir rappelé les paroles de « la tribu de Dana » à chaque soirée Favela ! Mégane, tu vas tellement me manquer mon chat noir adoré ! Je pense que tu as réussi admirablement à être notre colocataire « friends » de la favela. Merci pour tes histoires incroyables. Merci claire pour ta patience notamment pour l'impression de mon manuscrit. Merci aussi, à toi Felix pour ta bonne humeur et les soirées dans ta coloc'. Chunmei, je suis content de te connaitre, merci pour tes repas chinois et d'être toujours prête à m'accueillir avec Elton. Bon courage aux nouvelles et nouveaux doctorants notamment Sabrina et Mathilde.

Je voudrais aussi remercier les étudiants qui ont participé à mes travaux de thèse, Héloïse Olivier, Jean-Charles Paulin, Mélissa Moulart, Lauriane Lauwers, Yohan Galesne, Milène Mutio, Manon Rozier, Pierre Turpin, Irene Pierini, Morgane Ferandou, Flore Zygband, Garance Leroy et Hélène Lovato.

Christophe et Anne, merci pour votre soutien indéfectible, vous m'avez accueilli comme un fils, comme un ami dans votre famille que ce soit à Boston ou à Compiègne. Je ne vous remercierais jamais assez pour tous ces bons moments autour d'un tarot, d'une belote, ou d'un repas. Merci aussi à Mathieu, pour m'avoir laissé t'embêter dans la neige de Boston. Merci aussi à Lisa, ne t'inquiète pas je t'apprendrais à jouer à mario kart.

Je voudrais aussi remercier Nabil, mon ami de toute une vie ! Merci Franck et Lucas pour votre amitié à toutes épreuves. Merci à Amélie, on est dans la même galère depuis BL01. J'ai confiance en toi et tes projets. Ton amitié compte à mes yeux. Merci aussi à Pierre, Marie, JP, pour m'accueillir à Paris et d'être venu à Compicity. Merci Candice, Romain, mes colocs' favoris de la boat house, vous me manquez trop. Merci Corentin, Léopold. Je remercie aussi tous mes amis que je n'ai pas cités.

Enfin un remerciement tout particulier à mes parents sans qui je n'aurais pu réaliser toutes ces années d'études. Merci aussi Simon, Victor, Eléonore, mais aussi ma petite filleule trop choupi Hélène.

# List of publications and communication

## Scientific articles

Lerebours, A., Marin, F., Bouvier, S., Egles, C., Masquelet, A.C. and Rassineux, A.," Trends in Trapeziometacarpal implant design : a systematic survey based on patents and administrative databases. *J. Hand Surg. Am.,* 2019.

Lerebours, A., Marin, F., Bouvier, S., Egles, C., Masquelet, A.C. and Rassineux, A., 2019. A voxel-based method for designing a numerical biomechanical model patient-specific with an anatomical functional approach adapted to additive manufacturing. *Computer methods in biomechanics and biomedical engineering*, *22*(3), pp.304-312.

Lerebours, A., Marin, F., Bouvier, S., Egles, C., Masquelet, A.C. and Rassineux, A.," Numerical method to rejuvenate highly deformed bones for a prosthesis design and additive manufacturing. Case study: the trapezium bone. Submitted in *Computer methods in biomechanics and biomedical engineering*, 2020.

Lerebours, A., Bouvier, S., Rassineux, A., Dembinski, L.and Egles, C., "From the medical images to the articular implant ready for implantation: Assessing the surface quality and the geometrical deviation" Manuscript ready for submission in *Plos one*

Lerebours, A., Vigneron, P., Bouvier, S., Rassineux, A., Bigerelle, M. and Egles, C., 2019. Additive manufacturing process creates local surface roughness modifications leading to variation in cell adhesion on multifaceted TiAl6V4 samples. *Bioprinting*, p.e00054.

Lerebours, A., Demangel, C., Dembinski, L., Bouvier, S., Rassineux, A., and Egles, C., Effect of the residual porosity of selective laser melted CoCrMo parts on wear of polyethylene under lubricated conditions. Submitted in *Biotribology*, 2020.

## Patents and technical know-how

Lerebours A., Masquelet A. C., Jihaz N., Bouvier S., Marin F., and Egles C., **Patent WO2018210953**: Method for producing a trapeziometacarpal prosthesis and resulting prosthesis, 2018.

Lerebours, A., Marin, F., Bouvier, S. and Rassineux, A., **Patent WO2019162636A1**: Method of manufacturing a complex substitution object from the real object, 2019.

Lerebours, A., Lauwers, L., **Technical know-how**: Toolkit for trapezometacarpal surgery, 2019.

**International and national congress**

Lerebours, A., Masquelet, A.C., Marin, F., Bouvier, S., Egles, C. and Rassineux, A. Geometrical analysis of the trapezium bone's morphology variability. *WCB*, 2018, Poster

Lerebours, A., Marin, F., Bouvier, S., Egles, C., Masquelet, A.C. and Rassineux, A. A new method adapted to 3d printing for the design of a patient-matched carpo-metacarpal prosthesis, *proceedings of the 3rd ITOW*, 2018, Oral presentation

Lerebours, A., Vigneron, P., Bouvier, S., Rassineux, A., Bigerelle, M. and Egles, C. Heterogeneity of surface texturing created by selective laser fusion and cellular adhesion. *Assises de la fabrication additive*, 2019, Oral presentation

Lerebours, A., Marin, F., Bouvier, S., Egles, C., Masquelet, A.C. and Rassineux, A. Additive design of a complex hand replacement bone. *Assises de la fabrication additive*, 2019, Oral presentation

**Other scientific communications**

Lerebours, A. L'impression 3D métal à portée de main. *Ma thèse en 180 secondes*. Final Sorbonne université

Lerebours, A., Vigneron, P., Bleicher V. De Capitaine Crochet à Iron Man. *Fête de la science 2017 Université de Technologie de Compiègne*. Oral presentation

# Teaching activities

| Teachings | Person in charge | Date | Type of teaching carried out | Number of hours |
|---|---|---|---|---|
| MQ17 - introduction to materials science | P. Revel | Sept-16/Dec-16 | Practical work | 20h |
| MQ17 - introduction to materials science | M. Risbet | Fev-17/Ju-17 | Practical work | 20h |
| NP90 - Nano-projects | J. Favergeon | Fev-17/Ju-17 | Project management | NA |
| PS21- Physical mechanics | P. Feissel | Sept-16/Dec-16 | Tutorial work | 14h |
| TX- Laboratory project | C.O. Sarde | Sept-16/Dec-16 | Project management | NA |
| TN04- Realization | S. Moreau | Sept-17/Dec-17 | Project management | NA |
| PS21- Physical mechanics | P. Feissel | Sept-17/Dec-17 | Tutorial work | 21h |
| MQ17 - introduction to materials science | P. Revel | Sept-17/Dec-17 | Practical work<br>Project management | 32h |
| TX- Laboratory project | C.O. Sarde | Sept-17/Dec-17 | Project management | NA |
| TX- Laboratory project | C.O. Sarde | Juil-18 | Project management | NA |
| MQ17 - introduction to materials science | P. Revel | Sept-18/Dec-18 | Practical work | 20h |
| TX- Laboratory project | C.O. Sarde | Sept-18/Dec-18 | Project management | NA |
| TX- Laboratory project | C.O. Sarde | Fev-18/Ju-18 | Project management | NA |
| TN20- CAD: geometric modeling | A. Rassineux | Fev-19/Ju-19 | Practical work<br>Lecture course | 31h |

# Table of contents

# List of figures and tables

## Chapitre 1



### Article 1

## Chapitre 2

# Chapitre 3

## Article 2:



## Article 3:

# Chapitre 4

## Article 4:

**Figure 1**: a) Sketch of the atomization process; b) SEM images showing the CoCrMo powder particle morphology; c) granulometry measurement and d) chemical composition of the CoCrMo powder particles
**Figure 2**: Design of a trapezial implants based on patient data; M1: 1st metacarpal contact surface; M2: 2nd metacarpal contact surface; SCP: scaphoid contact surface; TPZ: trapezoid contact surface
**Figure 3**: a) Selective laser melting sketch and b) parameters used
**Figure 4**: Analysis of the geometrical analysis
**Figure 5**: Mirror-like implant processed by SLM and superfinished
**Figure 6**: SEM images of the CoCr surface of the implant after, SLM, sandblasting and superfinishing
**Table 1 :** The chemical composition (mass %) of CoCrMo specimens
**Figure 7**: SEM images of the pores: a) round pores due to gas entrapment and b) irregular pores due to sintering process; c) diagram of the pores distribution (size and circularity).
**Figure 8**: a) Number of pores per $mm^2$ depending on the area of the implant. b) Average wall thickness (µm). c) Mean area ($\mu m^2$) of the pores depending on the area of the implant. d) Circularity of the pores depending on the area of the implant.
**Figure 9**: a) Principal component analysis showing the average values of pores parameters of each defined zone of interest in the two version of the implant, b) Presence of large and irregular pores through the defined zone of interests
**Figure 10**: a) Surface texture after the superfinishing post-treatment and b) average roughness of the surface of interest of both version of the implant
**Figure 11**: Principal component analysis of the roughness parameters and boxplot of the Sa values depending of the specimens and zones; visualization of the surface and main orientation
**Figure 12**: histogram of the deviation distance of the scanned implant after sandblasting and after superfinishing.
**Figure 13**: Detailed histogram of the distance after the superfinishing post-treatment.
**Figure 14**: 3D colorization map by Hausdorff distance analysis. Principal component analysis of the roughness parameters and boxplot of the Sa values depending of the specimens and zones; visualization of the surface and main orientation
**Figure 15**: histogram of the distance between the medical image data and the numerical model

# Chapitre 5

## Article 5:

**Figure 1**| Typical Selective Laser Melting layout
**Figure 2**|**a)** Multifaceted stem-like specimen and inclination in the SLM manufacturing chamber with 4 distinctive surfaces defined by an angle with the AM build plate; **b)** Multifaceted specimen created by selective laser melting; **c)** Morphology of the Ti6Al4Vpowder; **d)** granulometry of the Ti6Al4V powder
**Figure 3** | cell covering rate and nuclei counting experimental design
**Figure 4** |Material characteristic of the Ti64-specimens-as-SLM: **a)** porosity, **b)** fully entangled martensitic hcp α' lathes microstructure inside the prior-β grains **c)** prior-β grains

### Article 6:



## Chapitre 6

# List of abbreviations

| | | | |
|---|---|---|---|
| **SCP** | Scaphoid | **Ti6Al4V /Ti64** | Titanium-6Aluminium-4Vanadium |
| **TPZ** | Trapezoïd | **UHMWPE /PeHd** | Ultra Hight Molecular Weight Poyethylene |
| **M1/M2/…** | First metacarpal bone/ 2nd metacarpal bone/… | **IL** | Interleukins |
| **TMC/CMC** | Trapeziometacarpal/ Carpo-metacarpal joint | **TNF-α** | Tumor Necrosis Factor |
| **OA** | Osteoarthritis | **COF** | Coefficient Of Friction |
| **MOP /MOM /COC** | Metal-On-Polyethylene Metal-On-Metal Ceramic-On-Ceramic | **FBS** | foetal bovine serum |
| **AM** | Additive manufacturing | **Ra/Sa** | arithmetical mean roughness (2D/3D) |
| **SLM** | Selective Laser Melting | **SEM** | Scanning Electron Microscope |
| **EBM** | Electron Beam Melting | **EBSD** | Electron backscatter diffraction |
| **FDM** | Fused Deposition Modelling | **DMEM /α-MEM** | Dulbecco's Modified Eagle Medium / Minimum Essential Medium Eagle - alpha modification |
| **SLA** | StereoLithogrAphy technology | **L929** | Mouse fibroblast cell line |
| **CAD** | Computer-aided design | **MC3T3** | Mouse osteoblastic cell line |
| **STL file** | Stereolitography file | **CT** | Computer tomography |
| **DfAM** | Design For Additive Manufacturing | **FDA** | Food and Drug administration |
| **CSG** | Constructive Solid Geometry (CSG). | **CE** | European Certificate |
| **B-rep** | Boundary representation | **FAST** | Function Analysis System Technics |
| **CoCr** | Cobalt-Chromium | | |

# Avant-propos

L'arthroplastie prothétique est le remplacement d'une articulation humaine par un système mécanique. Celle-ci est une des solutions thérapeutiques pratiquées couramment dans le cas de l'arthrose qui est une destruction ou une dégénération des surfaces articulaires. Actuellement l'arthroplastie se pratique par remplacement des surfaces articulaires par des éléments métalliques, en polyéthylène haute densité, en céramique ou en pyrocarbone sensé mimer les caractéristiques géométriques morpho-fonctionnelles de l'articulation. Ainsi il apparaît que le design de la prothèse influe sur la performance fonctionnelle de l'articulation. Dans le cas particulier de la main, ce sont les articulations interphaliennes, métacarpo-phalangiennes et pour le pouce l'articulation trapézo-métacarpienne qui sont exposées à l'arthrose et donc potentiellement sujettes à une arthroplastie. Toutefois les taux d'échec sont pour la main de 8 à 21% ou bien avec des reprises fonctionnelles limitées entraînant une perte de qualité de vie du patient et des taux de remplacement à 10 ans de 25% pour certains modèles.

Dans ce contexte, l'analyse des échecs dans le but d'améliorer la conception de l'arthroplastie est un thème majeur de recherche en biomécanique. Ainsi sur la base de modèles numériques, il a été montré que chaque individu avait des caractéristiques mécaniques articulaires qui lui étaient propres en terme de cinématique (amplitude de mouvement, axes instantanés de rotation,…) et en terme dynamique (force de contact, répartition de la pression de contact,….) du fait des spécificités musculosquelettiques de la personne par la géométrie des os, localisation des insertions musculaires, composantes physiologiques. En conséquence la personnalisation et l'identification de paramètres spécifiques du sujet ou du patient sont devenues pertinentes aussi pour l'analyse et la conception de prothèse et de procédure d'arthroplastie. Dans le cas de la main, cette problématique est d'autant plus exacerbée qu'il y a des variations anatomiques et de taille très importantes. Néanmoins la mise en œuvre de conceptions personnalisées de prothèses articulaires bien que faisable techniquement n'a pas été très appliquée en routine du fait de l'inadaptation des processus de fabrication traditionnels basés sur la standardisation des tailles et des formes géométriques de prothèses. Or depuis 2-3 ans la démocratisation de l'impression 3D de petits

objets a complètement changé les paradigmes de la conception personnalisée de dispositifs médicaux de par la flexibilité qu'elle donne et de par l'accessibilité pour sa mise en œuvre.

Cette thèse fait suite à une idée prospective issue du projet de recherche HANDY (11/2015 – 06/2016) financé par l'Institut Universitaire de l'ingénierie de la santé (IUIS - Sorbonne Universités SU). Ce projet HANDY a montré la faisabilité de réalisation d'un implant à géométrie complexe pour la chirurgie réparatrice de la main par les technologies émergentes de fabrication additive via une implantation sur cadavre. Des essais préliminaires ont été menés pour examiner la capacité de deux techniques de fabrication additive (Direct Metal Deposition (DMD) (E.C. Nantes) et Selective Laser Melting (SLM) (EnsamMarisTech) à reproduire une géométrie anatomique complexe telle que l'os trapèze de la main en alliage métallique.
Un essai clinique limité à la pose de l'os sur cadavre réalisé par le Pr Alain Charles MASQUELET a montré les potentialités de rétablissement des patients souffrant de rhizarthrose par rapport aux solutions thérapeutiques existantes (trapézectomie, arthrosplastie totale, l'ostéomie, l'arthrodèse), toutefois il a mis en exergue des problématiques concernant l'approche chirurgicale d'implantation.

Ce travail de thèse s'inscrit dans la continuité de cette approche, en proposant un implant articulaire géométriquement adapté au patient et réalisé par fabrication additive métal qui viendrait compléter l'arsenal des solutions thérapeutiques de la rhizarthrose. Il s'agit plus globalement de développer, analyser et valider les étapes de réalisation d'un implant à géométrie complexe quelconque. Il s'agit de prendre en compte de l'aspect biologique (réaction du système immunitaire), l'aspect mécanique (propriété de frottement), l'aspect morphologique (quantification des déviations géométriques) et de l'aspect clinique (approche chirurgicale, design de l'implant).

Dans ce cadre, pour faciliter la compréhension des travaux effectués au cours de cette thèse, une introduction générale est proposée. La bibliographie porte dans un premier temps sur la complexité de l'environnement articulaire trapezio-métacarpienne sur la pathologie

de la rhizarthrose. Par la suite les solutions thérapeutiques sont exposées en s'attardant sur l'arthroplastie prothétique. En effet, un article intitulé « **Trends in Trapeziometacarpal implant design: a systematic survey based on patents and administrative databases** » présente les différentes stratégies de design de ces prothèses et leurs évolutions au cours du temps. L'introduction se poursuit en présentant de façon succincte la fabrication additive par lit de poudres, les biomatériaux métalliques d'intérêts compatibles à cette technologie et les méthodologies de conception adaptée au potentiel de ce procédé. Enfin, les spécifications des prothèses articulaires en termes de biocompatibilité et de biotribologie sont abordées.

Ces travaux ont démontré dans un premier temps la nécessité d'intégrer en amont l'aspect clinique notamment l'approche chirurgical afin de mieux appréhender les spécifications géométriques de l'implant. L'objectif étant d'assurer une stabilité et un bon positionnement afin de diminuer les complications cliniques. Ce travail a débouché sur un brevet présenté dans l'annexe n°2: **WO2018210953: « Procédé de réalisation d'un implant prothèse trapézo-métacarpienne et de l'implant obtenu ».**

La seconde partie de cette étude explore la mise au point d'un système numérique permettant de prendre en compte les spécifications géométriques et par extension de retrouver la morphologie d'un os tel qu'il le fut avant sa pathologie. Il s'agit également d'intégrer les contraintes de la fabrication additive et de l'ajout d'élément prothétique. Ce travail s'appuie sur une approche fonctionnelle et par lissage d'une représentation par voxels. Ce travail de recherche est présenté sous la forme de deux articles: **« A voxel-based method for designing a numerical biomechanical model patient-specific with an anatomical functional approach adapted to additive manufacturing »** et **« Numerical method to rejuvenate highly deformed bones for a prosthesis design and additive manufacturing. Case study: the trapezium bone ».** Par ailleurs un brevet a été déposé **WO2019162636A1 : « Procédé de fabrication d'un objet complexe de substitution à partir d'un objet réel ».** Il est présenté dans l'annexe n°3.

Des prototypes avancés de l'implant ont été réalisé dans le but d'atteindre les spécifications des prothèses articulaires notamment d'état de surface. Ce procédé inclus la fabrication additive par technologie de fusion sélective par laser. Le matériau sélectionné est l'alliage à base cobalt. Par ailleurs, le procédé est suivi d'une superfinition physico-catalytique adapté aux géométries complexes. L'impact de ces étapes de fabrication a été évalué sur les critères de déviations de géométrie, rugosité de surface et porosité. Ce travail est présenté sous la forme d'un article : « **From the medical images to the articular implant ready for implantation : Assessing the surface quality and the geometrical deviation** ». Des prototypes réalisés par fusion sélective par laser en acier inoxydable 316L et revêtu en céramique ont également été réalisés et sont présenté dans les annexes 4 a) et b).

Il s'agit ensuite de comprendre l'impact de cette qualité de surface induite par la chaine de fabrication (fusion sélective par lit de poudre, superfinition) sur la résistance aux frottements du polyéthylène haute densité. Ce travail est présenté sous la forme d'un article: « **Effect of the residual porosity of selective laser melted CrCoMo parts on the wear of polyethylene under lubricated conditions** ». Une étude biotribologique comparative entre des échantillons en alliage cobalt-chrome et 316L par laser réalisés par fusion sélective par laser et forgeage a été réalisée et est présenté dans l'annexe n°5 a). Ces travaux nous ont permis de mieux appréhender les mécanismes d'usure du polymère en milieu biologique suivant les différences microstructurales et de porosité des contreparties métalliques induite par les deux procédés de fabrications. Des essais sur des échantillons revêtus par de la céramique ont été réalisés et sont présenté dans l'annexe n° 5 b). Une étude préliminaire de biocompatibilité nous a permis d'appréhender la cytocompatibilité des échantillons réalisés par fabrication additive superfinis et recouvert par de la céramique. Cette étude examine également l'inertie des biomatériaux vis-à-vis de la réponse inflammatoire précoce. Ces travaux sont présentés dans l'annexe n°6.

L'effet du procédé sur la partie controlatérale du trapèze prothétique, soit la tige métacarpienne a également été abordé. Il s'agit d'une pièce nécessitant un ancrage avec la matière osseuse. Dans ce contexte, l'effet de la variation de la texturation de surface inhérent à la fabrication additive sur l'adhésion cellulaire d'une lignée ostéoblastique a été étudié. Ce

travail est présenté sous la forme d'un article : « **Additive manufacturing process creates local surface roughness modifications leading to variation in cell adhesion on complex TiAl6V4 samples. »**

Ce travail se termine par une étude philosophique et psychologique afin de comprendre l'importance du geste de la préhension dans le contexte des nouvelles technologies. En effet le travail scientifique et technique jusqu'alors réalisé ne revêt par le regard du patient. Il s'agit de fait de mettre en exergue les implications pour les patients de recouvrer la préhension dans un spectre plus large que les considérations cliniques (regard sur soi, définition du soi par des activités ne pouvant plus être faites, etc).

Enfin une discussion générale souligne la contribution de recherche originale des résultats de cette thèse pour la réalisation d'implant personnalisé par fabrication additive. Des perspectives sont également proposées pour la continuité du projet.

# CHAPTER 1 :

# State of the art

*Ce chapitre propose un bref état de l'art permettant de mieux appréhender les travaux scientifiques de cette thèse. Elle porte dans un premier temps sur la complexité de l'environnement articulaire trapezo-métacarpien et la pathologie de la rhizarthrose. L'ensemble des solutions thérapeutiques sont exposés notamment l'arthroplastie prothétique, détaillée par un article. Ce dernier présente notamment les différentes stratégies de design de ces prothèses et leurs évolutions au cours du temps. L'introduction se poursuit en présentant de façon succincte la fabrication additive par lit de poudres, les biomatériaux métalliques d'intérêts compatibles à cette technologie et les méthodologies de conception adaptée au potentiel de ce procédé. Enfin, les spécifications des prothèses articulaires en termes de biocompatibilité et de biotribologie sont abordées.*

# 1. Hand's anatomy and osteoarthritis of the trapeziometacarpal joint

## 1.1. The hand

The human hand allows a great diversity of movement because of its fundamental function: prehension. Some animals (e.g. bonobos and chimpanzees) also have this faculty but it attains this degree of maturity only in humans. It is due to the thumb's characteristic to oppose all other fingers. From a physiological point of view, the hand represents the effector end of the upper limb. In addition it is also a very sensitive and precise sensory receiver [1].

The hand, seen from the front, has the palm, following the wrist and is articulated with five fingers. On either side of the palm are two protuberances: the thenar eminence at the base of the thumb and the hypo-thenar eminence at the distal end under the little finger. The five fingers are the little finger, ring finger, middle finger and index finger, and a short finger, the thumb. All long fingers have three phalanges, while the thumb has only two. The five fingers do not have the same importance in the motor function of the hand.

- **The thumb**: a predominant role because of its opposability,
- **The clamp area**: It includes the middle finger, index finger and thumb (bi-digital clamp: thumb/index: tri-digital clamp: thumb index finger/major),
- **The grip area**: It includes the ring finger and the little finger, essential to ensure the firmness of the full palm grip and in particular to develop strength through the hand.

The skeleton of the hand can be divided into three parts: **the carpus, the metacarpus and the phalanges.** The carpus is the set of bones forming the skeleton of the wrist, it is composed of two rows:

- **The first row (proximal)**: scaphoid (SCP), semi lunar (SL), pyramidal (Pl) and pisiform (Pf) (lateral to medial)
- **The second row (distal)**: trapezium (T), trapezoid (TPZ), large bone (Lb) and hooked bone (Hb) (lateral to medial)

The metacarpal is the set of bones forming the skeleton of the palm, consisting of five long bones, the metacarpals, each connected to the bones of one of the five fingers of the hand. The phalanges are the bones of the skeleton of the fingers. Similarly to metacarpal bones,

they have a proximal epiphysis as the base, a distal head and a body. The digging movement is possible by the thenarian and hypo-thenarian muscles whose upper insertions stretch the tranverse carpal ligament, bringing the scaphoid/ trapezoid bone pair closer to the pisiform/hooked bone.

### 1.2. The thumb

The osteo-articular column of the thumb consists of five bones: the scaphoid (S), the trapezium (T), the first metacarpal (M1), the first thumb phalanx (P1) and the second thumb phalanx (P2). There are four joints: the scapho-trapezium (ST): the trapeziometacarpal (TMC); the metacarpal-phalangeal (MP): the interphalangeal (IP). Five degrees of freedom allows the bending movements (opposition). The role of the thumb in gripping is due to its position in front of the palm. Its functional flexibility is also due to the organization of its osteo-articular column and its motor muscles [1]. In this manuscript we will use the Anglo-Saxon nomenclature of the different joint movements of the thumb.

**Table 1**: Anglo-Saxon nomenclature of the TMC kinematics.

| **Anglo-saxon nomenclature** | **French Nomenclature** |
|---|---|
| Flexion | Opposition |
| Extension | Contre opposition |
| Abduction | Antéposition |
| Adduction | Rétroposition |
| Axial rotation | Pronation supination |
| Circumduction | Circumduction |
| Palmar abduction | Abduction |

**Flexion** is the movement of the thumb towards the base of the little finger and **extension** is the return movement, bringing the thumb column into the plane of the palm. **Abduction** refers to the movement that places the thumb perpendicular to the palm plane, while adduction places the thumb in the palm plane, about 60° from the M2. The **flexion/extension** and **abduction/adduction** movements start from the neutral position defined by the muscular rest (30° between M1 and M2; 40° between M1 and the sagittal plane; 40° between M1 and the transverse plane) [1].

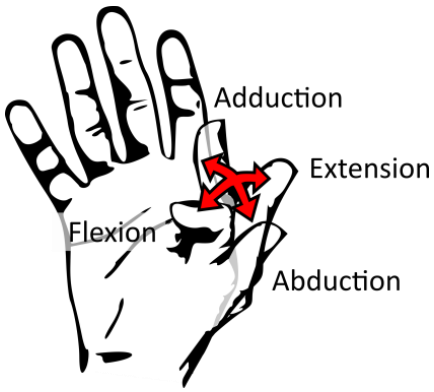


**Figure1:** Movement of the thumb

The flexion-extension range of motion is 17°±9°. The amplitude is slightly different between men and women (women: 18°±9°; men: 16°±8°). The abduction/adduction range of motion is 22°±9° (women: 24°±9°; men: 19°±8°) [1]. **Axial rotation** can also be defined around the longitudinal axis of the thumb and **circumduction** consists in describing the greatest amplitude of the thumb. The **opposition movement** corresponds to all the movements from the neutral position at the base of each of the long fingers except the index finger. It refers more generally the ability to wear the thumb pulp in contact with the pulp of each of the other four fingers. These movements involve flexion, abduction and axial rotation.

### 1.3. The trapeziometacarpal joint (TMC)

The trapeziometacarpal joint (TMC) is at the base of the osteoarticular column of the thumb. It is the main articulation allowing opposition mechanisms. It is described in the literature as a toroid-negative joint, also known as "saddle" joint [2,3]. In the dorso-volar direction, the curves are concave while in the radio-ulnar direction, the curves are convex. The curves have local variations depending on the location [1]. This point is further developed in the chapter 3 of this manuscript. Mathematics models can be used to approach this geometry as seen in figure 2.

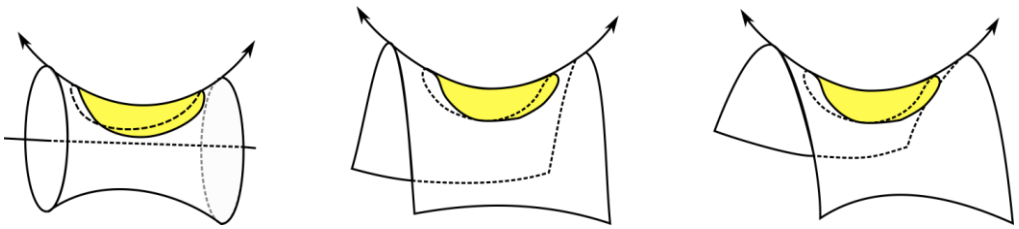

**Figure 2**: From left to right: hyperboloid segment of revolution / parabolic hyperboloid segment / hyperboloid hyperboloid segment

In addition, it has been shown that this surface is asymmetric because the radio-ulnar segment is curved laterally. This allows axial rotation along this trajectory [2]. The TMC

joint surfaces; ligament and tendon insertions are described in the next paragraphs. Understanding the complexity of the joint environment allows us to better address the need for a surgical approach in the development of an implant with a disruptive geometry compared to standard designs (e.g. ball-and-socket). This point is further examined in the chapter 2 of this manuscript.

### 1.3.1. Surface topography of the trapezium

The trapezium is located between the scaphoid and the first metacarpal. It possesses 4 joint faces.

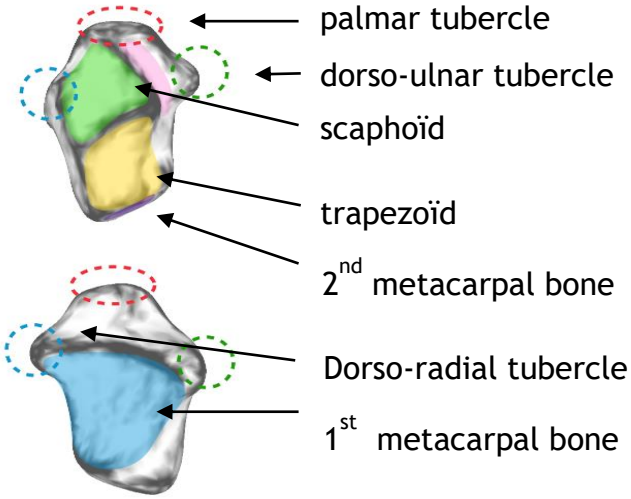


**Figure 3**: Trapezium anatomy

### 1.3.2. Topography of the surfaces of the 1st metacarpal (M1)

Like all metacarpals, it is a long bone with a body or diaphysis, a base at its upper end (upper epiphysis) and a head at its lower end (lower epiphysis). The upper base has an articular surface with the trapezium concave from front to back and convex transversely. On the palmar part there is a triangular tuberosity opposite the trapezium tubercle in neutral position. On the dorsal side, there are two tuberosities on either side of the base of M1, the point of insertion of the dorsal-radial ligament and the inter-metacarpal ligament. The lower epiphysis is articulated with the base of the first phalanx of the thumb and two small sesamoid bones, an area of tendon and ligament insertion. The articular surface of interest, i.e. the one in contact with the trapezium, is inversely shaped. It has a ridge corresponding to the furrow of the trapezium surface and a depression applying to the trapezium ridge [1]. Applied to the surface of the trapezium, the concordance is not absolute as the curvature radii are slightly different.

### 1.3.3. Coaptation

The TMC joint capsule is known for its laxity allowing the movement of the metacarpal surface on the trapezium in the manner of a pivot working in compression [1]. The capsule's role is to orient M1 in all directions following the tension of the thenarian muscles. The stability of the joint known as coaptation, is mainly ensured by active elements including the thenarian muscles, and passive elements ligament constraints [4]. The role of the joint capsule (2 to 4 mm) in coaptation is minor [1]. The TMC ligaments lead the movement and ensure coaptation in each position in dependence of the degree of tension. In this manuscript, we will use the nomenclature of TMC joint ligaments described by Bettinger et al. [5].

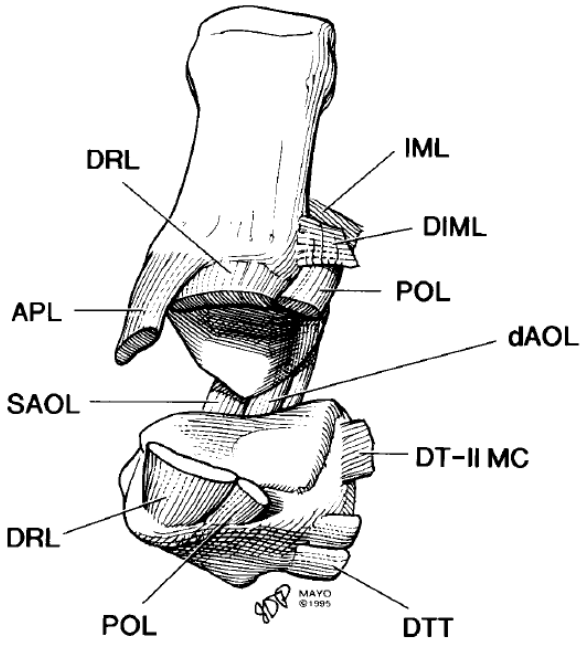


**Figure 4**: Main TMC joint ligaments [6]

- **The posterior oblique ligament (POL)** is inserted into the dorsal ulnar tubercle of the trapezium. It converges with the inter-metacarpal ligament (IML) and reaches the palm tubercle of the M1. LOP is a broad ligament and its shape is semi-lunar.
- **The inter-metacarpal ligament (IML)** is short and thick. It is inserted on the dorsal-radial surface of the M2 and joins the oblique posterior ligament. It resists extreme abduction, supination and flexion.

- **The upper oblique anterior ligament (SAOL)** is attached to the palmar tubercle of the trapezium and to the palmar tubercle of M1. It is a thick, wide and solid structure that stretches in pronation and extension of the TMC joint.
- **The dorsal-radial ligament (DRL)** is inserted into the dorsal-radial tubercle of the trapezium and terminates on the dorsal edge of the M1. It is contracted only in extreme supination, and adduction flexion.
- **The inner oblique anterior ligament (DAOL)** is inserted into the anterior edge of the trapezium and terminates on the 1st metacarpal, deeper than the SAOL. To a certain extent, it ensures the pronation movement of the thumb during adduction. It acts as an axis of rotation during flexion and extension movements of the thumb.
- **The internal inter-metacarpal ligament (IIML)** is a separated part of the IML that has an insertion on the dorso-radial tubercle of M2 towards the dorso-ulnary edge of M1. It resists thumb pronation and radial sublimation.
- **The ulnar collateral ligament (UCL**) is attached to the ulnar base of M1 and terminates on the transverse ligament of the carpus (reticulum of the flexors).
- **Other ligaments**: The dorso-trapezoidal (DTT) and dorsal trapezoidal-second metacarpal ligaments (DT-II MC) are opposed to M1 pronation, while the ventro-trapezoidal (VTT) and ventral trapezio-second metacarpal (VT-II MC) ligaments resist supination. The trapezium-third metacarpal ligament (T-III MC) is the most inserted ligament on the trapezium.

Below is a summary of the action of the ligaments in relation to the different movements of the TMC joint according to A.I. Kapandji [1]. We notice that the IML is always in tension whether it is in abduction or adduction. POL and DAOL are controlling the rotational stability of M1 as they are wound in opposite direction at the M1 base.

**Table 2**: Summary of the ligaments action for all its movements [1]

| | **Abduction** | **Adduction** | **Flexion** | **Extension** | **pronation (Axial rotation)** | **supination (Axial rotation)** | **Intermediate position** |
|---|---|---|---|---|---|---|---|
| IML | Tension | Tension | | | | Tension | Slackening |
| POL | Tension | Slackening | Tension | Slackening | Slackening | Tension | Slackening |
| DAOL | Tension | Slackening | Slackening | Tension | Tension | Slackening | Slackening |
| DRL | Slackening | Tension | Slackening | Tension | | | Slackening |

### 1.3.4. Motor muscles in the joint

The thumb is bound with nine motor muscles. It allows a great mobility and to perform the essential function of opposition with the other fingers. There are two groups of muscles:

- **The extrinsic muscles.** There are four of them. Their proximal insertions are located on the radius and ulnar side of the thumb. Three are extensors and allow the slackening, while the other one is an abductor and allow the tension. The abductor is therefore essential for the supply of power.
- **The intrinsic muscles.** There are five of them. Their proximal insertions are located on the carpus or metacarpus, in the eminence of the thenar. They allow the control of precision and coordination.

The characteristics of intrinsic muscles [1] are:

- **The Abductor Pollicis Brevis (APB)** is a flat, thin muscle located under the skin. It begins from the scaphoid bone tubercle and the anterior carpal ligament (LAAC) and terminates on the lateral tubercle of the first phalanx, and in conjunction with the other palm and lateral abductor muscles, allows abduction in the TMC joint and extension in the IP joint.
- **The Opponens Pollicis (OP)** is a small triangular muscle located under the APB. It originates on the palmar tubercle of the trapezium and on the LAAC and is inserted on the radial edge of the first metacarpus. It allows flexion and pronation in the TMC joint
- **The flexor pollicis brevis** (FPB) is formed by two bundles. The first one is superficial (trapezium tuber, LAAC) while the other is deeper (anterior surface of the trapezoid and large bone). It is oblique to reach the lateral tubercle of first phalanx's base and the lateral metacarpal-phalangeal sesamoid. It allows flexion and pronation in the TMC joint.
- **The adductor Pollicis (AP)** is a thick, triangular-shaped muscle with two proximal origins. One beam is oblique and originates on the anterior surface of the trapezoid and the large bone. The other beam is transversal and originates on the anterior face of the base of the M2 and M3. The muscle ends on the medial tubercle of P1. It is a thick muscle with a triangular shape. It allows the adduction into the MP joint and allows the extension of the IP joint.

- **The Interosseux Palmaris Primus (IPP)** consists of two beams. It takes its origin on the adjacent surfaces M1 and M2 and is inserted on the basis of the first phalanx of the index. It causes the flexion, abduction and pronation of the metacarpal-phalangeal joint of the index finger. It also allows adduction in the TMC joint with other adductor muscles.

The characteristics of extrinsic muscles [1] are:

- **The abductor pollicis longus (APL)** takes its roots on the posterior surface of the radio side of interosseous membrane. It allows palmar abduction in the TMC joint as well as the abduction of the wrist as a whole.
- **The flexor pollicis longus (FPL)** is inserted on the anterior surface of the radius and interosseous membrane up to the 2nd phalanx of the thumb. It allows thumb flexion in the interphalangeal and the metacarpal-phalangeal joints. Its role in the movements of the TMC joint has not been demonstrated.
- **The extensor pollicis longus (EPL)** is anchored on the posterior surface of the radius and interosseous membrane and extends to the posterior surface of the 2nd phalanx of the thumb. It allows the extension of the thumb.
- **The extensor pollicis brevis (EPB)** is inserted on the posterior surface of the radius and on the posterior surface of the 1st phalanx of the thumb. It allows the extension of the thumb in the MP joint and causes a slight abduction in the interphalangeal and the metacarpal-phalangeal joints.

Its insertions have a role of mechanical stabilization of the joint and in the kinematics of the thumb column. The table below summarizes the predominance of muscles in the main movements of the thumb.

**Table 3** : Motor muscles action in the different movement of the TMC joint [1]

| **Joint movements** | **Motor muscles** | | | | | | | | |
|---|---|---|---|---|---|---|---|---|---|
| | **APB** | **OP** | **FPB** | **AP** | **IPP** | **APL** | **FPL** | **EPL** | **EPB** |
| Abduction | x | x | | | | x | | | x |
| Adduction | | | | x | x | | | x | |
| Extension | | x | | | | x | | | x |
| Flexion | | | x | x | x | | | | |
| Opposition (Flexion-Abduction-Pronation) | x | x | x | | | x | | | |
| Counter-opposition (Extension-Adduction-Supination) | | | | | | | | x | x |

### 1.3.5. Osteoarthritis of the trapeziometacarpal joint

TMC Osteoarthritis (OA) is the 2nd most common site of arthritis of the upper extremities. It corresponds to the wear of the cartilage in the joint between the trapezium bone and the base of the first metacarpal [7]. The trapezium bone will change its geometrical configuration through the pathology [8]. Osteoarthritis is often bilateral [9].

There are 3 main progressive models of osteoarthritis:

- Asymptomatic osteoarthritis which may evolve into a deformity;
- Occasional symptomatic osteoarthritis;
- Symptomatic osteoarthritis with chronic aggravation.

The therapeutic indications mainly concern the latter group. In clinical practice, it is necessary to take into consideration in the therapeutic act:

- The age of patients, with slightly different etiological characteristics between an elderly patient (> 60 years of age) and a young patient;
- The evolution of the osteoarthritis;
- The location of the osteoarthritis: isolated trapezo-metacarpal or peritrapezial.

### 1.3.6. Prevalence and factors contributing to the pathology

It is high-prevalence disease, affecting between 24.5% to 38% of the population after 66 years old [10]. Only 30% of osteoarthritis is associated with pain at the base of the thumb. Trapeziometacarpal (TMC) OA is particularly common in post-menopausal women (>45 years). Studies have shown that it affect women between 2 and 6 times more than men [11–13]. The origin of this female prevalence has not found a consensus in the literature. Some studies suggest that it is due the size of the trapezium. As females are known to have significantly smaller trapeziums than males, it results in a smaller contact area and a smaller congruency [14]. Under similar loading conditions, the female trapeziometacarpal joint would be subject to greater stresses than the male joint. The prevalence of osteoarthritis also increases with age [15]. Other predisposing factors include obesity [16,17], hysterectomy, ethnicity, genetics, history of inflammatory joint disease, and metabolic, congenital and developmental defects [18].

TMC osteoarthritis may arise after certain trauma [18] and repetitive use [10]. Certain occupations or hobbies predispose people to developing pain at the trapeziometacarpal

joint, particularly when the specific task requires sustained loading through the thumb [10]. For instance, manual work with vibratory tools in metal foundry has been associated with hand OA. Similarly, a study found the use of chopsticks predisposed to hand OA, especially in women [19]. Recent studies indicate that repeated use of the thumb for mobile phone use, in non-physiological movements requiring particular strength, may eventually induce more cases of OA in younger populations. Surgeons are currently observing only an increase in cases of thumb pain [20]. In addition, the use of smartphone leads to extensive flexion/extension of the thumb which likely increase load on these joints [20]. The consequences of smartphone use on this joint are currently studied at the Mayo Clinic since 2014 [21]. Additionally, two cases (32 and 33 years old) of OA due to mobile phone overuse have already been reported [22].

The chapter 6 of this manuscript studies in part the impact of the loss of the prehension gesture in the context of new technologies area. The aim is to highlight the importance for patients to recover grip in a broader spectrum than clinical considerations (self-awareness, definition of the self by activities that can no longer be done, etc.).

### 1.3.7. Impairments

Pain is the most common and disabling disability in people with TMC OA. Pain is usually localized on the palmar surface of the joint. Some report dull-aching pain, but most of the time, pain is often sudden and sharp aggravated by the execution of certain movements and activities such as turning a key, writing, using scissors or holding a needle. More rarely, patients consult for pure functional discomfort due to a limited range of motion. Finally, sometimes it is the deformation of the thumb in itself that leads them to consult. With the progression of joint degeneration because of advancing OA, impairments worsen, including weakness, thumb contracture and a decrease of the joint mobility. These symptoms are significantly affecting the overall function of the hand. Pain of OA limits many activities requiring manipulation of objects in the hand. Such activities include but are not limited to opening jars and bottles and fastening buttons.

### 1.3.8. Classification

Two radiographic classification systems are commonly used to determine the evolution of TMC OA [23,24]. The tables below describe both classifications.

**Table 4**: Classification of Dell [23]

| Stade | |
|---|---|
| **I** | Joint pinching or subchondral sclerosis but without subluxation or osteophytes. Stress pains |
| **II** | To the previous lesions is added a small osteophyte at the ulnar edge of the distal articular surface of the trapezius and a subluxation lower than one third of the articular surface. Clinically the subluxation is reducible |
| **III** | The osteophyte is bigger. Subluxation is equal to one-third of the joint surface and reduction is impossible. "some patients" have a deformity in the adduction of the first metacarpal and secondary metacarpal-phalangeal hyperextension. |
| **IV** | Total disappearance of the joint space. The joint is totally stiff. The pain is relatively reduced. |

**Table 7** : Classification of Eaton et Litter [24]

| Stade | |
|---|---|
| **I** | Small enlargement of the joint space by effusion or laxity |
| **II** | Slight joint pinch. subchondral sclerosis. osteophytes or foreign bodies do not exceed 2 mm in diameter. |
| **III** | Joint pinch mark with subluxation and osteophytes or foreign bodies of a diameter exceeding 2 mm. no scapho-trapezotrapezoidal lesions |
| **IV** | Scapho-trapezotrapezoid involvement |

These systems provide the radiological stage of OA TMC. They allow surgeons to determine the most appropriate management of the pathology. These systems will be used throughout this manuscript.

Many clinical cases have shown individuals with radiographic characteristics of OA without having the symptoms [25]. This is why in clinical condition, the treatment is rather determined according to the severity of symptoms such as pain, loss of strength than the radiological stage. Other classification systems are developing for the choice of optimal therapeutic treatment [26].

## 2. Management of osteoarthritis of the trapeziometacarpal joint

Management of TMC OA aims to decrease pain, weakness and contracture, and improve hand function. To meet the needs of patients, therapeutic treatments and surgical techniques are many and varied. The diagnosis looks at whether the dorsal palpation of the TMC joint is painful. Two clinical tests complete the diagnosis.

- **The grinding test**: it consists in applying an axial compression of the thumb combined with a rotational movement. It is used to highlight cracks that are signs of a damaged seal.

- **The Glickel test**: it highlights any dorsal instability of M1. It consists in reducing the subluxation of M1 by pressing at its base.

Depending on the results and the radiographic stages either conservative or surgical approach will be proposed.

### 2.1. Conservative management

Non-surgical techniques are measures taken primarily for patients at an early stage (Eaton stage I) of OA before any surgical measures are considered. Common interventions include [27]:

- Drugs (analgesics) and intra-articular injection (cortisone, hyaluronate)
- Orthoses
- Strengthening exercises
- Activity modification (patient education in joint protection)

Initially, the treatment consisted of taking non-steroidal anti-inflammatory drugs (NSAIDS) to reduce pain and inflammation. Since the effect is only short-term, alternative treatments by cortico-steroids and hyaluronate injections have been used. Studies have found that there is some evidence for pain relief with both injections [27]. Based on the present literature, hand therapy (strengthening exercises, and activity modification) provides some pain reduction but does not restore pinch and grip strength [28]. To treat pain more deeply, orthoses can be used to immobilize the joint. However clinical studies have shown that orthoses are well tolerated and give some pain reduction [27]. However it does not eliminate entirely the pain and the inflammation [29].

Despite conservative management some people still have persistent pain and dysfunction at the base of the thumb. Surgery is therefore considered. This is because patients are seen at an advanced stage, making conservative treatments ineffective.

### 2.2. Surgical management

Surgical management includes:

- **Ligament reconstruction:** The procedure consists in strengthening the volar ligament and reinforcing the dorsal joint capsule [30]. It is for painful hypermobile pre-OA TMC joint [31] (Stage I).
- **Metacarpal osteotomy:** It consists in removing a radially-based wedge of 20-30º from M1 followed by four weeks of fixation with Kirschner wires. It is mainly used for stage II-III. The procedure aims to redistribute stresses from compromised volar TMC side to the dorsal side [32].
- **Arthrodesis :** It consists in resecting both articular surfaces of the metacarpal and trapezium, and fusing them together with internal fixation such as plate and screw [33]. It is indicated for younger, active people with Stage II-III OA without any scaphotrapezial joint involvement. It provides stability, strength and pain relief. The thumb is therefore blocked in a certain position leading to a significant loss of motion and the inability to flatten the hand [33].
- **Trapeziectomy:** It is based on the principle of removing pathological joint areas by extracting one of the bones in friction, the trapezium. Proposed in 1943 [34] as it was for a long time the only surgical treatment for this pathology. A number of variants of trapeziectomy have been proposed: partial, isolated, total, with or without tendon interposition, with or without ligament reconstruction or both. It is performed mainly for elderly patient with advanced disease. However, it does not prevent proximal migration of the M1 which results in impingement between M1 and SCP with loss of thumb length.
- **Arthroplasty implants:** It consists in implanting prosthesis to replace partially or entirely the TMC.

## 2.3. Arthroplasty implant

CURRENT CONCEPTS

# Trends in Trapeziometacarpal Implant Design: A Systematic Survey Based on Patents and Administrative Databases

Augustin Lerebours, MA,* Frederic Marin, PhD,† Salima Bouvier, PhD,* Christophe Egles, PhD,‡ Alain Rassineux, PhD,* Alain-Charles Masquelet, MD‡

Hand function is inseparably linked to the condition of the thumb. The trapeziometacarpal (TMC) joint that provides the different movements of opposition is one of the joints most affected by osteoarthritis, which causes an irreversible deformation of the bone. The ideal thumb carpometacarpal implant must restore range of movement, prevent complications, be biocompatible, and have good mechanical properties (ie, low wear, high corrosion resistance, and osteointegration properties where it is anchored in a bone). The integrity of the implant and the surrounding biological structures must be long-lasting and withstand constant stresses induced by the prosthesis. Three main types of implant systems for the thumb are currently clinically available; others are under investigation in human subjects. This systematic review is based on administrative databases, patents, the literature, and information from orthopedic companies. It provides a summary of strategies and design changes and an overview of the biomechanical characteristics of currently available carpometacarpal implants for treating osteoarthritis of the thumb. *(J Hand Surg Am. 2019;■(■):■−■. Copyright © 2019 by the American Society for Surgery of the Hand. All rights reserved.)*

**Key words** Hemiarthroplasty, interposition arthroplasty, osteoarthritis, patents, systematic review.



HAND FUNCTION IS LINKED TO THE condition of the thumb, which makes human prehension[1] all the more complex. Functionally, the most important thumb joint is the carpometacarpal (CMC) joint, located at the base of the thumb between the trapezium and the first metacarpus. The articulation is a concavo-convex joint stabilized by ligaments that also limit the range of movement (ROM). The CMC joint is often affected by arthritis. This can result in pain, diminished strength of the pollici-digital grasp, and a smaller ROM, making everyday activities difficult. For this reason, implant arthroplasty is often recommended after a trial of nonsurgical treatments as soon as painful symptoms occur.[2] From a biomechanical point of view, the aim of implant arthroplasty is to restore normal CMC kinematics in a way that prevents loosening. The biomaterial has to be chosen with consideration regarding its interaction with the biological environment. The parts are under several mechanical constraints (shear stress, compressive, wear, etc). Therefore, for such an articular implant, the material needs (1) to be low-wear, (2) to have an elasticity modulus similar to that of bone, along with (3) a high resistance to corrosion and (4) properties of

*From the *Royallieu Research Center and †Department of Biomechanics and Bioengineering, Royallieu Research Center, Sorbonne University Alliance, University of Technology of Compiègne, Compiègne; and the ‡Department of Orthopedics, Trauma, and Hand Surgery, Saint Antoine Hospital, Paris, France.*

Received for publication October 4, 2018; accepted in revised form November 15, 2019.

No benefits in any form have been received or will be received related directly or indirectly to the subject of this article.

**Corresponding author:** Augustin Lerebours, MA, Sorbonne Universités, Université de Technologie de Compiègne, CNRS, UMR 7337 Roberval, Centre de Recherche Royallieu, CS 60 319, 60203 Compiègne Cedex, France; e-mail: augustin.lerebours@utc.fr.

0363-5023/19/■ ■ -0001$36.00/0
https://doi.org/10.1016/j.jhsa.2019.11.015

 

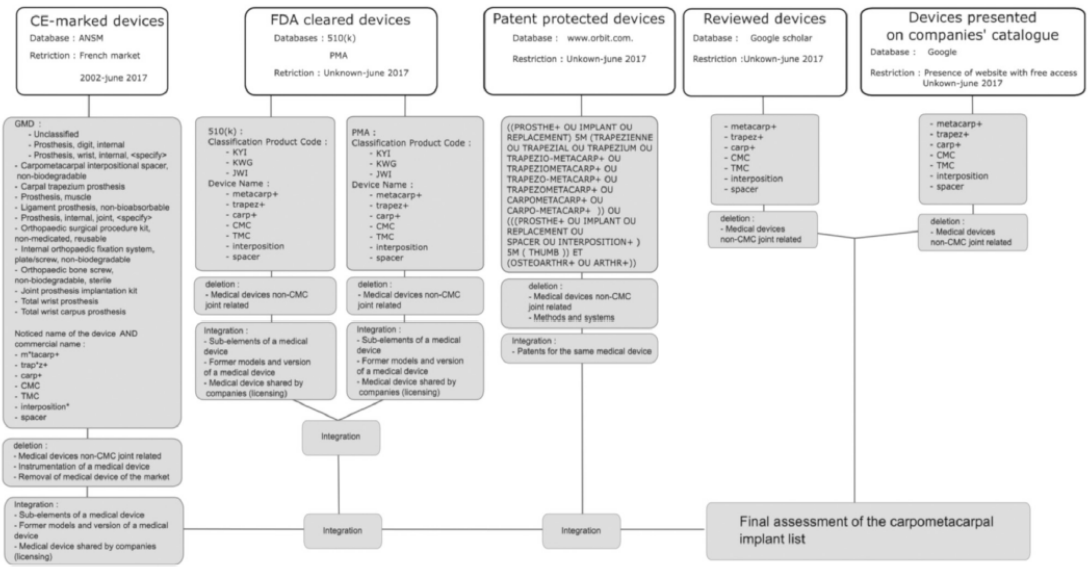


**FIGURE 1:** Schematic view of the methodology used for the literature review and the search results based on reviewed devices, patent-protected devices, FDA-cleared devices, CE-marked devices, and companies 'information. To be classified, the implant had to be well-described.

osteointegration (anchored part). The prosthesis also needs to withstand the forces that act on the CMC joint. A large range of implants are currently available on the market.

In this work, we classify CMC arthroplasty implants for treating osteoarthritis (OA) according to the principal design types: total joint replacement, hemiarthroplasty (HA), and interposition arthroplasty. The objective of this precise classification is to observe how each of these design types is evolving. Ours is the first classification to be based on a systematic review of US Food and Drug Administration (FDA)-cleared implants, European Conformity (CE)-marked implants, patents, the scientific literature, and information provided by companies in the orthopedic sector. Figure 1 describes the protocol.

Information on CMC medical devices was obtained as follows: 60 were from the scientific literature, 47 were from patents, 24 were CE-marked, 25 were FDA-cleared. Altogether, we assessed 105 CMC prostheses.

Four design types were identified: (1) total joint replacement, (2) HA, (3) interposition arthroplasty, and (4) miscellaneous designs.

## TOTAL JOINT REPLACEMENT

Total joint replacement replaces both articulating surfaces. It is composed of 2 main elements: trapezial and metacarpal components. The trapezial component either replaces the trapezium completely or is fitted into a resurfaced trapezium. The metacarpal component is fixed into the medullary cavity of the opposite bone. Table 1 shows the proposed classification.

## HEMIARTHROPLASTY

Hemiarthroplasty (HA) implants replace only the metacarpal surface of the joint. The base of the metacarpal component is in contact with either a resected trapezium or the scaphoid. Hemiarthroplasty is an alternative that preserves the bone stock. The proposed classification can be seen in Table 2.

## INTERPOSITION ARTHROPLASTY

Interposition arthroplasty is a one-piece implant placed at the interface of 2 articulating surfaces. It acts as either an entire trapezium replacement or a cartilage replacement placed between slightly resected TMC surfaces. The proposed classification can be seen in Table 3.

## MISCELLANEOUS DESIGNS

These include any other strategies used for stabilizing the thumb. There are too few miscellaneous designs to undertake a proper classification (Table 4).

**TABLE 1. Classification of Total Joint Replacement Implants**

| | | | | | | | |
|---|---|---|---|---|---|---|---|
| **Total Replacement** | 1. Partial trapeziectomy | 1.1 Constrained (inseparable components) | 1.1.1 Ball-and-socket | 1.1.1.1 Simple mobility | 1.1.1.1.1 Trapezial rotation center | | Roseland (DePuy Inc)*, Steffee (Laure Prosthetics)*, **Nahigan prosthesis***(c), Carat/Ledoux (IOTA)*(c), Carpofit (Implantcast)*, **De la Caffinière (Fixano)***(a), TMCJ-T/II (Beznoka)*, TMCJ-T/III (Beznoka)*, **Bedeschi***(b), Alnot-Bichat*, Link*, Steffee (1979)*, **Tripodal (Lima France)**(b), Braun-Cutter/CMC (Avanta) implant (Avanta Orthopaedics), Prothèse de pouce (Mathys Orthopédie), Braun- Carter (Cutter Labs) |
| | | | | | 1.1.1.1.1.2 Metetacarpal rotation center | | Guepar II (Guepar group)*, **Mayo (DePuy Inc)***(e), Rubis Modulaire/FR2980105 (3S Ortho), Lewis WO2007022342 (Mayo Foundation, 2006)† |
| | | | | 1.1.1.2 Double mobility | 1.1.1.2.2.1 Trapezial rotation center | | Evolutis Isis (f) (Evolutis), Moovis/FR3004921/US2015342745 (Avanta Orthopeadics), Maïa/FR3027213/EP3009107/ FR2883723 (Groupe Lepine, double mobility, 2014) (IOTA, geometric features, 2004), Touch (Kerimedical)* |
| | | | | | 1.1.1.2.2.2 Metetacarpal rotation center | ∅ | |
| | | | 1.1.2 Helical spring | | | W02017037686 (CMC sert, 2016)† | |
| | | | 1.1.3 Nonrigid tissue link (Cardan, others) | | | ∅ | |
| | | 1.2 Unconstrained (separable components) | 1.2.1 Saddle/anatomical shaped | | | | **(Avanta) SR TMC implant (g)** (Avanta Orthopaedics), CH711485/DE102014115301 (Handiplants, 2014)†, FR2836822 (Bouvet Jean Claude, 2002)†, FR2805152 (Cremascolli Ortho, 2000)† |
| | | | 1.2.2 Ball-and-socket | | 1.2.2.1.1 Trapezial rotation center | | Arpe (Biomet), Ivory (Stryker), Motec/W02014077750/ SE0801001 (Swemac)†, Elektra/FR2770770 (Fixano, 1997)†, **Moje Acamo-CMC 1 (Moje) (ceramic) (d)**, US2013226306 (Remi Sciences, 2012) (Pyrocarbon)† |
| | | | | | 1.2.2.2.2 Metacarpal rotation center | | US2008269908 (Piper Medical)†, TW201607521/US2014128984/ CN103815989 (National Cheng Kung University, 2012)† |
| | 2. Total trapeziectomy | 2.1 Constrained (inseparable components) | 2.1.1 Ball-and-socket | 2.1.1.1 Simple mobility | 2.1.1.1.1.1 Trapezial rotation center | | **TMCJ-TR/CZ20150793 (Beznoka, 2015)**† **(f)**, US2013338784 (Pallia Christopher Sterling, 2012)† |

(Continued)

**TABLE 1. Classification of Total Joint Replacement Implants (Continued)**

| | | | | |
|---|---|---|---|---|
| | | | 2.1.1.2 Metacarpal rotation center | ∅ |
| | | 2.1.1.2 Double mobility | 2.1.1.2.1 Trapezial rotation center | Ebony (Stryker)/ FR2931059 (Memometal Technology, 2008)† |
| | | | | CA2862622 (Aptis Medical, 2012)† |
| | | | 2.1.1.2.2 Metacarpal rotation center | ∅ |
| | 2.1.2 Nonrigid tissue link (Cardan, others) | | | Implant total cardan de Kapandji/FR2954691 (ITEM/Pallier Christopher Sterling, 2009)* |
| | 2.2 Unconstrained (separable components) | 2.2.1 Saddle/anatomical shaped head | | W02014075114 (Solomons Michael Wayne, 2013)† |

*No longer on the market at the date of the systematic reviewing process.
†Not yet on the market at the date of the systematic reviewing process.

## TOTAL JOINT REPLACEMENT: TRENDS OBSERVED

The first CMC total arthroplasty prosthesis (Table 1 [1.1.1.1.1.a]) was similar to a hip prosthesis with a trapezial polyethylene cup and a cemented metacarpal one-piece stemmed head. There have been extensive reports with overall good clinical results at first, but some series found alarming rates of trapezial component loosening (Table 5 [a]). Similar designs followed (Table 1 [1.1.1.1.1]). The development of fixation features such as screw threads, spurs, and spikes (Table 1 [1.1.1.1.1.b]]) allowed the design of the first cementless implants (Table 1 [1.1.1.1.1.c]).

In response to an alarming number of reports of the cup loosening,[3] unconstrained implants were developed (Table 1 [1.2.2.1]) conjointly with modular necks and heads of different sizes and orientations. Materials typically used for the articular interface of the implants included metal on polyethylene, ceramic on ceramic, and metal-on-metal. The first ceramic-on-ceramic implant (Table 1 [1.2.2.1.d]) had a high rate of complications owing to osteolysis and loosening of the cup[4] (Table 5). Despite some improvements, novel characteristics, such as the unconstrained ball and socket, the modular neck and head, and the hydroxyapatite coating, were often insufficient to prevent loosening of the cup entirely[5] (Table 5 [a]). None of the designed primary stabilization components, such as grooves, spikes, and screw thread, led to a significant improvement in the stability of the cup[4,6] (Table 5 [b]).

Because of degeneration of the joint, it sometimes becomes impossible to fix the cup on the trapezium. Some total joint arthroplasty implants (Table 1 [2]) were associated with a total trapezectomy. These implants are sometimes preferred when the trapezium is highly deformed or bone density is low, and for CMC implant revision when preservation of the bone is impossible.

Some ball-and-socket implants feature a metacarpal center of rotation (Table 1 [1.1.1.1.2], Fig. 2). Although dislocation and loosening were reported for one of the implants (Table 1 [1.1.1.1.2.e]), it has not been shown that the reverse center of rotation leads to complications (Table 5 [c]).

Certain implants are no longer marketed. These include De la Caffinière, Steffee (1979), Steffee (1986), and Bedeschi.

Most changes occurred in the ball-and-socket subfamily. Currently, total joint arthroplasty prostheses tend to involve secondary osteointegration over a primary stabilization by cement. Most models are sprayed with an osteoconductive coating such as a

**TABLE 2. Classification of HA Implants**

| | | | | |
|---|---|---|---|---|
| **Hemiarthroplasty** Bone/implant mobility | 1. Partial trapeziectomy | 1.1 Flat/convex head | 1.1.1 Silicone | **Swanson Silastic implant HP (a)** (Dow Corning Corp, Wright Medical) Eaton prosthesis*, Niebauer prosthesis* |
| | | | 1.1.2 Pyrocarbon | US2013226306 (Remi Sciences, 2012) |
| | | 1.2 Hemisphere head | 1.2.1 Silicone | Kessler Prosthetic (Dow Corning Corp, Wright Medical)* |
| | | | 1.2.2 Metallic | **Biopro modular thumb implant (d)** (BioProfile)/ US8021431, **Swanson titanium trapezium implant (c)** (Dow Corning Corp. Wright Medical), **SERPENS *(d)** Modular CMC Implant System (hnm total recon)* |
| | | | 1.2.3 Ceramic | Moje Hemi-CMC1 (Moje)* |
| | | | 1.2.4 Pyrocarbon | **CMI/EP1437104 (Tornier/Bioprofil/Nexa) (e)** |
| | | 1.3 Saddle head | 1.3.1 Metallic | **Stablyx (Skeletal Dynamics LLC) (g)** |
| | | | 1.3.2 Pyrocarbon | Pyrocarbon CMC (3S Ortho/integra) |
| | 2. Total trapeziectomy | 2.1 Flat head | 2.1.1 Silicone | **Swanson Silastic trapezium (b)** (Dow Corning Corp. Wright Medical), Oxalys (OSD), **TIE-IN (f)** / US2005251264 (Biotech Ortho, Wright Medical) |
| | | | 2.1.2 Pyrocarbon | US2013226306 (Remi Sciences, 2012) |
| | | 2.2 Hemisphere head | 2.2.1 Pyrocarbon | **Nugrip/PyrohemiSphere/WO2010033691 (3S Ortho/Integra) (e)** |

*No longer on the market at the date of the systematic reviewing process.

microtextured hydroxyapatite,[4] tricalcium phosphate, a resorbable calcium phosphate combination, or a plasma-sprayed, microtextured titanium enhancing bone fixation.

The metacarpal stem is often anatomic to distribute stress along the stem. No stem loosening has been reported, which suggests that this is not an essential characteristic, but it can improve the osteoconductive property of the hydroxyapatite coating as it operates in close contact.[7]

More recently, prostheses have been able to provide the basal thumb joint with double mobility through either a partial trapeziectomy (Table 1 [1.1.1.2]) or a total trapeziectomy (Table 1 [2.1.1.2]). This innovation is aimed at preventing subsequent loosening of the cup by reducing the stress induced by friction on the bone interface of the cup. Part of the residual couple is absorbed by the larger articulation while only a small couple remains[8] (Fig. 3).

The first dual-mobility ball-and-socket (Fig. 4) was associated with a total trapezium replacement, and it was subject to instability of the trapezial component caused by the ligamentoplasty anchoring system.[8] This highlights the importance of stabilizing the trapezial component. Therefore, the subsequent designs of dual-mobility implants included several stabilization features using the radial carpal flexor and cortical screws anchored into the trapezoid and the second metacarpus (Table 1 [2.1.1.2.f]).

Another patent (US2013338784) also describes a trapezium-shaped replacement component. However, the lack of securing elements and the monolithic metacarpal component may be insufficient to outperform existing solutions (Fig. 5).

The development of total joint arthroplasty has mirrored improvements in total hip arthroplasty. However, several studies have shown that simplifying the TMC joint to a ball-and-socket articulation has deleterious effects by altering the kinematics, changing musculotendinous moment arms and altering force transmission.[9,10] The prosthesis is thus overstressed, which partly explains the short life span of the ball-and-socket design. To address this problem, the design of Avanta SR CMC (Avanta Orthopaedics) was intended to mimic the anatomical shape of the joint (Table 1 [2.1.1.2.g], Fig. 6). Once implanted, the cadaveric model had kinematics similar to that of a normal temporomandibular joint, and similar stability was provided by a ligamentous tension.[11] However, the noncongruent and unconstrained characteristics of the implant and the high probability of malposition

**TABLE 3. Classification of Interposition Arthroplasty Implants**

| | | | | | |
|---|---|---|---|---|---|
| **Interposition arthroplasty** | 1. Partial trapeziectomy | 1.1. Unconstrained | 1.1.1. Nonrigid material | 1.1.1.1. Nonresorbable | CA2949606 (Columbia University, 2015)†, US2010324693 (Hardenbrook Frederick H)†, US2016135956 (Cedars Sinai Medical Center, 2015)†, Cartiva SCI (Biovation)/US2016286407, Ashworth button implant* |
| | | | | 1.1.1.2 Resorbable/biological compounds | ∅ |
| | | | 1.1.2. Rigid material (metallic, ceramic, pyrocarbon, other) | 1.1.2.1 Sphere | **Metallic spherical CMC implant (g)** (Wright Medical), **SONATA(g)** (Science et Medecine); **Orthosphere ceramic spherical CMC implant (f)** (Wright Medical), **PyroSphere HaPy Pyrocarbon Sphere (h)** (Tornier /Bioprofile/3S Ortho) |
| | | | | 1.1.2.2. Cylinder/disc | ∅ |
| | | | | 1.1.2.3 Saddle/anatomical-shaped | Pyrocardan/EP2263614 (Ascension/Tornier) |
| | | 1.2. Constrained | 1.2.1. Nonrigid material | 1.2.1.1 Nonresorbable | |
| | | | | 1.2.1.2. Resorbable/biological compounds | **Artelon CMC Spacer (a)** (Stryker/Artimplant) Artelon Arthroscopic (Stryker/Artimplant); SE0100127 (Artimplants, 2001)†; WO2010097724 (Ortho Space, 2010)†, US2011054627 (2010) (Bear Brian)†, **Regjoint (i)** (Arex/medandcare /Scaffidex)* |
| | | | 1.2.2. Rigid material (metallic, ceramic, pyrocarbon, other) | 1.2.2.1 Cylinder/disc/annular-shaped | Porous Nonbioresorbable WO2012003037/US2010268337/WO2010114578 (Intellectual property chale/Synasive Technology, 2009), **Pyrodisk (j)** / WO2004093767 (3S Ortho/Integra), WO2011032043 (2010) **(Articulinx [k])**†, FR2801194 (Fixano, 1999)† |
| | | | | 1.2.2.2. Saddle/anatomical-shaped | Strickland trapezial implant (Wright Medical) |
| | 2.Total trapeziectomy | 2.1. Unconstrained | 2.1.1. Nonrigid material | 2.1.1.1. Nonresorbable | Proplast-stabilized (Vitek)*, **Marlex (c)**, **Tecoflex* (d)**, Gelfoam* |
| | | | | 2.1.1.2. Resorbable/biological compounds | **Gore-Tex (b)**/WO9847449 (Gore Medical)*, **Permacol Porcin dermal collagen xenograft*** **(e)**, Graftjacket (Wright Medical)*, Costochondral allograft*, Rolled ligaments (Orthomed SAS) |
| | | | 2.1.2. Rigid material (metallic, ceramic, pyrocarbon, other) | 2.1.2.1. Cylinder | Theol (Stryker)* |
| | | | | 2.1.2.2. Sphere | Pi2/EP1112753/US6090145 (Tornier/Bioprofile) |
| | | 2.2. Constrained | 2.2.1. Nonrigid material | 2.2.1.1. Nonresorbable | ∅ |
| | | | | 2.2.1.2. Resorbable/biological compounds | Anchovy Resorbaid Arex 615R (Arex/Cousin Biotech) |
| | | | 2.2.2. Rigid material (metallic, ceramic, pyrocarbon, other) | 2.2.2.1. Sphere | Helal (OEC Europe limited)*, WO2016166641 (Lanzetta Marco, 2016)† |
| | | | | 2.2.2.2. Trapezium-shaped | **TrapEZX (m)** / USD655008/USD619718/US2009254190 (Lavender Medical/Extremity Medical LLC), EP2687189/US2013304223 (TORNIER, 2013)† |
| | | | | 2.2.2.3. Unknown | Pinch (Cousin Biotech) |
| | 3. Unknown/undecided | | | | Trapeziometacarpal joint spacer (Scientific Data Systems Israel Ltd), US2010057215 (Upex Holdings, 2008)†, Trapezium shaped : WO2010129882 (Tornier, 2010)†, W02014075114 (Solomons Michael Wayne, 2013)† |

*No longer on the market at the date of the systematic reviewing process.
†Not yet on the market at the date of the systematic reviewing process.

**TABLE 4. Classification of Miscellaneous Implants**

| | | |
|---|---|---|
| Miscellaneous | Total trapeziectomy | CMC mini tightrope (a) (Arthrex Inc), CMC cable fix (Instratek Inc), Mersilene suspension suture (Ethicon) (b) |

**TABLE 5. Clinical Outcomes of Total Joint Replacement Implants**

| Total Joint Replacement | Clinical Outcomes |
|---|---|
| Isis (Guepar III) (a) | (n = 30; 30 mo follow-up; 97% survivorship, 10% complications mainly owing to loosening of cup) Seng et al (*Chir Main*, 2013) |
| Maïa (Arpe) (b) | (n = 36; 42 mo follow-up; 97% survivorship; 6% dislocation and loosening) Kubat et al (*Acta Chir Orthop Traumatol Cech*, 2012)<br>(n = 100; 48 mo follow-up; 95,6% survivorship) Teissier et al (*Chir Main*, 2011) |
| Rubis II Modulaire (c) | (n = 104; 120 mo follow-up; unspecified survivorship; 9.5% dislocation and 0.87% loosening) Dehl et al (*Chir Main*, 2014)<br>(n = 61; 143 mo follow-up; unspecified survivorship; 9.8% dislocation and 3.28% loosening) Laterza-Leroy et al (*Chir Main*, 2011)<br>(n = 118; 88 mo follow-up; 92% survivorship; 9.8% dislocation, 23.3% pain) Maes et al (*Chir Main*, 2011) |
| Roseland | (n = 79; 44 mo follow-up; 96% survivorship; 2,53% dislocation, and 1% trapezius fracture) Guardia et al (*Chir Main*, 2010)<br>(n = 45; 14 mo follow-up; 82% survivorship; 2.2% dislocation and 22.2% loosening) Schuhl et al (*Chir Main*, 2001)<br>(n = 64; 150 mo follow-up; 91% survivorship; 25% complication with some dislocation [1.6%], and loosening [3.12%]) Semere et al (*Chir Main*, 2015) |
| Motec (a) | (n = 53; 22,8 mo follow-up; 91% survivorship; 8% complication with some dislocation [6%], and loosening [3.12%]) Krukhaug et al (*J Hand Surg Eur Vol*, 2014)<br>(n = 42; 26 mo follow-up; 60% survivorship; 40% complication including dislocation [21%] and loosening [7%]; pain often associated) Thillemann et al (*J Hand Surg Br*, 2016)<br>(n = 22; 29 mo follow-up; 78% survivorship; 9% complication) Hansen et al (*J Hand Surg Br*, 2013) |
| Arpe (a) | (n = 32; 86 mo follow-up; 78% survivorship; 22% complication including 16% loosening and 6.25% dislocation) *Apard and Saint cast* (*Chir Main*, 2007)<br>(n = 64; 127 mo follow-up; 95% survivorship; 10% dislocation, and 6% loosening) Martin and Ferrero (*J Hand Surg Br*, 2014)<br>(n = 35; 72 mo follow-up; 91% survivorship; and 12% complications including dislocation (4.65%), loosening, and perforation of the polyethylene cup owing to wear [2.33%]) Vander Eecken et al (*Acta Orthopæd Belg*, 2012) |
| Steffee | (n = 45; 48 mo follow-up; 91% survivorship, and 38% dislocation) Ferrari et al (*J Bone Joint Surg*, 1986) |
| Ledoux/Carat | (n = 43; 26 mo follow-up; 58.9% survivorship, 9.3% dislocation, and 32.56% loosening) Wachtl (*J Hand Surg*, 1996) |
| Mayo (c) | (n = 31; 53 mo follow-up; unspecified survivorship; and 12.9% loosening) Amadio et De Silva et al (*Ann Chir Main Memb Super*, 1990)<br>(n = 63; 60 mo follow-up, 19% survivorship, and 52% dislocation) Cooney et al (*Clin Orthop Relat Res*, 1987) |
| TMCJ-T/II (a) | (n = 11; 12 mo follow-up, unspecified survivorship, 18% complications owing to dislocation; infection in resection interposition, and transient paresthesia) Jurča et al (Acta Chirurg Orthop Traumatol Cech, 2016) |
| Moovis | (n = 20; short follow-up duration and 100% survivorship) Regnard et al (*BMC Proc.*, 2015) |
| De la Caffinière | (n = 77; 102 mo follow-up; 79% survivorship; 31.31% loosening, and 3.9% dislocation) VanCapelle et al (*J Hand Surg Am*, 1999)<br>(n = 43; 68 mo follow-up; 77% survivorship, 20,93% loosening, and 2.33% dislocation) Wachtl et al (*J Bone Joint Surg Br*, 1998)<br>(n = 31; 48 mo follow-up; 87% survivorship, 6% complications) Boeckstyns et al (*J Hand Surg*, 1989) |

(Continued)

**TABLE 5. Clinical Outcomes of Total Joint Replacement Implants (Continued)**

| Total Joint Replacement | Clinical Outcomes |
|---|---|
| Guepar II (c) | (n = 36; 42 mo follow-up; unspecified survivorship and 14.71% loosening) Alnot et al (*Ann Chir Main Memb Super,* 1993)<br>(n = 84; 50 mo follow-up; 99% survivorship, 6% loosening, and main complication of pain) Lemoine et al (*Orthop Traumatol Surg Res,* 2009)<br>(n = 64; 29 mo follow-up; 98% survivorship and 3.1% loosening) Masmejean et al (*Chir Main,* 2003) |
| Avanta SR | (n = 20; 30 mo follow-up; 70% survivorship, 55% dislocation, 15% ankylosis related to prosthetic calcification, and 20% revision with ligamentous reconstruction) Perez-Ubeda et al (*J Hand Surg,* 2003)<br>(n = 62; 36 mo follow-up; 89% survivorship, 19% loosening of cup) Pendse et al (*J Hand Surg Br,* 2009) |
| Moje Acamo-CMC | (n = 12; 50 mo follow-up; 68% survivorship, 100% loosening) Kaszap et al (*J Hand Surg Br,* 2012)<br>(n = 9; unspecified follow-up duration; 67% survivorship, 33% loosening associated with pain, and 67% osteolysis around implant associated with lack of stability) Hellegaard et al (*Rheumatology [Sunnyvale]),* 2014)<br>(n = 9; 12 mo follow-up; 67% survivorship and 89% loosening of cup) Hansen et al (*J Hand Surg Br,* 2008) |
| Braun-Carter | (n = 50; 96 mo follow-up; 94% survivorship, 10% dislocation) Braun et al (*Clin Orthop Relat Res,* 1985)<br>(n = 29; 48 mo follow-up; 90% survivorship, 14% dislocation, and 21% cement extrusion) Braun et al (*J Hand Surg,* 1982) |
| CMC (Avanta) -Braun-Cutter | (n = 26; 59 mo follow-up; 96% survivorship, 3,85% dislocation, and 3,85% loosening) Badia et al (*J Hand Surg,* 2006) |
| Elektra (a) | (n = 29; 60 mo follow-up; 90% survivorship, 3.5% dislocation, 3.5% loosening, and 3.5% instability) Krukhaug et al (*J Hand Surg Br,* 2014)<br>(n = 39; 48 mo follow-up; 56% survivorship, 33.3% dislocation, 3% loosening) Klahn et al (*J Hand Surg Br,* 2012)<br>(n = 100; 54 mo follow-up; 83% survivorship, 15% insufficient osteointegration, 7% dislocation) Regnard et al (*J Hand Surg,* 2006) |
| Ivory (b) | (n = 20; 37 mo follow-up; 85% survivorship mainly owing to loosening of cup) Spaans et al. (*J Wrist Surg,* 2016)<br>(n = 39; 47 mo follow-up; 77% survivorship only owing to loosening of cup and instability of trapezial component; principal complication was SBR dysesthesia) Goubeau et al (*J Hand Surg Eur Vol,* 2013) |
| Nahigian | (n = 42; 47 mo follow-up; 77% survivorship only owing to loosening of cup) Hannula and Nahigian (*J Hand Surgery,* 1999) |

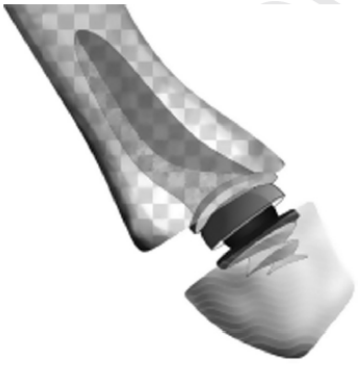

**FIGURE 2:** Total joint replacement model based on a metacarpal center of rotation, ball-and-socket implant associated with a partial trapeziectomy.

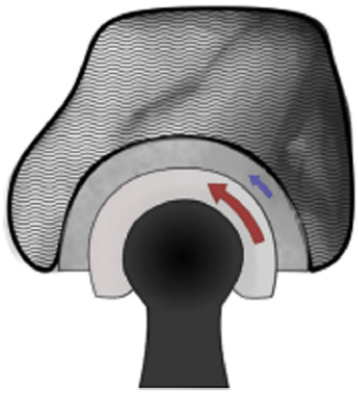

**FIGURE 3:** Double-mobility ball-and-socket CMC feature.

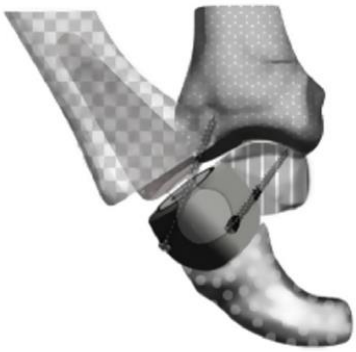

**FIGURE 4:** Total joint replacement model based on a double-mobility ball-and-socket implant associated with a total trapeziectomy (Patent Number CA2862622).

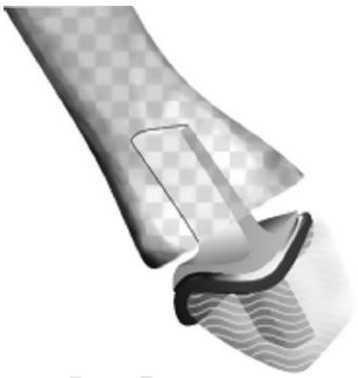

**FIGURE 6:** Total joint replacement model based on the saddle shape.

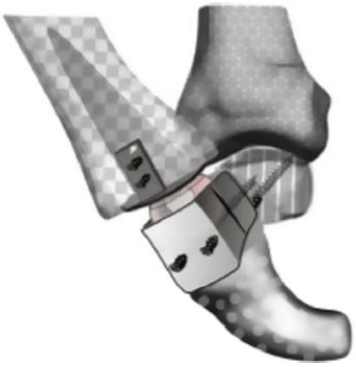

**FIGURE 5:** Total joint replacement model based on a constrained ball-and-socket associated with a total trapeziectomy (Patent Number US20130338784A1).

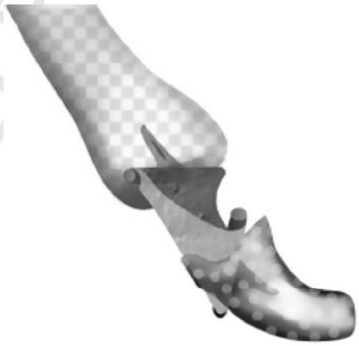

**FIGURE 7:** Total joint replacement model based on an implant with an original and flexible material link between the metacarpal and trapezial compounds.

resulting from a non-adapted ancillary caused a high loosening rate.[6] This type of implant was abandoned when the health care industry market adopted risk-averse behavior for different CMC designs, and the various patents filed (FR2836822, FR2805152, DE102014115301, and CH711485) have had little commercial uptake.

An example of an implant known to consider the physiology of the joint was the Kapandji implant (ITEM, FR2954691), but we were unable to find a cohort of patients in the literature (Fig. 7).

The CMC Sert prosthesis (WO2017037686) is the only total joint replacement prosthesis constrained by a flexible helical spring (Fig. 8). Elements in the internal volume of the helical spring limit shear deformation.

**FIGURE 8:** Total joint replacement model based on a constrained implant with a helical spring between the metacarpal and trapezial compounds (Patent Number WO2017037686).

**TABLE 6. Clinical Outcomes of HA Implants**

| HA | Clinical Outcomes |
|---|---|
| CMI (d) | (n = 54; 22 mo follow-up; 80% survivorship, 19% dislocation, 6% loosening, 2% trapezium trapezius fracture, and pain) Martinez de Aragon et al (*J Hand Surg,* 2009). |
| Swanson Silicone Trapezium Implant (a) | (n = 326; 120 mo follow-up; 89% survivorship, 6% dislocation, 1% loosening, 2% instability, and 6% pain) Krukhaug et al (*J Hand Surg Br,* 2014)<br>(n = 66; 196,8 mo follow-up, unspecified survivorship, 26% complication including 19% subluxation and implant failure) Bezwada and Webber (*J Hand Surg,* 2002)<br>(n = 22; 117,6 mo follow-up, unspecified survivorship, 50% luxations and subluxations, 70% implant wear, and 39% silicone synovitis) Allieu et al (*Ann Chir Main Memb Super,* 1990) |
| Niebauer (b) | (n = 27; 109 mo follow-up, unspecified survivorship, 3% silicone synovitis, and 83% subluxation increased over time) Sotereanos et al (*J Hand Surg*, 1993)<br>(n = 22, 28.8 mo follow-up, unspecified survivorship, 50% subluxation, and 9% instability). Adams et al (*J Hand Surg,* 1990)<br>(n = 30, 78 mo follow-up, 83% subluxation and 13% pain) Sotereanos et al (*J Hand Surg,* 1993) |
| NuGrip (d) | (n = 10; 9,5 mo follow-up; 90% survivorship, 10% dislocation, 10% too-large implant, and 10% instability and remaining osteophytes) Van De Kimmenade et al (*Internet J Ortho Surg,* 2014) |
| Tie-in (e) | (n = 17; 9.5 mo follow-up; 82% survivorship, 5% complications including 18% postoperative swelling, pain, and silicone synovitis, and 36% subluxation) Poppen et al (*J Hand Surg,* 1978) |
| Swanson Titanium Trapezium Implant | (n = 71; 120 mo follow-up; 94% survivorship, 6% complications including dislocation [1%], pain [4%], and loosening [1%]) Krukhaug et al (*J Hand Surg Br,* 2014) |
| BioPro Modular Thumb Implant (c) | (n = 159; 72,1 mo follow-up; 94% survivorship and 1% loosening) Pritchett et al (*Clin Orthop Relat Res,* 2012) |

## HEMIARTHROPLASTY: TRENDS OBSERVED

In 1969, Swanson introduced the concept of HA. This was designed to treat not only OA of the CMC joint but also multi-surface trapezial arthritis. The implant (Table 2 [1.1.1.a]) was made of silicone elastomer, with a slightly concave base, placed against a partially resected trapezium. A similar model exists for a total trapezium replacement (Table 2 [2.1.1.b]).

Because of initial good results (Table 6 [a]), together with ease of insertion and an acceptable ROM, a large range of silicone HA implants were developed (Table 2 [1.1.1], [1.2.1], and [2.1.1], Fig. 9). However, most of the studies showed a high rate of subluxation and implant failures owing to fracture or silicone synovitis[11] (Table 6 [b]). Silicone implants were therefore declared unsuitable for young, active patients (who subject implants to considerable loads); other materials such as ceramics, metal, and pyrocarbon were preferred.

Moje Hemi-CMC1 (Moje) (Fig. 10) is the only ceramic HA implant (Table 2 [1.2.3]). So far, no concerns relating to degradation have been raised, which may be a consequence of better stabilization resulting from preservation of the trapezium and from capsular and ligament tensioning.[6]

The first HA metallic implant (Table 2 [1.2.2.c]) was a one-piece implant with a convex base

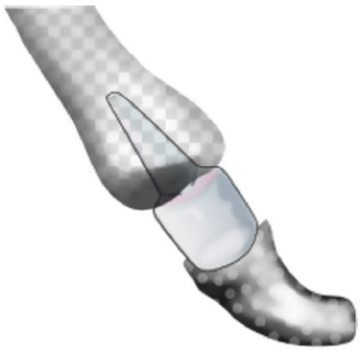

**FIGURE 9:** Hemiarthroplasty model based on the first silicone implants designs.

inserted into a slightly resected trapezium. Implants with plasma-sprayed coating for cementless fixation rapidly followed (Table 2 [1.2.2], [1.3.1]). These implants (Fig. 11, (Table 2 [1.2.2.d]) featured different innovations: (1) the varus angle (adduction) mimicked the orientation of the anatomical saddle TMC joint, and (2) the modularity allowed different base sizes independently of the stem and an additional adjustment of ligament tension, thus stabilizing the implant. The survivorship of 94% suggests the benefit of these features[12] (Table 6 [c]).

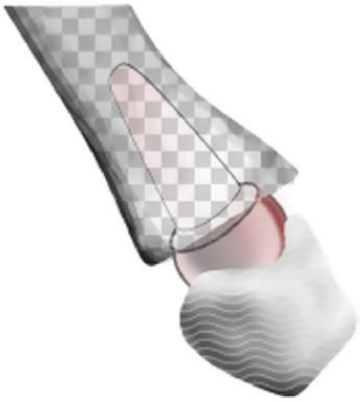

**FIGURE 10:** Ceramic HA implant design.

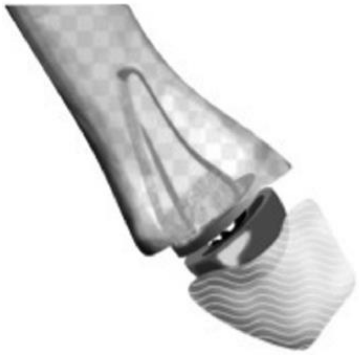

**FIGURE 11:** Metal HA implant with a modular head (Patent Number US8021431).

Pyrocarbon, a material developed in the early 1970s, has been used in patients since 1989. The main difference from the commonly used material for orthopedic implants (TA6V-alloy, 316L, CrCoMo alloy, silicone) is that it has the same mechanical properties as cortical bone.[13] This theoretically leads to reduced stress at the bone−implant interface. Pyrolytic carbon has been found to have good long-term biocompatibility[13] and good bio-tribological properties.[13]

The first pyrocarbon implants to be marketed (Fig. 12) are shown in Table 2 ([1.2.4.e], [2.2.1.e]). However, metacarpal subluxation was a concern in some series[14] (Table 6 [d]). These studies highlight that pyrocarbon implants are often subject to loosening, dislocation, and subluxation.

Because instability is one of the most often-cited complications, there has been a trend toward increasing the stability of the HA implants rather than changing the material. As seen in other designs, stabilization is a key feature for avoiding subluxation. However, the different nonmetallic materials used (silicone, pyrocarbon, and ceramics) are incompatible with bone-in-growth coating; consequently, there has been a need for primary stabilization strategies.

A joint capsule by itself cannot offer enough stability to the implant, mainly because it is not attached to the implant. In addition, the capsular tissue after a trapezium resection often prevents a good encapsulation.[15] Eaton improved the stability of the Swanson silastic implant by passing a ligament through the cannulated base and inserting it in the trapezoid.[14] The most recent silicone prosthesis (Fig. 13) (Table 2 [2.1.1.f]) features a tapered neck, which means that a reinforced structure can be created with a segment of nearby tendon. Fewer implant removals caused by dislocation have been reported[11] (Table 6 [e]). The low incidence of synovitis is attributed to improved stability of the prosthesis, which reduces frictional forces and particle formation.

Metallic implants (Fig. 14, Table 2 [1.3.1.g]) have also primary stabilization features combined with a bone-in-growth coating. The suture holes allow a suspensionplasty with the flexor carpi radialis tendon.

## INTERPOSITION ARTHROPLASTY: TRENDS OBSERVED

Synthetic resorbable spacers have been used in an arthroscopic approach to preserve the joint capsule. The synthetic allograft made by degradable polyurethane (Table 3 [1.2.1.2.a]) showed initial promise, but foreign body reactions were often reported[11] (Table 7 [a]). Similar concerns were raised in relation to the polytetrafluoroethylene material (Table 3 [2.1.1.2.b]), which was linked to osteolytic lesions consistent with reactive particulate synovitis[16] (Table 7 [b]). Other synthetic, nonresorbable, nonautogenous materials have been used, including polypropylene (Table 3 [2.1.1.1.c]). So far, polypropylene grafts have not been seen to induce synovitis[14] (Table 7 [c]). The Gelfoam thrombogenic sponge (1959) has been used without specific complications and with good patient satisfaction[14] (Table 7 [d]). The trapezium bone has also been replaced by a polyurethane implant (Table 3 [2.1.1.1.d]). Biological materials such porcine dermal collagen xenograft (Table 3 [2.1.1.2.e]) have also been used for interposition. This was a biological porcine tissue from which cells could be removed without damaging the 3-dimensional collagen matrix, but the implant was discontinued after occurrences of foreign body reactions.[16] The Graft Jacket is an

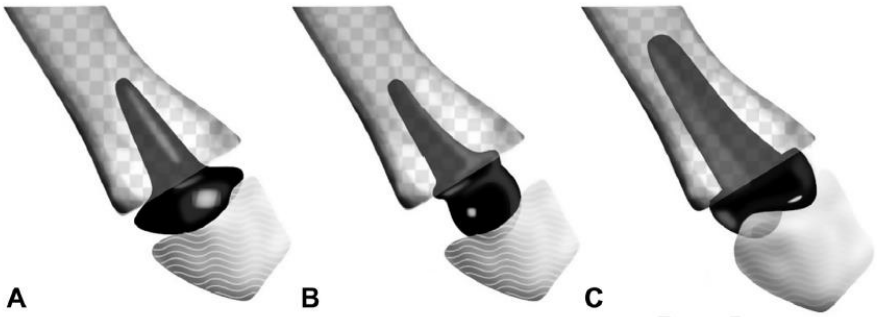


**FIGURE 12:** Hemiarthroplasty models based on the range of pyrocarbon implants. **A** Implant associated with partial trapeziectomy. **B** Spherical head implant associated with a partial trapeziectomy. **C** Saddle-shaped head implant associated with a slight trapezium resection.

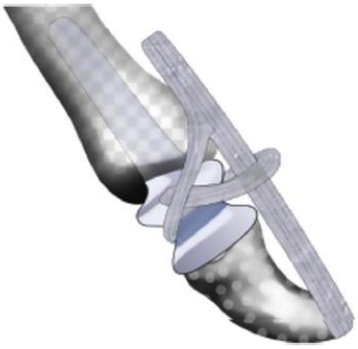

**FIGURE 13:** Hemiarthroplasty model based on the most recent developed silicone implant featuring a ligamentous stabilization (Patent No. US2005251264).

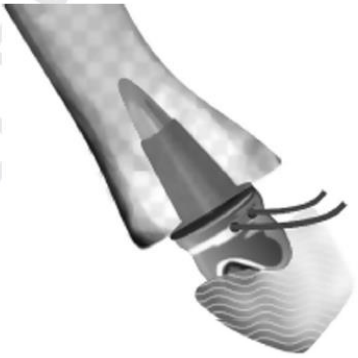

**FIGURE 14:** Hemiarthroplasty model based on a saddle-shaped implant associated with slight trapezium resurfacing.

acellular dermal allograft from cadaveric human skin tissue treated to retain only the collagen scaffold, to preserve the strength and integrity of native autografts without the allograft's immunologic response.[16] Despite relatively good outcomes, the variation in biocompatibility and the high cost without clear clinical benefits led to its withdrawal[17] (Table 7 [e]).

Interposition arthroplasty is a solution involving total replacement of the trapezium. One of the first implants was Helal (OEC Europe), a silicone spherical spacer with Dacron core stems at the pole that articulated with the scaphoid and the first metacarpus. Complications were reported, including subluxation of the prosthesis and silicone synovitis[14] (Table 7 [f]).

Original spherical implants (Table 3 [1.1.2.1]) were developed (Fig. 15). These implants are inserted after reaming the central metacarpal and trapezial articular surfaces. Among them, a spherical implant made of yttrium-stabilized zirconia ceramic (Table 3 [1.1.2.1.f]) had promising preliminary results, but subsequently there were reports of the implant sinking into the bone[11] (Table 7 [g]). This complication was attributed to the hardness of the material coupled with stress induced by the implant on the bone, causing eroding of the cancellous bone.[11] Similar implants exist that are made of metal (Table 3 [1.1.2.1.g]) or pyrocarbon (Table 3 [1.1.2.1.h]).

A porous poly-L/D-lactide copolymer implant (Table 3 [1.2.1.2.i) was developed at Tampere University of Technology. Reports mentioned insufficient stabilization of the implant and a high frequency of osteolysis[18] (Table 7 [h]). Other strategies were developed to improve stability. For instance, an implant has a slightly biconvex torus shape through which a cord or a tendon can be passed to reinforce stability (Table 3 [1.2.2.1.j]). No dislocations have been reported, but significant pain occurred in some patients[11] (Table 7 [i]). Another implant also presents tethers to adjust the implant position and stability with braided polyester suture material (Table 3 [1.2.2.1.k]). A study suggested that design

**TABLE 7. Clinical Outcomes of Interposition Implants**

| Interposition | Clinical Outcomes |
|---|---|
| Arex 615R | (n = 68, unspecified follow-up duration, unspecified survivorship, 12% pain, 1.5% body reaction) Semere et al. (*Chir Main,* 2013) |
| Gore-Tex (b) | (n = 34; 41 mo follow-up, unspecified survivorship and unspecified high rate of osteolytic lesions consistent with reactive particulate synovitis) Greenberg et al (*J Hand Surg,* 1997) |
| Gelfoam (d) | (n = 34; 60 mo follow-up, 32% pain during activities, 20% mild pain, and 4% moderate pain) Nusem et al (*J Hand Surg,* 2003) |
| Graft Jacket (e) | (n = 89; 30 mo follow-up, 6% complications including 2% pain, instability, and temporary paresthesias [2% revisions]) Kokkalis et al (*Hand Surg Am,* 2009) |
| Helal (f) | (n = 22; 13,6 mo follow-up, unspecified survivorship, 9% infection, 23% subluxation, and 14% nerve damage) Grange and Helal (*Hand,* 1983)<br>(n = 23; 59 mo follow-up, unspecified survivorship, and 26% pain) O'Leary (*J Hand Surg,* 2002) |
| Orthosphere (g) | (n = 7; 33 mo follow-up, 28% survivorship, 86% pain, weakness, and stiffness, and 14% dislocation) Athwal et al (*J Hand Surg,* 2004) |
| Pyrosphere | (n = 24; 12 mo follow-up, unspecified survivorship, 29% complications including 23% dislocation and related pain and 6% displacement) Colgate-Stone (*Hand Surg,* 2011)<br>(n = 50, 36 mo follow-up, 14% subluxation, 6% revision, 2% heterotopic ossification, and 4% pain) Adams et al (*J Hand Surg,* 2009) |
| Regjoint (h) | (n = 23, 12 mo follow-up, 30% foreign body reaction, 8% pain, and osteolysis) Mattila et al (*J Hand Surg Br,* 2016) |
| Pyrodisk (i) | (n = 19; 70 mo follow-up, 90% survivorship, 10% instability, and 10% pain) Barrera-Ochoa et al (*J Hand Surg,* 2014) |
| Articulinx (j) | (n = 8; 24 mo follow-up, 75% survivorship, and 25% instability) Fiente et al (J Wrist Surg, 2013) |
| Pyrocardan (k) | (n = 27; 24 mo follow-up, 14% persistent pain, 4% grinding, and 11% dislocations) Lauwers et al (*Hand Surg Rehabil,* 2016)<br>(n = 27; 16,6 mo follow-up and 100% survivorship) Bellemère et al (*Chir Main,* 2011) |
| Marsilen (c) | (n = 38; 60 mo follow-up and 100% survivorship) Wehbé et al (*Hand Clin,* 2013) |
| Pi2 | (n = 42, 124.5 mo follow-up, 100% survivorship, and 4.6% dislocation) Agout et al (*Hand Surg Rehabil,* 2016) |
| Artelon (a) | (n = 32, unspecified follow-up duration, unspecified survivorship, and complication 8% to 37%) Nilsson et al (*Acta Orthop,* 2010) |

**FIGURE 15:** Interposition arthroplasty model based on a metallic spherical implant associated with a partial trapeziectomy.

modifications were needed because of a radiopaque marker complication and potential displacement of the optimal position over time[19] (Table 7 [j]).

Trends are mainly toward resorbable materials[16] and anatomical shapes. As described earlier, foreign body reaction has been a major concern, creating the need for a highly biocompatible device that can be inserted using a minimally invasive arthroscopic approach. Patents have been filed (SE0100127, WO2010097724, and US2011054627) for implants designed to meet these criteria. A wide range of implants seek to mimic the complexity of the concavo-convex joint. Among these, the Strickland trapezoidal implant (Wright Medical) is a metallic saddle-shaped implant anchored in the trapezium. The Pyrocardan pyrocarbon implant (EP2263614) has an unconstrained dual concave disk. Longer-term complications have been reported, including grinding and dislocation[13] of the implant (Table 7 [k]). There are patents (EP2687189 and US2013304223, Tornier) describing trapezium replacement with a biconvex pyrocarbon disk. An anatomic metal trapezium replacement (Table 3 [2.2.2.1.m]) has also been

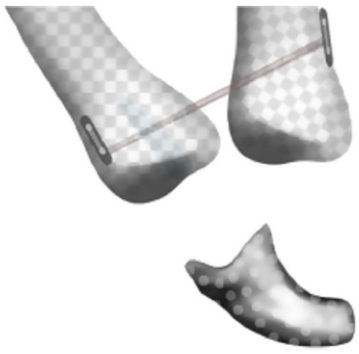

**FIGURE 16:** Miscellaneous model based on an implant featuring thread fixation between the first and second metacarpals.

developed. Stabilization is provided by a screw in the second metacarpus. There are also patents (WO2010129882 and WO2014075114) describing implants that tend to mimic the anatomic characteristics and function of the trapezium. No data are available on corresponding developments.

## MISCELLANEOUS DESIGNS: TRENDS OBSERVED

The small number of implants makes it difficult to discern trends within the category of miscellaneous designs, although different implants in this category use similar stabilization strategies. After a total trapeziectomy, the first and second metacarpals are fixed together by a thread to avoid displacement toward the vacant location. Threads[4] (Fig. 16) are made of FiberWire suture between 2 stainless-steel washers (Table 4 [a]); others are made of polymer (Table 4 [b]).

## RELEVANCE OF THE CLASSIFICATION

In the current classification of CMC arthroplasty implants, we did not want to depart from using the already well-established distinguishing feature of design: total joint replacement, HA, and interposition arthroplasty. However, to date, this is the first classification to incorporate new characteristic trends and innovations through a systematic survey of FDA-cleared implants, CE-marked implants, patents, the scientific literature, and information from companies in the orthopedic sector. This has yielded a standardized classification system including all arthroplasty implants for treating OA. We aimed to provide insights into how the different types of design are evolving and what sort of innovations are desirable.

## SUMMARY

Several factors need to be considered in choosing an implant, including kinematics, loads, and wear conditions, all of which affect the choice of biomaterial. The anatomical complexity of the TMC joint regarding its geometry leads to complex kinematics including pure flexion-extension and adduction-abduction movements, and composite circumduction movements. The axes of rotation of the TMC joint cannot be defined with respect to the classical reference planes, which makes movements hard to quantify. Traditional ways of manufacturing orthopedic implants (milling and turning) are more appropriate for manufacturing large series of prostheses with a specified size. New technologies such as additive manufacturing can pave the way for new kinds of TMC prostheses that are more anatomical and potentially patient-specific.[20]

## ACKNOWLEDGMENTS

The authors received funding from "Agence National de la Recherche" ANR-11-IDEX-0004-02 under Initiative D' Excellence "Sorbonne Universités" by an International Union of Immunological Societies project for the promotion of health care innovation.

## REFERENCES

1. Durand S, Marin F, Oberlin C, Ho Ba, Tho MC. Morphogenesis of the human palma arch using three-dimensional geometric modeling. *Clin Anat*. 2011;24(7):874–879.
2. Wajon A, Vinycomb T, Carr E, Edmunds I, Ada L. Surgery for thumb (trapeziometacarpal joint) osteoarthritis. *Cochrane Database Syst Rev*. 2015;2:CD004631.
3. De Smet L, Sioen W, Spaepen D, Van Ransbeeck H. Total joint arthroplasty for osteoarthritis of the thumb basal joint. *Acta Orthop Belg*. 2004;70(1):19–24.
4. Schmidt I. Surgical treatment options in thumb carpometacarpal osteoarthritis: a recent literature overview searching for practice pattern with special focus on total joint. *Curr Rheumatol Rev*. 2015;11(1):39–46.
5. Krukhaug Y, Lie SA, Havelin LI, Furnes O, Hove LM, Hallan G. The results of 479 thumb carpometacarpal joint replacements reported in the Norwegian Arthroplasty Register. *J Hand Surg Eur Vol*. 2014;39(8):819–825.
6. Huang K, Hollevoet N, Giddins G. Thumb carpometacarpal joint total arthroplasty: a systematic review. *J Hand Surg Eur Vol*. 2015;40(4):338–350.
7. Sun L, Berndt CC, Gross KA, Kucuk A. Material fundamentals and clinical performance of plasma-sprayed hydroxyapatite coatings: a review. *J Biomed Mater Res*. 2001;58(5):570–592.
8. Goorens CK, Van Schaik DEC, Goubau JF. Surgical treatment after a failed trapeziectomy: a case report. *Chir Main*. 2015;34(4):205–209.
9. Spartacus V, Mayoly A, Gay A, et al. Biomechanical causes of trapeziometacarpal arthroplasty failure. *Comput Methods Biomech Biomed Engin*. 2017;20(11):1233–1235.
10. Imaeda T, An KN, Cooney WP III. Functional anatomy and biomechanics of the thumb. *Hand Clin*. 1992;8(1):9–15.

11. Vitale MA, Taylor F, Ross M, Moran SL. Trapezium prosthetic arthroplasty (silicone, Artelon, metal, and pyrocarbon). *Hand Clin*. 2013;29(1):37−55.
12. Pritchett JW, Habryl LS. A promising thumb basal joint hemi-arthroplasty for treatment of trapeziometacarpal osteoarthritis. *Clin Orthop Relat Res*. 2012;470(10):2756−2763.
13. Bellemère P. Pyrocarbon implants for the hand and wrist. *Hand Surg Rehabil*. 2018;37(3):129−154.
14. Wajon A, Ada L, Edmunds I, Carr E. Surgery for thumb (trapeziometacarpal joint) osteoarthritis. *Cochrane Database Syst Rev*. 2005;(2):CD004631.
15. Badia A, Sambandam SN. Total joint arthroplasty in the treatment of advanced stages of thumb carpometacarpal joint osteoarthritis. *J Hand Surg Am*. 2006;31(10):1605−1614.
16. Kokkalis ZT, Zanaros G, Weiser RW, Sotereanos DG. Trapezium resection with suspension and interposition arthroplasty using acellular dermal allograft for thumb carpometacarpal arthritis. *J Hand Surg Am*. 2009;34(6):1029−1036.
17. Cobb TK, Walden AL, Cao Y. Long-term outcome of arthroscopic resection arthroplasty with or without interposition for thumb basal joint arthritis. *J Hand Surg Am*. 2015;40(9):1844−1851.
18. Mattila S, Waris E. Unfavourable short-term outcomes of a poly-L/D-lactide scaffold for thumb trapeziometacarpal arthroplasty. *J Hand Surg Eur Vol*. 2016;41(3):328−334.
19. van der Veen FJC, White DN, Dapper M, Griot J, Ritt M. Clinical evaluation of the Articulinx Intercarpometacarpal Cushion for the first CMC joint: a feasibility study. *J Wrist Surg*. 2013;2(3):276−281.
20. Trevisan F, Calignano F, Aversa A, et al. Additive manufacturing of titanium alloys in the biomedical field: processes, properties and applications. *J Appl Biomater Funct Mater*. 2018;16(2):57−67.

Unfortunately, no evidence has proven that one surgical treatment is better than another.

# 3. Metal additive manufacturing

Additive manufacturing (AM), also known as 3D printing, is a group of processes that produce component from three-dimensional (3D) model data, layer-by-layer. This process is opposed to conventional manufacturing processes such as milling, turning, forging and casting of bulk feedstock materials which results inevitably in large material waste. The most significant advantage is its freeform fabrication capability of complex parts. Furthermore, AM has a flexibility on feedstock material because unconsumed powders can be reused, making the manufacturing more cost-efficient.

According to ASTM F2792-12a, both selective laser melting (SLM) and electron beam melting (EBM) are classified as powder bed fusion technologies where thermal energy selectively fuse regions of a powder bed. Other standards exist and are related to individual processes, chains of processes (hardware and software), test procedures, quality parameters, customer-supplier agreements, and fundamental elements.

The AM technology used in this work is selective laser melting.

## 3.1. Technology of selective laser melting (SLM)

Selective laser melting (SLM) uses a fibre laser source (Nd:YAG laser (wavelength : 1064nm)) as the energy source. The whole process is carried out in an inert gas filled chamber such as such as $N_2$, Ar, $H_2$ which ensures higher purity by minimizing the oxygen in the environment and reduces the risk of hydrogen pick up.

Depending on the material, different process parameters [35] can be adjusted.

- **Laser parameters**. It includes power, scanning speed, beam diameter, etc., determine the width of the scanning beam. The manufacturing speed is related to the scanning speed.
- **System parameters**. It concerns the thickness of the powder layer, the treated powder surface, the distance between two adjacent strands; these parameters influence the quality of the part. Different scanning modes exist such as the commonly used 90° crossover strategy and the checkerboard strategy
- **Environmental parameters.** It includes the preheating temperature, the atmosphere and gas pressure

SLM technology also offers the advantage of a wide variety of raw materials such as stainless steel [36], Titanium and its alloy [37], cobalt-based alloy [38]. And it has virtually no geometric limits for the part model. In surgical prosthesis applications, SLM technology allows the customization and manufacturing of bone substitutes directly from tomography data.

## 3.2. Specimen manufacturing

The production of specimens by SLM necessitates three steps: (i) pre-treatment, (ii) powder melting and (iii) post-treatment.

### 3.2.1. Pre-treatment

Pre-processing includes converting CAD model data; (i) the orientation of the specimen in the manufacturing chamber; (ii) the addition of supports and (iii) the slicing. The 3D model of the part is generated by Computer-assisted-design (CAD) software including Catia, Pro-E, etc. In order for the SLM system to decode the digital file, the file must be converted to STL (for **ST**ereo-**L**ithography) format. The design of a numerical model adapted for additive manufacturing is discussed in the Chapter 3 of this manuscript. The STL file approches an object by its external surface. This surface is necessarily closed and is defined by a series of triangles (or facets). The design of parts for additive manufacturing is further described in the paragraph §3.3.

### 3.2.2. Powder melting

First, the powder is preheated to limit deformations. Then the laser melts the powder layer according to the trajectories established from the numerical model and the process parameters. The particles melted under the laser beam form a solid structure. The process stops when the last layer is finished.

### 3.2.3. Post-treatment

After the manufacturing process, it is necessary remove the supports and clean the parts from unmelted particles. Parts manufactured by SLM can also be heat treated to eliminate internal stresses and to reduce porosity.

## 3.3. Design for additive manufacturing (DfAM)

DfAM is the practice of designing and optimizing a product for the process chain of additive manufacturing. It aims at reducing development time and cost, and increase the

quality, and profitability of the products manufactured. AM technologies have allowed the creation of unique freeform design with different features and constraints than other manufacturing processes [39]. Therefore, process-specific numerical design methods and tools are necessary. Typical DfAM methods include:

- topology optimization,
- design for multiscale structures (lattice or cellular structures),
- Custom surfaces, textures, and porosity for improved
- Functionality multi-material design,
- Cost effective production of custom-fit and mass customized
- products part consolidation

Theses DfAM methods relies on CAD systems which are mostly based on two kinds of modeling [40]:

- **Constructive Solid Geometry (CSG)**. It consists in the combination of simple volumetric geometry such as sphere and cuboids, using Boolean operators to create more complex objects. It ensures that objects are "solid", or watertight. The creation of geometries are quick, but may be inappropriate for the representation of complex 3D shapes such as anatomical structures[40] which cannot be divided easily into simpler volumetric geometries.
- **Boundary representation (B-rep):** It consists in the local representation of faces, edges and vertices through the simplest geometric items. It includes points, curves and surfaces. It is therefore more flexible and often yields an accurate 3D representation but requires more sophisticated CAD skills. It is particularly the case for making the model watertight as required by AM system. Additionally, all the modeling is realized manually which is time-consuming.

The chapter 3 of this manuscript focuses of the design of a patient-specific numerical model for additive manufacturing based on a functional approach. AM processes allow the customization of surfaces, texture and porosities. The most popular application in the biomedical industries is the design of porous metals for bone scaffolds for orthopaedic implants [41,42]. It aims to imitate the bones' architecture to guide the proliferation and growth of cells.

In the chapter 5 of this manuscript, a section focuses on the local surface roughness variation induce by the SLM process and its impact on cell adhesion.

## 3.4. Articular implant's material compatible with SLM

Metals studied in this work are Ti6Al4V and CoCr alloy. They are common metals used in orthopaedic applications.

### 3.4.1. Titanium-6Aluminium-4Vanadium (Ti6Al4V)

Ti6Al4V alloy also known as Ti64, may be processed via SLM technology. It is an α+β titanium alloy with high strength, low density, high fracture toughness, excellent corrosion resistance and good biocompatibility. These properties are particularly attractive for implants. The chemical composition is described in the table below.

**Table 6**: Chemical composition of TiAl6V4 according to ASTM F136

| Al | C | Fe | H | N | O | Ti | V |
|---|---|---|---|---|---|---|---|
| 5.5-6.5% | <0.08% | <0.25% | <0.01% | <0.05% | <0.13% | Bal | 3.5-4.5% |

#### 3.4.1.1. Microstructure

The titanium element of the TiAl6V4 arranged in two different crystal structures: hexagonal closed packed (HCP) known as α-Ti which forms below the β-transus (980°C) temperature and body centred cubic (bcc) known as β-Ti above the β-transus temperature. Al stabilizes α while V stabilizes β. Therefore, at room temperature, the alloy has a dual phase α+ β. However, the phase modifies with the temperature history and cooling rate. Upon rapid cooling above the β-transus, there will be the formation of α ' martensitic microstructure from β grains. Therefore in the SLM process, α' microstructure is formed from columnar β grain (the size varies from 1 to 20mm in length and 0.2 to 4mm in width)[43].

#### 3.4.1.2. Properties

SLM produces in theory fully-dense parts, but even with optimized parameters, porosity remains which can deteriorate the mechanical properties. Two types of pores prevail: gas pores and lack of fusion pores. These pores are likely to become nucleation site for microcracks, particularly lack of fusion pores which are likely to be at boundary zone between two layers [43]. Ti6Al4V presents significant anisotropy in tensile properties regarding the different orientation due to the columnar β grains and grain boundary α. Longitudinal samples have lower tensile strength and yield strength and greater elongation (2%) than horizontal samples [43]. Parts produce by AM processes have also a high surface roughness. The surface texture is due to (i) the adhesion of partially melted particles, (ii) the staircase effect related to the layer width and (iii) the existence of open

pores [43]. Ra values are around 10–15µm. Several studies have demonstrated a sufficient biocompatibility of as-SLM Ti6Al4V parts and confirmed its adoption for the fabrication of custom orthopaedic implants. Additionally, it was found that the topography of SLM parts was associated with good bone regeneration in-vivo. The authors concluded that the topography made by SLM is a promising alternative to conventional implant surface topographies such as sandblasting [44].

### 3.4.2. Cobalt-Chromium (CoCr)

The cobalt chromium alloy can be shaped by SLM. It has been defined as effective metallic biomaterials in the ASTM Standards [45] because of its good mechanical properties, high corrosion resistance, and high wear resistance. It is particularly its excellent wear resistance properties compared to the other metallic biomaterials such as titanium (Ti6Al4V) alloys and stainless steels (316L). It therefore makes a good choice for sliding parts in artificial joints [46]. The chemical composition of CoCrMo alloy is described in the table below.

**Table 7**: Chemical composition of CoCrMo according to ASTM F75

| **Co** | **Cr** | **Mo** | **F** | **Al** | **Si** | **Mg** | **W** | **P** | **S** | **Ni** | **Ti** | **N** |
|---|---|---|---|---|---|---|---|---|---|---|---|---|
| Bal | 27-30% | 5-7% | <0.75 | <0.1 | <1 | <1 | <0.2 | <0.02 | <0.01 | <0.5 | <0.1 | <0.25 |

#### 3.4.2.1. Microstructure

CoCrMo parts are also characterized by a melt pool microstructure. It is composed of long columnar grains along the building direction. The material is composed of both face-centered-cubic Co-base phase and a carbide-dispersed Co-base phase which are regularly distributed. The resulted microstructure is a fine and homogeneous structure due to the rapid melting and solidification processes.

#### 3.4.2.2. Properties

Dense parts up to 0.9% have been manufactured. The porosity was mainly gas pores.
The tensile strength and yield strength of the as-SL parts have been found to be greater than the ASTM F75 standard alloy (casting), but a lower elongation [47]. The distinctive features at 45° compared to 90° are similar to 316L alloy and Ti6Al4V results. CoCrMo alloy processed by SLM featured a reduction of metal release compared to traditional manufacturing, suggesting a better biocompatibility [38].

# 4. Articular implant specification

## 4.1. Biocompatibility: the biological effects of implant

Biocompatibility is the ability of a material to exist in an *in vivo* environment for an acceptable period of time with no detrimental effect on the host. All materials used in medical devices have to be biocompatible. The degree of biocompatibility depends on the application. Therefore, biocompatibility doesn't only refer if there are any adverse biological reactions to a material, but if the material performs satisfactorily in the application.

There are many guidelines and regulations regarding the biocompatibility requirements, tests and minimum standards which include the series of standards ISO 10993-1 to 10.

The term biocompatibility covers a large set of properties including adhesion to tissues (e.g. muscles and ligaments, bone, etc), chemical and mechanical stresses, cell growth and differentiation.

### 4.1.1. Effect of implant degradation in the inflammatory process

Inflammation is a non-specific physiological response due different factors such as trauma, infection, intrusion of foreign materials. The signs of inflammation are redness, swelling, pain and heat.

Neutrophils and eosinophils are the first active line of defense against foreign material. Among the freely circulating leukocytes, mocnocytes are the largest. Some monocytes can differenciate rapidly into macrophage and go to the infected site after the neutrophils. They phagocytise and digest the material, which activate some metabolic pathways such as the synthesizing and the releasing of cytokines. Cytokines are molecules that cell use to communicate with each other, particularly to regulate processes where different type of cells are involved. Cytokines that are implicated in the implant degradation process are some interleukins (IL-1, IL-6), tumor necrosis factor (TNF-α) and prostaglandin $E_2$. In the presence of small particles, cytokins stimulate large phagocyte cells called osteoclast to resorb bone. Osteoclasts are naturally present on bone surface along with osteoblasts cells which form bones; a balance between bone resorption and formation led principally by osteocytes. Mechanoreceptors allow it to measure bone pressure, and thus manage this balance, making bone a material that adapts to its environment. However an increased osteoclasts activity by cytokins results in bone loss. The results directly affect the integrity at the bone-implant interface, that could lead to pain, loosening and surgical revision a seen in paragraph §2.3.

Macrophage may multiply and fuse to form a foreign body giant cell that is more active and phagocytise larger size particles. The phagocytic activity is related to the size of the particle, with a maximum stimulus between 0.1-1.0 µm. If the particle is toxic, it induces accumulation of dead neutrophils and macrophages, accompanied with bacterial infection.

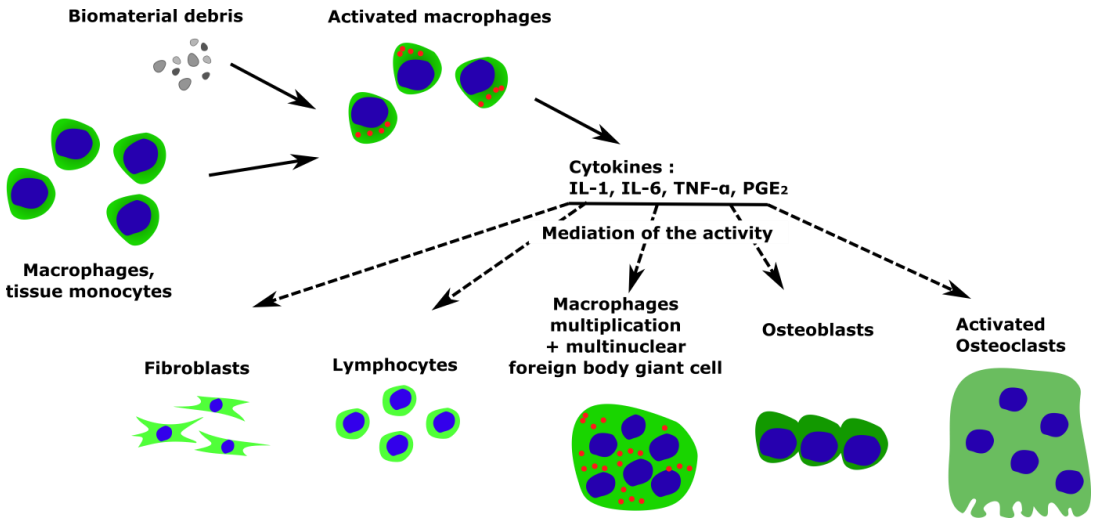


**Figure 5**: Inflammation response to biomaterial debris

The Annex 6 of this manuscript covers the effect of the as-SLM materials degradation in the inflammatory process through cytokins measures.
Observations of lymphocytes suggest a specific immune response. The effect of the as-SLM materials on the specific immune system has not been studied in this work.

There are different final states where no progressive biological changes occur:

- **Extrusion**: The implant is near an epithelial tissue. The local host response results in the formation of a pocket at the interface.
- **Resorption**: The implant is resorbable. The implant sites disappear or resolves with a scar.
- **Integration:** The implant is integrated. There is no capsule, although some inflammatory cells persist. It is the case of implant made of titanium and its alloy implant with cell-adhesive surface.
- **Incapsulization**: a capsule is created around the implant and mineralizes. It is an unusual response.

### 4.1.2. Bone remodelling near implants

The success of orthopaedic implants aimed to be anchored to bone material is linked to the bone remodelling process at the interface known as osseointegration. This involves complex biological processes which are influenced by surface properties such as topography, chemistry or surface energy properties of the implant [48]. Among the material available, titanium alloys such as Ti6Al4V-ELI has been found to chemically adhere with bone due to the $TiO_2$ oxide film. Different modifications of these surfaces were proposed for enhancing osseous integration such as hydroxyapatite coating [49,50] and Calcium Phosphate (CaP)coating [51].

The chapter 5 of this manuscript will discuss on the challenging question: how to take advantage of the additive manufacturing characteristics and the biological principle of osseointegration to design orthopaedic implants with clear clinical benefit.

## 4.2. Biotribology

Tribology is the science of interacting surfaces; when these surfaces are in a biological system, it is called as biotribology. Basic tribological concepts are discussed in terms of friction, wear and lubrication.

- **Friction**: general resistance to motion of one material over another
- **Wear**: modification of the interface by different processes known as *wear*.
- **Lubrication**: introduction to a material at the interface to make the relative motion easier.

Different pairs of material are used in artificial joint replacement such as metal-metal, ceramic-ceramic, ceramic-polymer, and metal-polymer as seen in the previous paragraph. The life expectancy of these implants is limited by the tribological deficiency of the friction materials. Lubrication regimes, wear debris, friction coefficient are factors that affect their durability. Wear debris leads to adverse tissue reactions that cause aseptic loosening of the components and finally lead to implant failure. Friction may also change in the surface of the bearing materials and in the lubricant properties.

A section of the chapter 5 of this manuscript focuses on the biotribological behaviour of the SLM parts against polyethylene high density (HMWPE) in terms of friction, lubrication, wear, frictional heating, and wear evaluation referring the basic biotribological rules.

### 4.2.1. Friction, lubrication and wear

In contact with UHMWPE, three wear mechanisms have been identified: (i) fatigue wear and (ii) adhesion wear and (iii) abrasion wear.

- **Fatigue wear**. It occurs because of a cyclic loading that destroys the surface of the material.
- **Adhesion wear**. It is generated by the transfer of material from one surface to another under load.
- **Abrasion wear**. It is set up when there is asperities on the surface or a third body particles are trapped between the surfaces.

#### 4.2.1.1. Friction

During the motion of a body over the surface of another one, there is a force that resists the motion, known as frictional force. It is given by:

$$F_f = \mu F_\perp \qquad \textit{Équation 1}$$

$F_\perp$: Force perpendicular to the interface (compressive force, gravity, etc)

$\mu$: Coefficient of friction

The coefficient of friction (COF) is the ratio which varies usually between 0 and 1. It gives the relationship between the frictional force and the perpendicular force. It is a characteristic of the interface which depends upon (i) the material pair, (ii) the surface texture (roughness parameters) and (iii) the lubricant involved.

COF usually has greater values just before the initiation of the movement ($\mu_i$) than when the surfaces are in steady motion ($\mu_s$). Both $\mu_i$ and $\mu_s$ are independent of $F_\perp$ and also stress which is therefore related to the geometric interfacial surface area.

#### 4.2.1.2. Lubrication

The principle of lubrication is to provide a layer that separates the two surfaces during relative motion reducing both frictional forces and wear. Lubrications modes are classified by the nature and the magnitude of the surface separation.

- **Fluid-film lubrication:** The sliding surfaces are separated by a continuous fluid-film. It can be described in two subcategories:
    - **Hydrodynamic**. The fluid-film formation depends on the shape of the bearing surfaces, the relative motion and the viscous pressure. All the work of friction is dissipated by viscous shear of the lubricant. (surface separation: $10^{-3}$, $10^{-4}$ cm)

- **Elastohydrodynamic.** The fluid-film properties are defined by the elastic properties of the contacting bodies. Forces of one body are transmitted in the lubricant generated enough stress to deform elastically the other body. It may lead to localized fatigue failure and an increased wear rate. The surface separation is smaller ($10^{-4}$, $10^{-5}$ cm).

- **Boundary**: The lubricant interacts chemically with both surfaces. I resulting in a thin coating both bearing surfaces rather than acting as a low-shear interface. These surfaces are therefore coated with chemical-bonded components that act as a protection layer. Surface separation is often less than $10^{-5}$ cm. The chemical and physical natures of the surfaces and the lubricant are of major importance in the frictional behaviour.
- **Mixed**: Both fluid-film and boundary lubrication regimes act simultaneously.

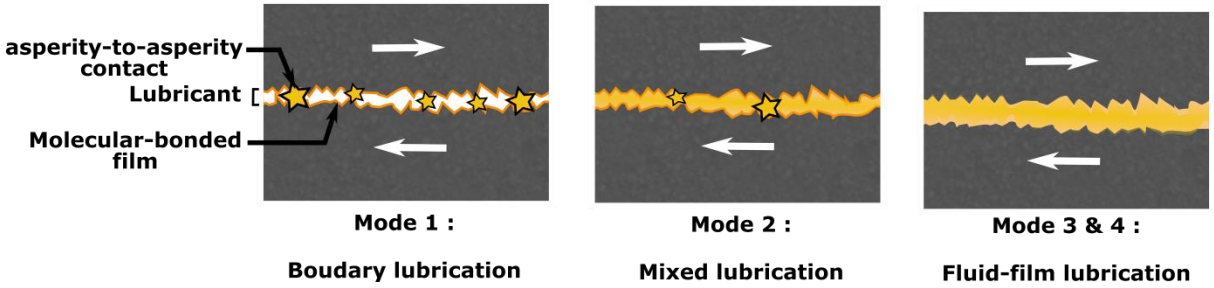


**Figure 6**: Schematic drawing of the lubrication mode

Synovial fluid is the natural lubricant of joints. It is an ultrafiltrate of serum. Therefore, foetal bovine serum (FBS) has often been employed as a model of synovial fluid.

#### 4.2.1.3. Wear

Wear is the main pronounced problem of joint replacement implants because it (i) produces biologically "active" particles that activate the inflammatory response and modifies the shape that affect the function. Different types of wear have already been defined:

- **Abrasive wear**. Wear is caused by a harder body that abrade softer one(s). Two categories can be distinguished.
  - two-body abrasion: The asperities of the harder surface abrade the softer one
  - Three-body abrasion: Hard particles are trapped between surfaces and abrade one or both of the surfaces. Literature studying retrieved articular implants showed that third-body abrasive wear is affecting significantly their service life.

- **Adhesive wear:** It is due to high local friction. This type of wear is generally defined as transfer film of material from one surface to another during relative motion. It leads to tearing and fracture. It is produced when softer material such as UHMWPE moves on hard material such as metal. It creates a film across the asperities, increasing the contact area and therefore reducing the local stresses. The film is either stable (wear rate reduced after the film formation), or unstable (increased wear by abrasive wear)
- **Corrosive wear**: wear is governed by both mechanical wear and chemical reaction because of metal ions releasing.
- **Fatigue wear**: It is caused by the displacement of the particles. It may lead to the generation of debris from the surfaces or/and propagation of cracks.
- **Erosive wear**: hard particles attack the surface layer. It may lead to plastic deformation and brittle fracture. This type of wear is no common in total joint replacement.

### 4.2.2. Measurement of wear in artificial joints and factors

Systems have been designed to evaluate the tribological behaviour of materials. These systems include ball-on-disc, pin-on-disc, and pin-on-plate.

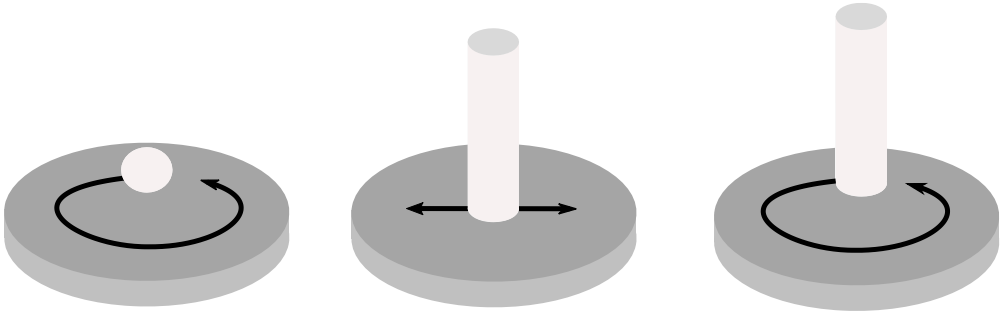

**Figure 7**: System to evaluate the tribological behaviour of materials: ball-on-disc, pin-on-disc, and pin-on-plate.

The most commonly used techniques to assess wear and tear are:

- the gravimetric method: measurement of weight change and
- the volumetric method: measurement of dimensional changes

ASTM standards F2025-06, F171414-96 and ISO 14242-2 are based on the gravimetric method for measuring wear of total joint prostheses. This method consists of measuring the initial weight difference and the weight after the wear test. The ISO 14242-2:2000 standard specifies that a balance with an accuracy of 0.1 mg must be used. Due to the fluid absorption properties of the polymers, weight measurements are affected. In order to

reduce the error due to fluid absorption, standards recommend pre-soaking the polyethylene samples in the lubricant until saturation. This process can take days or even weeks.

Gravimetric is calculated:

$$W_n = W_{an} + S_n \quad \text{Equation 1}$$

$W_n$ : net mass loss after n loading cycles,

$W_{an}$: average uncorrected loss of mass

$S_n$ : average increase in the mass of the control sample over the same period

The average wear rate $a_G$ can be calculated using a linear adjustment relationship between $W_n$ and the number of load cycles n:

$$W_n = a_G.n + b_n \quad \text{Equation 2}$$

$W_n$ : net mass loss after n loading cycles,

$b$: constant

This method is effective in determining the amount of experimental wear in vitro.

It is important to couple this method with SEM and optical profilometer analyses on both contact surfaces at different time intervals to establish wear mechanisms by analyzing changes in surface properties and plastic deformation of the specimens. These analyses will also help determining an eventual transfer of material that could cause a significant error in the determination of weight loss.

Surface laser profilometry is a popular method that allows to determine easily wear in primitive tests such as pin-on-disc, ball-on-disc. The wear volume can be calculated using the cross-section, wear track and length. Thus, the wear factor (k) of the sample can be determined as follows:

$$k = {}^{V}/_{NS} \quad \text{Equation 3}$$

k : wear factor ($mm^3/(N\ m)$),

V : wear volume ($mm^3$),

N: applied load (N),

S : friction distance (m)

### 4.2.3. Factors influencing wear in artificial joints

Different factors influence the wear behaviour and are discussed in the following paragraphs.

#### 4.2.3.1. Lubrication

Lubrication is one of the most important and complex factors that affect the implant friction and wear. The ideal lubrication regime is fluid-film and besides the lubricant, the key parameters that influence its formation is the surface quality and surface texturing.

The average surface roughness Ra of the surfaces is relevant for the determination of the lubrication regime.

$$\lambda = \frac{h_{min}}{Ra} = \frac{h_{min}}{(Ra_{(surface\,1)})^2 + (Ra_{(surface\,2)})^2} \qquad \text{Équation 2}$$

With
$0.1 < \lambda < 1$: boundary lubrication,
$1 \leq \lambda \leq 3$: mixed lubrication,
$\lambda > 3$: fluid-film lubrication.

#### 4.2.3.2. Surface quality and surface texturing

The surface profile, texture and topography are playing a role in the wear behaviour.
ISO standard 4287: 2000 defines the surface texture specification. The standard distinguishes the following surface profiles; the basic surface profile P, the surface waviness profile W and the surface roughness profile R.

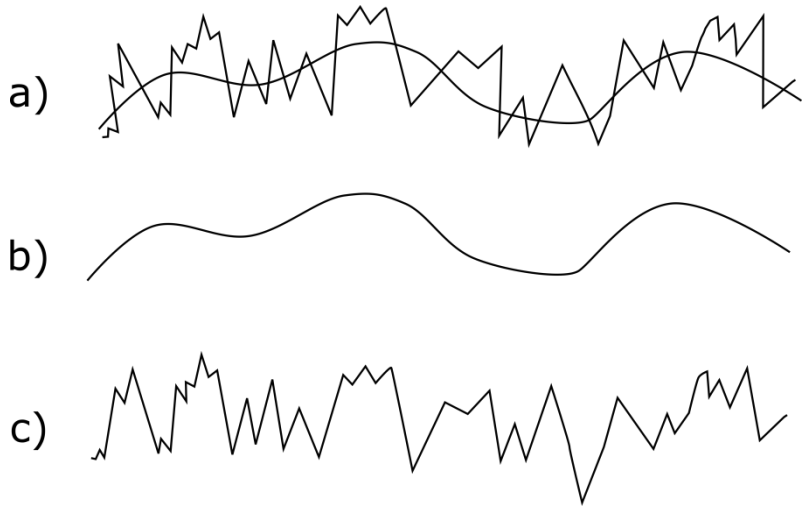


**Figure 8** : profiles according to EN ISO 4287 (1999) (a) basic surface profile P (b) surface waviness profile W (c) surface roughness R.

The waviness profile is the low frequencies and high amplitudes of the surface peaks and valleys while the roughness profile is the high frequencies and low amplitudes of the surface peaks and valleys.
Surface roughness can be quantified using a profile method through either a contacting stylus or a non-contacting technique using a laser source. Although the arithmetical mean

deviation (Ra (2 dimensions); Sa (3 dimensions)) is the most commonly used parameters for wear studies particularly to measure the type of lubrication, it only refers to roughness height and does not provide spacing information. Other surface texture parameters exist as described in ISO 25178. It includes spacial, functional and, hybrid parameters which can be used to characterize more complexes surface texturing aimed to reduce wear in artificial implants. For instance, studies found reduction of wear between CoCr against UHMWPE by texturing the cobalt-based part. The surface texturing consisted in introducing dimples of different size [52,53]. The authors concluded that it was an effective way to control the lubricant volume in boundary lubrication type.

Additive manufacturing parts possess porosity on its surface; the effect on the wear behaviour will be discussed in the chapter 5 of this manuscript.

#### 4.2.3.3. Hardness

Hardness of metals and alloys is a mechanical property that has been demonstrated to influence wear. It is therefore an indicator to determine the wear resistance in the literature [54]. It has been admitted in the literature that if the hardness of the softer bearing part increases, then the wear decrease [55].

#### 4.2.3.4. Geometry

The geometry tolerance of the bearing parts such as the size and the curvature also influence the life-span of the implants. An inadequacy of the bearing part will induce abnormal wear. The origin may be an inappropriate positioning of the implant or the tolerance of the manufacturing process. This problem has been reported mainly for ball-in-socket configurations. Furthermore, it has been found that polyethylene compensate this problem with creep [56] against the metal contrarily to metal-on-metal bearing parts.

#### 4.2.3.5. Patient related factors

However, the factors that influence the tribological behaviour of joint implants are not only related to the choice of materials and implant design, but also to patient-specific parameters. These parameters include the lifestyle of the patient, the body weight, the age, the sex and synovial fluid. Additionally, few studies has measured precisely the contact patterns and the pressure distribution between the contact areas of joints particularly the trapeziometacarpal joint [57]. Therefore, the incorporation of these parameters cannot be adequately simulated by in vitro tests.

## 5. Refences list


[1] A.I.Kapandji, Anatomie Fonctionnelle I Membre supérieur, 6th editio, 2011.

[2] K. Kuczynski, Carpometacarpal joint of the human thumb., J. Anat. 118 (1974) 119–126.

[3] K. Kuczynski, The Thumb and The Saddle, Hand. (1975) 120–122.

[4] T. Imaeda, K.. An, W.P. Cooney, R. Linscheid, Anatomy of trapeziometacarpal ligaments, J. Hand Surg. Am. 18 (1993) 226–231.

[5] P. Bettinger, R. Linscheid, R. Berger, I.W. Cooney, K. An, An anatomic study of the stabilizing ligaments of the trapezium and trapeziometacarpal joint, J. Hand Surgery. 24 (1999) 786–98.

[6] P.C. Bettinger, R.L. Linscheid, R.A. Berger, W.P. Cooney, K.N. An, An anatomic study of the stabilizing ligaments of the trapezium and trapeziometacarpal joint, J. Hand Surg. Am. 24 (1999) 786–798.

[7] V. Pellegrini, Osteoarthritis of the trapeziometacarpal joint: the pathophysiology of articular cartilage degeneration. I. Anatomy and pathology of the aging joint, J. Hand Surg. Am. 26 (1991) 967–74.

[8] E. Halilaj, D.C. Moore, D.H. Laidlaw, C.J. Got, A.P.C. Weiss, A.L. Ladd, J.J. Crisco, The morphology of the thumb carpometacarpal joint does not differ between men and women, but changes with aging and early osteoarthritis, J. Biomech. 47 (2014) 2709–2714.

[9] A. Damen, B. Van Der Lei, P.H. Robinson, Bilateral Osteoarthritis of the Trapeziometacarpal Joint Treated by Bilateral Tendon Interposition Arthroplasty, J. Hand Surg. Am. 22 (1997) 96–99.

[10] T.D. Hart, D. J., & Spector, Definition and epidemiology of osteoarthritis of the hand: a review, Osteoarthr. Cartil. 8 (2000) S2–S7.

[11] B.Y.S.D. Young, E.A. Mikola, A RTHROSIS, 4 (2004).

[12] L. Xu, R.I. Strauch, G.A. Ateshian, R.J. Pawluk, V.C. Mow, M.P. Rosenwasser, Topography of the Osteoarthritic Thumb Carpometacarpal Joint and Its Variations With Regard to Gender , Age , Site , and Osteoarthritic Stage, (1998) 454–464.

[13] R.O.Y.M. Acheson, Y. Chan, A.R. Clemett, New Haven Survey of Joint Diseases XII : Distribution and symptoms of osteoarthrosis in the hands with reference to handedness, (1970) 275–286.

[14] L. Xu, R. Strauch, G. Ateshian, R. Pawluk, V. Mow, M. Rosenwasser, Topography of the osteoarthritic thumb carpometacarpal joint and its variations with regard to

gender, age, site, and osteoarthritic stage, J. Hand Surg. Am. 23 (1998) 454–64.

[15] J. Busby, J. Tobin, W. Ettinger, K. Roadarmel, C.C. Plato, A longitudinal study of osteoarthritis of the hand: the effect of age, Ann. Hum. Biol. 18 (1991) 417–424.

[16] H.A.P. Dahaghin, S., Bierma-Zeinstra, S. M. A., Koes, B. W., Hazes, J. M. W., & Pols, Do metabolic factors add to the effect of overweight on hand osteoarthritis? The Rotterdam Study, Ann. Rheum. Dis. 66 (2007) 916–920.

[17] A. Haara, M. M., Heliövaara, M., Kröger, H., Arokoski, J. P., Manninen, P., Kärkkäinen, A., ... & Aromaa, Osteoarthritis in the carpometacarpal joint of the thumb: prevalence and associations with disability and mortality, JBJS. 86 (2004) 1452–1457.

[18] G. Martou, K. Veltri, A. Thoma, Surgical treatment of osteoarthritis of the carpometacarpal joint of the thumb: a systematic review, Plast. Reconstr. Surg. 114 (2004) 421–432.

[19] D.J. Hunter, Y. Zhang, M.C. Nevitt, L. Xu, J. Niu, L.-Y. Lui, W. Yu, P. Aliabadi, D.T. Felson, Chopstick arthropathy: The Beijing Osteoarthritis Study, Arthritis Rheum. 50 (2004) 1495–1500.

[20] E.E. İNal, K. Demİrcİ, A. Çetİntürk, M. Akgönül, S. Savaş, Effects of smartphone overuse on hand function, pinch strength, and the median nerve, Muscle Nerve. 52 (2015) 183–188.

[21] A. Goto, S. Leng, K. Sugamoto, W.P. Cooney, S. Kakar, K. Zhao, In Vivo Pilot Study Evaluating the Thumb Carpometacarpal Joint During Circumduction, Clin. Orthop. Relat. Res. 472 (2014) 1106–1113.

[22] F. Canillas, A. Colino, P. Menéndez, Cellular phone overuse as a cause for trapeziometacarpal osteoarthritis: a two case report, J. Orthop. Case Reports. 4 (2014) 6.

[23] P.C. Dell, T.M. Brushart, R.J. Smith, Treatment of trapeziometacarpal arthritis : Results of resection arthroplasty, J. Hand Surg. Am. 3 (1978) 243–249.

[24] R. Eaton, S. Glickel, Trapeziometacarpal osteoarthritis. Staging as a rationale for treatment., Hand Clin. 3 (1987) 455–71.

[25] S. Young, E. Mikola, Thumb carpometacarpal arthrosis, J. Am. Soc. Surg. Hand. 4 (2004) 73–93.

[26] L. Cheze, R. Dumas, J. Comtet, C. Rumelhart, M. Fayet, Determination of the number of degrees of freedom of the trapeziometacarpal joint–an in vitro study, IRBM. 33 (2012) 272–277.

[27] G.M. Spaans, A. J., Van Minnen, L. P., Kon, M., Schuurman, A. H., Schreuders, A. T., & Vermeulen, Conservative treatment of thumb base osteoarthritis: a systematic review, J. Hand Surg. Am. 40 (2015) 16–21.

[28] J.H. Villafañe, J.A. Cleland, C. Fernández-de-las-Peñas, The Effectiveness of a Manual Therapy and Exercise Protocol in Patients With Thumb Carpometacarpal Osteoarthritis: A Randomized Controlled Trial, J. Orthop. Sport. Phys. Ther. 43 (2013) 204–213.

[29] C. Swigart, R. Eaton, S. Glickel, C. Johnson, Splinting in the treatment of arthritis of the first carpometacarpal joint, J. Hand Surgery,. 24 (1999) 86–91.

[30] R.G. Eaton, S.Z. Glickel, J.W. Littler, U. 1985, Tendon interposition arthroplasty for degenerative arthritis of the trapeziometacarpal joint of the thumb, J. Hand Surg. Am. 10 (1985) 645–654.

[31] S.Z. Freedman, D. M., Eaton, R. G., & Glickel, Long-term results of volar ligament reconstruction for symptomatic basal joint laxity, J. Hand Surg. Am. 25 (2000) 297–304.

[32] J.L. Hobby, H.A. Lyall, B.F. Meggitt, First metacarpal osteotomy for trapeziometacarpal osteoarthritis, J. Bone Joint Surg. Br. 80-B (1998) 508–512.

[33] F. Chamay, A., & Piaget-Morerod, Arthrodesis of the Trapeziometacarpal Joint, J. Hand Surg. Am. 19 (1994) 489–497. doi:10.1016/0266-7681(94)90215-1.

[34] W. Gervis, Osteo-arthritis of the trapezio-metacarpal joint treated by excision of the trapezium, (1947).

[35] B. Vandenbroucke, J.P. Kruth, Selective laser melting of biocompatible metals for rapid manufacturing of medical parts, Rapid Prototyp. J. 13 (2007) 196–203. doi:10.1108/13552540710776142.

[36] Y. Sun, A. Moroz, K. Alrbaey, Sliding Wear Characteristics and Corrosion Behaviour of Selective Laser Melted 316L Stainless Steel, J. Mater. Eng. Perform. 23 (2014) 518–526. doi:10.1007/s11665-013-0784-8.

[37] F. Trevisan, F. Calignano, A. Aversa, G. Marchese, M. Lombardi, S. Biamino, D. Ugues, D. Manfredi, Additive manufacturing of titanium alloys in the biomedical field: Processes, properties and applications., J. Appl. Biomater. Funct. Mater. 16 (2018) 57–67.

[38] Y. Hedberg, I. Odnevall Wallinder, Metal release and speciation of released chromium from a biomedical CoCrMo alloy into simulated physiologically relevant solutions, J. Biomed. Mater. Res. - Part B Appl. Biomater. 102 (2014) 693–699.

[39] M. Thompson, G. Moroni, T. Vaneker, G. Fadel, R.I. Campbell, ... & Gibson, I., F. Martina, Design for Additive Manufacturing: Trends, opportunities, considerations, and constraints, CIRP Ann. 65 (2016) 737–760.

[40] Martti Mäntylä, An introduction to solid modeling, Computer S, New York, NY, 1987.

[41] S. Arabnejad, R. Johnston, J. Pura, B. Singh, M. Tanzer, D. Pasini, undefined 2016, High-strength porous biomaterials for bone replacement: A strategy to assess the interplay between cell morphology, mechanical properties, bone ingrowth and, Acta Biomater. 30 (2016) 345–356.

[42] N. Taniguchi, S. Fujibayashi, M. Takemoto, K. Sasaki, B. Otsuki, T. Nakamura, T. Kokubod, S. Matsudaa, Effect of pore size on bone ingrowth into porous titanium implants fabricated by additive manufacturing: an in vivo experiment, Mater. Sci. Eng. C. 59 (2016) 690–701.

[43] S. Liu, Y. Shin, Additive manufacturing of Ti6Al4V alloy: A review, Mater. Des. 164 (2019).

[44] A.T. Sidambe, Biocompatibility of advanced manufactured titanium implants-A review, Materials (Basel). 7 (2014) 8168–8188.

[45] V.A. Mayer, annual book of ASTM standards, section thirteen, medical devices and services., (2008).

[46] K.S. Katti, Biomaterials in total joint replacement, Colloids Surfaces B Biointerfaces. 39 (2004) 133–142. doi:10.1016/J.COLSURFB.2003.12.002.

[47] A. Takaichi, Suyalatu, T. Nakamoto, N. Joko, N. Nomura, Y. Tsutsumi, S. Migita, H. Doi, S. Kurosu, A. Chiba, N. Wakabayashi, Y. Igarashi, T. Hanawa, Microstructures and mechanical properties of Co-29Cr-6Mo alloy fabricated by selective laser melting process for dental applications, J. Mech. Behav. Biomed. Mater. 21 (2013) 67–76.

[48] K. Anselme, Osteoblast adhesion on biomaterials, Biomaterials. 21 (2000) 667-681.

[49] Stephen J. Kelly, Stephen J. Incavo, Bruce Beynnon, The use of a hydroxyapatite-coated primary stem in revision total hip arthroplasty, J. Arthroplasty. 21 (2006) 64-71.

[50] S. Saber-Samandari, S. Baradaran, B. Nasiri-Tabrizi, K. Alamara, W.J. Basirun, Microstructural evolution and micromechanical properties of thermally sprayed hydroxyapatite coating, Adv. Appl. Ceram. 117 (2018) 452–460.

[51] K. Park, S. Kim, Y. Jeong, H. Moon, H. Song, Y. Park, H. Moon, … H.S.-M.S. and, undefined 2018, Fabrication and biological properties of calcium phosphate/chitosan composite coating on titanium in modified SBF, Mater. Sci. Eng. C. 90 (2018) 113–118.

[52] H. Sawano, S. Warisawa, S. Ishihara, U. 2009, Study on long life of artificial joints by investigating optimal sliding surface geometry for improvement in wear resistance, Precis. Eng. 33 (2009) 492–498.

[53] H. Ito, K. Kaneda, T. Yuhta, I. Nishimura, K. Yasuda, T. Matsuno, Reduction of polyethylene wear by concave dimples on the frictional surface in artificial hip joints, J. Arthroplasty. 15 (2000) 332–338.

[54] A. Ruggiero, E. Gómez, M. Merola, Experimental comparison on tribological pairs UHMWPE/TIAL6V4 alloy, UHMWPE/AISI316L austenitic stainless and UHMWPE/AL2O3 ceramic, under dry and, Tribol. Int. 96 (2016) 349–360.

[55] Z. Jin, M. Stone, E. Ingham, (v) Biotribology, Biotribology. Curr. Orthop. 20 (2006) 32–40.

[56] T. Stewart, Tribology of artificial joints, Orthop. Trauma. 24 (2010) 435–440.

[57] T. Momose, Y. Nakatsuchi, S.S.-T.J. of hand Surgery, U. 1999, Contact area of the trapeziometacarpal joint, J. Hand Surg. Am. 24 (1999) 491–495.

# CHAPTER 2:

# Technical feasibility of Implantation and geometric requirements

*Ce chapitre démontre la faisabilité d'implanter une prothèse trapézo-métacarpienne basée sur la géométrie d'un trapèze sain. La technique d'implantation et les éléments prothétiques de l'implant ont été optimisés afin d'assurer une bonne stabilité de l'articulation reconstruite. La prothèse se comporte de manière anatomique avec une amplitude de mouvement satisfaisante en flexion/extension, adduction/abduction. Les résultats de l'expérience ont abouti à un brevet sur la conception de l'implant et un savoir-faire sur les ancillaires. Les difficultés rencontrées lors de l'implantation de la prothèse ont conduit à développer un implant patient-spécifique afin de réduire les complications constatées en clinique.*

## 1. General context

The development of a trapezo-metacarpal joint prosthesis must take into account the actual implantation conditions in order to satisfy the surgical constraints (tools, surgical procedure, etc.) and the clinical environment (operating room) as well as the complexity of the osteoarticular environment. The objective of this chapter is to:

- Design a carpometacarpal prosthesis;
- Develop a surgical approach to implant the prosthesis;
- Understand the clinical concerns of the prosthesis and the implantation procedure;
- Optimize the prosthetic elements of the implant, the ancillary and the implantation procedure to ensure a durable stability and good positioning of the prosthesis.

Four tests of implantation on cadavers were carried out led by Professor Alain-Charles MASQUELET in collaboration with the school of surgery of the Paris hospitals (AP-HP).
The design of the prosthesis (anchoring means, prosthetic trapezius, and metacarpal insert) and its realization process are patented by a valorization organization named "Satt Lutech". In addition, surgical tools are being developed through know-how.

## 2. Scientific article and patent

- *Patent WO2018210953: « Method of making a trapezo-metacarpal prosthesis and prosthesis obtained » A. LEREBOURS, F. MARIN, S. BOUVIER, C. EGLES, N. JIHAZ, A.C. MASQUELET (2018) (see Annex 1)*

## 3. Introduction

Osteoarthritis of the carpometacarpal joint often modified irreversibly and extremely the trapezium bone morphology [1–3]. Whereas the adjacent subchondral metacarpal bone surface and its cartilage do not remodel significantly with the disease [4]. The changes including the development of osteophytes, wear removal of cartilaginous and osseous materials and loss of density, occur in the trapezium [4,5], affecting all the function of the joint, the thumb opposition and thus the hand prehension.

Arthroplasty is more and more suggested for treating osteoarthritis, as soon as the symptom of strong pain occurs. A large range of implants and options are available on the market to treat the basal joint arthritis depending on the severity of the disease. Classifications of the evolution of osteoarthritis [6,7] help the surgeon to assess the best arthroplasty option between an interposition arthroplasty, a hemiarthroplasty or a total joint replacement.

All the current designed implants: interposition arthroplasty [8,9], hemiarthroplasty [10,11] and total joint replacement [10,12,13], present a high rate of complication such as dislocation of the trapezial cup in the ball-and-socket implants [10,12,13], persistent pain [14] and silicone synovitis [15]. The reasons are unclear, and implant failures may be caused by multiple independent factors such as implant design, insertion technique, and patient-related factors. However, the high damage of the trapezium bone (morphology and density) seems to be greatly responsible of the poor results of the current trapeziometacarpal prostheses. None of these designed implants can be expected to restore all the function of the joint: force transmission, kinematic range of motion, grasping force, stability. The replicate of a healthy trapezium shape particularly its kinematic surface with the first metacarpal bone, may have a positive influence on the thumb kinematics and more globally carpal kinematics. The design of the instrumentation for the surgical procedure is also important to success the surgical approach. Two study showed that the non-congruent and unconstrained characteristics of a CMC implant coupled with a high probability of malposition because of non-adapted ancillary cause high loosening rate [11,16].

This work reports our preliminary cadaveric testings results of a carpometacarpal prosthesis based on 3D printing technology. In addition, ancillary tools were specifically developed for the aforementioned design implant and were used in the cadaver test.

# 4. Material and methods

## 4.1. Extraction and digitalization of the specimen

Two trapeziums and metacarpal bones were excised from a diseased body provided by the surgery school of Paris (Fig.1 and 2)). All subjects died within 15 days of the sampling. Trapeziums and first metacarpal bones (M1) were collected from two subjects. Information such as weight, height and "dominant" hand (right-handed, left-handed) was unfortunately not available.

**Figure 1**: Subject 1: Left hand sampling, Subject 1: Right hand: dorsal view of the trapezium position and M1.

The surgeon has not noticed any kind of evidence of osteoarthritis pathology for the first subject and an advanced osteoarthritis pathology for the 2nd subject.

The specimens were cleaned in two steps: (i) standard dissection (i.e. scalpels, scrapers) and immersion of the bones in acetone; (ii) a fat-removal procedure, allowing a full removal of the cartilage and soft tissue.

The cadaveric specimens were then scanned using a clinical computed tomography (CT) (slice thickness = 0.625 mm and pixel size = 0.328125 mm x 0.328125 mm) (Fig.2.b)). Manual segmentation was performed using 3D Slicer® (Slicer.4.8), allowing a 3D modelling. As segmentation parameters, a mask was applied with a thresholding value for extracting cortical bone (CT-AAA2: 129.54) (Fig.2.c)). 3D images were reconstruct using the following procedure in 3D slicer: discrete marching cubes; 0 number of smoothing iterations, 0 target reduction in number of polygons (decimal percentage) (Fig.2.d)). The 3D models were then exported in STL files (Fig.2.e)). It must be noted that the soft tissue removal protocol is reported to have a shrinking effect on the superficial bone layer up to 0.43 mm (Gelaude, Vander Sloten, and Lauwers 2008; Van der Broeck et al., 2014).

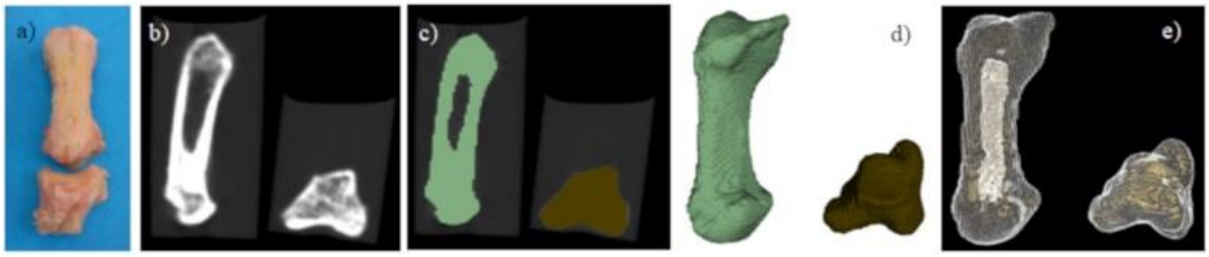


**Figure 2**: Steps of 3D reconstruction: a) Right hand: dorsal view of the trapezium and metacarpal bones after excision in the diseased body; b) CT-scan; c) segmentation (threshold value: 143.59); d) 3D reconstruction using marching cubes; e) exportation of the 3D model in STL files.

### 4.2. Choice of the rapid prototyping technology

The additive manufacture technology e.g. 3D printing for the prosthesis prototype was manufactured to approach the required implant characteristics. Selective laser melting (SLM) will be preferred for manufacturing the implant for its ability to print accurately complex shape in biocompatible metal currently used in orthopedic surgery [19,20]. However, the SLM technology is expensive, making it not appropriate to test the surgical approach, and the kinematic and stabilization performance of an implant design. In a concern to have cheaper construction materials and more flexibility in planning 3d printed prototypes in clinical application research, direct photo-chemical alteration of liquid polymer or stereolithography (SLA) technology was chosen. SLA technology was selected over fused deposition modelling (FDM) because of its reachable minimum layer thickness (0.1 mm) and its good surface finish (surface roughness < 10 μm, Ra) close to the one required for frictional surfaces of prosthesis [21]. Specific ancillary tools were also 3-dimensionnal printed using the same technology and tested during the cadaveric test but are not shown in this manuscript.

SLM technology was selected to understand its ability to reach the complex geometry morphology of the trapezium in a biocompatible metal commonly used for orthopedic prosthesis (Fig.3) as SLA technology performs in photo sensible resin. However, our cadaveric test was performed with SLA prototypes to be more flexible in design modification post implantation. Finally, by homothetic transformation, five different size of prosthetic trapezium from 22.5cm to 26,25cm (height) were manufactured, and their respective prosthetic metacarpal.

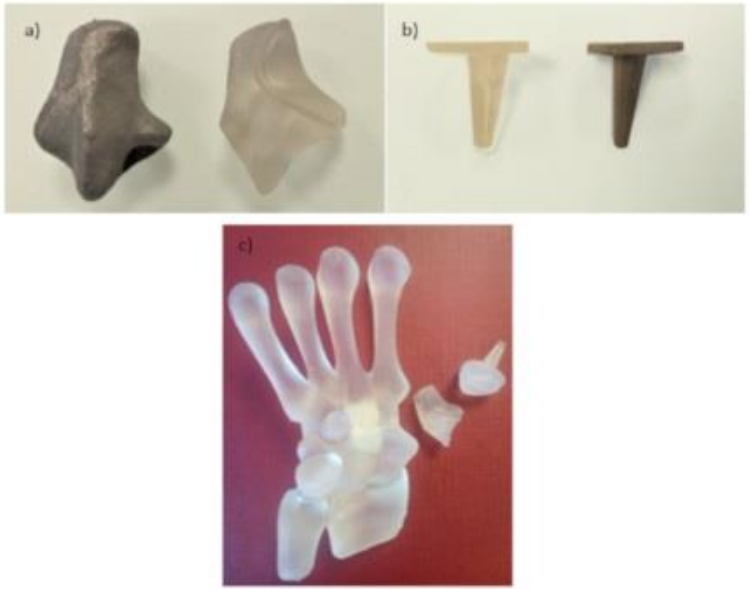


**Figure 3**: Choice of the 3-dimensional printing technology for prototyping: Prototyping choice is done regarding the topology accuracy and the potential printable material. a) SLM (TA6V) and SLA (clear photo-resin) prosthetic trapezium prototype (TA6V); b) SLM (TA6V) and SLA (clear photo-resin) metacarpal stem prototype; c) Position of the implant prototype (clear-resin) into a biomechanical model of the wrist (palmar view).

### 4.3. Dynamic motion analysis

After each implantation test, the orthopaedic hand surgeon qualitatively assessed range of motion (flexion, extension, abduction, adduction and circumduction), stability, and integrity of the nearby biological structures under physiological wrist motion (flexion, extension, supination, and pronation, ulnar and radial deviation). Videos of these motions were done post-implantation.

## 5. Cadaver experience n°1 and 2

The cadaver experience n°1 and 2 are not presented in this manuscript because the procedure of implantation were not entirely performed due to a lack of specific ancillary tools. However, both implantation tests resulted in an improved design of the implant used for the two implantation tests presented in the following paragraph §5.1.

# 6. Cadaver experience n°3

## 6.1. Implant design

### 6.1.1. Prosthetic trapezium part

The two scanned trapezium bones were used to design trapezo-metacarpal implants. The 1st trapezium bone morphology has not been modified. The 2nd trapezium bone model with advanced osteoarthritis has been modified morphologically to recover the healthy characteristics that have been impacted such as the concavo-convex radius of curvature of the 1st metacarpal contact surface. The angulation between the scaphoid, 2nd metacarpal bone, and the trapezoid has been remained untouched. The procedure is further described in the next chapter of this manuscript. The figure 2 allows us to visualize the geometrical differences, especially the angulations between the differences in contact surfaces (Fig.4).

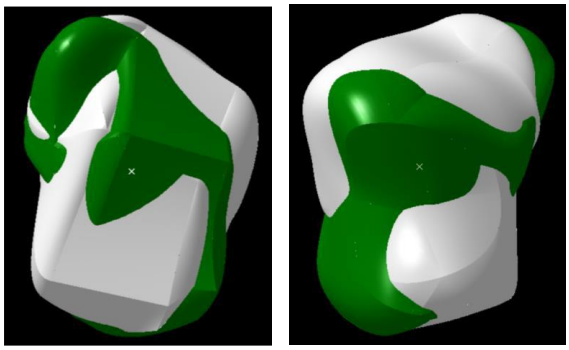

| Angle between : | Version n°1 (white) | Version n°2 (green) |
|---|---|---|
| 2nd metacarpal-trapezoid | 41,591° | 69,302° |
| 2nd metacarpal-scaphoid | 77,777° | 70,031° |
| Trapezoid-scaphoid | 118,484° | 138,974° |
| Trapezoid-1st metacarpal | 56,045° | 36,373° |
| 1st metacarpal-2nd metacarpal | 92,831° | 100,749° |
| Scaphoid-1st metacarpal | 17,046° | 15,586° |

**Figure 4**: Highlighting of geometric differences between the trapezium models: version 1 (green) and version 2 (white)

Items were included for the fixation of the further prosthesis. First a channel was added. It aimed to fuse the prosthetic compound in the trapezoid bone with a cortical screw (Fig.4), anchorage spikes were also added. They aimed at strengthening the fusion and secure the trapezium prosthesis' adequate location by preventing its rotation around the screw axis. The geometric variability of the inter-individual osteoarticular environment makes it difficult to position the implant correctly, particularly the positioning of the two parts of the implant (trapezium prosthesis and metacarpal prosthesis) opposite each other. These elements are aimed to overcome this implantability difficulty. Cortical screws are adapted to the hard parts of the bone and are characterized by a narrow thread over the entire length of the screw. A trapezoid fixation was chosen because the joint with the trapezium is considered to have little motion, and is known to play a role in stabilization and force transmission role rather than a kinematics (Moritomo et al., 2000;

Sonenblum et al., 2004). As both bones are tightly linked and move together on a single path relative to the scaphoid, a fusion of the prosthetic trapezium to the trapezoid might not change the wrist kinematic. A prehension mean coupled with its respective ancillary tool allows the manipulation of the prosthesis while keeping the integrity of its required surface finish, a bulge around the frictional surface also prevent any deterioration of this high controlled surface finish surface during the implantation procedure.

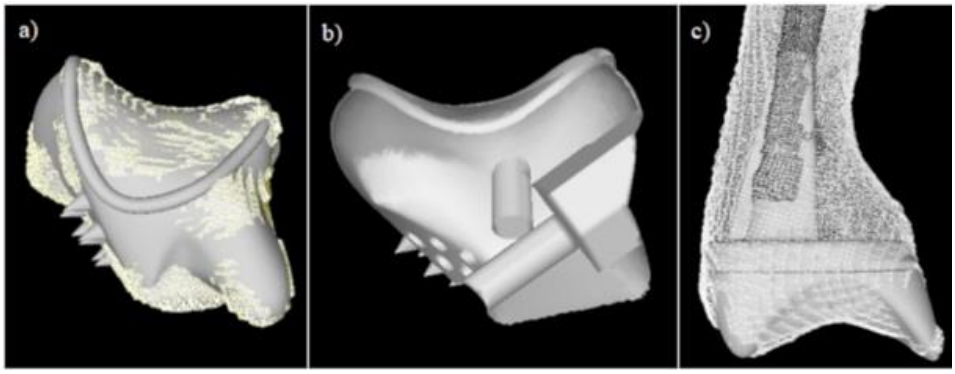


**Figure 5**: Anatomical prosthesis design: Prosthesis design based on the complex morphology of a healthy carpo-metacarpal joint from a CT-scan of a diseased body composed of a prosthetic trapezium, a metacarpal stem and a metacarpal insert. Visualization of the prosthetic compounds design.

### 6.1.2. Prosthetic metacarpal part

The geometry of the metacarpals acquired by medical imaging were used to design the metacarpal parts of the implant which are the stem and the insert. The metacarpal stem is design to fit the medullar of the metacarpal bone as because of its low osseous density and thus the most probable location of the stem. A square-based anti-rotation system has been added to ensure that the insert is correctly positioned in the metacarpal stem. The contours of the flat area of the metacarpal stem were created from B-splines based on 4 points of the metacarpal taken as a reference. The metacarpal insert was designed to keep the integrity of the joint capsule and ligament insertions known to play stabilization feature of the joint (Fig. 4 and 5) [24–26]. The concave-convex surface of the inserts was created with 8 B-splines generated from points from the 3D metacarpal model. Both digitally acquired metacarpals have the particularity of having a larger anatomical volar protuberance and a medullary tube axis that is more focused on the radial zone. These are reliable anatomical indication against dorsal subluxations. Accentuated volar protuberance have been designed for both versions (Table 1). The flat section of the insert has the same geometric characteristics as the metacarpal stem. The "press fit" system of the insert has been created to fit into the metacarpal stem without forcing.

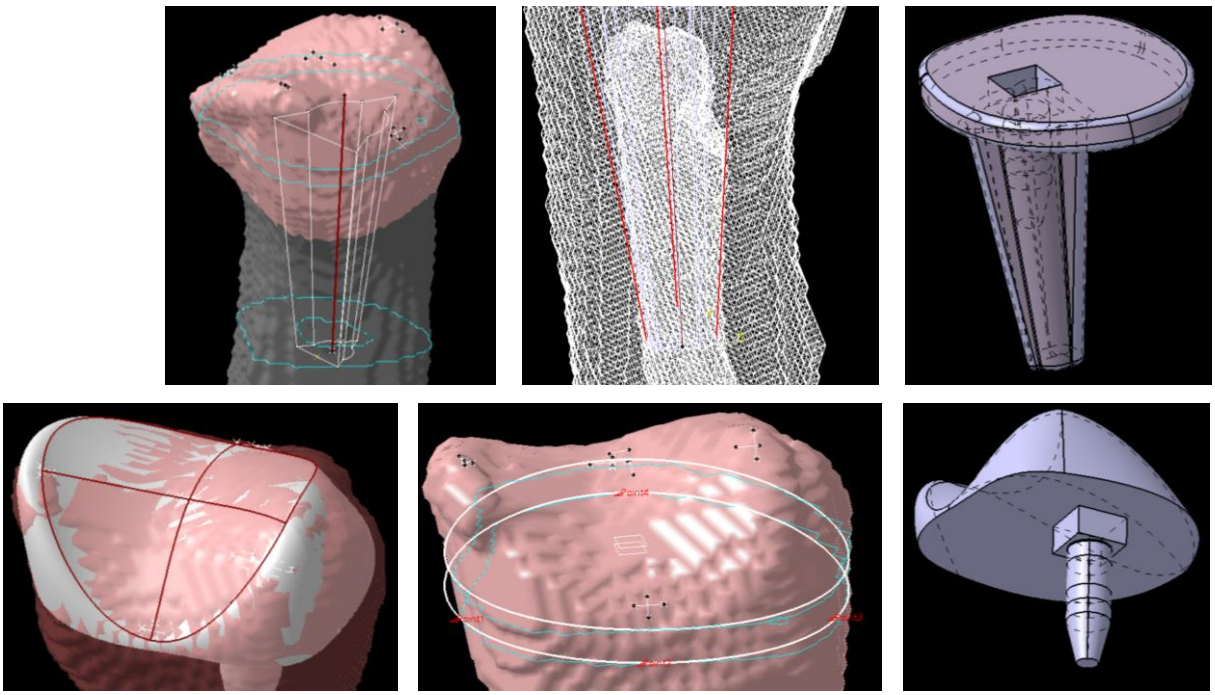

**Figure 6**: Design elements of the stem and the insert

**Table 1**: Protuberance characteristics of the metacarpal inserts

| | Protuberance P.0 | Protuberance P.1 | Protuberance P.2 |
|---|---|---|---|
| Visualisation Version 1 | 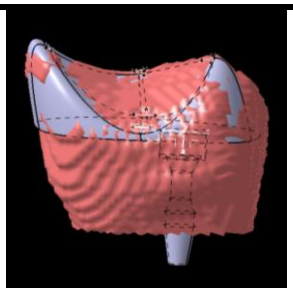 | 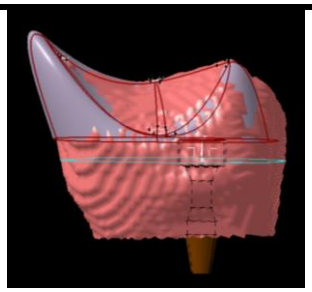 | 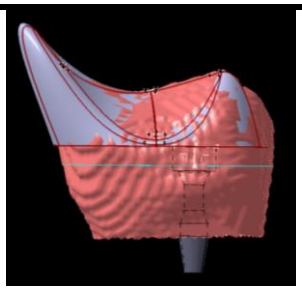 |
| Characteristics Version 1 | Anatomical volar protuberance | Accentuated volar protuberance of 1,95mm | Accentuated volar protuberance of 3,85mm |
| Visualisation Version 2 | 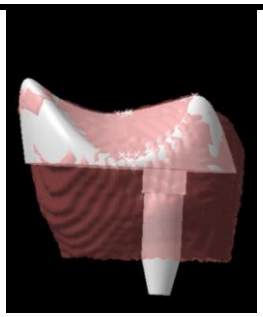 | 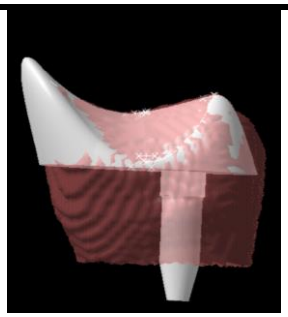 | 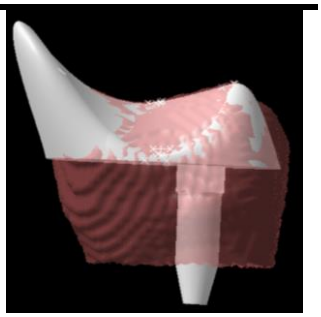 |
| Characteristics Version 2 | Anatomical volar protuberance | Accentuated volar protuberance of 1,95mm | Accentuated volar protuberance of 3,85mm |

## 6.2. Surgical technique

Dorsal approach

A centered curvilinear incision of 5-6cm was made on the trapezium area. After identifying the radial nerve, dissection was performed below the retinaculum tendon sheath located above the abductor pollicis longus (APL) and extensor pollicis brevis (EPB) tendons (Cf chapter 1). A scalpel incision in the interval between the two tendons allows the trapeziometacarpal joint capsule to be reached (Fig.7).

In an exploratory approach, we widened the opening compared to a conventional 3-4cm operation and cut the veins. A small part of the APL tendon was resected while retaining its distal insertion in order to stabilize the implant with it (Fig.7). In addition, the palmar component of the tendon, which is the long abductor, is a subluxating component of the joint.

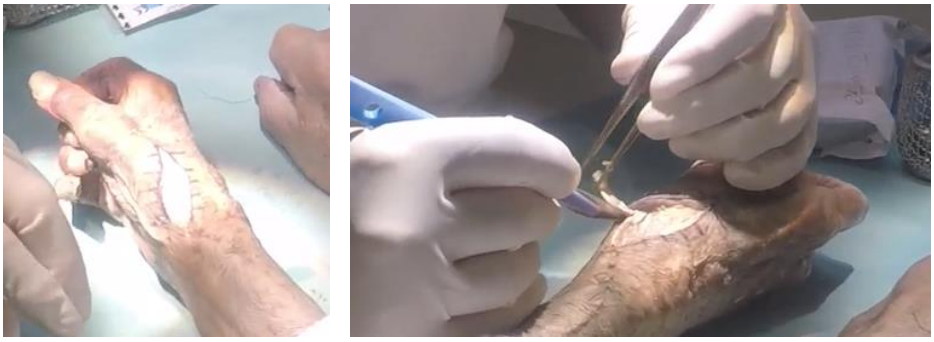

**Figure 7**: curvilinear incision; Partial resection of the APL tendon.

Extraction of the trapezium

The original trapezium was removed with a traditional trapezectomy procedure (Fig.8). The trapezium may either be extracted in integrity or in different pieces. Special care must be taken to avoid any injuries to the surrounding structures. In practice the trapezium is most often extracted in pieces. In the case of our experience, it was extracted in a single block allowing to compare its geometry and size compared to the different version of the prosthetic trapeziums. It should be noted that in our experience, we have incised the EPB tendon crossing vertically through the dorsal zone of the trapezium to the 1st metacarpus, in order to widen our work plan. However during a standard operation, the EPB must remain untouched. The extraction has been complicated by the narrow joint space between the trapezium and trapezoid, which has an extremely limited range of movement. This observation reinforces our choice to stabilize the prosthetic trapezium by fusion with the trapezoid.

**Figure 8**: Resection of the EPL tendon, Incision of the articular capsules around the trapezium, vacant loge which results of the total trapezectomy.

The approach adopted to open the joint capsule is an "H" incision. The original trapezium was removed with a traditional trapezectomy procedure based on a dorsal radial incision initial approach. The proximal part of the first metacarpal bone was excised of 3-4 mm parallel to the radio-ulnar and dorso-volar extremities with its respective ancillary tool. A drill hole completed by a grating process allows to prepare the metacarpal bone prior the stem insertion. Both part composing the prosthetic metacarpal bone (stem and insert) are implanted. The prosthetic trapezium is then inserted and screwed in the trapezoid bone. Joint capsules and articulation are then sutured back.

Choice of the implant version

With regard to the angles between the different articular surfaces, the choice was made for the version 2 of the implant. In addition, we have chosen the 85% reduced size corresponding to a length of 24.65cm of the prosthetic trapezium. Compared to the extracted trapezium from the cadaver, this corresponds to a size reduction of 86.5%. The anatomical volar protuberance of the insert has been chosen (Fig.9).

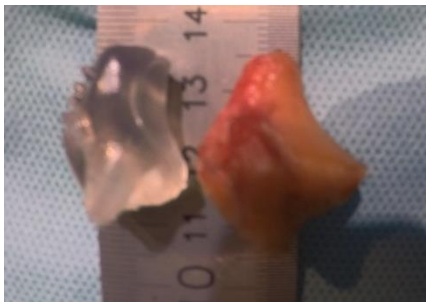

**Figure 9**: Size difference of the prosthetic trapezium and the extracted trapezium.

Preparation of the proximal surface of the 1st metacarpal bone

After clearing a part of the joint capsule relative to the proximal part of the 1st metacarpal bone, while keeping the tendon insertions, a 3,2mm drilling hole was made in the medullar canal. 3-4 mm of the proximal part was extracted parallel to the radio-ulnary and ulno-volar extremities (Fig.10). This extraction was carried out using a gouge clamp. Therefore, the flatness and angulation of the plane could not be adjusted. Based on the

drill hole, a widening was carried out using a rasp (Fig.10). This operation is facilitated by the fact that the operation is performed on a cadaver, the bone having lost its consistency. To ensure that the proximal part of the 1st metacarpal is sufficiently ready, the prosthetic metacarpal was inserted and then removed several times to continue the surface preparation (resection and/or enlargement of the stem-insertion hole).

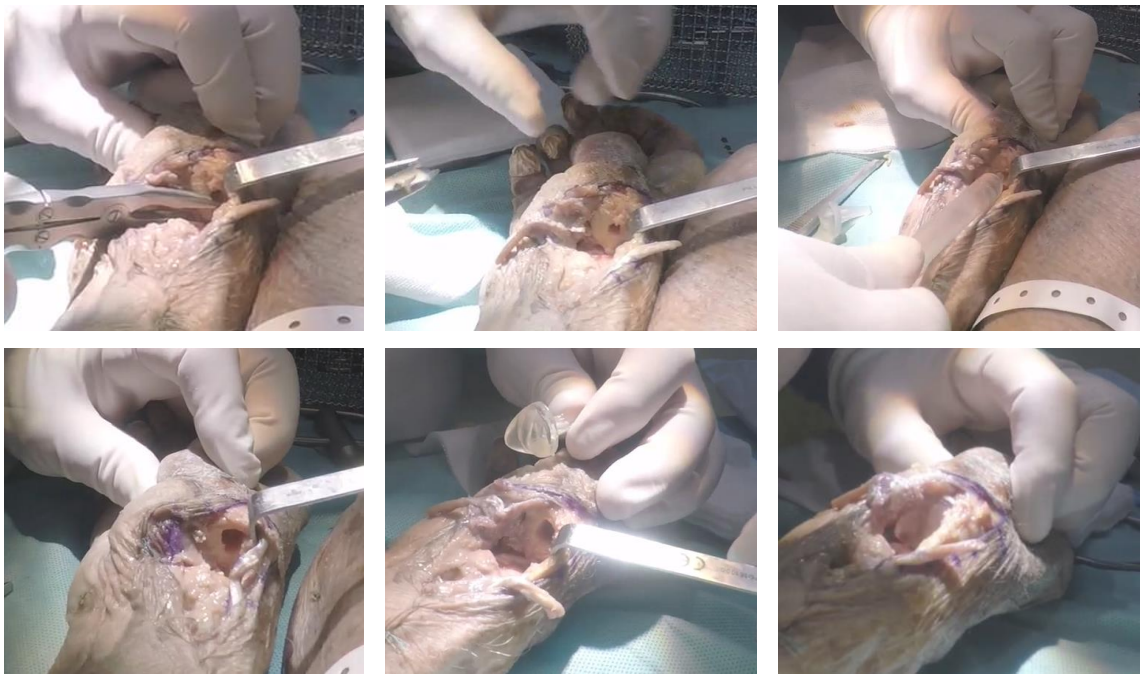

**Figure 10**: Preparation of the proximal part M1: resection with a gouge clamp. Preparation of the proximal part M2: result of the resection. Preparation of the proximal part M1: Enlargement of the hole for the metacarpal stem via a rape. Preparation of the proximal part M2: result of the enlargement of the hole for the metacarpal stem. Insertion of the prosthetic metacarpal. Result of the insertion of the prosthetic metacarpal.

<u>Preparation and anchoring of the prosthetic trapezium on the trapezoid</u>

The prosthetic trapezium was then inserted into the loge left empty by the trapeziectomy, the objective is to ensure that it is properly positioned by matching the contact areas with the surrounding bones (scaphoid, trapezoid, and M2) and the metacarpal insert (Fig.11). The bulge around the trapezometacarpal surface was also a good indicator of the implant positioning. In the case of our experience, this good positioning was achieved with and without the metacarpal insert. During this step, we observed that the entire prosthetic metacarpal, i.e. the stem and metacarpal insert, requires a higher resection than that which can be achieved. A compressive force between the prosthetic trapezium and the prosthetic metacarpal was observed, making trapezometacarpal mobility difficult. Therefore, in this experience, we extracted the metacarpal stem to put only the

metacarpal insert. However, by doing this operation, the insert could rotate in the axis of the medullary canal of the metacarpal, causing an instability of this component.

A drilling hole through the prosthetic trapezium in the trapezoid was made by a 2.4mm drill bit, the screw then anchored the two parts, compressing the anchor spikes.

It is important that the prosthetic trapezium does not move in the direction of rotation of the anchor screw. In the case of a real operation, the preparation of the anchorage will be done with a prosthetic trapeze test. The tension between the two metacarpal and trapezial components was considered satisfactory because it was possible to slightly detach the two parts.

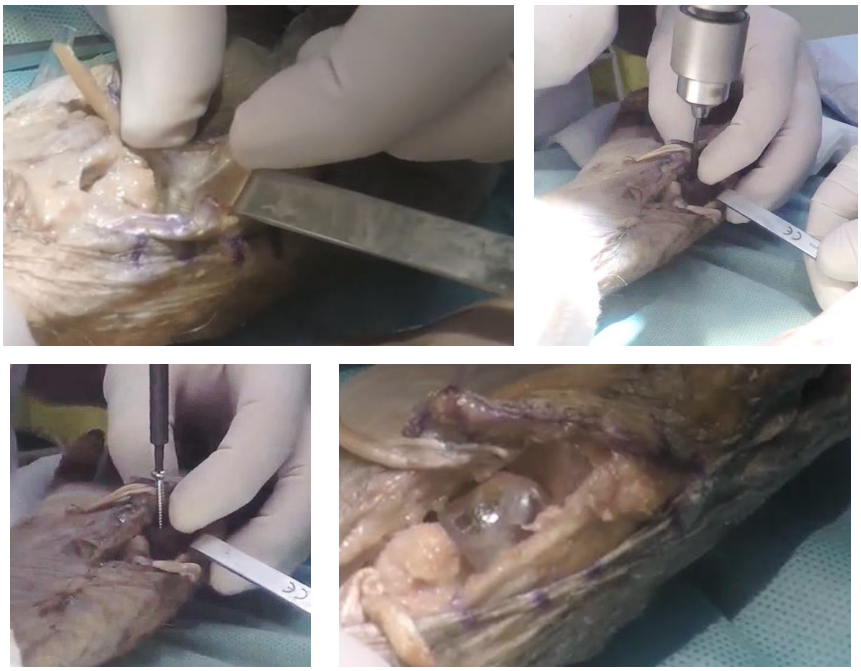

**Figure 11**: Positioning of the prosthetic trapezium. Preparation of the prosthetic trapezium anchor by pre-drilling the trapezoid. Anchoring the prosthetic trapezium by the anchoring screw. Result of the implantation.

Suture of the joint

The capsule joint was sutured back with the resected part of the APL tendon (Fig.12).

**Figure 12**: Suturing of the capsule joint and the APL tendon altogether.

### 6.3. Results post-implantation

By opening the palmar surface of the wrist, the bone compresses on the scaphoid and then causes the scaphoid to move relative to the other bones, which means that partial resection of the scaphoid is not necessary.

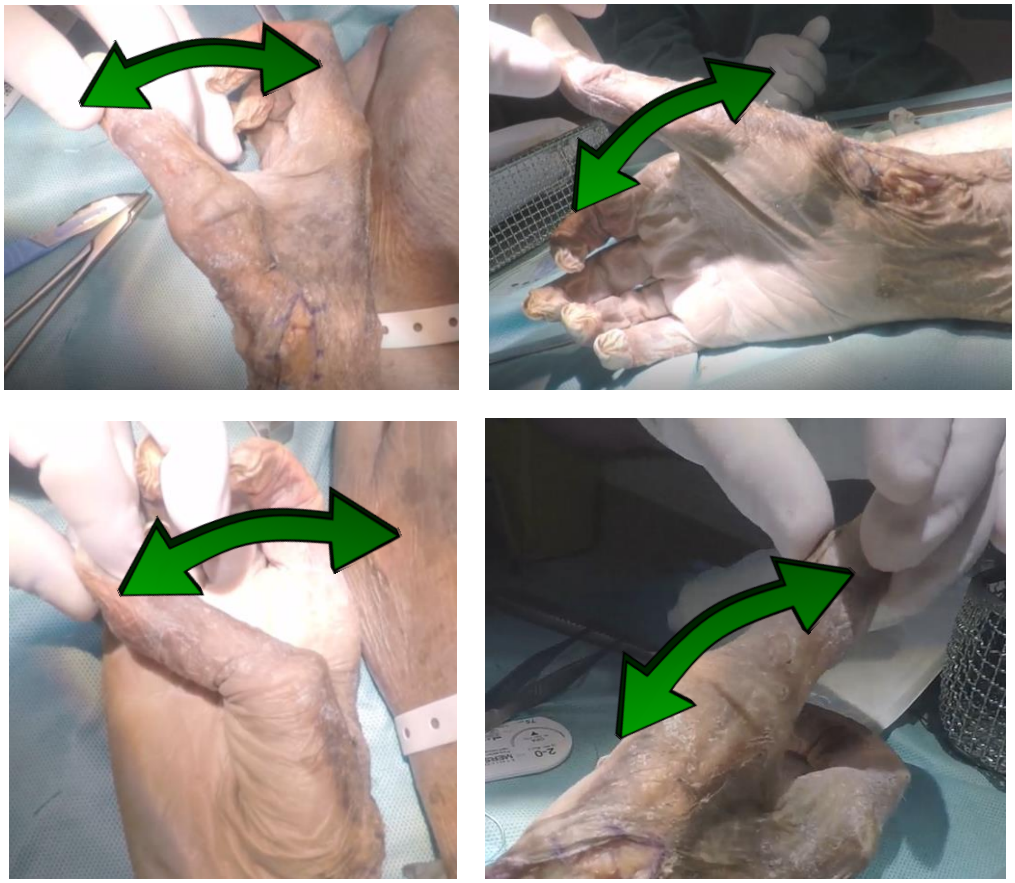

**Figure 13**: Cadaver experience n°3: mobility post-implantation: Flexion; Extension; Adduction; Abduction.

At the end of our experience, the Kapandji index obtained is normal without forcing. This proves that the spatial encumbrance is adequate. Eventually the tendons can be completely disinserted and then reinserted into the base of the 1st metacarpus by means of a small anchor to increase the stability. A mobility tests realized after the surgery showed similar range of motion between the prosthesis and the original carpometacarpal joint as it is practiced during surgery procedure. The prosthesis behaved in an anatomically way with satisfied range of motion regarding flexion/ extension, adduction/abduction (Fig.13). Wrist motions were also well-performed without any impingement syndrome or blockage due to the nearby biological structures. The prosthesis demonstrated a primary mechanical stability throughout all physiological positions of the wrist. The applied subluxated force leads to an observable slight mobility of the implant without subluxation.

## 7. Cadaver experience n°4

### 7.1. Implant design

Both prosthetic trapeziums and metacarpals bones were prototyped with no changes.

### 7.2. Surgical technique

Dorsal approach

The same approach as the previous cadaver experience, has been realized. A 5-6cm centered curvilinear incision was made on the trapezium area between the APL and EPB tendons. In the exploratory approach, we widened the opening compared to a conventional 3-4cm operation. Veins were cut. Unlike the previous experiment, the APL tendon was not resected.

Extraction of the trapezium

The extraction of the trapezium was carried out by preserving it entirety (Fig.14).

**Figure 14**: Extraction of the trapezium after incision of the trapezium joint capsules

Choice of the implant version

The version 1 of the prosthetic trapezium was chosen in relation to the angles of the articular surfaces. In addition, the prosthetic trapezium measuring 25cm in length has been chosen. A difference of 3.5mm can be measured compared to the extracted trapezium, corresponding to a reduction of 87.7%. The anatomical volar protuberance of the insert has been chosen (Fig.15).

**Figure 15**: Size difference between the prosthetic trapezium and the extracted trapezium

Preparation of the proximal surface of the 1st metacarpal bone

Unlike the previous experience, we opted to first resect the proximal part of the 1st metacarpal bone, and then make the hole for the insertion of the stem. The proximal part of M1 was cleaned and the tendon insertions were preserved. Tendon insertions plays a role in the stability. The resection cut of the proximal part was therefore chosen at 3-4mm from the radio-ulnary and ulno-volar extremities (Fig.16). A specifically designed tool was used to ensure the correct flatness and angulation of the plane. The tool is not presented in this manuscript as it has been protected by a "know-how".

**Figure 16**: Preparation of the proximal part of the first metacarpal bone: resection with the designed cutting guide and a scalpel. Highlighting of the difference in thickness between the prosthetic metacarpal and the resected area.

Based on the drill hole, a widening was carried out using a rasp. The stem and the insert were then applied into the widened medullary canal.

Preparation and anchoring of the prosthetic trapezium on the trapezoid

Difficulties were found to properly position the prosthetic trapezium and reproduce the kinematics of the previous experiment. The prosthetic trapezium has been rotating while it was anchored in the trapezoid bone (Fig.17). To overcome this problem, a hole was made with a drill bit in the prosthetic trapezium to maintain its correct position during the anchoring process (Fig.18). We finally obtained similar implementation results compared to the previous experience.

**Figure 17**: Highlighting of the incorrect positioning of the prosthetic trapezium due to its rotation by the screw (off-center bulge) and extraction of the prosthetic trapezium.

**Figure 18**: Procedure to prevent the rotation of the prosthetic trapezium from rotating when anchoring it a) drilling b) screwing of the prosthetic trapezium

Suture of the joint

The joint was closed with conventional surgical thread with a number of surgical stitches (Fig.19).

**Figure 19**: Closing the joint with surgical thread

### 7.3. Results post-implantation

**Figure 20**: Cadaver experience n°4: applied subluxated force to test the stability of the implant

A small mobility was felt, but the implant did not subluxate even by forcing the movement (Fig.20). This is an interesting point since the capsule no longer plays any role mechanically. It should be noted that there is a stability that will be given by the axial forces through muscle contraction.

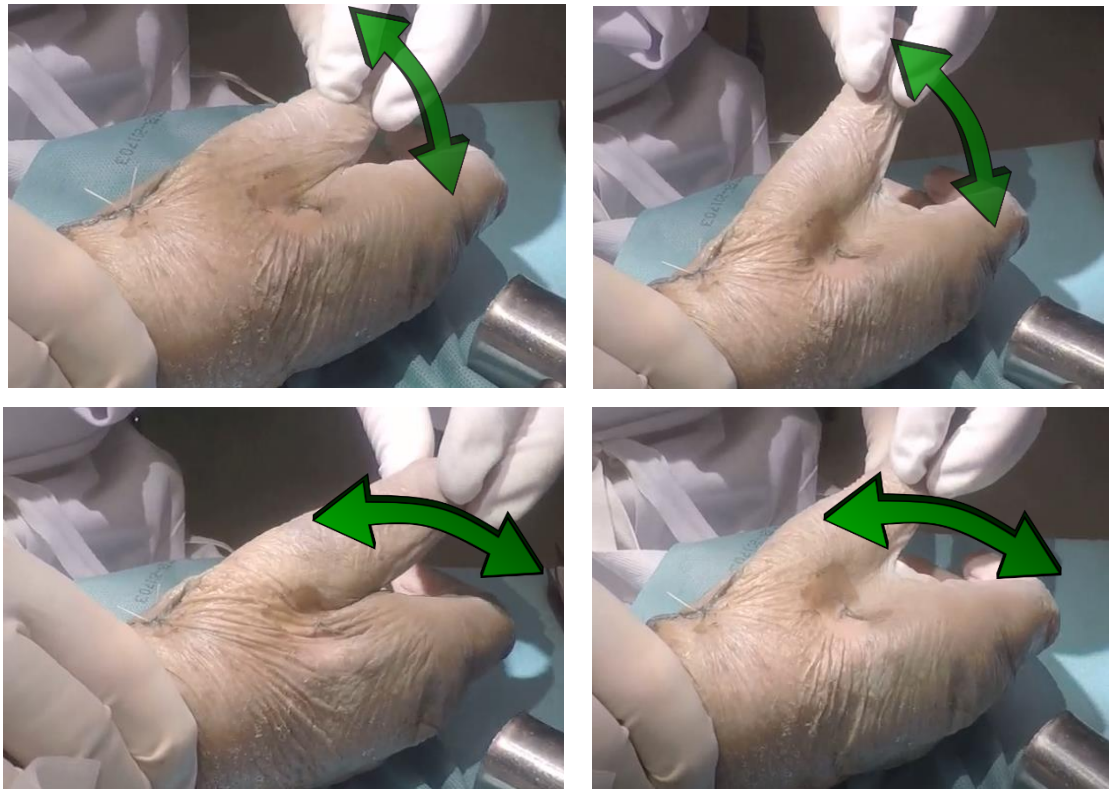

**Figure 21**: Cadaver experience n°4: mobility post-implantation: Flexion; Extension; Adduction; Abduction

Similarly to the first experience, the prosthesis behaved with satisfied range of motion regarding flexion/ extension, adduction/abduction. No impingement syndrome or blockage were found (Fig.21).

## 8. Discussion

This work demonstrated the feasibility of implanting a 3D printed replica of a healthy trapeziums and testing their motion behavior. The 3rd cadaver experience had promising results regarding post-implantation performance however the stem of the implant could not be placed due to an excessive compressive force between the prosthetic trapezium and the prosthetic metacarpal. The 4th cadaver experience also had promising post-implantation results. It should be noted, however, that the implantation was made difficult due to an unstable positioning of the prosthetic trapezium.

This work supports further investigation, such as imaging to support these results, and comparison with other trapeziometacarpal prostheses. Furthermore, investigation of the safety with carefully controlled trials need to be assessed before a potential introduction in clinics. All new concepts for product design must be prototype. The assessment of the implant design in physical terms and the implantability tests in cadaver have highlighted flaws that could not been found otherwise. These experiences have shown us the difficulty

of implanting the prosthesis and the need to implement multi-scale solutions to promote the correct positioning of the entire implant in order to obtain the expected results. The solutions that have been tested include (i) the installation of prosthetic anchoring elements (spikes, screw hole, bulge), (ii) specific surgical tools and (iii) the choice of different version of the implant (size, morphology). However further investigations needs to be assessed to ensure a well-performed implantability of the implant.

Due to the fact that the trapezium's geometry shows complex pattern of concavo-convex curvatures [2,27] and articulates with three other bones, the trapezium prosthesis has to replicate its complex shape to minimize non-physiological kinematics, wear and stability. In addition, studies have shown significative inter-individual differences in the shape of the carpal and particularly the trapezium bone [2,4,28].

However, morphology changes are often extreme [1–3] making it difficult to produce patient-specific implants based on the trapezium bone. One would argue that the design of the prosthetic surfaces on the less damaged surface of the metacarpal would be more logical, rather than trying to replicate a healthy trapezium. However, the curvatures of the metacarpal and trapezium surfaces are significantly different [29]. With the rapid progress in 3D printing of different materials during recent years, complex geometry and large range of prosthesis size have become a realistic option.

The designed carpometacarpal implant and its surgical approach take into account the instability and loosening of previous implants [9,10,13]. A loss of osseous density of the bone during osteoarthritis was said to be significant [30] and persuade us not to base the stability and fixation of the prosthesis on a resected trapezium. Thus, our prosthetic trapezium replica replaces entirely the former diseased trapezium bone and is firmly fixed on the trapezoid by a screw and spikes. Even though the trapezoid and prosthetic trapezium fusion was not seen to affect the different wrist motion in our cadaveric test, a another cadaveric study [23] found that although the relative motions between the trapezoid and trapezium is small, it is statistically significant (up to 0.4 mm) and at least 10° (flexion and radial deviation). This fusion might impact somehow the wrist mobility.

The concept of replacing the trapezium with a solid implant is not new. In 2009 a metal trapezium (TrapEZX Extremity Medical) was introduced and subsequently implanted in more than 100 patients between 2010-2012 [31] . The design approximates the articulating surfaces (scaphoid, trapezoid and metacarpal bones). However, it does not consider the high variability of morphology of the trapezium bones which could affect the stability of the implant. The prosthesis articulates with the patient metacarpus which is

also affected by OA but at a lower degree. And the prosthesis is fixed on the 2nd metacarpus which could surely (i) affect the kinematic of the middle finger, (ii) arise subluxation between the prosthesis and the 1st metacarpus.

Our study presents limitation. First, the original bones are healthy without osteophytes and deformations. The strategy to base its design on the contralateral bone was not selected as it often has the morphological deformation although at a lower degree because of aging [2,32]. Current research are done to recompute healthy morphological features from advanced osteoarthritis stage geometry [33].

Second, as the test was performed in a cadaver, the stability of the implant by the axial forces during muscular contraction was not possible. However passive primary mechanical stability which was performed is a good indicator of a longer-term stability [34].

Third, the designed prototype might be used in patient as an ancillary tool to test the appropriate size of the different compounds of the prosthesis. The couple of materials used for the frictional parts is still an open question and will be assessed by long-term biomechanical tests and wear resistance investigation.

To conclude, anatomical designs for additive manufacturing e.g. 3D printing gives new opportunity to prosthesis manufacturing by reducing the development design duration and supply chain, and allowing subject specific prosthesis. Further investigations need to focus on the reduction of the required skills in computer-assisted-design to conceive efficient geometry design and improved modelling regarding printability in additive manufacturing. In this context, the following chapters will be focused on the design of an additive manufactured patient-specific carpometacarpal prosthesis, aimed particularly to optimize the good positioning and stability of the implant.

The main clinical specifications that results from the cadaveric tests are:

- Recover mobility related to the trapezo-metacarpal joint.
- Replace the stabilization induced by ligament, tendon and joint insertions due to their excision during arthroplasty of the osteoarthritic trapezium to avoid any complications, particularly subluxation (spatial integrity).
- Transmit stresses easily into other carpal bones during wrist and thumb movements to avoid material wear and recover the grip and pinch forces.
- Reduce pain in relation to the arthritic joint.
- Be easily implantable (time to set up, ancillary).

- Be implantable while maintaining the integrity of the surface finish (roughness) of the contact surfaces.
- Maintain the surface and topological integrity and its surrounding biological structures over time.

These clinical specifications allows us to elaborate in a more exhaustive way the geometrical specification of the trapezium model. These specifications are:

- The contact surfaces with the scaphoid, trapezoid and 2nd metacarpal bones have to be closed to their respective adjacent bones.
    - patient's angulation of the described articular surfaces
    - patient's surface area of the described articular surfaces

*These joints plays a role mainly in the stabilization of the bone due to their tight characteristics. The accuracy needed is medium.*

- The contact surface with the prosthetic metacarpal must reflect the contact surface with a metacarpal under healthy conditions.
    - healty angulation
    - healty surface features (concavo-convex radius of curvature)
    - healty surface area

*This joint plays a role mainly in the kinematics of the thumb. The accuracy needed is high.*

- The surfaces defining the passage of the FCR tendon must be defined.
- The other surfaces must reflect a healthy bone condition and allow the addition of the various prosthetic elements.

*These areas do not necessitate a high accuracy.*

A more detailed list of the specifications is shown in Annex n°1.

## 9. Reference list


[1] Cooke, S. Kenneth, D.S. Rolando, Z.G. Steven, G.E. Richard, Degenerative changes of the trapeziometacarpal joint: radiologic assessment, Skeletal Radiol. 24 (1995) 523–527.

[2] E. Halilaj, D.C. Moore, D.H. Laidlaw, C.J. Got, A.P.C. Weiss, A.L. Ladd, J.J. Crisco, The morphology of the thumb carpometacarpal joint does not differ between men and women, but changes with aging and early osteoarthritis, J. Biomech. 47 (2014) 2709–2714.

[3] S. Van Nortwick, A. Berger, R. Cheng, E. Al, Trapezial topography in thumb

carpometacarpal arthritis, J. Wrist Surg. 2 (2013) 263.

[4] L. Xu, R. Strauch, G. Ateshian, R. Pawluk, V. Mow, M. Rosenwasser, Topography of the osteoarthritic thumb carpometacarpal joint and its variations with regard to gender, age, site, and osteoarthritic stage, J. Hand Surg. Am. 23 (1998) 454–64.

[5] V. Pellegrini, Osteoarthritis of the trapeziometacarpal joint: the pathophysiology of articular cartilage degeneration. I. Anatomy and pathology of the aging joint, J. Hand Surg. Am. 26 (1991) 967–74.

[6] R. Eaton, S. Glickel, Trapeziometacarpal osteoarthritis. Staging as a rationale for treatment., Hand Clin. 3 (1987) 455–71.

[7] P. Dell, T. Brushart, R. Smith, Treatment of trapeziometacarpal arthritis: results of resection arthroplasty, J. Hand Surg. Am. 3 (1978) 243–9.

[8] Belcher HJ, R. Zic, Adverse Effect of Porcine Collagen Interposition after Trapeziectomy a Comparative Study, J. Hand Surg. Br. Eur. Vol. 26 (2001) 159–164.

[9] P. Bellemère, L. Ardouin, Pi2 spacer pyrocarbon arthroplasty technique for thumb basal joint osteoarthritis, Tech. Hand Up. Extrem. Surgery. 15 (2011) 247–52.

[10] Y. Krukhaug, S.A. Lie, L.I. Havelin, O. Furnes, L.M. Hove, G. Hallan, The results of 479 thumb carpometacarpal joint replacements reported in the Norwegian Arthroplasty Register, J. Hand Surg. (European Vol. 39 (2014) 819–825.

[11] M. Pérez-Úbeda, A. García-López, F. Martinez, E. Vilanova, M. Martos, L. Stern, Results of the cemented SR trapeziometacarpal prosthesis in the treatment of thumb carpometacarpal osteoarthritis, J. Hand Surg. Am. 28 (2003) 917–25.

[12] L. Hellegaard, T. Hansen, Long Term Follow Up in Patients with Radiologically Loose Trapeziometacarpal Total Joint Implants, Rheumatol. 4 (2014) 2161–1149.

[13] A. Klahn, M. Nygaard, R. Gvozdenovic, M.E.H. Boeckstyns, Elektra prosthesis for trapeziometacarpal osteoarthritis: a follow-up of 39 consecutive cases, J. Hand Surg. (European Vol. 37 (2012) 605–609.

[14] C. Taleb, S. Berner, G.. Ruggiero, First metacarpal resurfacing with polyvinyl alcohol implant in rhizarthrosis: Preliminary study, Chir. Main. 33 (2014) 189–95.

[15] C.A. Peimer, Long-term complications of trapeziometacarpal silicone arthroplasty., Clin. Orthop. Relat. Res. 220 (1987) 86-98. http://europepmc.org/abstract/med/3297454 (accessed April 9, 2018).

[16] A. Pendse, A. Nisar, S.Z. Shah, A. Bhosale, J.V. Freeman, I. Chakrabarti, Surface replacement trapeziometacarpal joint arthroplasty – early results, J. Hand Surg.

(European Vol. 34 (2009) 748–757.

[17] F. Gelaude, J. Vander Sloten, B. Lauwers, Accuracy assessment of CT-based outer surface femur meshes, Comput. Aided Surg. 13 (2008) 188–199.

[18] V. den B. Joyce, V. Evie, W.-S. Roel, V.S. Jos, Segmentation accuracy of long bones, Med. Eng. Phys. 36 (2014) 949–953.

[19] Y. Hedberg, I. Odnevall Wallinder, Metal release and speciation of released chromium from a biomedical CoCrMo alloy into simulated physiologically relevant solutions, J. Biomed. Mater. Res. - Part B Appl. Biomater. 102 (2014) 693–699.

[20] A.T. Sidambe, Biocompatibility of advanced manufactured titanium implants-A review, Materials (Basel). 7 (2014) 8168–8188.

[21] R. Campbell, M. Martorelli, H. Lee, Surface roughness visualisation for rapid prototyping models, Comput. Des. 34 (2002) 717–25.

[22] H. Moritomo, S. Viegas, K. Elder, K. Nakamura, M. DaSilva, R. Patterson, The scaphotrapezio-trapezoidal joint. Part 2: a kinematic study, J. Hand Surg. Am. 25 (2000) 911–20.

[23] S. Sonenblum, J. Crisco, L. Kang, E. Akelman, In vivo motion of the scaphotrapezio–trapezoidal (STT) joint, J. Biomech. 37 (2004) 645–52.

[24] P. Bettinger, R. Linscheid, R. Berger, I.W. Cooney, K. An, An anatomic study of the stabilizing ligaments of the trapezium and trapeziometacarpal joint, J. Hand Surgery. 24 (1999) 786–98.

[25] B. Van Brenk, R. Richards, M. Mackay, E.A. Boynton, A biomechanical assessment of ligaments preventing dorsoradial subluxation of the trapeziometacarpal joint, J. Hand Surgery. 23 (1998) 607–11.

[26] D.A. Neumann, T. Bielefeld, The Carpometacarpal Joint of the Thumb: Stability, Deformity, and Therapeutic Intervention, J. Orthop. Sport. Phys. Ther. 33 (2003) 386–399.

[27] H. Dathe, C. Dumont, R. Perplies, J. Fanghänel, D. Kubein-Meesenburg, H. Nagerl, M.M. Wachowski, The thumb carpometacarpal joint: curvature morphology of the articulating surfaces, mathematical description and mechanical functioning, Acta Bioeng. Biomech. 18 (2016).

[28] Loisel, F., S. Chapuy, P.B. Rey, L. Obert, B. Parratte, L. Tatu, D. Lepage, Dimensions of the trapezium bone: a cadaver and CT study., Surg. Radiol. Anatomy,. 37 (2015) 787–792.

[29] D'agostino Priscilla, Benjamin Dourthe, Faes Kerkhof, G. Harry Van Lenthe, Filip

Stockmans, Evie E. Vereecke, In vivo biomechanical behavior of the trapeziometacarpal joint in healthy and osteoarthritic subjects, Clin. Biomech. 49 (2017) 119–127. https://www.sciencedirect.com/science/article/pii/S0268003317302000 (accessed September 19, 2018).

[30] J.J. Schreiber, T.J. McQuillan, E. Halilaj, J.J. Crisco, A.P. Weiss, T. Patel, D. Kenney, A.L. Ladd, Changes in local bone density in early thumb carpometacarpal joint osteoarthritis, J. Hand Surg. Am. 43 (2018) 33-38.

[31] M.A. Vitale, F. Taylor, M. Ross, S.L. Moran, Trapezium prosthetic arthroplasty (silicone, Artelon, metal, and pyrocarbon), Hand Clin. 29 (2013) 37–55.

[32] L. Xu, R.I. Strauch, G.A. Ateshian, R.J. Pawluk, V.C. Mow, M.P. Rosenwasser, Topography of the Osteoarthritic Thumb Carpometacarpal Joint and Its Variations With Regard to Gender , Age , Site , and Osteoarthritic Stage, (1998) 454–464.

[33] A. Lerebours, F. Marin, S. Bouvier, C. Egles, A.-C. Masquelet, A. Rassineux, A voxel-based method for designing a numerical biomechanical model patient-specific with an anatomical functional approach adapted to additive manufacturing, J. Numer. Sci. Biomech. Bioeng. (2019).

[34] J. Lignon, J.P. Friol, F. Chaise, Historique des prothèses totales trapézo-métacarpiennes, Ann. Chir. La Main Du Memb. Supérieur. 9 (1990) 180–188.

## 10. Intermediate conclusion

In this chapter, we have demonstrated the feasibility to implant a carpometacarpal prosthesis based on the geometry of a healthy trapezium shape. The implantation technique and the prosthetic elements of the implant has been optimized so as to ensure a good stability of the reconstructed joint. The prosthesis behaved in an anatomically way with satisfied range of motion regarding flexion/ extension, adduction/abduction. The results of the experience have led to a patent on the design of the implant and a know-how on the ancillary tools. However, the difficulty of the prosthesis' implantation has led us to develop a patient-matched implant aimed to reduce drastically the complications found in clinic. The development of a patient-matched model is described in the following chapter.

# CHAPTER 3:

# Numerical method to rejuvenate highly deformed bones for a prosthesis design and additive manufacturing. Case study: the trapezium bone

*Ce chapitre aborde l'étape préliminaire de conception du modèle numérique adapté au patient mais aussi à l'impression 3D. L'idée est de « rajeunir » numériquement l'os du patient afin de retrouver sa forme pré-pathologique. La procédure numérique proposée est basée sur une configuration réduite de paramètres par une conception fonctionnelle et sur un processus à base de voxels. Le principal avantage du modèle configurable est sa capacité à compenser un manque d'informations dans les données brutes d'imagerie médicale ou une morphologie déformée due à une maladie comme la rhizarthrose. L'approche à base de voxels permet de transformer les régions distinctes en une structure unique. Cela permet d'ajouter aisément des opérations topologiques. Combiné à un processus de lissage simple, le résultat donne un modèle triangulé homogène, exempt d'erreurs d'imprimabilité, tout en rendant le modèle configurable plus réaliste sur le plan anatomique. L'approche a été appliquée sur les os du trapèze profondément touchés par l'arthrose. Des paramètres configurables ont été définis pour restaurer la morphologie de la pré-arthrose tout en préservant les spécificités non-affectées par la pathologie. Cette procédure de "rajeunissement" permet par ailleurs, de connaître les zones de déformations dues à l'arthrose spécifiques à chaque patient, ce qui peut être utile pour l'examen clinique et le choix d'un traitement optimal.*

## 1. General context

The implantation trials resulted in the need for a trapezium bone replacement model that can geometrically match the patient's osteoarticular environment. The trapezium bone has a highly functional and complex morphology, with some areas largely involved in stabilizing the bone and transmitting the forces of the osteoarticular column from the thumb to the various bones of the carpus. In addition, the trapezius bone has significant inter-individual morphological variability and is slightly less pronounced between bilateral trapezius bones. In addition, osteoarthritis at the base of the thumb irreversibly deforms this bone, causing pain, loss of mobility and reduced strength. In this chapter we propose a two-steps approach. The first step consists in setting up a computer-aided design method to model a configurable healthy bone specific to a given individual. This method also ensures the integrity of the output model in terms of printing by a technique based on voxel representation. Other advantages of this method include the ability to control the degree of accuracy, perform addition and removal operations known as Boolean operations, make neighbouring surfaces initially unconnected into a continuous surface and finally not require extensive design skills. The 2nd step consists in identifying the configurable parameters of the model to "rejuvenate" an arthritic bone to obtain an optimal digital trapezium replacement model for the patient. This approach is based on a geometric analysis of bones in healthy and arthritic conditions. These works are summarized in two articles and have been patented.

## 2. Scientific article

- *Lerebours, A., Marin, F., Bouvier, S., Egles, C., Masquelet, A.C. and Rassineux, A., 2019. A voxel-based method for designing a numerical biomechanical model patient-specific with an anatomical functional approach adapted to additive manufacturing. Computer methods in biomechanics and biomedical engineering, 22(3), pp.304-312.*

- *Lerebours, A., Marin, F., Bouvier, S., Egles, C., Masquelet, A.C. and Rassineux, A.," Numerical method to rejuvenate highly deformed bones for a prosthesis design and additive manufacturing. Case study: the trapezium bone." Submitted in Computer methods in biomechanics and biomedical engineering*

- *Patent WO2019162636A1« Method of manufacturing a complex substitution object from the real object» A.Lerebours, F.Marin, S.Bouvier, A.Rassineux, (2018) (Annexe n°2)*

# Article 2:

COMPUTER METHODS IN BIOMECHANICS AND BIOMEDICAL ENGINEERING
https://doi.org/10.1080/10255842.2018.1552684



## A voxel-based method for designing a numerical biomechanical model patient-specific with an anatomical functional approach adapted to additive manufacturing

Augustin Lerebours[a], Frederic Marin[b], Salima Bouvier[a], Christophe Egles[b], Alain-Charles Masquelet[c] and Alain Rassineux[a]

[a]Centre de recherche de Royallieu, Sorbonne Universités, Université de technologie de Compiègne, CNRS, FRE-2012 Roberval, Compiègne cedex, France; [b]Centre de recherche Royallieu, Sorbonne Universités, Université de technologie de Compiègne, CNRS, UMR 7338 BioMécanique et BioIngénierie (BMBI), Compiègne cedex, France; [c]Orthopaedic, Trauma, and Hand Surgery, Saint Antoine Hospital APHP, Paris, France

**ABSTRACT**

Here, we describe an original and efficient geometry design approach, based on voxels resulting in a validated model for printability in additive manufacturing. The proposed approach is also designed to be accessible to non-specialists as it does not require specialist skills in computer-assisted-design (CAD). It focuses on biomedical applications, particularly the geometry design of a configurable digital biomechanical model with selected anatomical features based on medical imaging compatible with customization, as might be needed for prosthetic elements. The methodology is based on two main steps. First, an accessible parametrization to medical employees of a configurable biomechanical model is matched specifically to the patient. The configurable model is designed to palliate any kind of potential lack of information from the Digital Imaging and Communication in Medicine (DICOM) file of the medical imaging or partial topological defects but with the least and sufficient number of parameters. For this purpose, the configurable model is segmented in topological areas with a complexity facing solely the desired specification, without regards of potential numerical errors prior AM such as boundary edges, intersecting faces and non-manifold edges. The second step is the voxel-based modelling, easily accessible for medical employees unfamiliar with CAD. Voxels stores the geometric information in a discrete format to facilitate customization by topological operations such as addition and subtraction. The voxelization representation coupled with a smoothing filter, results in a more realistic, robust and closed triangulated model, freed from errors of printability. This method is presented in the context of a trapezium replacement prosthesis prior to selective laser melting (SLM) and diverse post-treatments.

**ARTICLE HISTORY**
Received 15 May 2018
Accepted 22 November 2018

**KEYWORDS**
Implantable prosthesis; Design for Additve Manufacturing; Enhanced voxe-based method; Functional design; Trapezium replacement

### 1. Introduction

Additive manufacturing (AM) (Caudillo et al. 2002), also referred to as 3D printing, (Zadpoor and Malda 2017), is having a huge impact in the healthcare industry. Innovative AM-specific designs for implants have begun to emerge. AM offers more patient-specific and better osteointegration properties, since it allows the design of precise complex anatomical shapes, both external and internal, and the use of a wide range of biomaterials (ASTM 2012; Emmelmann et al. 2011; Gao et al. 2015).

The process of obtaining an AM physical model based on patient medical imaging by converting images directly into triangulated mesh files has already been applied, particularly for 3D visualizations that are done to better understand a pathological condition and to predict surgical outcomes (Huotilainen et al. 2014; Lethaus et al. 2012; Rengier et al. 2010). Some hearing prostheses (Liacouras et al. 2011; Mohammed et al. 2018) and dental implants (Barone et al. 2016; Tunchel et al. 2016) have involved semi-automated processes from patient data to part production. The modelling system used in these applications unfortunately does not allow configurability, and the system in itself is not adapted to a time-efficient additive manufacturing process.

Prostheses are most often manufactured using subtractive machining technology such as milling and turning. Some research has focused on implantable medical devices with complex anatomical shapes designed for AM (Pradel et al. 2018). Most research

CONTACT Augustin Lerebours augustin.lerebours@utc.fr

focuses on topological design of porous metals for bone scaffolds for orthopaedic implants (Arabnejad et al. 2016; Taniguchi et al. 2016; Wang et al. 2016). These interconnected pores aimed to imitate the architecture of real bones to guide the proliferation, growth of cells appropriately in the scaffold. A wide range of design strategies exists to create a periodic scaffold using Computer Aided Design (CAD) tools such as the use of polyhedral solids to create graded porous aspect (Wang et al. 2016). Several patents have also been approved for generating patient-specific design by AM such as US6932842B1, US20060136058A1 and US8086336B2.

The general process chain for 3D-printed customized implants includes:

1. Acquisition of the patient data through medical images (MRI, CT-scan)
2. Design of the implant using CAD software (solid)
3. Creation of the meshed model (STL or OBJ file)
4. Slicing of the file in the building software. Each slice corresponds to the layer thickness of the AM process
5. AM (powder-bed fusion, material extrusion, material jetting, direct-energy deposition, vat photopolymerization, sheet lamination)
6. Removal of undesirable material components (unmelted powder, support structures)
7. Additional post-processing (cleaning, polishing, sterilization, etc.)

Combining improved designs for additive manufacturing (DfAM) with a shortened supply chain has great potential benefits for the healthcare industry (Pradel et al. 2018).

Computer-assisted design (CAD) systems are mostly based on two kinds of modelling, namely Constructive Solid Geometry (CSG), and Boundary representation (B-rep) (Mäntylä 1987). CSG modelers allow the creation of objects that combine simpler objects known as primitives (cones, sphere, cuboids, pyramids), using Boolean operators. CSG has the advantage of ensuring that objects are 'solid', or watertight. It also provides a quick way of creating geometries, but surface representation may not be accurate enough when the objects to be represented have complex 3D shapes, which is generally the case for anatomical structures (Mäntylä 1987). B-rep, on the other hand, allows a local representation of connecting faces, edges and vertices through simple geometric items (points, curves and surfaces). B-rep is therefore more flexible and often yields an accurate 3D representation. However, it requires more sophisticated CAD skills, particularly when making the model watertight, as there are no algorithms for topological operators (Mäntylä 1987). All the modelling therefore has to be done manually, which is time-consuming.

Consequently, neither CSG nor B-rep is well-suited to the design 3D-printed customized implants.

Moreover, the file generated prior to additive manufacturing is a faceted triangulated representation of a 3D CAD model (STL or OBJ files). AM models require a careful avoidance of numerical errors such as boundary edges, intersecting faces, and non-manifold edges (Huang et al. 2013) that could lead to instable slicing algorithms and even manufacturing failure. These two modelling approaches still lack an optimized digital file prior to 3D-printing that could effectively eliminate these printability errors. Therefore, a modelling system that allows an error-free final file before printing and with a basic CAD toolset for the design of AM-based implants has become essential. The basic CAD toolset includes:

1. Patient-specific feature design from the patient's data
2. Configurable topological features to recover missing information in the medical imaging and anatomical regions distorted by a pathology
3. Design of watertight objects
4. Boolean operations (addition, subtraction) for prosthetic elements (prostheses require stabilization features such as spikes and screw holes
5. A meshed model containing no printability errors and with a homogeneous triangulated representation

This work presents an original approach combining B-rep and a voxel-based representation. This modelling system has a number of features that make it a valuable alternative, namely an ability to control accuracy at a desired level, Boolean and algebraic operations, connection of slightly discontinuous surfaces, and undemanding modelling. Voxelization involves converting geometric objects into a set of voxels (configurable numerical cuboids) that best approximates the original object (Jense 1989). Voxel-based model are insensitive to object complexity and make for ease of display and model manipulation (Boolean operations) (Jense 1989). Little work has been published on the use of voxel-based models for geometric reasoning in engineering design (including for AM).

In this article we present a quick, reliable method for producing a patient-matched numerical biomechanical model. It requires no specialist skills in CAD, and is based on an anatomical functional approach adapted for prosthesis design and AM. The case study used as an example of applying this method relates to a trapezium replacement prosthesis.

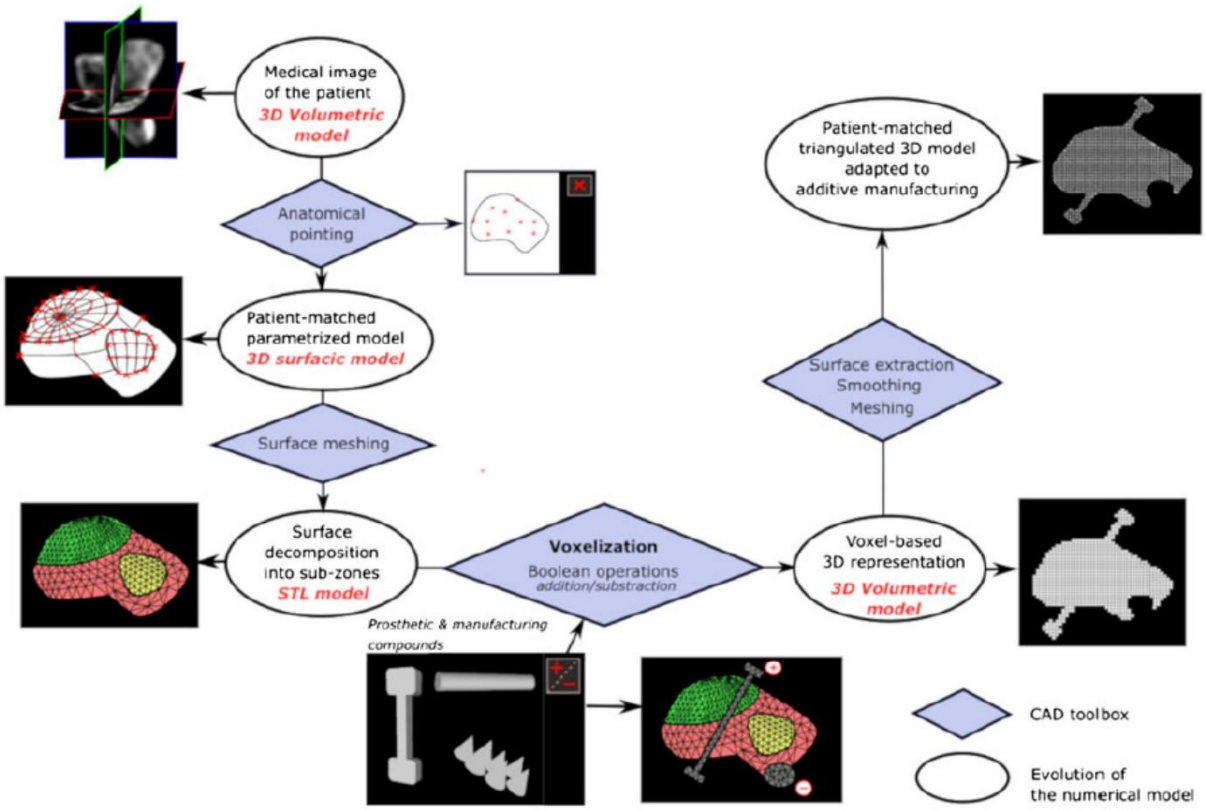


Figure 1. Methodology of designing a patient-matched implant for additive manufacturing.

## 2. Methods

The methodology comprises two main steps. First, a reduced parametrization of a configurable biomechanical model is matched specifically to the patient using B-rep modelling. Second, a voxel-based approach coupled with a smoothing filter is used to improve this intermediate model in in relation to three aspects: the improved model is anatomically more realistic, compatible with an undemanding addition of functional elements, and contains no errors of printability (Figure 1).

### 2.1. Definition of the configurable model

This paragraph describes the first step. The main objectives of this first process step are the following:

1. Configurability of the model: palliating any potential lack of information in the medical imaging and any potential topological defects in the pathological structure.
2. Universality of location points: points defined with an anatomical or geometrical property are universal, meaning that a model can be adapted from one person to another.
3. A small number of parameters (configurable points and vectors) and low computational load in reconstructing the desired complexity. To what extent this objective is met will depend greatly on the biomechanical structure.

A biological structure often possesses distinct regions with specific roles. Our idea was to design these regions independently and to make patient adaptation easier. With our method, the complexity modelling can be configured for each region using solely a functional approach and considerably fewer parameters (Table 1). A highly frictional surface of a bone must be carefully designed and faithfully reflect the real geometry because not only the kinematic behavior, but also the wear behavior and the force transmission will be affected. An osseous groove that let the passage of a tendon does not require such fidelity of the geometry.

For our trapezium replacement example, three anatomical regions were defined, each having its own desired level of complexity (Table 1).

A first configurable model was created on single trapezium by positioning points according to Table 1 specifications on the 3D volumetric model from medical image data, splines were thereafter designed with additional vectors (magnitude and direction) and finally surfaces were

Table 1. Design complexity assessment depending on the degree of functionality of segmented areas.

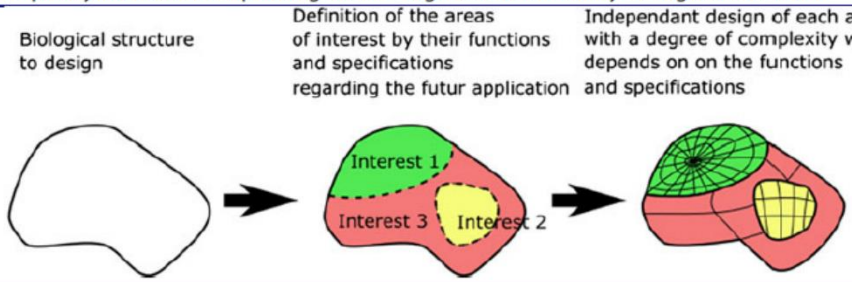


Trapezium bone example for a further implant design adapted to additive manufacturing

| Structure of interest | Specifications and functions | Required complexity | Number of designed points per area ($cm^{-2}$) |
|---|---|---|---|
|  Trapezo-metacarpal joint contact | Highly cinematic contact surface with concavo-convex curvatures; Force transmission; No subluxation complication | High | 17.77 |
|  Trapezoïd-2nd metacarpus-scaphoïd joint contact | Highly stabilization surface contact; Force transmission low cinematic area | Medium | 5.20 |
|  Global shape | Defined global shape; Sufficient surface for prosthetic and manufacturing elements | Low | 2.78 |

designed from edge curves. Configurability of each region is therefore possible by moving each defined point in the 3-dimensional space with potential restrictions (e.g. a distance from a point, along a direction) and by modifying vectors (direction and magnitude).

### 2.2. Application on specimens

To test the configurability and the universality of the designed model we used four healthy trapezium bones removed from two diseased patients (males aged 61 and 66, left and right trapeziums). The bones were provided by the *Académie Nationale de Chirurgie* in Paris, and any evidence of pathology was reported by the surgeon. Specimens were stripped of cartilage and soft tissue, dried by immersion in acetone and underwent a fat-removal procedure. All the specimens were scanned with a clinical computed tomography (CT) (slice thickness of 0.625 mm and pixel size of 0.328 mm × 0.328 mm). Manual segmentation (3D Slicer® (Slicer.4.8)), with a threshold value suitable for extracting cortical bone (CT-AAA2: 129.54), was applied prior to the 3D reconstruction using discrete marching cubes with no iterations of smoothing (Lorensen and Cline 1987). 3D models were exported as STL files. The left trapeziums were mirrored, and all were scaled in order to make the distance between the center of the second metacarpal and the scaphoid contact surfaces correspond to an average value (16.846 mm).

The configurable model was thus fitted to the four trapeziums (Figure 2).

Distance deviation was measured using Hausdorff distances between the adapted configurable model and the reconstructed DICOM file. The Hausdorff distance $d_H(X, Y)$ of X and Y, two non-empty subsets of a metric space (M, d), is defined as follows:

$$d_H = max\{\text{supinf}d(x,y), \text{supinf}d(x,y)\}$$

Hausdorff distance analysis gives the shortest distance between each of the points defining a model and its corresponding point among those that define another model, known as the target. The result is often represented visually by a 3D model colorized by a distance correlation.

### 2.3. Voxelization and smoothing process

This paragraph describes the second step. The main objectives of this second process step are the following:

1. Transforming the model: from a number of different volumes a single watertight volume has to be obtained.

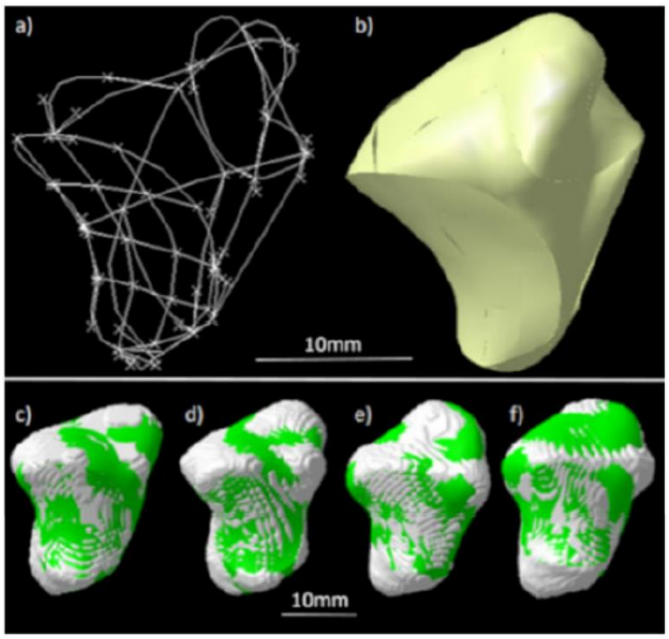


Figure 2. Adaptation of the configurable model on a set of 4 healthy trapezium bones: a) Curve and b) surface visualization of the configurable model of the trapezium, c) to f) from left to right: subject 1: right hand trapezium, left hand trapezium, subject 2: right hand trapezium, left hand trapezium.

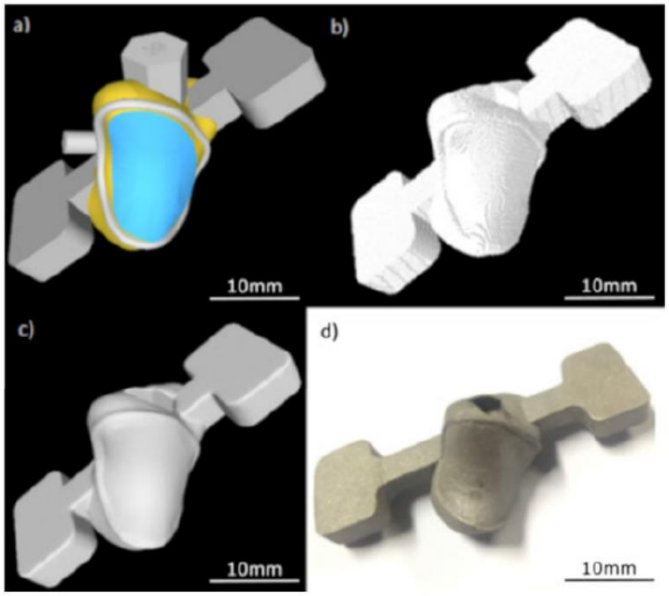


Figure 3. Process of implant design with Boolean operation and AM based on voxelization, a) Separated STL file, b) Boolean operation and Voxelization, c) Resulting smoothed numerical file (STL), d) AM sample by SLM technology.

2. Customizing the model to obtain a functional prosthesis through model manipulations (Boolean operations).
3. Smoothing the unrealistic continuity between surfaces (potentially sharp and thus unacceptable for a prosthesis) in the input patient-matched model.
4. Smoothing the jagged effect of the grid.
5. Obtaining a homogeneous meshed model containing no printability errors.

Independent regions are denoted as solids. Each solid is represented by one or a set of STL files. The decomposition of the model in the trapezium example is detailed above in §2.1 and §2.2. Each topological structure was exported as an STL file with a sufficient accuracy (average value: 8.3E + 04 faces/cm$^2$) to avoid the loss of design information. These STL files are input files for the voxelization process. The main idea is to create a

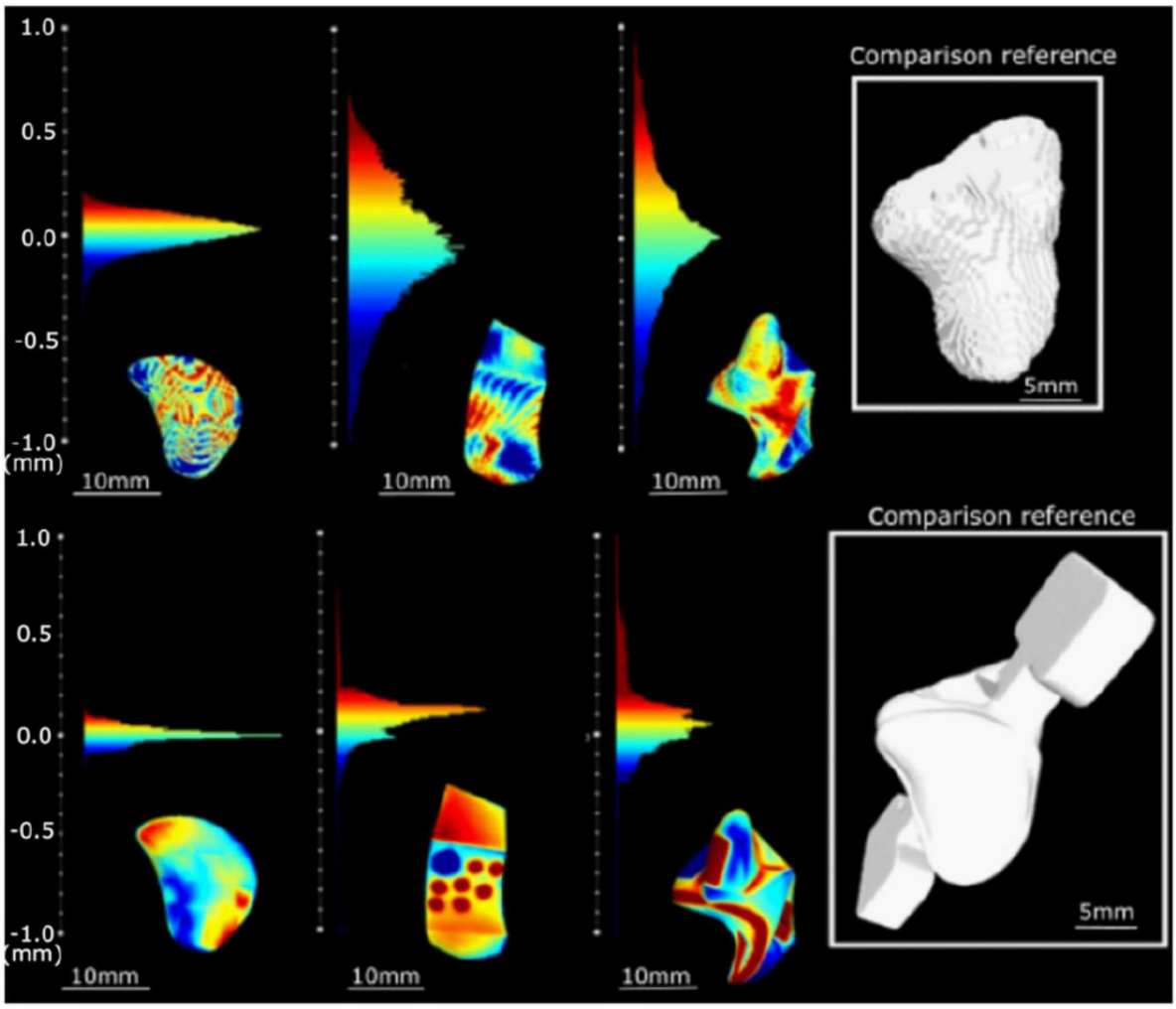


Figure 4. a) Excellent correspondence of the topological accuracy of each designed area with their defined accuracy specifications. Distance comparison with the bone of reference (segmented medical image) visualized by a range of color and histograms of the measured distance between sampled points of the right hand of subject 1. b) Distance comparison with the final triangulated 3D model (smoothed-voxel based representation).

voxelization of each volume. A voxel model displays a volume with a matrix of discrete digital blocks known as voxels. Voxel model are often designed by assigning a logic value to each voxel, indicating whether it is a solid space or a void space (Sobierajski et al. 1993). Topological operators such as the union of or the difference between voxelized objects can then easily be employed to build the final model. No continuous geometrical model is created. These kinds of topological operations cannot reliably be applied on STL meshes because of the complexity of the meshes (elongated elements, high number of elements coincident to a node, non-conforming meshes in each edge of the mesh may not be connected to 2 triangles). STL files are gathered into sets which constitute a solid. The process of voxelization from triangles is detailed in Huang et al. (1998). Once the procedure has been carried out for each volume, topological operators can be employed. In the trapezium example, a Boolean operation was performed to functionalize the trapezium model into a prosthesis (Figure 3). The jagged effect of the grid is then smoothed by a Catmull-Clark (Catmull and Clark 1978) procedure in which only vertices are updated and no additional face nodes are added, which means that no additional nodes are created. In order to reduce the effect of shrinkage in areas of high curvature variations, an 'inflate and shrink procedure' as described by Taubin (1995) is used (Figure 3). The goal is to control the distance between the original STL mesh and the smoothed model. This distance does not exceed the size of one voxel. Even though sharp edges are smoothed, the voxelization process can be done with a level of accuracy that provides an acceptable model for additive manufacturing. Following this, quadrangles are split into triangles and a global STL mesh is created. The resulting conforming mesh is suitable for numerical calculus (finite element analysis). In addition,

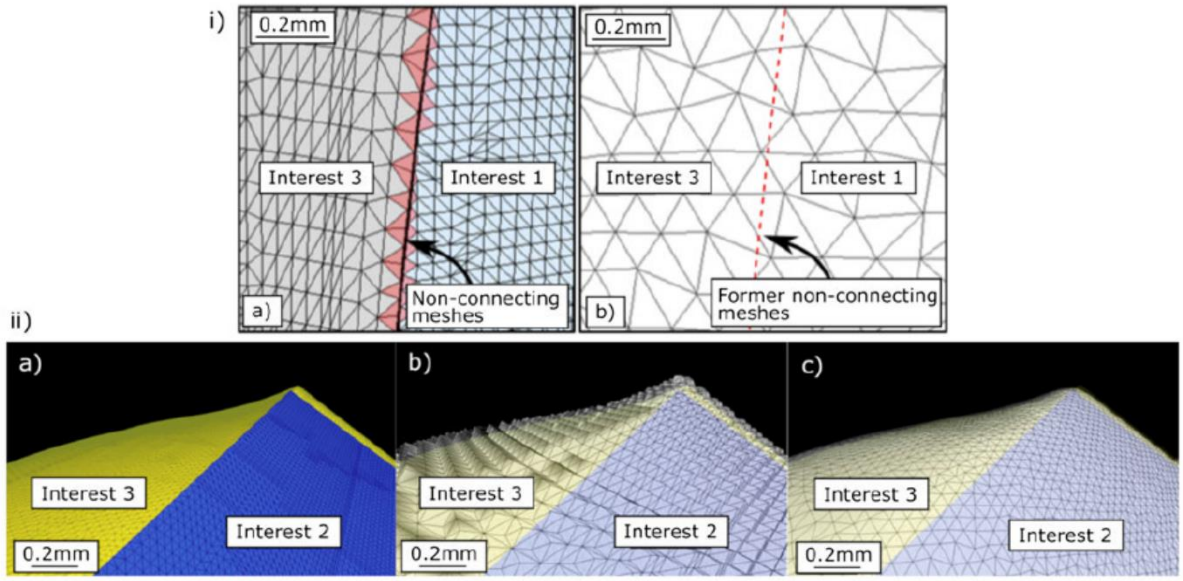


Figure 5. Excellent 3D mesh model guarantied with no-self-intersection, non-manifold edges and a homogeneous mesh. a) presence; i): a) Visualization of a mismatched and non-connecting triangles of the meshes; b) closed mesh after the voxel-based and smoothing process, ii) visualization of the process; a) Extracted meshed files from the different segmented areas of the configurable model; b) Voxelization process of the structure; c) Final numerical stage structure smoothed by a Catmul filter.

the process allows thin gaps or intersections between solids (STL) where the size of the gap is less than the size of a voxel, which facilitates geometrical modelling. In our example, given the accuracy of the medical imaging used and given that the largest gap detected was 0.01 mm (Figure 4), we chosed a voxel width of 0.175 mm.

The simplicity of the designed surfaces means a potential unrealistic continuity between surfaces in the input patient-matched model. The smoothing process was therefore necessary, not only to smooth the cubic shape of the voxels, but also to make the model more anatomically realistic.

Distance deviation was measured using Hausdorff distances between the final meshed file and the adapted configurable model.

## 3. Results

Deviations may occur during any of the steps in the design process. As an example, to illustrate potential deviation that may occur, we analyze data relating to the right trapezium of the first subject.

### 3.1. Surface quality of the topological structures

There were marked differences between the adapted configurable model and the reconstructed DICOM file (Figure 3). However, every distinctly designed region attained its respective specified level of detail. Distance analysis done using 3D mesh processing software system (MeshLab 2016) shows that the greatest distances were 0.35 mm (Figure 3) for 'interest 1'. The mapping of deviations (Figure 3) featured a pattern of blue and red colors that were evenly distributed as a result of the digitized layer-by-layer medical image. Given the slice thickness of 0.625 mm that we used, the level of detail attained may be considered as excellent. The deviation mapping of the anatomical regions 'interest 2' and 'interest 3', gave the greatest differences, being respectively 2.5 and 3 times as large (Figure 3).

### 3.2. Mesh quality of the smooth voxel-based structure

Comparative deviation inspection was also performed between the designed anatomical regions and the final triangulated mesh after the voxelization and smoothing process. The color mapping was not uniform because of the presence of prosthetic elements, resulting in high values (sharp blue and red colors) (Figure 4b). The non-affected areas had a distribution deviation ranging between ±0.15 mm (Figure 4b), which is less than the slice thickness of the medical imaging.

Deviations were to be expected, because the voxelization and smoothing process were also intended to make the biomechanical model more realistic by smoothing the unrealistic continuity between surfaces resulting from the relatively simple configurable model (Figure 5).

When distinct regions are designed independently there will be gaps (Figure 5i), which is unsuitable for

AM. The voxel-based approach resulted in a single homogeneous triangulated mesh after the smoothing filter (Figure 5). All printability issues relating to the intermediate files are thus no longer a concern (Figures 3 and 5a).

## 4. Discussion

If users lacking specialist CAD skills (for example, healthcare workers) are to create complex digital files for printing with any degree of accuracy, constraints need to be reduced to a minimum. Closing boundaries makes the modelling considerably more complex, but this is an unequivocal condition for printability. Poisson Surface Reconstruction is an effective way of closing gaps in triangulated mesh files (Kazhdan and Hoppe 2013). However, if the dataset of points is particularly disconnected, a volumetric voxel-based approach can be a valuable alternative. Voxelization has already been used to represent solids obtained from CT and MRI scans (Tiede et al. 1998). Using voxelization for AM is however less common (Doubrovski et al. 2015), given that voxelization still requires considerable computer power, and voxel-based sculpting is not yet highly developed, making it difficult to get rid of the B-rep modelling prior to the process.

Using a voxel-based approach coupled with a smoothing filter has two purposes. First, to effectively render the model free of self-intersection and manifold edges by having a single homogeneous mesh particularly suitable for AM. Second, to give the simply designed model a more anatomically realistic shape. The voxel-based representation also makes customization easier using topological operations, so designing an implant can become quite straightforward. The triangulated 3D model is also suitable for finite element analysis, once voxels are split into tetrahedrons.

The most commonly used algorithm for medical image segmentation is thresholding. However, threshold values for specific tissues are possibly error-prone. In our case, since the voxel width was 0.328 mm, an error of three voxels corresponds to a deviation of 1 mm. This problem was not considered in the scope of the work. We obtained our DICOM using a precise (and commonly used) parametrization of a CT scan in order to demonstrate the actual pros and cons and to avoid the constraint of changing medical imaging standards. However, much more precise medical imaging parametrizations exist that would have allowed a more accurate model.

The manual adaptation of the function-based configurable model requires user experience (e.g. knowledge of anatomy), which can be a potential source of errors.

The design approach described in this manuscript emerged from an individual case study involving a trapezium replacement prosthesis. Further study will be required to determine whether this method can be extended to other types of implants.

Errors may also be found during the manufacturing process, particularly in the AM and the finishing processes. Thus, further research is undoubtedly required.

## 5. Summary

This article presents a quick, reliable procedure, accessible to non-specialists, for obtaining a configurable numerical model from biomedical data, a model suitable for functionalization and AM. The proposed procedure relies on a reduced parametrization based on an independent functional design of distinct regions and a voxel-based process. The main advantage of the configurable model is its ability to palliate a lack of information in the raw medical imaging data, as well as a deformed morphology that may be caused by diseases such as osteoarthritis. The voxel-based approach transforms the distinct regions into a single structure and allows additional topological operations. In combination with a simple smoothing process, it yields a homogenous triangulated model containing no printability errors and makes the simply configurable model more anatomically realistic in shape.

In the case of a trapezium replacement prosthesis design, this method proved to be reliable and time-efficient.

**Conflict of interest:** The authors report no conflict of interest, financial or otherwise.

## Funding

The research leading to these results received funding from the French Agence Nationale de la Recherche (ANR-11-IDEX-0004-02 under the "Sorbonne Universités" Idex) through an IUIS project for the promotion innovation in healthcare.

## ORCID

Augustin Lerebours http://orcid.org/0000-0003-0124-5627

## References

Arabnejad S, Burnett Johnston R, Pura JA, Singh B, Tanzer M, Pasini D. 2016. High-strength porous biomaterials for

bone replacement: a strategy to assess the interplay between cell morphology, mechanical properties, bone ingrowth and manufacturing constraints Acta Biomater. 30:345–356.
ASTM. 2012. Standard terminology for additive manufacturing technologies. West Conshohocken (PA): ASTM International.
Barone S, Casinelli M, Frascaria M, Paoli A, Razionale AV. 2016. Interactive design of dental implant placements through CAD-CAM technologies: from 3D imaging to additive manufacturing. Int J Interact Des Manuf. 10(2): 105–117.
Catmull E, Clark J. 1978. Recursively generated B-spline surfaces on arbitrary topological meshes. Comput Aid Des. 10(6):350–355.
Caudillo M, Herrera-Trejo M, Castro MR, Ramírez E, González CR, Juárez JI. 2002. On carbide dissolution in an as-cast ASTM F-75 alloy. J Biomed Mater Res. 59(2): 378–385.
Doubrovski EL, Tsai EY, Dikovsky D, Geraedts JMP, Herr H, Oxman N. 2015. Voxel-based fabrication through material property mapping: a design method for bitmap printing. Comput Aid Des. 60:3–13.
Emmelmann C, Scheinemann P, Munsch M, Seyda V. 2011. Laser additive manufacturing of modified implant surfaces with osseointegrative characteristics. Phys Procedia. 21:375–384.
Gao W, Zhang Y, Ramanujan D, Ramani K, Chen Y, Williams CB, Wang CCL, Shin YC, Zhang S, Zavattieri PD. 2015. The status, challenges, and future of additive manufacturing in engineering. Comput Aid Des. 69: 65–89.
Jense GJ. 1989. Voxel-based methods for CAD. Comput Aid Des. 21(8):528–533.
Huang J, Yagel R, Filippov V, Kurzion Y. 1998. An accurate method for voxelizing polygon meshes. IEEE Symposium on Volume Visualization; p. 119–126.
Huang P, Wang C, Chen Y. 2013. Intersection-free and topologically faithful slicing of implicit solid. J Comput Inf Sci Eng. 13(2):021009.
Huotilainen E, Jaanimets R, Valášek J, Marcián P, Salmi M, Tuomi J, Mäkitie A, Wolff J. 2014. Inaccuracies in additive manufactured medical skull models caused by the DICOM to STL conversion process. J Cranio Maxill Surg. 42(5):259–265.
Kazhdan M, Hoppe H. 2013. Screened Poisson surface reconstruction. ACM Trans Graph. 32(3):1.
Lethaus B, Poort L, Böckmann R, Smeets R, Tolba R, Kessler P. 2012. Additive manufacturing for microvascular reconstruction of the mandible in 20 patients. J Craniomaxillofac Surg. 40(1):43–46.
Liacouras P, Garnes J, Roman N, Petrich A, Grant GT. 2011. Designing and manufacturing an auricular prosthesis using computed tomography, 3-dimensional photographic imaging, and additive manufacturing: a clinical report. J Prosthet Dent. 105(2):78–82.
Lorensen WE, Cline HE. 1987. Marching cubes: a high resolution 3D surface construction algorithm. ACM Siggraph Computer Graphics.
Mäntylä M. 1987. An introduction to solid modeling. New York (NY): Computer Science Press, Inc.
Mohammed MI, Cadd B, Peart G, Gibson I. 2018. Augmented patient-specific facial prosthesis production using medical imaging modelling and 3D printing technologies for improved patient outcomes. Virtual Phys Prototyp. 13(3):164–176.
Pradel P, Zhu Z, Bibb R, Moultrie J. 2018. Investigation of design for additive manufacturing in professional design practice. J Eng Des. 29(4–5):165–200.
Rengier F, Mehndiratta A, von Tengg-Kobligk H, Zechmann CM, Unterhinninghofen R, Kauczor H-U, Giesel FL. 2010. 3D printing based on imaging data: review of medical applications. Int J Comput Assist Radiol Surg. 5(4):335–341.
Sobierajski L, Cohen D, Kaufman A, Yagel R, Acker DE. 1993. A fast display method for volumetric data. Visual Comput. 10(2):116–124.
Taniguchi N, Fujibayashi S, Takemoto M, Sasaki K, Otsuki B, Nakamura T, Matsushita T, Kokubo T, Matsuda S. 2016. Effect of pore size on bone ingrowth into porous titanium implants fabricated by additive manufacturing: an in vivo experiment. Mater Sci Eng. 59:690–701.
Taubin G. 1995. Curve and surface smoothing without shrinkage. IEEE International Conference on Computer Vision; p. 852–857.
Tiede U, Schiemann T, Hohne KH. 1998. High quality rendering of attributed volume data. Visualization'98. Proceedings of IEEE Conference on Visualization.
Tunchel S, Blay A, Kolerman R, Mijiritsky E, Shibli JA. 2016. 3D printing/additive manufacturing single titanium dental implants: a prospective multicenter study with 3 years of follow-up. Int J Dent. 2016:1–9.
Wang X, Xu S, Zhou S, Xu W, Leary M, Choong P, Qian M, Brandt M, Xie YM. 2016. Topological design and additive manufacturing of porous metals for bone scaffolds and orthopaedic implants: a review. Biomaterials. 83:127–141.
Zadpoor AA, Malda J. 2017. Additive manufacturing of biomaterials, tissues, and organs. Ann Biomed Eng. 45(1):1–11.

# Article 3:

# Numerical method to rejuvenate highly deformed bones for a prosthesis design and additive manufacturing. Case study: the trapezium bone

Augustin Lerebours [1], Alain Rassineux [1], Frederic Marin [3], Salima Bouvier [1],

Alain-Charles Masquelet [2], Christophe Egles [2]

[1]*Alliance Sorbonne Universités, Université de technologie de Compiègne, CNRS, FRE 2012 Roberval, Centre de recherche Royallieu, CS 60 319, 60 203 Compiègne cedex, France*

[2]*Alliance Sorbonne Universités, Université de technologie de Compiègne, CNRS, UMR 7338 BioMécanique et BioIngénierie (BMBI), Centre de recherche Royallieu, CS 60 319, 60 203 Compiègne cedex, France*

[3]*Orthopaedic, Trauma, and Hand Surgery, Saint Antoine Hospital Paris France*

**Submitting for the journal of Computer Methods in Biomechanics and Biomedical Engineering (*Research article*)**

**CORRESPONDING AUTHOR**

Augustin LEREBOURS
Alliance Sorbonne Universités, Université de technologie de Compiègne,
CNRS, FRE 2012 Roberval,
Centre de recherche Royallieu,
CS 60 319,
60203 Compiègne cedex,
France
augustin.lerebours@utc.fr
Phone +33658019946

**Abstract**

Some pathologies deform bones irreversibly which affect their associated functions such as a bone's resistance to daily stresses, as well as adversely affecting its stability and kinematics. In this work was developed a numerical guideline to "rejuvenate" deformed bones in a consistent CAD framework requiring a minimum set of computer-aided design tools. It allows us to design numerical models adapted to the design of patient-specific implants and to additive manufacturing technologies. The process consists of different steps including (i) the creation of a reduced configurable model that matches the patient's data, (ii) the rejuvenation deformed zones, (iii) Boolean operations to implement functional elements and (iv) the adaption of the model to additive manufacturing systems by a voxel-based method. The last step guarantees a watertight triangular meshed model without any printability errors.

This work focuses on the numerical "rejuvenation" of trapezium bones at advanced osteoarthritic stage, to get a numerical model for the design of a patient-specific carpometacarpal implant (CMC) which is adapted to additive manufacturing. In addition, the rejuvenation process provides a clear overview of the arthritic deformation of the trapezium that occurred specifically for each patient. The location of preferential wear was seen to be in the volo-ulnary quadrant.

**Keywords**

Computer-assisted rejuvenation; Trapezium; Prosthesis; additive manufacturing; voxel-based method; arthroplasty, carpometacarpal joint; osteoarthritis,

# Introduction

Bone are known to adapt to stress and strain by remodeling i.e Wolff's law making the morphology “topologically optimized” specifically for each people [1]. However, among pathologies, some deform bones irreversibly affecting the associated functions i.e. withstand daily stresses, while keeping its stability and movement ability. Osteoarthritis (OA) is a common pathology which affect particularly the bones of the hand [2]. The geometric features of OA include the development of osteophytes and subchondral cysts [3]. Erosion of the osseous articular surfaces occurs after a complete loss of cartilage which causes changes in the topology of the joint which alter the joint alignment [3]. At an advanced stage, articular surfaces become extremely distorted with a collapse in the subarticular region [3]. The alteration of the joint axes affects negatively the load transmission and thus decrease the maximal force that can be applied [3].

Surgical treatments for such pathologies often involve the implantation of a prosthesis aiming to replace partially or entirely the bone(s) affected. However, every bone has a unique shape and condition, the dissimilarities of shape among people are particularly significant for small bones [4]. Most manufacturers’ solution for compensating this variation of shape is to create a range of standard implants with modular parts. This solution has been chosen mostly because of the subtractive machining technologies which are beneficial for large and identical series. However, depending on the level of experience of the surgeon, it may result in an inaccurate size and positioning of the implant leading to implant failures [5–7].

Additive manufacturing (AM) technologies are currently improving upon this limitation by allowing complex internal and external shapes of implants with various biocompatible materials [8]. Patient-matched solution therefore seems a tenable way to respond to these clinical complications [9].

Many anatomical Computer-assisted-design (CAD) model reconstruction guidelines have been proposed, however most methods are time-consuming employing manual interactions which require specific CAD skills to be performed [10]. In general, anatomical structure is numerically reconstructed through either segmentation or volumetric representation from medical imaging [11]. Some studies have developed automatic reconstruction procedures without any manual operations [12] particularly with the emergence of statistical shape models [13]. As bone shape is affected by some pathologies, the configurability of the model for a further “rejuvenation” need to be integrated in the CAD framework, just as additive and subtractive operators i.e. Boolean

operators and AM adaptation i.e. water-tight triangulated mesh must also be integrated. Some studies have touched upon numerical restoration process of anatomical structure for prosthesis surgery. The procedure is mainly based on computer mirroring techniques, mostly applied for maxillofacial implants [14,15]. It implies that the symmetric part has not been morphologically deformed by a specific pathology.

With new Food and Drug administration (FDA) guidelines for the technical consideration of AM medical devices [16] and the clearance of several AM implants by the Center for Devices and Radiological Health (CDRH) [17], more time-effective numerical methods for the conversion of medical image data such as computer tomography scan or magnetic resonance imaging, to patient-matched numerical model adapted to AM need to be developed. Moreover, methods specifically adapted for non-CAD skilled specialists need also to be considered.

The main goal of this work is to develop a comprehensible numerical method for the "rejuvenation" of deformed bones in a consistent CAD framework for additive manufacturing. It enables us to create an accurate model adapted for the design of patient-matched implants adapted to AM from medical image data. The framework used is based on voxel representation. This work focus on the numerical "rejuvenation" of trapezium bones with advanced osteoarthritis stage, to get a numerical model that allows the design of a patient-specific carpometacarpal (CMC) implant. CMC patient-matched implant for palliating osteoarthritis has been studied because (i) the trapezium bone presents highly functional and complex morphology with some areas involved largely in the stabilization of the bone, (ii) osteoarthritis deformed irreversibly the trapezium bone while having a significant morphology's variability [18,19] and (ii) all the current designed implants present high rate of revision [20–22].

## Materials and methods

The CAD framework concept used [23] is presented in the Figure 1. It is composed of four main steps which are:

- Creation of a configurable model (B-spline) with a reduced number of parameters that matches the patient's data.
- Rejuvenation of the deformed zones
- Boolean operations (additive and subtractive) for implementing functional elements in a voxel-based representation
- Additive manufacturing adaptation of the model

This CAD framework allows us to easily “rejuvenate” anatomical structure for AM-based implants which will be described through the case study of osteoarthritic trapezium bones.

Geometrical morphological variability was first studied and then used to investigate the numerical method for restoring deformed anatomical structures.

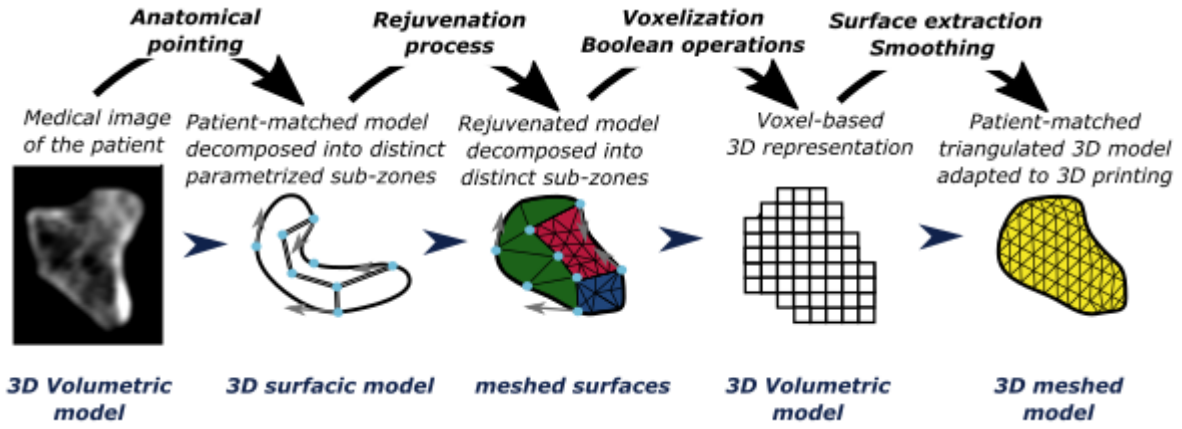


**Figure 1**: CAD Framework for the design of a patient-match implant adapted to additive manufacturing

**Specimens**

The geometrical variability and the pathological deformation studies were focused on the trapezium bone. Therefore eight trapezium bones were excised from cadavers, cleaned and dried by a fat-removal procedure and then 3D digitalized by a CT-scan (GE lightspeed VCT, 0.625mm slice thickness and 0.328x0.328mm$^2$ pixel size, cortical bone thresholding value (3D Slicer®)). Half of them were not diagnosed with advanced osteoarthritis stages (Table 1 and Fig.2). Left hand trapezium bones were mirrored, and all trapezium bones were scaled so that the distance between the center of the 2$^{nd}$ metacarpal and the scaphoid correspond to an average value (16.846mm). This allows us to avoid bias due by size during the examination of the articular surfaces (1$^{st}$ metacarpal (M1), trapezoid (TPZ), the scaphoid (SCP) and the 2$^{nd}$ metacarpal (M2).

**Preprocessing: patient-match configurable modelling**

The main objective of this process is to transform the medical image data into a configurable numerical model that kickstarts the “rejuvenation” process by recovering anatomical deformation.

**Table 1**: Description of the specimens

| Name | Subject | sex | Age | Left/Right | Condition |
|---|---|---|---|---|---|
| RT1 | Patient 1 | Male | 61 | Right | Healthy state |
| LT1 | | | | Left | Healthy state |
| RT2 | Patient 2 | Male | 66 | Right | Healthy state |
| LT2 | | | | Left | Healthy state |
| RT3 | Patient 3 | Female | 91 | Right | Advanced OA (Eaton III-IV): absence of cartilage tissue). Presence of large osteophytes (osseous excrescence) which blocked the trapezo-metacarpal joint particularly on the ulno-volar quadrant. |
| LT3 | | | | Left | |
| RT4 | Patient 4 | Female | 75 | Right | Advanced OA (Eaton III-IV) / Chondrapathy (cartilage damage) and large osteophytes |
| LT4 | | | | Left | |

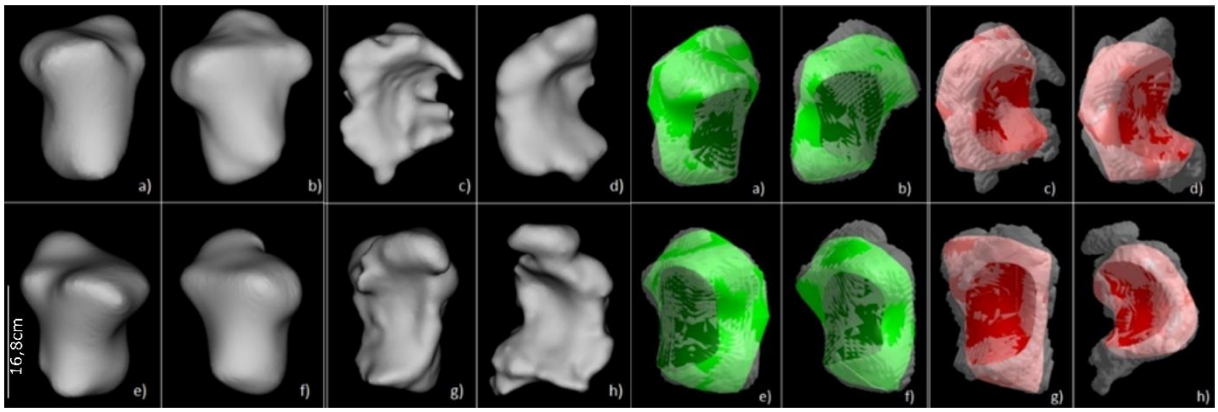


**Figure 2**: (i) OA pathology of the excised trapezium bones from deceased bodies (<15 days). Numerical visualization after computed tomography. a), e) & b), f) Trapezium of subject 1 (RT1 & LT1) and subject 2 (RT2& LT2). c) & g) Trapezium bones subject 3 (RT3 & LT3) with an advanced OA stage d) & h) Trapezium bones of subject 4 (RT4 & LT4) (ii) Patient-matched configurable model of both healthy (green) and OA (red) trapezium bone. Size normalized (Length defined by both center of SCP and M2: 16.846mm (average value))

A model was designed with Boundary representation (B-rep) techniques. Thus model featured configurable points at anatomical or geometrical location which may be easily adapted from one person to another. It was also designed to have the least and sufficient number of configurable points and vectors to rapidly reconstruct the deformed area [23]. The different articular surfaces were distinctly designed with a number of parameters

dependent on both the geometrical complexity and the specification of a further CMC implant (M1: 17.77 points/mm$^2$, M2-SCP-TPZ: 5.20 points/mm$^2$) [23]. The configurable model was applied on the eight trapezium bones (Fig.2). It was facilitated by the higher relative absolute curvature of the articular boundaries than articular surfaces[24].

**Morphological examination**

We extracted a set of parameters to study the morphology and the orientation of the articular surfaces of each patient matched configurable model:

- Areas of the articular surfaces;
- Angle between the plane of the articular surfaces;
- The ratio between the length defined by the center of gravity of SCP and a defined point of M1, and the elongation of this length until the plane of M1;
- Concave curvature along the ulno-radial direction and convex curvature along the volo-dorsal direction (defined by an interpolation of the maximum of concave/convex curvature). The concave curvatures were measured at three locations: (i) center of the volar side, (ii) maximum curvature, (iii) center of the dorsal side, on 19 curves. Similarly the convex curvatures were measured at three locations: (i) center of the ulnar side, (ii) maximum curvature, (iii) center of the radial side, on 19 curves

**Numerical rejuvenation of the osteoarthritic subjects**

Through the pathology, osteophytes and osseous depletions are developing around M1, making it difficult to properly assess the edge of the articular surface. Some are occasionally discovered around the boundary of M2, SCP and TPZ. Furthermore, osteoarthritis affects also the specific concavo-convex curvatures of M1.

Thus, the specification of the rejuvenation procedure was designed to:

- withdraw any osseous defect (osteophytes and depletion)
- recover healthy concavo-convex curvatures of M1
- recover a good orientation of M1 regarding the other articular surfaces

The rejuvenating process is described in figure 3.

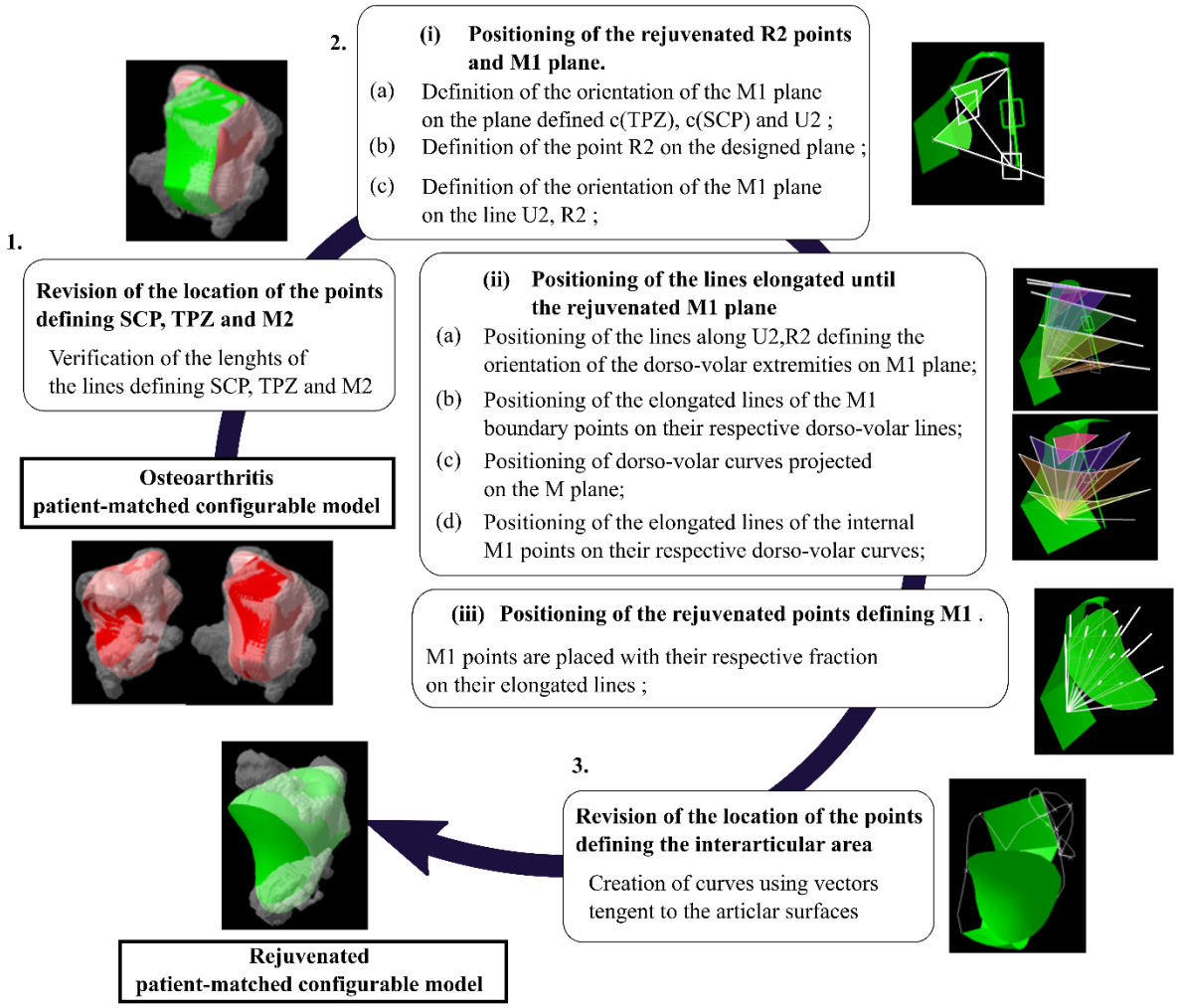


**Figure 3**: Procedure of the numerical trapezium rejuvenation

All the parameters described in figure 3 are configurable resulting in direct changes in the morphology of the numerical model as seen in figure 4.

**A smoothed voxel-based representation dedicated to Boolean operation and additive manufacturing**

At this point, the model requires modifications (i) to be anatomically more realistic, (ii) to be compatible with Boolean operations and (iii) to be a water-tight triangulated mesh with no printing errors.

STL (stereolithography) files are widely used for additive manufacturing processes. However, the configurable model at this step is a surface geometry of unstructured triangles constructed from a non-ideal data set. One major requirement of the process is necessary to provide a closed mesh, free of intersections, overlappings or gaps (printability errors). In addition, each edge of the conforming mesh must share two triangles exactly. One of the difficulties is not only to create a C0 continuous model

(closed) but also to connect the different surfaces with tangency conditions (C1) in order to avoid sharp edges in the mesh, what may require advanced CAD skills.

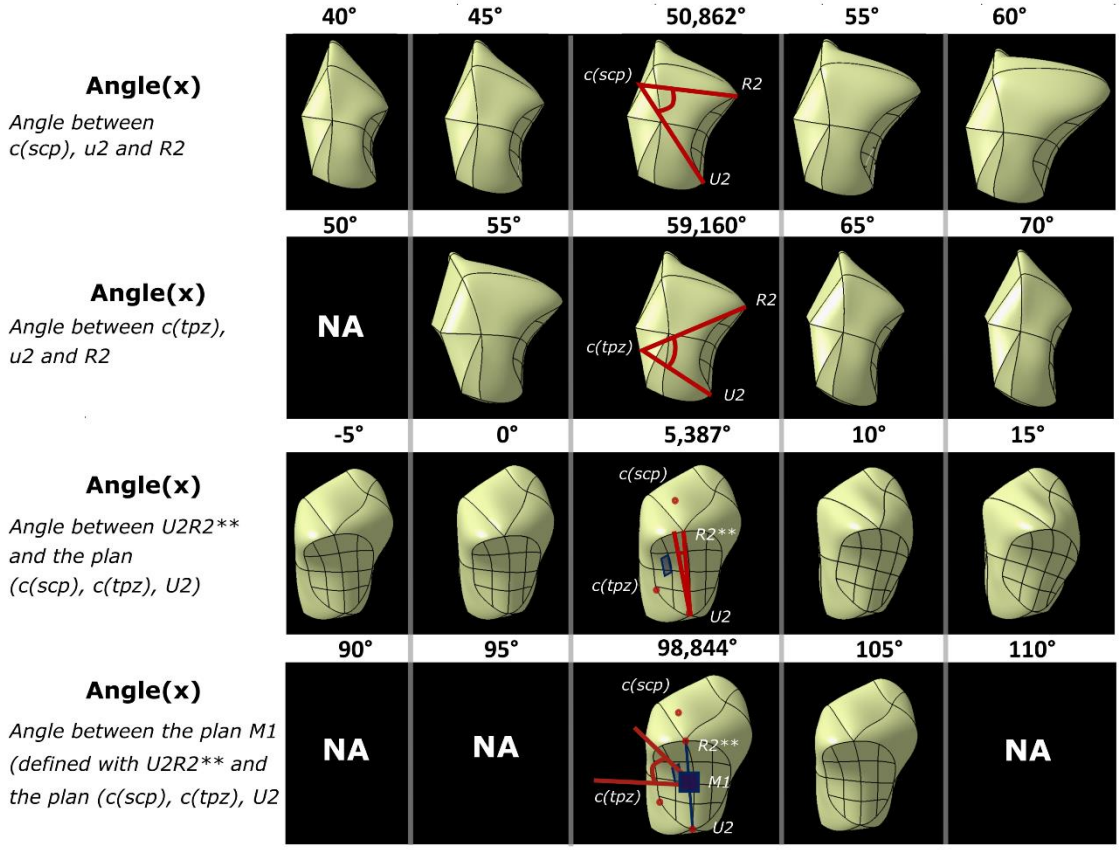


**Figure 4**: Evolution of the model with the variation of some configurable parameters

The process proposed here consist in the ability to integrate various geometrical data such as surfaces to create volume and elements which may be added to or subtracted from the final object. Surfaces may be created independently through surface modeling or obtained directly from a 3D image.

The first step of the process is to create an outer surface model from the assembly of these various data sets. All surfaces and volumes are converted into STL files and the outer surface is composed of triangles which are not necessarily connected and that may intersect (fig.5.a & a').

The approximation of these complex geometries consists in using a grid composed of voxels of configurable size as a model representation. The surface to represent can be given by the outer faces of the grid which provides a shagged effect. The object to represent is decomposed into volumes which must be added and volumes to be subtracted. The following process is performed for these two groups of objects.

In the first step, the initial data (triangles or points) are enclosed in a regularly spaced three-dimensional voxel grid which encloses the two groups of volumes. If a STL file is

provided, triangles are discretized using the element shape functions so that the maximum space between neighboring points does not exceed 10% of the chosen voxel size. Voxels which contain one point of the discretized STL files are identified (fig.5.b & b'). The input data is therefore a set a points. An empty voxel is chosen on the top of the grid and an advancing front algorithm based on face adjacency is applied to fill all cells around the object [25]. Inner voxels can be thereafter identified easily. In order to identify a closed volume of the outer surface, gap between surfaces must not exceed the size of one voxel. This constitutes the only requirement of the technique. Isolated voxels as well as unit layer of voxels are identified and removed. This enables to remove spurious voxels at the interface of adjacent and overlapping surfaces. At this step, the process allows Boolean operations as seen in fig. 5.a') to c') necessary for customizing the model in order to obtain a functional prosthesis.

The second step of the process consists of smoothing the shagged effect of the voxelized model and the unrealistic continuity between surfaces. We have applied here a standard Catmul-Clark algorithm in which no additional faces nodes or edge nodes are added but only vertices are updated (fig.5.c & c'). It is a subdivision technique [26] whose principle is to localize a point to a place calculated by a weighted combination of its neighbors' position. Therefore the connectivity of the mesh is unchanged. Repeated operations of such smoothing have a shrinkage effect of the mesh and a shrink and inflate procedure as described by Taubin [27] must be applied. In practice, 200 iterations were applied. The tangency between adjacent surfaces is ensured by the smoothing process leading to a more anatomically realistic model.

The final step consists in splitting the quadrangles into triangles with respect to a geometrical quality criterion. The numerical model is therefore composed of a homogeneous triangulated mesh (STL) closed which contains no printing errors for a further AM process.

# Results

### Inter-specimen analysis

Healthy condition

The morphological analysis of the healthy models highlights various aspects of the osseous variability.

After scaling, the healthy trapezium featured similar areas of the articular surfaces (Fig.6.a). However, the angles between articular surfaces were much more sensible to variation (± 5° around the average value) (Fig.6.b). The ratio of the distance of the points

featuring M1 by their elongated length to the M1 plan gave values with reduced variability among specimens (Fig.6.c-d). The concavo-convex patterns featured by these ratios translate and were therefore good configurable parameters for the rejuvenation process.

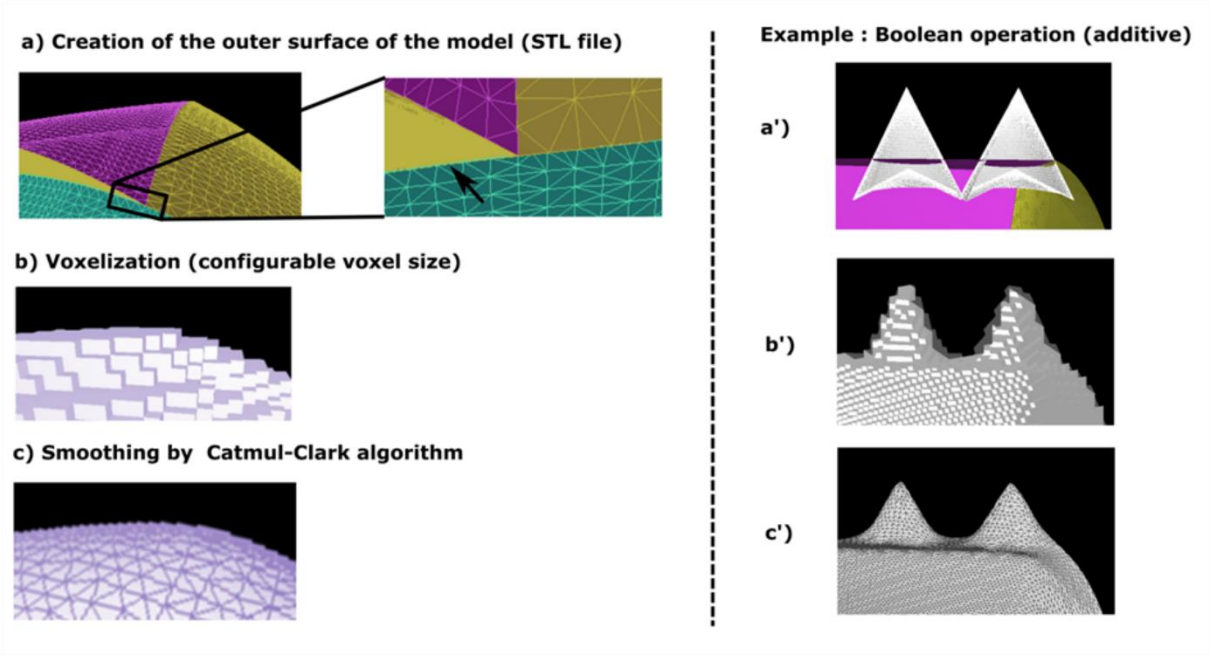


**Figure 5**: a) Unstructured triangulation of the outer surfaces that not necessarily connected, or/and that may intersect; b) Each triangle is discretized by a point in its center. A voxels is identifies if it contains at least one point. The result gives a set of voxels; c) Smoothing of the shagged effect of the grid by Catmul-Clark algorithm (200 iterations) followed by an inflation procedure and the splitting of the quadrangles into triangles. a') to c') Process management of boolean operations

The concave and convex curvatures varied along their respective centerlines. The concave curvature decreased uniformly along the ulno-radial line while the convex curvature, twice less pronounced, increases along the volo-dorsal line (Fig.6.a-b-e). The concave curvature was noticeably higher in the center than the dorsal and radial sides allowing the delimitation of both sides, whereas similar values were observed for the convex curves both at the sides (ulnar and radial) and at the centerline (Fig.7.f-g-j).

Osteoarthritic condition

The morphological analysis of the osteoarthritic models highlights the positioning and the degree of the deformations that have occurred during the pathology development.

The osteoarthritic trapeziums had larger M1 area which can be explained by the presence of osteophytes around the surface leading to overestimate the boundary of the surface. TPZ and SCP surfaces were more often subjected to osseous depletion leading to lower area estimation. The location of M2 near the osteophytes of M1 might also increase the

estimated area (Fig.6.a). Osteoarthritis also affected the relative orientation of M1 as lower angle were assessed with TPZ (-19°) and higher angle with SCP (+7°) (Fig.6.b).

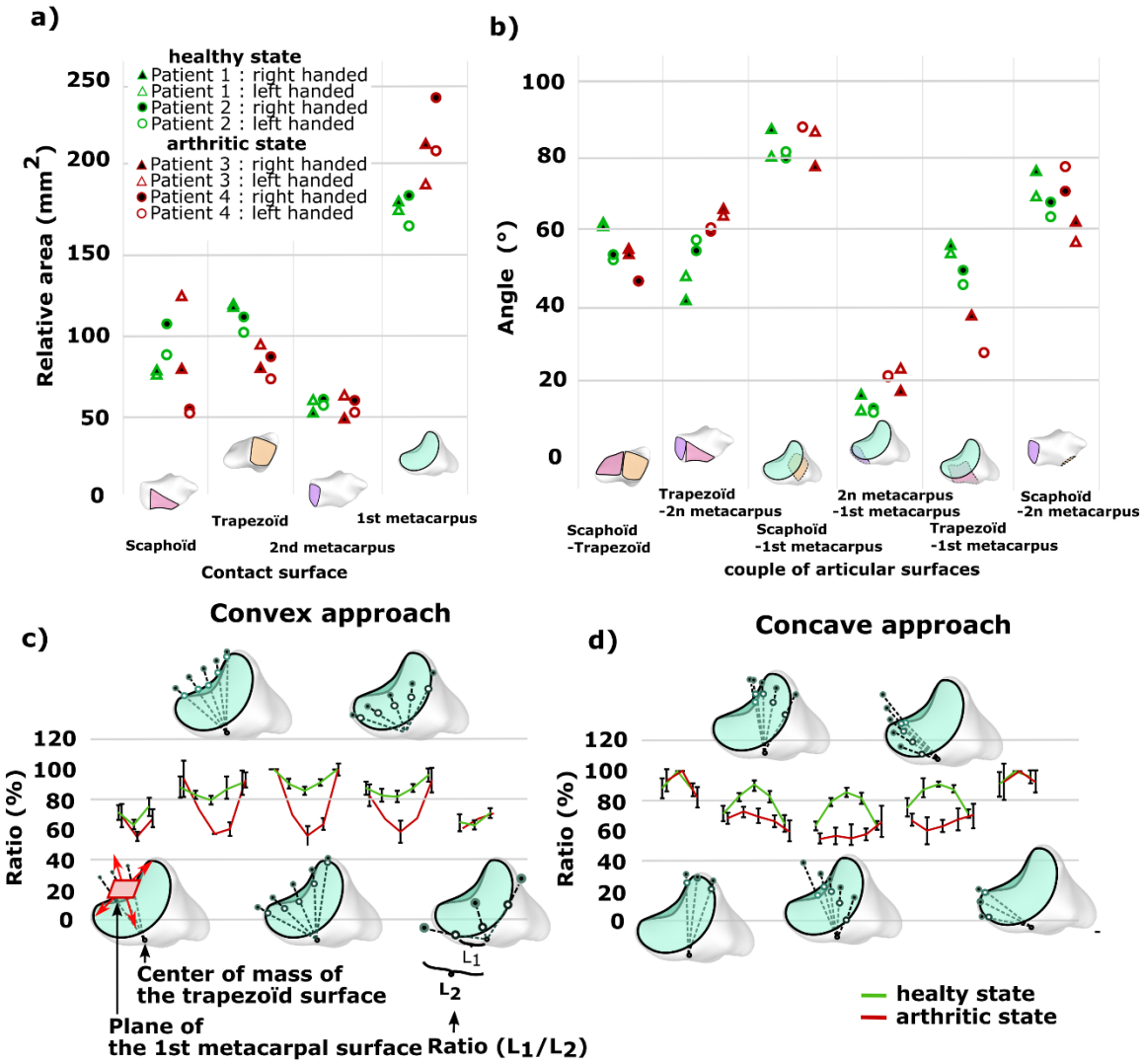


**Figure 6**: a) Articular area analysis b) Angle between articular surfaces analysis c) M1 Fraction analysis, a concave approach; d) M1 Fraction analysis, a convex approach; R: Right, L: Left, T: Trapezium, 1-4 : subject 1-4, blue : healthy bones, red : osteoarthritic bones.

Furthermore, the osteoarthritic trapeziums had highly different pattern of concavo-convex curvature (Fig.6.c.d and Fig.7). The concave curvature was close to zero and often negative in certain area featuring “dish” patterns. Only LT3 had a pronounced concave curvature close with healthy values in certain areas (ulno-dorsal and ulno-volar) which might indicate a less advanced stage of the disease (Fig.7.c-d-e). In all osteoarthritic trapeziums the sides (dorsal and volar) had distinct concave values compared to the centerline. The convex curvature was twice higher than the healthy trapezium and slightly

decrease from 0.2mm$^{-1}$ to 0.1mm$^{-1}$ with values on both sides (radial and ulnar) less pronounced than the centerline (Fig.7.h-i-j).

The volar quadrants had the highest difference of curvature, followed by volo-dorsal quadrant and the radio-dorsal quadrant. However, these indications alone are not sufficient to localize the preferential wear area of osteoarthritis.

**Rejuvenated specimen analysis**

The process of rejuvenation was applied on all osteoarthritic trapeziums with different sets of values. Figure 8 shows that all the rejuvenated models had (i) a removal of the osteophytes and osseous depletions, (ii) articular surfaces orientation similar to those of healthy trapezium, and (iii) M1 curvature similar to those of healthy trapeziums. The rejuvenated morphology is therefore significantly different from its arthritic stage, particularly the M1 articular surface regarding the concavo-convex curvature.

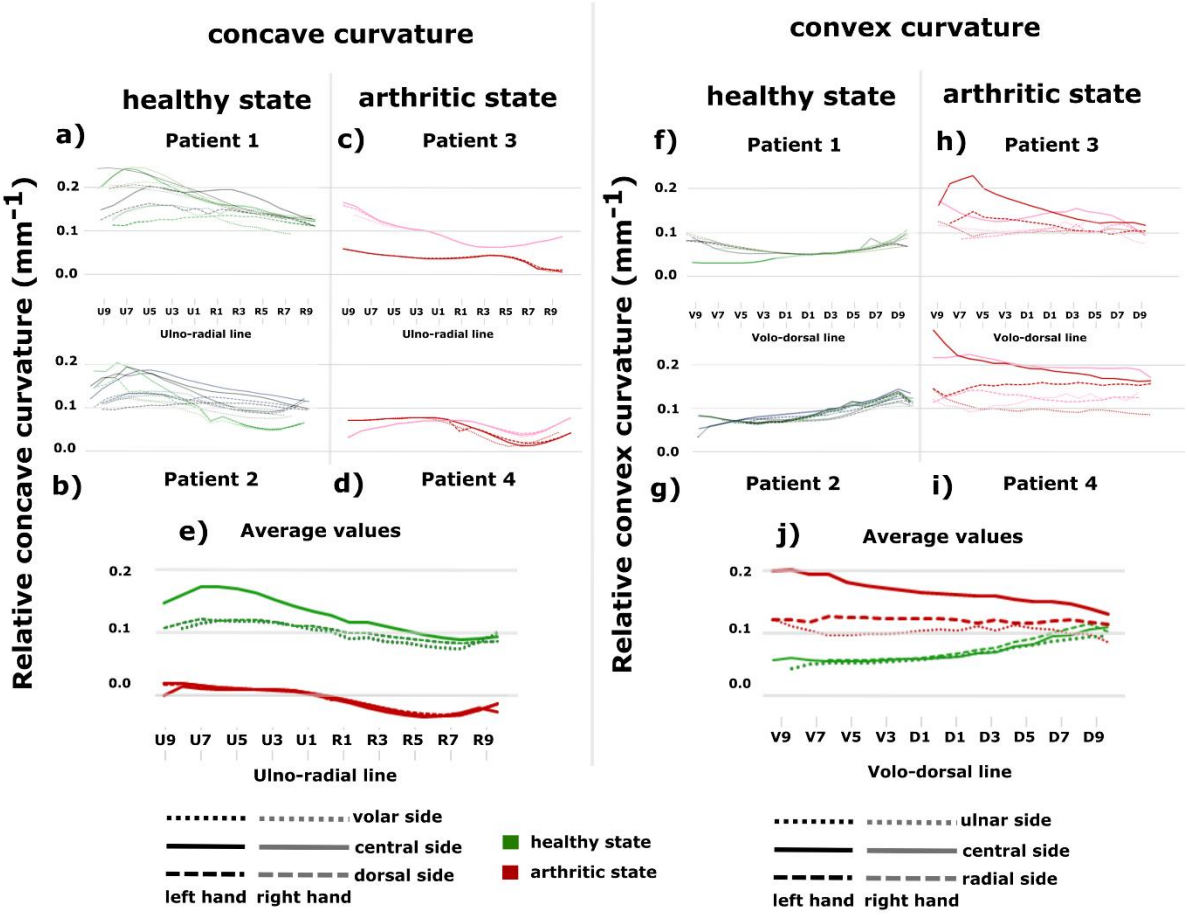


**Figure 7**: a) to d) Evolution of the relative concave curvature along the ulno-radial line (dashed line: volar side; full line: center; dotted line: dorsal side) and the convex curvature along the volo-dorsal line (dashed line: ulnar side; full line: center; dotted line: radial side Comparison of the left (dark blue) and right hand (light blue) trapezium bone for each subject.

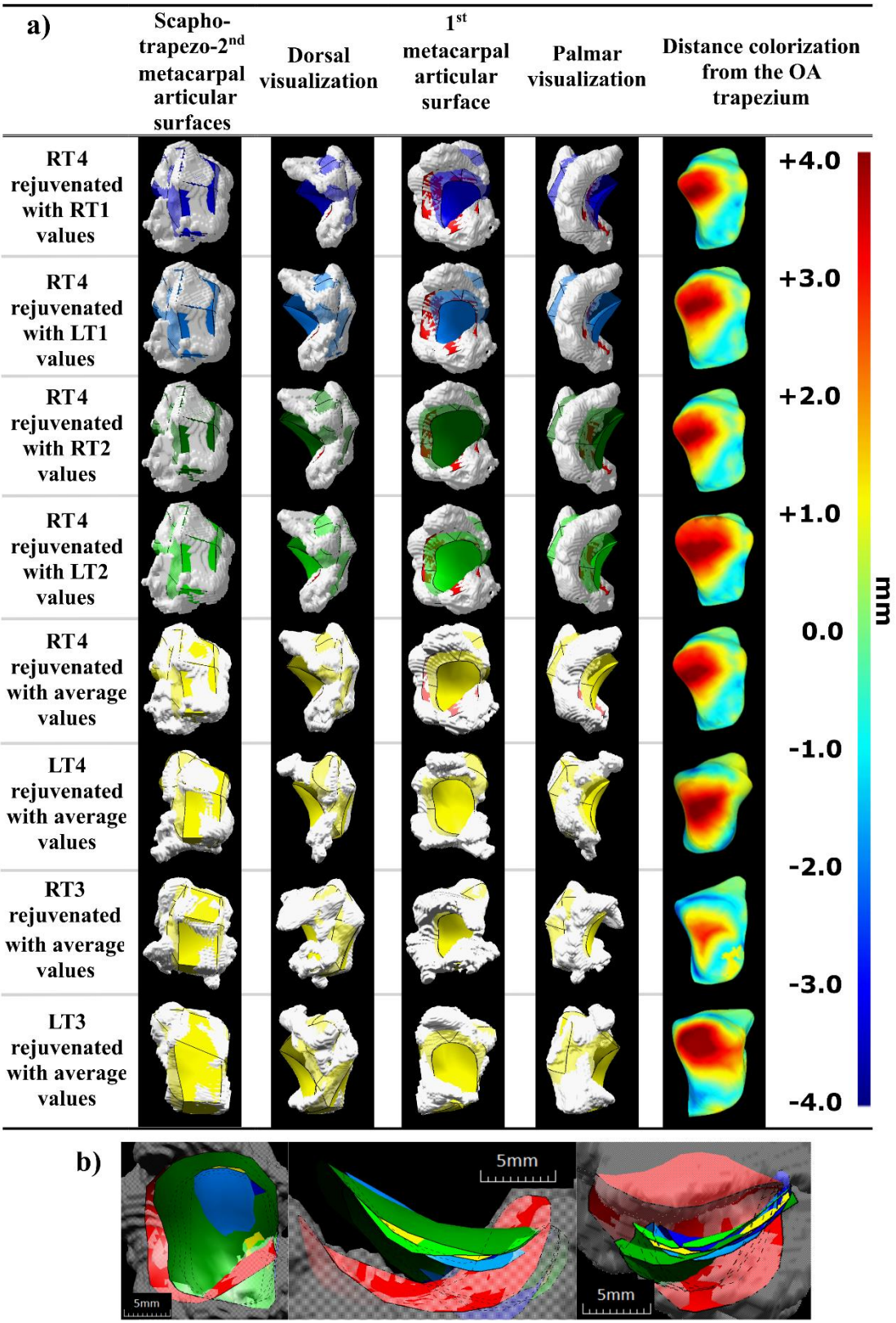


**Figure 8**: Rejuvenation of osteoarthritic trapeziums with different sets of values: dark blue: RT1; light blue: LT1; dark green: RT2; light green: LT2; yellow: average values. a) Global morphology and the rejuvenated bones and analysis of distance with the osteoarthritic trapezium of reference; b) zoom on the M1 rejuvenated surfaces from the RT4 osteoarthritic trapezium.

It allows us to visually understand the potential deformation that was caused by osteoarthritis. The analysis of distance of the rejuvenated bone with their respective original arthritic trapezium indicated that the VU quadrant was region that had the largest removal of osseous material, and the dorso-radial quadrant was often affected by osseous formation. The fact that all the rejuvenated M1 surfaces designed from a single arthritic trapezium were relatively close one to another although the sets of values were different indicates the robustness of the rejuvenation procedure (Fig.8). The verification of the concavo-convex curvature on the rejuvenated trapezium based on TR1 and TR2 values from the TR4 osteoarthritic trapezium indicated that all of the healthy curvature characteristics were recovered, and that the values were closed from their values of reference (RT1 and RT2) (Fig.9).

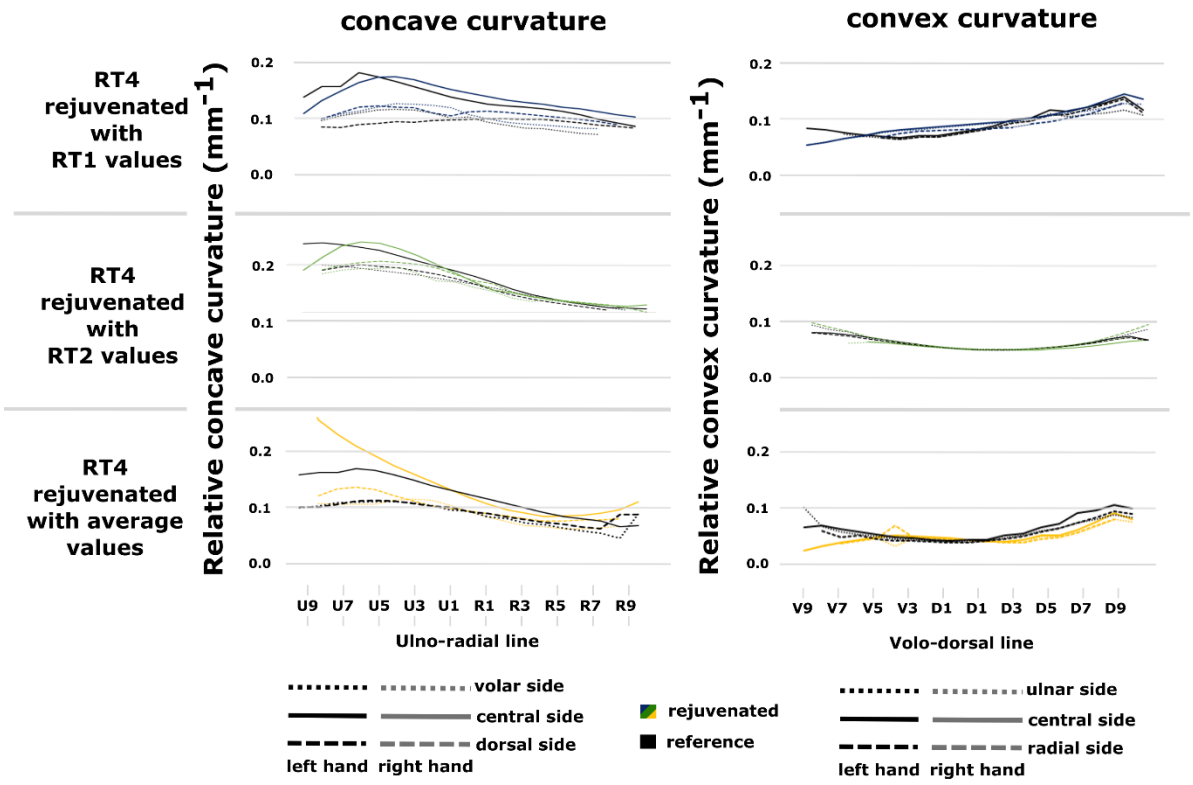


**Figure 9**: Evolution of the relative concave curvature of the rejuvenated right-hand trapezium of subject 4 respectively along the ulno-radial line (dashed line: volar side; full line: center; dotted line: dorsal side) and the volo-dorsal line (dashed line: ulnar side; full line : center; dotted line : radial side). Comparison with the values of references (yellow: average; orange: RT1; green: RT2)

**Model adaptation for additive manufacturing by voxel-based representation**

The model adaptation proposed ensured the data integrity towards the final printable model and reduce the computational processing cost for data operations. The voxel-based framework coupled with a smoothing filter guaranteed a numerical model adapted to AM. The smoothing step is not only used to smooth the shagged effect induced by the voxelization but also to create a more natural and continuous surface to the derived anatomy from the relatively simple configuration of the model. No tangency requirement is imposed between adjacent surfaces.

The computational time spent to obtain the smoothed model does not exceed 3 minutes (intel® Xeon® CPU-2683 V4) for models composed of 250000 triangles and 8M voxels. The gap between the smoothed model and the initial data does not exceed the half size of a voxel.

# Discussion

The methodology developed in this work to numerically rejuvenate a deeply affected trapezium by osteoarthritis can be extended to other biological systems for two purposes: to understand the pathology through the morphological deformations and to design a treatment that matched the initial and healthy morphology.

**Rejuvenation: Analysis of the deformation of osteoarthritic trapezium bones**

This work has demonstrated that there is a significant inter-subject variability of the morphology that highlights the importance of a patient-specific implant. It also demonstrates that the arthritic morphology is significantly different from its initial morphology (Fig.2) affecting not only the concavo-convex-curvature of the CMC articular surface (Fig.4) with localized wear removal and osteophytes formation but also its relative orientation regarding the other articular surfaces (Fig.3). These changes are confirmed by the literature [19,28–32]. The rejuvenation process gives a clear insight on the deformation that has occurred specifically for each patient. The fact that the VU quadrant was the preferential wear location is supported in the literature [30,33], although the entire wear pattern is still controversial [34]. Lee et al. found that the volo-ulnar quadrant also had the greatest trabecular bone volume, thickness, and connectivity, providing evidence that the compressive loads at the CMC joint occur mainly at this quadrant resulting in a consistently affected region of wear in osteoarthritic stage [32]. Our results support that the complex kinematics of the pollici-digital mobility favors loading in the volo-ulnar quadrant [32]. Limitations of our study include small sample size featuring both arthritic patterns: the “dish” and the “cirque” [29]. However, compared to

previously reported data of osteoarthritic and normal bone, the samples and the resulted rejuvenated bone matched cohort statistical analysis. The decrease of the concave curvature and the increase of the convex curvature in the CMC articular surface agrees previous studies [19,29]. It is important to consider that the analysis was carried out on subchondral bone surfaces, and thus may not be representative when adding the cartilage over the articular surfaces.

**Rejuvenation: Analysis of the process**

In this work, a model reconstruction guideline has been proposed adapted for implant design and AM that is time efficient and does not need specific CAD skills to be performed. Some studies [35,36] have demonstrated that simplifying the "saddle" joint to a ball-and-socket design could overstress the prosthesis which partly explain the complications. Therefore, an implant that replicate the healthy trapezium shape of the patient might be a solution for these clinical complications. Several methods for generating patient-specific implants has been patented and reviewed in the literature [37–40]. Most of them are aimed for cranial surgery, dentistry, and maxillofacial surgery. The patent US6932842B1 [37] for instance, proposed "rejuvenation" step that can be realized by either (i) comparing the real-medical reference data to a database to the medical data taken from a healthy person or by comparing the symmetrical body regions [14,15]. Sutradhar et al [41] design framework for patient‑specific bone replacements uses topology optimization. A clear and accurate understanding of the applied load and constraints are therefore needed. However, the mechanical loads and constraints of some anatomical structures still remain to be solved, particularly for carpal bones [42].

None of the CAD framework used [37–40] were designed to be time-efficient and accessible to non-specialists while allowing configurability for a further restoration process. Additionally, the creation of a closed B-rep with no holes, overlapping can be a tedious and time consuming task. Compared to standard implants, 3D printed patient-matched implants cannot be manufactured in advance phase; implants should thereafter be manufactured in the shortest possible time, with respect to the shape deformation and surgeon's viewpoint. Our work was realized with this objective; therefore a minimum necessary CAD toolset was designed allowing (i) the configuration of topological features resulting in a final watertight meshed model containing no printability error and (ii) Boolean operations (addition, subtraction) for prosthetic elements. Our smoothed voxel based technique combines the advantage of an accurate surface modeling, the ability to perform Boolean operation as any CSG modeler while providing in a final step a high

quality mesh which could be even used for finite element analysis. Connectivity defects deleterious for additive manufacturing such as spurious gaps or intersecting surfaces are filtered by the voxelization.

The limitations of our “rejuvenation” procedure are the relative high number of parameters even though it has been already reduced to a certain degree, and the manual CAD operations which may lead to topological errors. Further work can be done to optimize both of these limitations with the emergence of statistical shape models [13] and dimensionality reduction approaches [43]. Further tendency of big data and artificial intelligence will offer additional opportunity to counterpart this current limitation [44].

## SUMMARY

This article presents a quick, reliable procedure, accessible to non-specialists, for obtaining a “rejuvenated” numerical model from biomedical data, a model suitable for functionalization and AM. The approach consisting in numerically rejuvenated a deeply affected trapezium by osteoarthritis, for designing a CMC implant specifically matched to the patient. The clinical outcomes are expected such as the decrease of complication related to the wear behavior, the transmission of the force, the stability of the implant and its adequate position.

## CONFLICT OF INTEREST

The authors report no conflict of interest, financial or otherwise.

## ACKNOWLEDGMENTS

The research leading to these results received funding from the French Agence Nationale de la Recherche (ANR-11-IDEX-0004-02 under the “Sorbonne Universités” Idex) through an IUIS project for the promotion innovation in healthcare.

## REFERENCES

[1] H. Frost, Wolff’s Law and bone’s structural adaptations to mechanical usage: an overview for clinicians, Angle Orthod. 64 (1994) 175-188.

[2] S. Batra, R. Kanvinde, Osteoarthritis of the thumb trapeziometacarpal joint, Curr. Orthop. 21 (2017) 135–144.

[3] D.B. Burr, M.A. Gallant, Bone remodelling in osteoarthritis, Nat. Rev. Rheumatol. 8 (2012) 665–673.

[4] J.J. Crisco, J.C. Coburn, D.C. Moore, M.A. Upal, Carpal bone size and scaling in men versus in women, J. Hand Surg. Am. 30 (2005) 35–42.

[5] N. de Beer, C. Scheffer, Reducing subsidence risk by using rapid manufactured

patient-specific intervertebral disc implants, Spine J. 12 (2012) 1060–1066.

[6] M.A. Vitale, F. Taylor, M. Ross, et al., Trapezium prosthetic arthroplasty (silicone, Artelon, metal, and pyrocarbon), Hand Clin. 29 (2013) 37–55.

[7] A.D. Speirs, M.O. Heller, W.R. Taylor et al., Influence of changes in stem positioning on femoral loading after THR using a short-stemmed hip implant, Clin. Biomech. 22 (2007) 431–439.

[8] X. Wang, Z. Xu, et al., Topological design and additive manufacturing of porous metals for\rbone scaffolds and orthopaedic implants: A review, Biomaterials. 83 (2016) 127–141.

[9] R.N. Maniar, T. Singhi, Patient specific implants: scope for the future, Curr. Rev. Musculoskelet. Med. 7 (2014) 125–130.

[10] J. Slamin, B. Parsley, Evolution of customization design for total knee arthroplasty, Curr. Rev. Musculoskelet. Med. 5 (2012) 290–295.

[11] T.M. Bücking, E.R. Hill, J.L. Robertson, et al., From medical imaging data to 3D printed anatomical models, PLoS One. 12 (2017) e0178540.

[12] D.-J. Yoo, Three-dimensional surface reconstruction of human bone using a B-spline based interpolation approach, Comput. Des. 43 (2011) 934–947.

[13] L. Joskowicz, Future Perspectives on Statistical Shape Models in Computer-Aided Orthopedic Surgery: Beyond Statistical Shape Models and on to Big Data, in: Comput. Assist. Orthop. Surg. Hip Knee, Springer Singapore, 2018: pp. 199–206.

[14] B. Lethaus, P. Lucas, B. Roland, et al., Additive manufacturing for microvascular reconstruction of the mandible in 20 patients, Ournal Cranio-Maxillo-Facial Surg. 40 (2012) 43–46.

[15] A. Jardini, M. Larosa, … R.M.F.-J. of C., undefined 2014, Cranial reconstruction: 3D biomodel and custom-built implant created using additive manufacturing, Jcmfs.Com. (n.d.).

[16] U.S.D. of Health, C. for B.E. and R. Services Administration, Food and Drug Health, Center for Devices and Radiological Research, Technical Considerations for Additive Manufactured Medical Devices. Guidance for Industry and Food and Drug Administration Staff, 2017.

[17] M. Di Prima, J. Coburn, D. Hwang, J. Kelly, A. Khairuzzaman, L. Ricles, Additively manufactured medical products – the FDA perspective, 3D Print. Med. 2 (2016) 1.

[18] A. Lerebours, A. Rassineux, M. Frederic, B. Salima, C. Egles, A.-C. Masquelet, Geometrical analysis of the trapezium bone's morphology variability., in: Word

Congr. Biomech., 2018.

[19] E. Halilaj, D.C. Moore, D.H. Laidlaw, et al., The morphology of the thumb carpometacarpal joint does not differ between men and women, but changes with aging and early osteoarthritis, J. Biomech. 47 (2014) 2709–2714.

[20] C. Taleb, S. Berner, G.. Ruggiero, First metacarpal resurfacing with polyvinyl alcohol implant in rhizarthrosis: Preliminary study, Chir. Main. 33 (2014) 189–95.

[21] Y. Krukhaug, S.A. Lie, L.I. Havelin, O. Furnes, L.M. Hove, G. Hallan, The results of 479 thumb carpometacarpal joint replacements reported in the Norwegian Arthroplasty Register, J. Hand Surg. (European Vol. 39 (2014) 819–825.

[22] L. Hellegaard, T. Hansen, Long Term Follow Up in Patients with Radiologically Loose Trapeziometacarpal Total Joint Implants, Rheumatol. 4 (2014) 2161–1149.

[23] A. Lerebours, F. Marin, S. Bouvier, C. Egles, A.-C. Masquelet, A. Rassineux, A voxel-based method for designing a numerical biomechanical model patient-specific with an anatomical functional approach adapted to additive manufacturing, J. Numer. Sci. Biomech. Bioeng. (2019).

[24] M.W. Tocheri, A. Razdan, R.C. Williams, M.W. Marzke, A 3D quantitative comparison of trapezium and trapezoid relative articular and nonarticular surface areas in modern humans and great apes, J. Hum. Evol. 49 (2005) 570–586.

[25] M. Berger, A. Tagliasacchi, L.M. Seversky, P. Alliez, G. Guennebaud, J.A. Levine, A. Sharf, C.T. Silva, A Survey of Surface Reconstruction from Point Clouds, Comput. Graph. Forum. 36 (2017) 301–329.

[26] and J.C. Catmull, Edwin, Recursively generated B-spline surfaces on arbitrary topological meshes, Comput. Des. 10 (1978) 350–355.

[27] G. Taubin, Curve and surface smoothing without shrinkage, IEEE Int. Conf. Comput. Vis. (1995) 852–857.

[28] Cooke, S. Kenneth, D.S. Rolando, et al., Degenerative changes of the trapeziometacarpal joint: radiologic assessment, Skel. Radiol. 24 (1995) 523-527

[29] S. Van Nortwick, A. Berger, R. Cheng, E. Al, Trapezial topography in thumb carpometacarpal arthritis, J. Wrist Surg. 2 (2013) 263.

[30] L. Xu, R. Strauch, G. Ateshian, et a., Topography of the osteoarthritic thumb carpometacarpal joint and its variations with regard to gender, age, site, and osteoarthritic stage, J. Hand Surg. Am. 23 (1998) 454–64.

[31] V. Pellegrini, Osteoarthritis of the trapeziometacarpal joint: the pathophysiology of articular cartilage degeneration. I. Anatomy and pathology of the aging joint, J.

Hand Surg. Am. 26 (1991) 967–74.

[32] A. Lee, A. Williams, J. Lee, R. Cheng, D.P. Lindsey, A.L. Ladd, Trapezium trabecular morphology in carpometacarpal arthritis, J. Hand Surg. Am. 38 (2013) 309–315.

[33] J. Pellegrini, D. Vincent, The ABJS 2005 Nicolas Andry Award: osteoarthritis and injury at the base of the human thumb: survival of the fittest?., Clin. Orthop. Relat. Res. 438 (2005) 266–276.

[34] M.F. Koff, O.F. Ugwonali, R.J. Strauch, et al., Sequential wear patterns of the articular cartilage of the thumb carpometacarpal joint in osteoarthritis1, J. Hand Surgery,. 4 (2003) pp.597-604.

[35] V. Spartacus, A. Mayoly, A. Gay, et al., Biomechanical causes of trapeziometacarpal arthroplasty failure, Comput. Methods Biomech. Biomed. Engin. 20 (2017) 1233–1235.

[36] T. Imaeda, K.N. An, Functional anatomy and biomechanics of the thumb., Hand Clin. 8 (1992) 9–15.

[37] P. Litschko, T. Henning, J. Beinemann, et al., US6932842B1 : Method for generating patient-specific implants, 2000.

[38] P. Tack, J. Victor, P. Gemmel, et al., 3D-printing techniques in a medical setting: a systematic literature review, Biomed. Eng. Online. 15 (2016) 115.

[39] J. Brie, T. Chartier, C. Chaput, et al., A new custom made bioceramic implant for the repair of large and complex craniofacial bone defects, J. Cranio-Maxillofacial Surg. 41 (2013) 403–407.

[40] J. Haq, N. Patel, K. Weimer, N.S. Matthews, Single stage treatment of ankylosis of the temporomandibular joint using patient-specific total joint replacement and virtual surgical planning, Br. J. Oral Maxillofac. Surg. 52 (2014) 350–355.

[41] A. Sutradhar, J. Park, D. Carrau, et al., Designing patient-specific 3D printed craniofacial implants using a novel topology optimization method, Med. Biol. Eng. Comput. 54 (2016) 1123–1135. -1418-0.

[42] M.J.F. Sandow, Computer Modelling Of Wrist Biomechanics - Translation Into Specific Tasks., Curr. Rheumatol. Rev. (2019).

[43] M. Kirby, Michael, Geometric data analysis : an empirical approach to dimensionality reduction and the study of patterns, John Wiley & Sons, 2001.

[44] L. Meng, W. Zhang, D. Quan, et al.,, From Topology Optimization Design to Additive Manufacturing: Today's Success and Tomorrow's Roadmap, Arch. Comput. Methods Eng. (2019) 1–26.

## 3. Intermediate conclusion

In this chapter, we have developed a method to numerically "rejuvenate" highly deformed bones in order to obtain a patient-specific implant adapted to additive manufacturing.

The proposed numerical procedure is based on a reduced configuration based on an independent functional design of distinct regions and a voxel-based process. The main advantage of the configurable model is its ability to compensate for a lack of information in raw medical imaging data or a deformed morphology due to a disease such as osteoarthritis. The voxel-based approach allows to transform the distinct regions into a single structure which enables additional topological operations. Combined with a simple smoothing process, it results in a homogeneous triangulated model, free of printability errors and makes the configurable model more anatomically realistic.

The approach was applied on trapezium bones deeply affected by osteoarthritis. Configurable parameters have been set up to restore the pre-arthrosis morphology while preserving the specificities not affected by the pathology. The concavo-convex radius of curvature characteristics of the rejuvenated models appear to be robust. Indeed, the sets of values of healthy patients integrated in the arthritic models give close results (surface, radius of curvature).

Additionally, this "rejuvenation" procedure makes it possible to know the areas of deformations due to osteoarthritis specific to each patient, which can be useful for clinical examination and the choice of an optimal treatment (total prosthetic arthroplasty, hemiarthroplasty, intervention, etc.)

The expected clinical results for a patient-specific trapezo-metacarpal prosthesis are (i) an easier implantability of the prosthesis, (ii) an adequate positioning of the implant in the osteoarticular environment and (iii) a stable post-operative implant. Lower complications of the implant are expected compared to the actual treatments.

# CHAPTER 4:

# From the medical images to the articular implant ready for implantation: Assessing the surface quality and the geometrical deviation

*Ce chapitre aborde les étapes de fabrications d'implants articulaires de forme complexe. L'objectif est de répondre aux spécifications préconisées par les normes concernant la texturation de surface. Nous avons démontré la faisabilité de produire de tels implants par fabrication additive métal par lit de poudre et d'atteindre la rugosité spécifiée par divers post-traitements. La superfinition physico-catalytique utilisée dans ce travail, fut jugée satisfaisant.*

*Cette étude constitue une référence pour la fabrication des implants articulaires de forme complexe en chrome-cobalt-molybdène. L'évolution de l'écart le long de la chaîne de fabrication des implants a été déterminée. Les principaux défauts des échantillons sont la présence de pores et de déviations géométriques locales ; défauts inhérents à la fabrication additive métal.*

## 1. General context

This part of my thesis aims at measuring the evolution of the deviation along the implant manufacturing chain. The goal is to understand which step has the greatest impact on the implant specifications from the medical imaging data to the final post-treated implant, from the concept to the real object.

A major problem in the manufacture of metal additives on powder beds is the post-treatment of complex surfaces. Polishing machines often allows us to finish implants with standard geometry which is not adapted to the morphology variability of our implant. The solution we found here was to use a physico-catalytic process that polish homogeneously samples in a tank therefore homogenizing the loss of matter along the full geometry of the piece. The objective of this research is double. First it aims to understand if this process is adequate for customized implants made by selective laser melting regarding the different quality standards. The texture, the porosity and the composition of the surface, were analyzed with particular focus on the articular contact surfaces and the prosthetic elements. Second it aims at understanding the evolution of the geometrical deviation along the manufacturing chain by laser scanning the manufactured implants. Three-dimensional surface deviation maps were created in order to inspect the accuracy of complex shapes through the manufacturing process.

This work provides a reference for the design and the manufacturing by selective laser melting and the post-treatment of articular medical implants made of chromium-cobalt-molybdenum and is presented through an article.

## 2. Scientific article

- Lerebours, A., Bouvier, S., Rassineux, A., Dembinski, L.and Egles, C., From the medical images to the articular implant ready for implantation: Assessing the surface quality and the geometrical deviation *Manuscript ready for submission in Plos one*

# Article 4:
# From the medical images to the articular implant ready for implantation: Assessing the surface quality and the geometrical deviation

Augustin Lerebours [1], Alain Rassineux [1], Frederic Marin [2], Salima Bouvier [1], Lucas Dembinski [3], Christophe Egles [2]

*[1]Alliance Sorbonne Universités, Université de technologie de Compiègne, CNRS, FRE 2012 Roberval, Centre de recherche Royallieu, CS 60 319, 60 203 Compiègne cedex, France*

*[2]Alliance Sorbonne Universités, Université de technologie de Compiègne, CNRS, UMR 7338 BioMécanique et BioIngénierie (BMBI), Centre de recherche Royallieu, CS 60 319, 60 203 Compiègne cedex, France*

*[3] LERMPS, ICB UMR 6303, CNRS, Univ. Bourgogne Franche-Comté, UTBM, F-90010 Belfort, France*

**Ready for submission for journal Plos One**

**CORRESPONDING AUTHOR**

Augustin LEREBOURS
Alliance Sorbonne Universités, Université de technologie de Compiègne,
CNRS, FRE 2012 Roberval,
Centre de recherche Royallieu,
CS 60 319,
60203 Compiègne cedex,
France
augustin.lerebours@utc.fr
Phone +33658019946

## Abstract

Additive manufacturing has allowed the manufacturing of complex parts from numerical models which may largely benefit the biomedical industry. Indeed, it facilitates the creation of anatomically-matched implants by using the medical imaging of the patient and complex geometric parts including porous structure, tortuous internal and external elements that would not be easily possible using traditional manufacturing approaches. Cobalt based alloys is a commonly used material for articular implant and has been available by metal additive manufacturing technologies including selective laser melting. However, the layer-by-layer fabrication process pose challenges in determining optimal characterization for the final finished articular implants. The success of the fabrication and the final performance of the device is tied to the material, the manufacturing parameters and the post-processing. In this study, SLM parts were superfinished by a physico-catalytic process which is adapted for complex geometric parts produce by additive manufacturing.

We aimed at understanding the full process and limits in the design and manufacturing phase. We particularly focused on how to achieve an adequate surface finish for metal articular implant parts regarding the acceptance criteria considerations indicated in medical devices standards. The innovative potential of metal AM also introduce geometrical variability which has been characterized for each manufacturing phase. This work used the case of a trapezium replacement implant to outlines different concerns of a metal additive manufacturing device that should be considered through the design phases. The results demonstrated the possibility to additive manufacture complex-shaped articular implants with an average roughness of 35nm. It also highligts the fact that selective laser melting is the process that have greatest impact on the implant specifications. Geometric deviations were mainly found in the areas that features the greatest surface porosity.

**Keywords**

Additive manufacturing, Selective laser melting, wear behavior, Cobalt-chromium-molybdenum alloy, polyethylene, porosity, biomedical implant

**Abbreviations**

AM, additive manufacturing; SLM, selective laser melting; 3D, three-Dimensional; CoCrMo, Cobalt-chromium-molybdenum alloy; SEM, Scanning Electron Microscopy.

## Introduction

Additive manufacturing (AM), also known as 3D printing is the "process of joining materials to make objects from 3D numerical model, usually layer-upon layer, as opposed to subtractive methodologies, such as traditional machining" according to ASTM standard F2792-10 [1]. The use of AM with metal powders is a growing industry in various sectors including aerospace, automotive, biomedical as it enables part customization and increased design complexity at no cost compared to conventional manufacturing [2]. It is no longer used only for prototyping [2].

Among the powder-based-AM technologies, selective laser melting has already being used to produce commercially metallic biomaterials such as titanium alloys, cobalt-chromium alloys or stainless steel for biomedical applications including orthopaedics [3], dental [4], and cardiovascular [5]. The orthopeadic industry has been particularly interested in metal-AM processes for their ability to produce orthopaedic implants with tailored properties which can enhance bone osseointegration through porous structure designs [6].

However, there are few studies that have been focused on processing a fully complex-shaped articular implant. Most of them are focused on lattice structure to enhance the anchoring properties of the implant at the interface with the trabecular bone [3].
The bearing surfaces should have low friction and good wear characteristics which are far different from the specifications of anchoring parts (e.g. stem, cup). Therefore, an efficient post-processing method is required for these surfaces. It is necessary to have a good understanding of entire manufacturing process from the medical data to the AM and the post-treatment particularly the impact on these bearing surfaces is needed. The quality of the bearing contact surfaces are a major concern in total joint replacement as the main cause of late revision is histiocytic response to *wear* debris known as osteolysis and surface damage with progressive loss of material known as wear [7,8].
Song et al. [9] have already studied the manufacturing of CoCrMo alloy by SLM for a femoral component. They found optimized SLM parameters that enable to 3D print CoCrMo parts with 99% density as well as their positioning in the SLM chamber. However the femoral component was polished by hand leading to process uncertainty due to uncontrolled surface texture finishing.

This work aims first at demonstrating the feasibility to produce a complex-shaped articular implant in CoCrMo by additive manufacturing and post-processing. By

measuring the evolution of the deviations along the implant manufacturing chain, the 2nd objective is to understand which design phase has the greatest impact on the bearing surface specifications. It particularly focus on the manufacturing process of a trapezium replacement implant to treat osteoarthritis at the base of the thumb based on a previous study [10].

The obtained results would provide guidance to manufacture and post-processing a complex customized implant by metal-additive manufacturing that comply articular implant specifications.

## Materiel and methods

### 1. Material selection

Cobalt -based alloys are widely used in orthopedic surgery because of its excellent wear behavior [11]. In the literature, there are some works that have focused on the process of an articular implant processed by Selective laser melting from cobalt-based alloy [12–14]. Selective laser melting (SLM) is a powder bed fusion technique which therefore, necessitates raw material in the shape of powder particles.

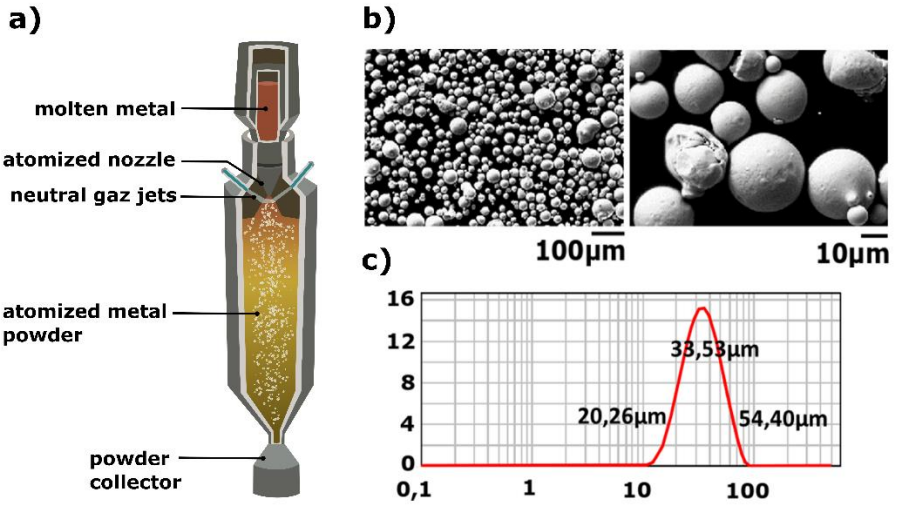


| | Co | Cr | Mo | F | Al | Si | Mg | W | P | S | Ni | Ti | Cu | N |
|---|---|---|---|---|---|---|---|---|---|---|---|---|---|---|
| Powder | Bal | 28.31 | 6.02 | 0.02 | 0.02 | 0.49 | 0.5 | <0.15 | <0.01 | <0.01 | 0.08 | <0.01 | Na | 0.08 |
| ASTM F75 | Bal | 27-30 | 5-7 | <0.75 | <0.1 | <1 | <1 | <0.2 | <0.02 | <0.01 | <0.5 | <0.1 | Na | <0.25 |

**Figure 1**: a) Sketch of the atomization process; b) SEM images showing the CoCrMo powder particle morphology; c) granulometry measurement and d) chemical composition of the CoCrMo powder particles

The cobalt-based alloy powder particles used are made by inert gas atomization under argon environment. The process begins with molten metal pouring from a nozzle. The stream of liquid metal is then hit by jets of inert gas (Argon) and atomized into fine metal

droplets which cool down and solidify when falling inside the atomized tower (fig.1.a). It is the most common process to produce metal powder for additive manufacturing. It offers perfectly spherical shape particles as seen in fig 1.b with an average particle diameter of 35.5 µm as seen in the powder size distribution of fig 1.c. The size distribution of the powder is a key feature in additive manufacturing as it can influence the powder flowability, the powder bed density, the energy input to melt the powder grains [15]. The chemical composition was verified and respect the specification of the ASTM F75 (fig.1.d) [16].

## 1. Designing the articular implant for a carpometacarpal arthroplasty

The first task of this work was to design a carpometacarpal medical implant. The carpometacarpal implant aims to replace entirely the trapezium bone deformed by osteoarthritis.

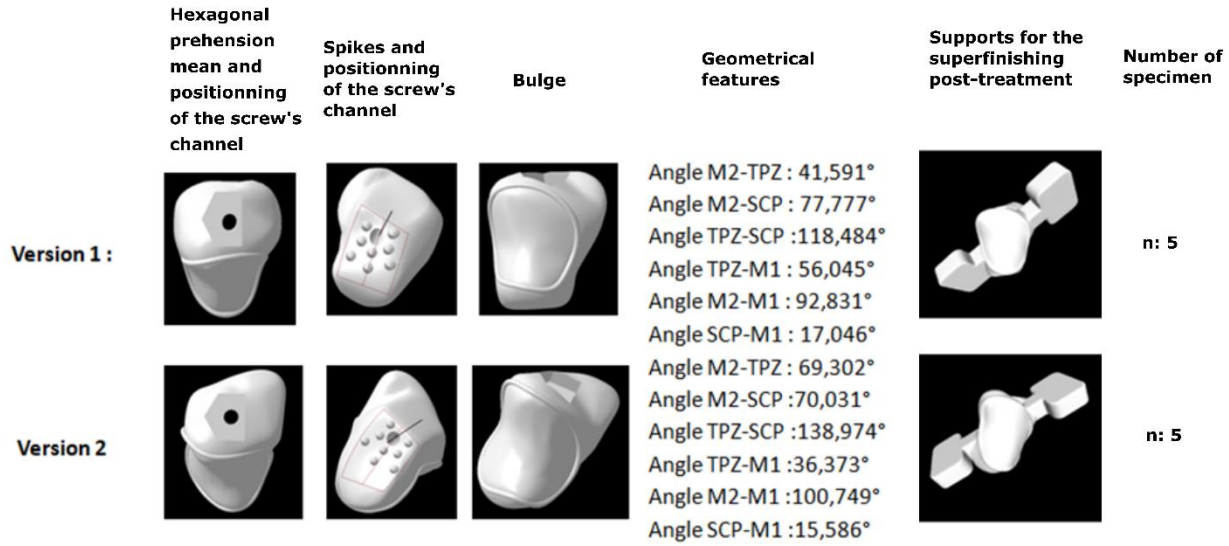


**Figure 2**: Design of a trapezium implants based on patient data; M1: 1st metacarpal contact surface; M2: 2nd metacarpal contact surface; SCP: scaphoid contact surface; TPZ : trapezoid contact surface

In order to study the feasibility of the SLM process for the manufacturing of complex and small-bone-like implant. Two implants were designed based medical data.

The implant comprises different areas of interests regarding the specification of the implant once implanted:

- Articulated area with the 1st metacarpal bone (m1).

  This area requires high quality (porosity, roughness, geometrical accuracy) because it is mainly involved in the movement of the thumb for prehensile activities. It has a concavo-convex shape also described as a 'saddle' with

degrees of curvatures that varies along the main direction (dorso-volar, ulno-radial).

- Articulated area with the 2nd metacarpal bone (m2)

  This area requires quality (porosity, roughness, geometrical accuracy) lower than M1 because it is mainly involved in the stability of the implant.

- Articulated area with the trapezoid bone (tpz)

  This area requires lower quality (porosity, roughness, geometrical accuracy) because it is mainly involved in the stability of the implant. However, the implant will be fixed with screws and spikes to this particular bone, therefore these elements (hole for the screws ; spikes) necessitate higher care regarding geometrical accuracy

- Articulated area with the scaphoid bone (scp)

  This area requires quality (porosity, roughness, geometrical accuracy) lower than M1 because it is mainly involved in the stability of the implant.

The bone reconstruction started with processing clinical computed tomography (CT) data of trapezium bones that have been previously extracted and cleaned from cadavers. Two trapezium bones were used. The surgeon has not noticed any kind of evidence of osteoarthritis pathology for the first subject and advanced osteoarthritis pathology for the 2nd subject. Therefore, the 2nd trapezium bone model with advanced osteoarthritis was modified morphologically to recover the healthy characteristics that have been impacted such as the concavo-convex radius of curvature of the 1st metacarpal contact surface. The numerical method is detailed in the previous chapter. The angulation between the scaphoid, 2nd metacarpal bone, and the trapezoid has been untouched from the original medical data. The figure 2 allows us to visualize the geometrical differences, especially the angulations between the differences in contact surfaces (Fig.2). Items were included for the fixation of the prosthesis. First a channel was added. It aimed to fuse the prosthetic compound in the trapezoid bone with a cortical screw (Fig.2), anchorage spikes were also added. They aimed at strengthening the fusion and secure the trapezium prosthesis' adequate location by preventing its rotation around the screw axis. Cortical screws are adapted to the hard parts of the bone and are characterized by a narrow thread over the entire length of the screw. A hexagonal prehension mean coupled with its respective ancillary tool allows us to manipulate the prosthesis while keeping the integrity of its required surface finish. A bulge was placed around the frictional surface

also prevent any deterioration of the surface finish surface during the implantation procedure. Finally supports have been added for the superfinishing procedure (Fig 2).
The final models were converted into a triangulated meshed model required by the additive manufacturing technologies.

## 2. Additive Manufacturing process of the patient-matched articular implant

The Selective laser melting process uses a laser to melt the powder layer by layer, generating the desired geometry as seen in Fig 3.a). Some key advantages of SLM are shape flexibility and the use of lattice structures. The manufacturing parameters used in this work are detailed in Fig.3 b). The specimens have been oriented in the manufacturing chamber so as to minimize the surface roughness and the staircase effect in the 1st metacarpal contact surface which is the most important zone of the implant. Part orientation also influences the build time and residual stress. Support structures have been added to support the specimens in case of overhang, conduct excess heat away and prevent warping or complete build failure.

a)

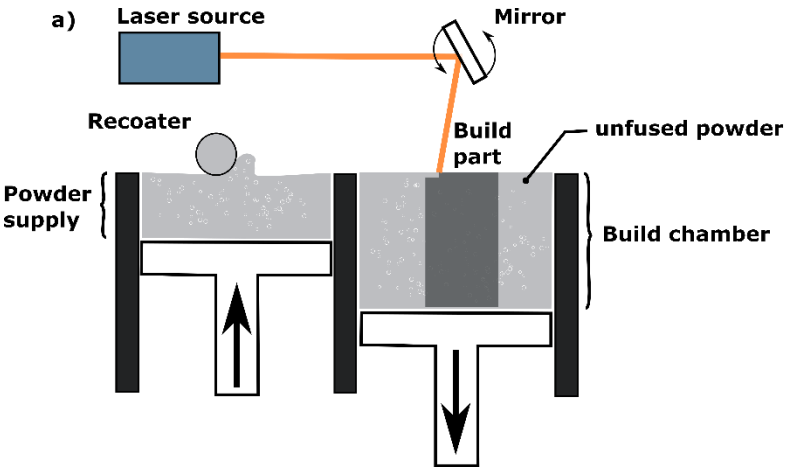


b)

| Parameters | |
|---|---|
| Filling Energy | 125 W |
| Speed | 1000 mm/s |
| Hatch vector | 105 µm |
| Layer width | 24 µm |
| Gaz de protection | Argon |

**Figure3**: a) Selective laser melting sketch and b) parameters used

## 3. Post processing

Once the samples were manufactured, the supports were removed manually. The implants were post-treated using two successive surface post-treatments: alumina sandblasting (aluminum oxide), superfinishing by micromachining process. The specimens were finally ultrasonic cleaned.

It is common that the surfaces produced by additive manufacturing are cleaned and smoothed by sandblasting process. Sandblasting smooths and cleans hard surfaces by forcing solid particles across that surface at high speeds using compressed air. The particles were in alumina (aluminum oxide).

The superfinishing also known as micromachining is a process that improves surface finish. The superfinishing used is a controlled automated process based on physico-catalytic method developed by BESTinCLASS. The specimens were placed inside a tank in which particles aggregated “in situ” by the catalyst are on a very-high-energy movements. The aggregates are microtools and nanotools component that match the roughness frequency that will be removed from the part being treated. Parts are surrounded by these particles in movement.

The implants were then cleaned in successive 15-minute ultrasonication baths in acetone, isopropyl alcohol and ultrapure water.

## 4. Surface characterization

### 4.1. Chemical composition

EDX was performed on the particle powder of CoCrMo and on the surface of the specimens.

### 4.2. Porosity Characterization

Surface porosity measurement were carried out using images from a confocal microscope laser (Sensofar) on the different areas of interests (m1, m2,scp, tpz) (Fig.1) using a 1746 x 1313µm zone. 2 to 5 images were done for each surface depending of their size (m1, scp :5 ; tpz, m2 : 2) in the the 5 specimens of each version of the implant. The following pores characteristics were extracted with imageJ :

### 4.3. Surface roughness analysis

Surface roughness of the different areas of interests (m1, m2,scp, tpz) was measurement with a confocal microscope laser (Sensofar)(Fig.1). A shape withdrawal of an order 10 polynomial filter was used to remove the 3-dimensional aspect of the samples. 2 to 5 measured were done for each surface depending of their size (m1, scp :5 ; tpz, m2 : 2) in the the 5 specimens of each version of the implant. Common amplitude parameters off the surface texture were measured including the average height roughness Sa and the root mean square: Sq. Hybrid roughness parameters were alos measured. It includes the root mean square gradient: Sdq and the developed interfacial area ratio: Sdr, among others.

### 4.4. Geometrical inspection

The manufactured trapezial component was scanned through 3D scanner and the acquired point cloud was exported as a STL file. The parts were compared to the numerical model after the sandblasting post-treatment and after the superfinishing treatment. Measurements of deviation were done by Hausdorff Distance with Meshlab

software. The Hausdorff distance is the distance from a point in one set to the closest point in the other reference set. To visualize the deviations, values were converted into colors.

$$d_H = max\{\sup\inf d(x,y), \sup\inf d(x,y)\}$$

Alignment of the specimens with the numerical model was done by ICP (iterative closest points) using 5 points at specified location.

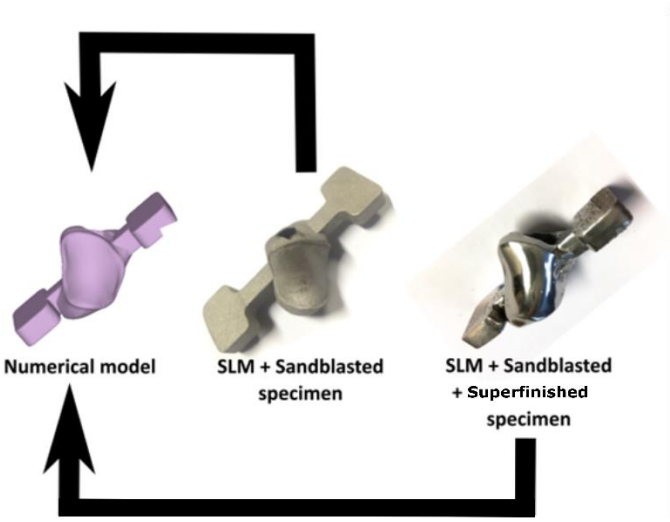


**Figure 4**: Analysis of the geometrical analysis

The numerical model was also compared to its original medical data using the same technics.

### 4.5. Principal component analysis

The variables of the porosity were all centered and reduced was well as the variables of the surface texture, in order to perform a principal component analysis (PCA). PCA is a statistical procedure that organizes the dataset to an orthogonal basis-set that maximizes the variance between observations and between variables. This gives a global view of the potential correlation between parameters and the potential similarities between observations.

## Results

### 1. Feasibility of manufacturing complex mirror-like implants

Figure 5 illustrates the two versions of the implant superfinished by a physico-catalytic method and processed by SLM. It is therefore feasible to manufacture complex geometric articular implant with a mirror-like finish. It should be noted that the optimal configuration of the SLM process parameters was done only for the exterior part and for the optimal roughness result. The manufactured implants were not stress relieved by a thermal treatment. Depending on the region of interest, the specification in term of

surface quality is different. The M1 region of interest *ie* the contact surface with the first metacarpal is the surface that needs the best surface quality. The chemical composition, the porosity, the roughness and the geometrical deviation are therefore analyzed in the next paragraphs.

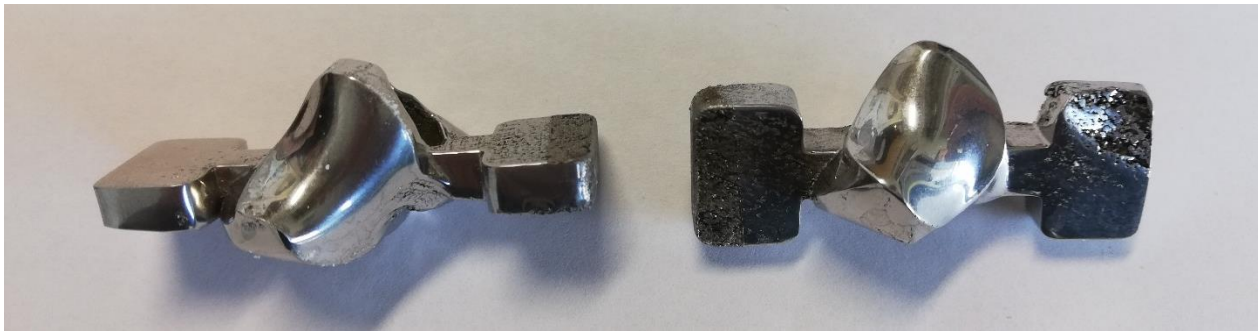

**Figure 5**: Mirror-like implant processed by SLM and superfinished

## 2. SEM and EDX investigations

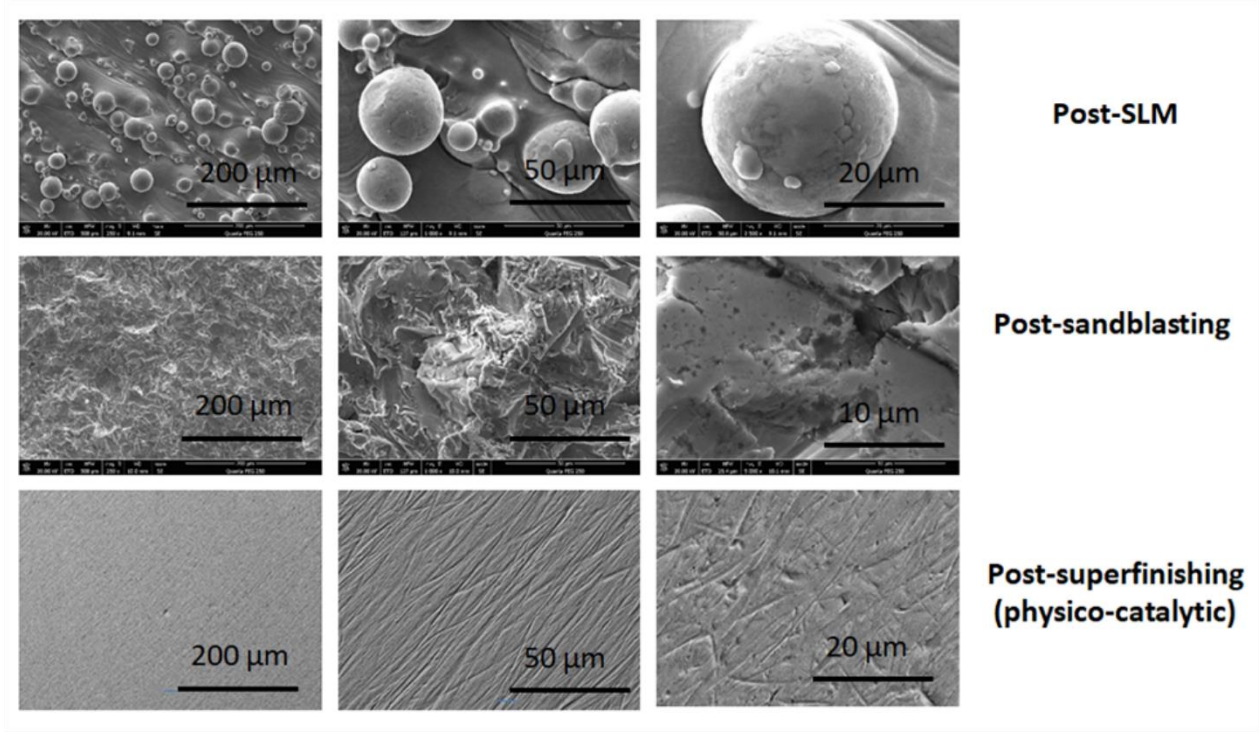


**Figure 6**: SEM images of the CoCr surface of the implant after, SLM, sandblasting and superfinishing

The SEM analyses were realized on the specimens' surfaces after the additive manufacturing steps, sandblasting post-treatment and after the superfinishing post-treatment. The SEM images from Figure 6 are showing the initial surfaces produced by SLM at different magnification. The obtained CrCoMo specimens have partially melted particles un-homogenously distributed on their surfaces (fig. 6). The sandblasting post-treatment removed all these particles. It results in a homogenous surface texture. The surperfinishing post-treatment resulted in a uniform removal and a smoothed surface

mirror-like finish. The surface had a texture which reflects the movement of the superfinishing tools in the tank. It has also highlighted the pores typical of additive manufacturing.

The chemical composition was measured with EDX on multiple surfaces after all performed post-treatments. An excess in the aluminum content has been measured. It chemical element came from the sandbasting post-treatment, it has been particularly found in the pores as shown in fig. 6 where the flux of superfinishing particles could hardly get. The other chemical elements found are similar with the powder chemical composition and fit the specifications of the ASTM standard.

**Table 1 :** The chemical composition (mass %) of CoCrMo specimens

| | Co | Cr | Mo | F | Al | Si | Mg | W | P | S | Ni | Ti | Cu | N |
|---|---|---|---|---|---|---|---|---|---|---|---|---|---|---|
| **Superfinished specimens** | Bal | 28.82 ±1.22 | 6.06 ±0.24 | <0.7 | 0.27 ±0.14 | 0.41 ±0.05 | <0.05 | <0.15 | <0.02 | <0.01 | <0.5 | <0.1 | 0 | <0.25 |
| **ASTM F75** | Bal | 27-30 | 5-7 | <0.75 | <0.1 | <1 | <1 | <0.2 | <0.02 | <0.01 | <0.5 | <0.1 | Na | <0.25 |

## 3. Porosity investigation

Two different pores' geometries are present in the specimens as shown in fig.6:

- Small (50 to 2000µm2) and circular,
- Large (up to 0,2mm2) and irregular.

The first family of pores are due to due to the entrapment of the inert (argon) gas in the build chamber [15]. The high cooling rate during the solidification process prevents dissolved gas from leaving the surface of the melt bath before solidification takes place. The 2nd family of pores are formed because of a lack of fusion also known as incomplete fusion holes. They are either poor bonding defects or defects with un-melted metal powders [15]. They are mainly due to a lack of energy input in the manufacturing process [15].

The two versions have a different number of pores (version 1: 30 pores/mm2; version 2: 19 pores/ mm2) which also vary with the location particularly for the 1st version as seen in fig.8.a. The region of interest M1 *ie* the contact surface with the 1st metacarpal have the lowest number of pores per mm2 while TPZ *ie* the contact surface with the trapezoid have the highest number of pores.

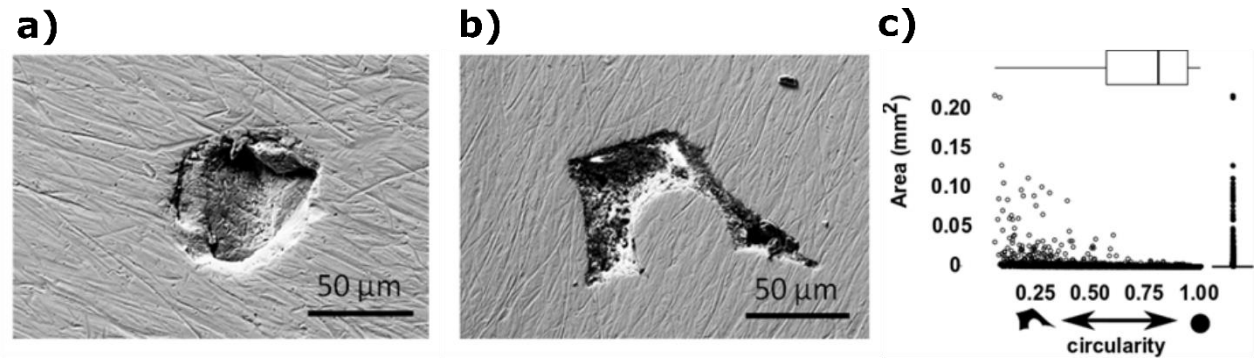


**Figure 7**: SEM images of the pores: a) round pores due to gas entrapment and b) irregular pores due to sintering process; c) diagram of the pores distribution regarding size and circularity.

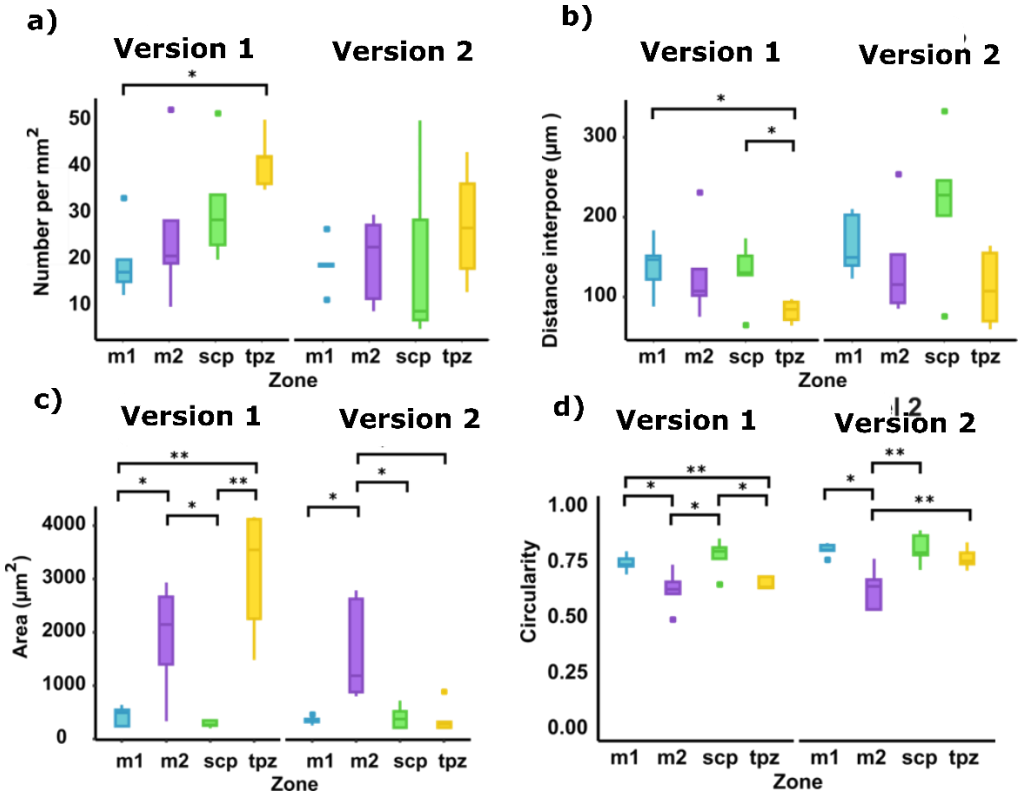


**Figure 8**: a) Number of pores per mm² depending on the area of the implant. b) Average wall thickness (µm). c) Mean area (µm ²) of the pores depending on the area of the implant. d) Circularity of the pores depending on the area of the implant.

The distance interpore was measured around 110µm for version 1 and 150µm for version 2 (fig.8.b). The values of distance differ from one region of interest to another. For both version of the implant, the region M2 and TPZ *ie* the contact surface with the 2nd metacarpal and trapezoid had the lowest distance interpore value around 100-70µm. M1 and TPZ *ie* the contact surface with the 1st metacarpal and scaphoid had a higher value around 130µm for the 1st version and around 150-220µm for version 2. These values seem correlated to the number of pores and also their areas as shown in fig.8. c). Indeed,

the larger the pores are the lower the distances interpore are. M2, TPZ of version 1 and M2 of version 2 have the larger pores from 1000µm2 to 4000µm2. The other regions of interests have smaller pores below 500µm2. As suggested by the nature of the pores, the circularity of the pores are much lower for these areas (fig.8.d).

Figure 9 is a principal component analysis of the observations and the variables. This 2-dimensional visualization allows us to confirm the observed trends. The arrows of the variables “number of pores” and “interpore distance” are opposite, indicating an inverse correlation.

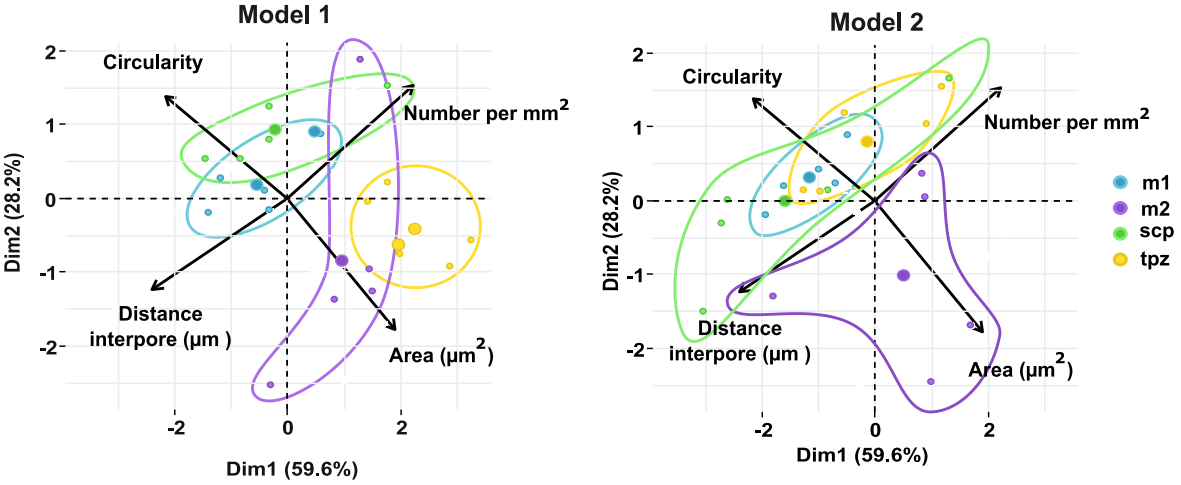


**Figure9**: a) Principal component analysis showing the average values of pores paramaters of each defined zone of interest in the two version of the implant, b) Presence of large and irregular pores through the defined zone of interests

The same correlation is shown for the variables "pore areas" and "circularity". For the 1st version, the pores features of M1 and SCP are not significantly different. For the 2nd version, the pores features of M1, SCP and TPZ does not vary significantly to distinguish one area to another. The couple of variable area and circularity allows us to distinguish some regions of interests M2 and TPZ in the first version and M2 in the 2nd version.

### 4. Surface texture investigation

Once the implant have been processed by SLM, the average roughness Sa is around 9-13µm. The surface texture is composed of partially melted particles and laser tracks. The sandblasting process withdraws the former surface texture to create a random surface texture with a matte gloss similar to cleft. It reduces the average roughness to 6.5-8µm. The final surface modification is processed by the physico-catalytic superfinishing. It results in a homogeneous surface texture with a mirror-like aspect composed of submicro-scratches that reflects the flux of the particles inside the tank as shown in fig. 10.a. The Sa is reduced all around the implant to about 35nm as shown in fig. 10.b. The

region of interest TPZ of the 1st version has the lowest Sa value while TPZ (30nm) of the 2nd version of the implant has the highest Sa value (42 nm). The roughness fit the specification recommended by the standard ISO 21534 :2007 : “Non-active surgical implants — Joint replacement implants — Particular requirements” [17]. Indeed, the standard indicates a Ra maximum of 0,100nm for the metallic part against UHMWPE, and a maximum of 50nm when the surface is convex. The roughness obtained after the superfinishing treatment does not correlate with nor the number of pores nor the size of the pores.

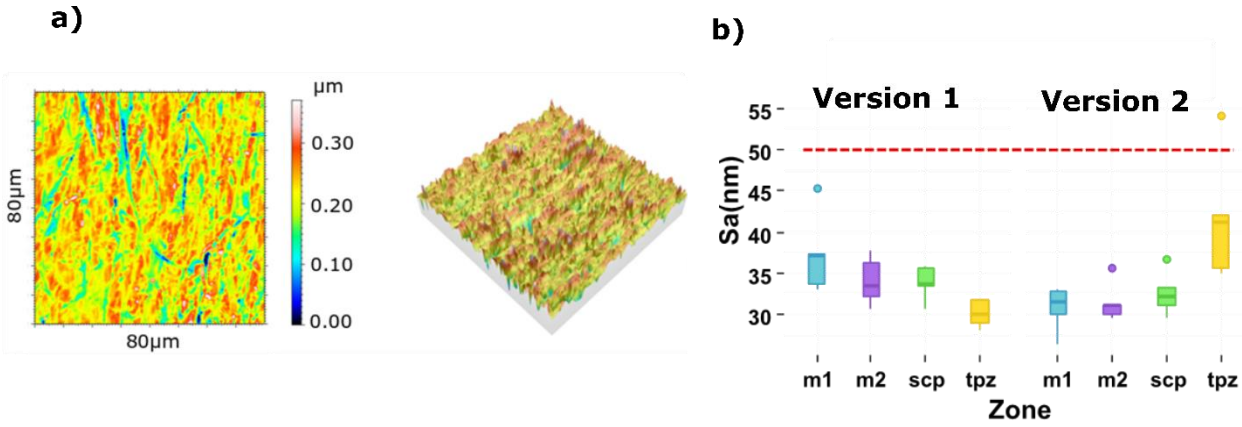


**Figure 10**: a) Surface texture after the superfinishing post-treatment and b) average roughness of the surface of interest of both version of the implant

Figure 11 shows a principal component analysis of the observations and a set of surface texture variables. No differences between the two versions are visualized. More than half of the variables' arrows are closed meaning that these parameters are interdependent. These include Sa, Sk, Sz, Vv, Vvc, among other parameters. The PCA was also done on the regions of interests, TPZ of the 1st version and M1 of the 2nd version were distinguished from the other surfaces composing their respective version of the implant. These differences do not seem to correlate with the pores characteristics.

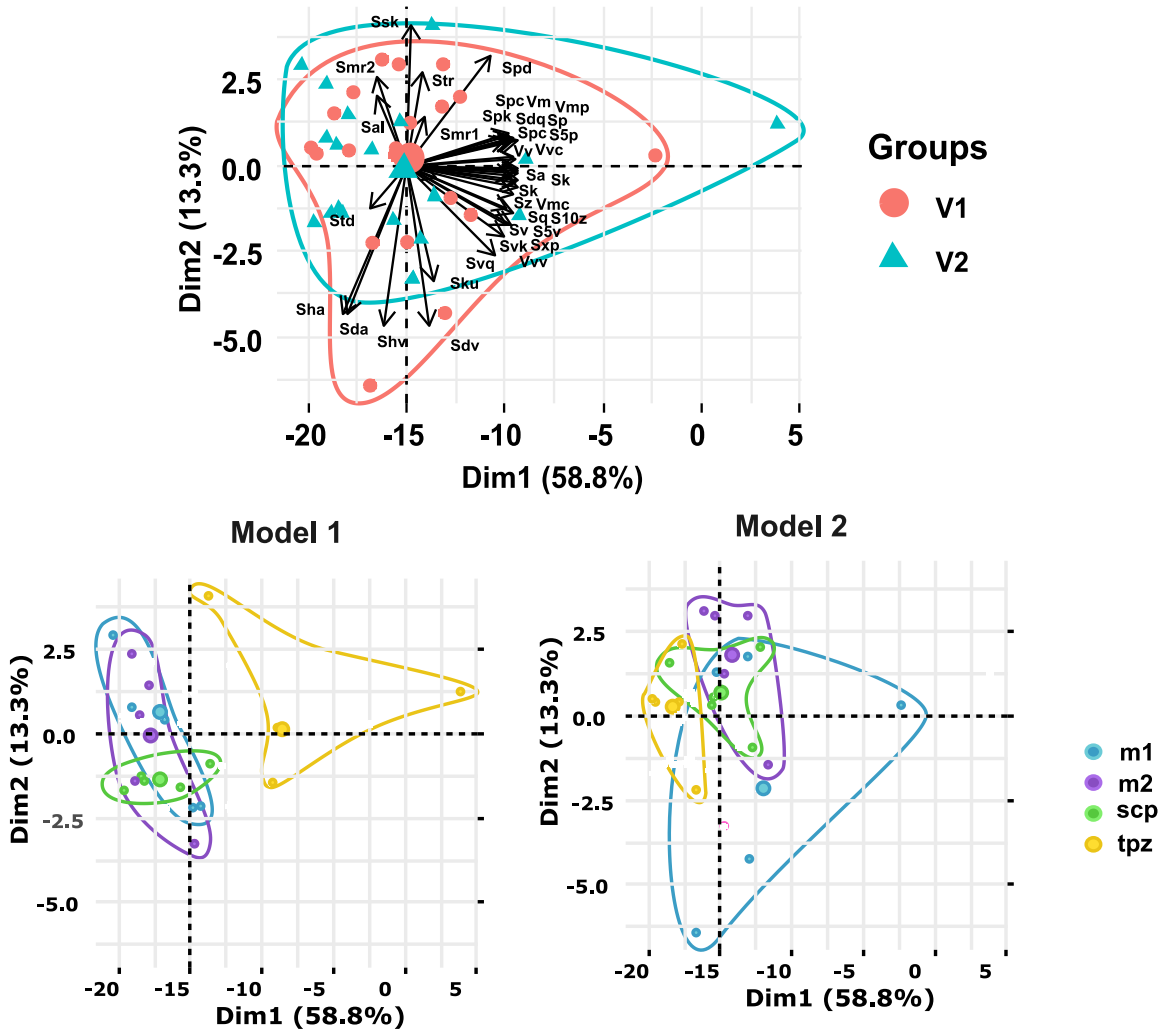


**Figure 11**: Principal component analysis of the roughness parameters and boxplot of the Sa values depending of the specimens and zones; visualization of the surface and main orientation

## 5. Geometric assessment

### 5.1. From numerical model to post-treatments

The accuracy of the surfaces was verified by 3D scanning the version of the implants with a laser robot arm after the sandblasting and the superfinishing processes. The obtained point cloud was compared with the designed implants by the Hausdorff distance measurement. The result of each point was then gathered in a histogram as seen in fig.12.a and b. Following the sandblasting, the average deviation was -43µm and +14µm respectively for the 1st version and the 2nd version of the implant. The values containing 5% and 95% of the distances are 664µm and 732µm respectively for the 1st version and the 2nd version. It suggests that major local deviations have occurred during either the selective laser melting process or/and the sandblasting process. All specimens feature the same trends. The manual nature of the sandblasting process suggests that the deviation has rather occurred during the SLM process. Following the superfinishing, the average

deviation was -97µm and -111µm respectively for the 1st version and the 2nd version of the implant. The values containing 5% and 95% of the distances are 746µm and 670µm respectively for the 1st version and the 2nd version. It suggests that the superfinishing process has not introduce major local deviations but rather a homogenous withdrawal around 50-150µm.

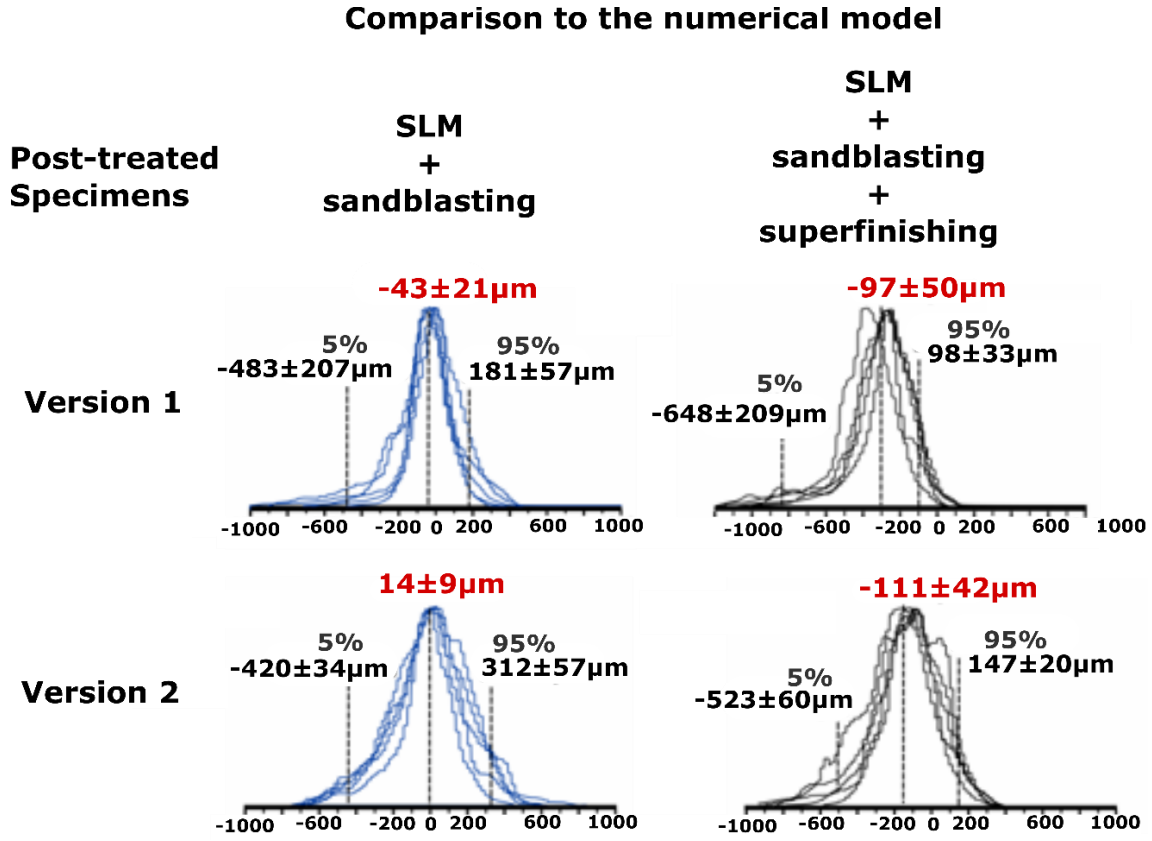


**Figure 12**: histogram of the deviation distance of the scanned implant after sandblasting and after superfinishing.

Figure 13 details the results obtained after the superfinishing for the regions of interests. The 1st version has its geometrical deviation mostly on M2, the other regions of interests feature an average deviation around -30µm. Most of the geometrical deviation of the 2 version is on SCP (-94µm), the other regions of interests feature an average value of -7µm. Furthermore, the distance values are also much closer one to another as shown by the 5% and 95% values.

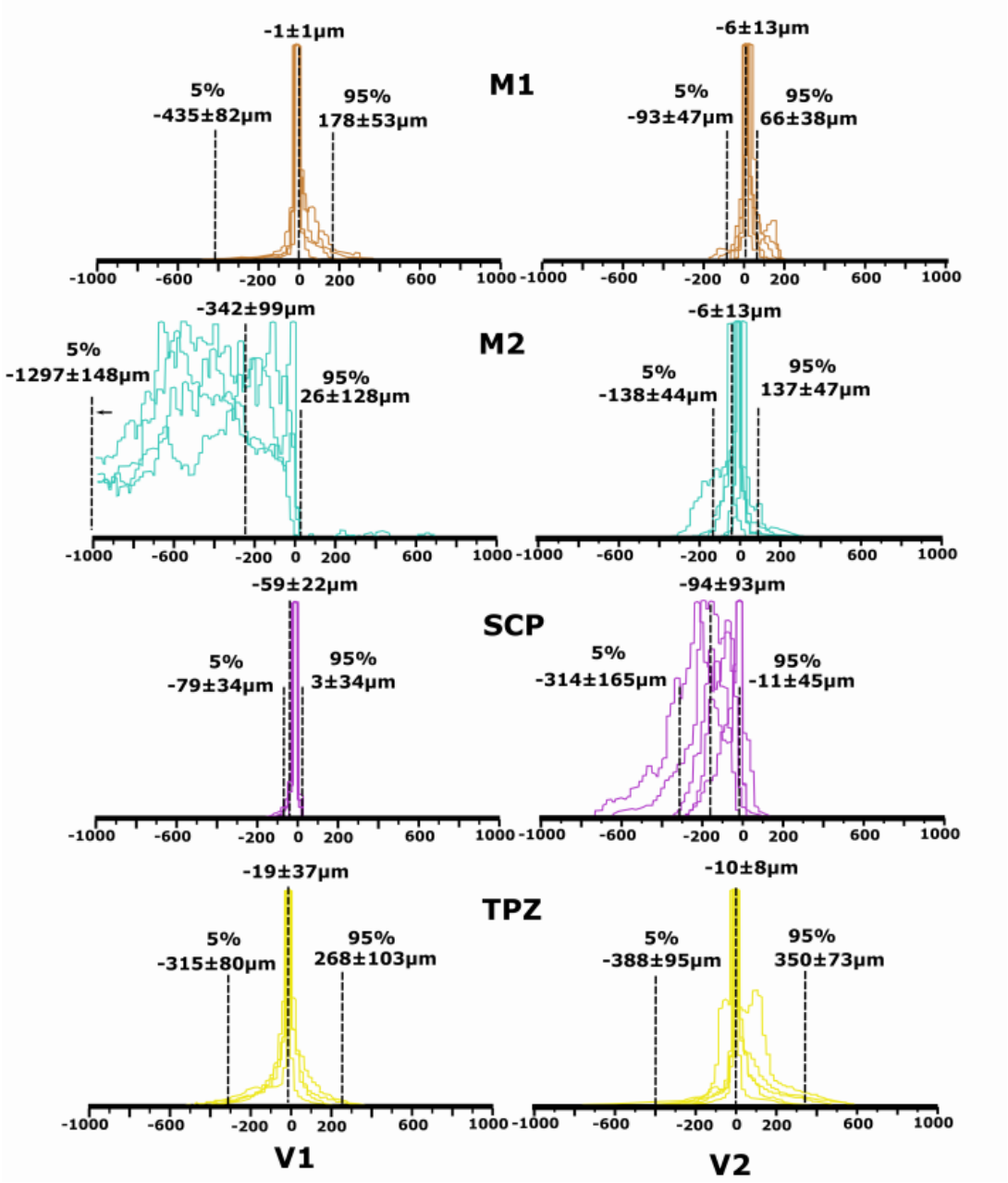


**Figure 13**: Detailed histogram of the distance after the superfinishing post-treatment.

The results are also shown by a color map to better picture the geometrical deviations that have occurred (fig 14).

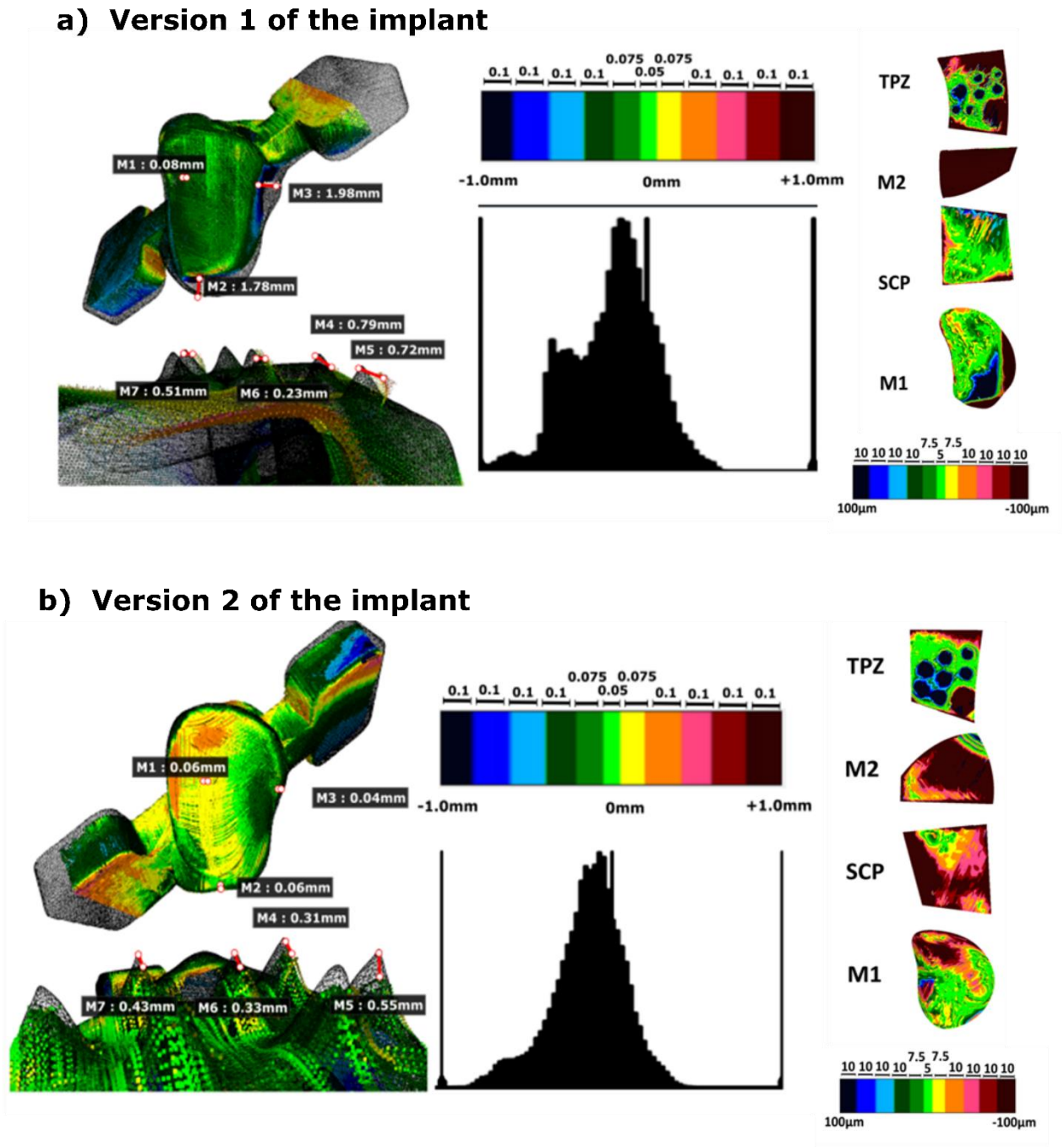


**Figure 14**: 3D colorization map by Hausdorff distance analysis Principal component analysis of the roughness parameters and boxplot of the Sa values depending of the specimens and zones; visualization of the surface and main orientation

Regarding the 1st version, the deviation of the M2 surface is confirmed but it seems to have affected the side of the M1 surface and TPZ. The spikes located on TPZ are clearly bend compared to the numerical model and. The important deviation found in M2 and on the side of TPZ suggests that it is due to a collapse of the structure due to inappropriate part positioning and lack of supports. It also explains the important number of irregular pores on these regions of interests.

Comparatively the 2nd version, the deviations are more homogeneous. M2 and SCP are the more affected regions. The important deviation found in M2 coupled with an important number of irregular pores suggests that a collapse of the structure has also occurred during the manufacturing process. The spikes located on TPZ are little smaller in size.

These geometrical deviation are due to the selective laser melting process due to the reproducibility of the geometrical deviation from on specimen to another.

The difference between the two versions suggest that the part orientation and the support has introduce different level of residual stresses which has led to a different level of part distortion although the manufacturing parameters set was identical for both specimens. A collapse of the structure has occurred on both M2 surface, it is due to a low overhang angle of these structure in the manufacturing chamber. Indeed, each new welding layer must be supported at least partly by the previous one. The angle between the part and the build platform was below 45°, the lack of support structures has led to a poor surface roughness as well as distortion and large pores. The post-treatment partly decreased the defects by mirror-like finishing the surfaces of the specimens.

### 5.2. From medical data to numerical model

The measured deviation during the manufacturing process and the post-treatments shall be compared to the geometrical deviation of the numerical model. Figure 15 shows the histogram of the distance of the 1st version. The 2nd version could not be realized because the trapezium of the patient was deformed due to arthrosis.

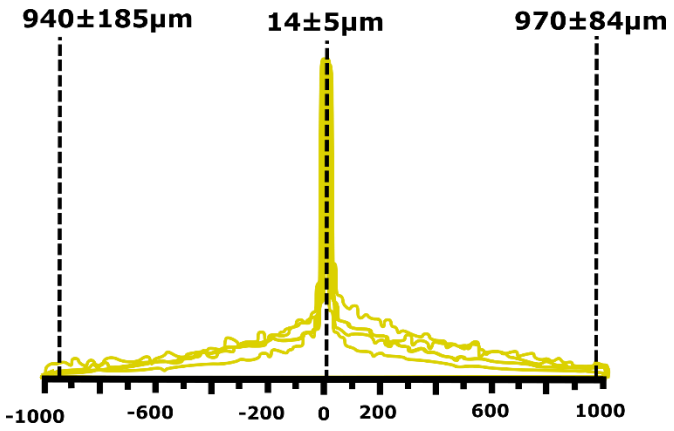


**Figure 15**: histogram of the distance between the medical image data and the numerical model

The average deviation is close to 14µm, however the 5% and 95% values are distant, around 955µm. It is mainly due to the size of voxels used in clinical computer tomography

(slice thickness = 0.625 mm and pixel size = 0.328125 mm x 0.328125 mm). Although geometrical deviations are found during this digitalization, the numerical model better pictures the real bone because of its smooth aspect.

## Discussion

This work aims at measuring the evolution of the deviation along the implant manufacturing chain. The aim is to understand which step has the greatest impact on the implant specifications.

This work demonstrates the feasibility to produce complex anatomically-shaped articular implants with a mirror-finish using additive manufacturing. Other studies has also been focused on the production of anatomical implant and controlled lattice structures by additive manufacturing [12,18,19]. With the selected manufacturing parameters, a number of defects specific of the SLM process appeared on the CoCrMo implants. At the end of the selective laser melting process, SEM analyses revealed particles partially melted in surfaces of the implants. The density of these partially melted particles was not homogenous on the entire surface of the specimens. Post-treatment was carried out by alumina sandblasting, superfinishing by physico-catalytic process and cleaning by successive ultrasonic baths. Some authors have also studied post-treatment after SLM for an implant application. Cosmo et al. [20] produced a customized implant in titanium and reached a Ra around 1,2µm after polishing the samples with carborundum abrasive discs mounted on an electric dental micro-motor. This process could not be done on our specimens due to their complex geometry. In order to get a more controlled geometric deviation, we used an automated process based on physico-catalytic method. This superfinishing have improved the quality of the anatomical surface, particularly the surface roughness, which complies with the ISO 21534: 2007. Indeed, the surface roughness was reduced to 35nm. However, the surfaces showed at the rate of pores distributed in a non-homogeneous way on both versions of the implant. This is a specific defect in additive manufacturing. The pore distribution was reproducible on the specimens. This method was already studied on Ti64 but for other application such as the enhancement of cutting tool life[21].

The increase in the aluminum content on the surface of the post-treated samples, particularly at the pore level has also been found in the study of Cosmo et al. [20]. It confirms the fact that the abrasive material of the sandblasting process is incrusted in the AM-based material and could not been completely cleaned by ultrasonication. A residual aluminum content was found after the superfinishing process inside the open-pores. A

decrease in the number of pores is therefore necessary to produced material with a controlled chemical composition that respects the standard specification. To achieve high density parts with minimal defects, a way is to optimize the set of laser parameters. The energy density is the key factor. At low energy densities, irregular pores may be found due to partial melting of the particles while at high energy densities, the pores are spherical and small due to gases trapped. The energy density varies with the laser power, the scanning speed, the hatch spacing and the layer thickness [15]. Monroy et al [22] studied the pores formation in CoCrMo parts produced by SLM. They found that the minor porosity was produced by the highest layer thickness. This strategy enhanced the thermal conductivity among the particles and subsequently permitting a successful densification. However increasing the layer thickness also decrease the accuracy of the produced parts. Another strategy to eliminate pores and defects is to apply a hot isostatic pressing (HIP) [23]. It consists to apply elevated temperatures up to 2000°C and high gas pressure up to 200Mpa. Pores close by plastic deformation. However this process is particularly efficient for internal porosity and defects but not for open-pores [23].

The geometrical inspection of the implants highlighted areas that were particularly deviated from the additive manufacturing process. This is the most critical step in terms of geometric deviation. Dimensional accuracy of CrCoMo parts fabricated by SLM was also studied by Taib et al. [24]. The geometry of their specimens allows them to perform dimensional measurements with the microscope which could not be done with our complex geometry implants. We therefore used a method based on the comparison of the scanned specimen by a laser sensor with the numerical model [25]. However this system lead to inspection uncertainty with a maximum of deviation of 100µm [26].

The most critical geometric deviations was found in the areas that features the greatest surface porosity suggesting an important thermal stress during the manufacturing a collapse of structures and the appearance of pores. Both versions of the implant showed different rates of porosity and geometric deviations, suggesting the importance of the position and quantity of the supports.

# Conclusion

The work demonstrates to produce, and post-process complex-shaped implants made by selective laser melting. The post-processing was done with corundum sandblasting, automated physico-catalytic superfinishing. The final implants complied with the surface texture specifications recommended by the standard ISO 21534 as the average roughness measured was around 35nm.

However, this study highligts the fact that the SLM is the process that have greatest impact on the implant specifications from the medical imaging data to the final post-treated implant. The laser energy, the support structures and the positioning are parameters that shall be finely controlled to obtain the desired material characteristics. Two kind of porosity was observed on the surface: round and circular pores and irregular pores, which were not homogeneously distributed on the surface of the implant. Geometrical deviations were mainly found in the areas that features the greatest surface porosity.

Although, this work discussed many manufacturing considerations, it does not address the full complexity of articular implants composed of multiple materials. The next study would be to evaluate the impact of the defects of CoCrMo part specific to SLM on the wear behavior of polyethylene material. The effect on the biocompatibility and the corrosion resistance are also concerns that should be addressed.

Different strategies to optimize parts quality would be interested such increasing the energy density during the SLM process and improving the support structures. Additional post-processing would also be a good study direction such as thermal treatment to release internal stresses and hot isostatic pressing to close internal pores.

# References list

[1] ASTM International, Standard Terminology for Additive Manufacturing Technologies, ASTM F2792 - 10. (2010).

[2] N. Guo, M.C. Leu, Additive manufacturing: technology, applications and research needs, Front. Mech. Eng. 8 (2013) 215–243.

[3] N. Taniguchi, S. Fujibayashi, M. Takemoto, K. Sasaki, B. Otsuki, T. Nakamura, T. Kokubod, S. Matsudaa, Effect of pore size on bone ingrowth into porous titanium implants fabricated by additive manufacturing: an in vivo experiment, Mater. Sci. Eng. C. 59 (2016) 690–701.

[4] W.C. Rodrigues, L.R. Broilo, L. Schaeffer, G. Knörnschild, F.R.M. Espinoza, Powder metallurgical processing of Co–28% Cr–6% Mo for dental implants: Physical, mechanical and electrochemical properties, Powder Technol. 206 (2011) 233–238.

[5] S. Cox, P. Jamshidi, N. Eisenstein, M. Webber, H. Hassanin, M.M. Attallah, M.M. Attallah, D. ET Shepherd, O. Addison, L.M. Grover, Adding functionality with additive manufacturing: Fabrication of titanium-based antibiotic eluting implants, Mater. Sci. Eng. C 64 (2016) 407–415.

[6] X. Wang, Z. Xu, S., X. S., L. W., C. M., Q. P., B. M., Y.M. Xie, Topological design and additive manufacturing of porous metals for bone scaffolds and orthopaedic implants: A review, Biomaterials. 83 (2016) 127–141.
[7] J.A. Davidson, Characteristics of metal and ceramic total hip bearing surfaces and their effect on long-term ultra high molecular weight polyethylene wear., Clin. Orthop. Relat. Res. (1993) 361–78.
[8] L. Zagra, E. Gallazzi, Bearing surfaces in primary total hip arthroplasty., EFORT Open Rev. 3 (2018) 217–224.
[9] C. Song, Y. Yang, Y. Wang, D. Wang, J. Yu, Research on rapid manufacturing of CoCrMo alloy femoral component based on selective laser melting, Int. J. Adv. Manuf. Technol. 75 (2014) 445–453. doi:10.1007/s00170-014-6150-7.
[10] A. Lerebours, F. Marin, S. Bouvier, C. Egles, A.-C. Masquelet, A. Rassineux, A voxel-based method for designing a numerical biomechanical model patient-specific with an anatomical functional approach adapted to additive manufacturing, Comput. Methods Biomech. Biomed. Engin. 22 (2019). doi:10.1080/10255842.2018.1552684.
[11] M. Nasab, M. Hassan, B. Sahari, Metallic biomaterials of knee and hip-a review, Trends Biomater. Artif. Organs. 24 (2010) 69–82.
[12] E. Liverani, A. Fortunato, A. Leardini, C. Belvedere, S. Siegler, L. Ceschini, A. Ascari, Fabrication of Co-Cr-Mo endoprosthetic ankle devices by means of Selective Laser Melting (SLM), Mater. Des. 106 (2016) 60–68. h.
[13] X.Z. Xin, N. Xiang, J. Chen, D. Xu, B. Wei, Corrosion characteristics of a selective laser melted Co-Cr dental alloy under physiological conditions, J. Mater. Sci. 47 (2012) 4813–4820..
[14] X.Z. Xin, N. Xiang, J. Chen, B. Wei, In vitro biocompatibility of Co-Cr alloy fabricated by selective laser melting or traditional casting techniques, Mater. Lett. 88 (2012) 101–103..
[15] B. Zhang, Y. Li, Q. Bai, Defect Formation Mechanisms in Selective Laser Melting: A Review, Chinese J. Mech. Eng. 30 (2017) 515–527.
[16] A. Internationnal, Standard Specification for Cobalt-28 Chromium - 6 Molybdenum castings and casting alloy for surgical implats, (2012).
[17] International Organization for Standardization, Non-active surgical implants — Joint replacement implants — Particular requirements, ISO 21534. (2007).

[18] A. Lerebours, P. Vigneron, S. Bouvier, A. Rassineux, M. Bigerelle, C. Egles, Additive manufacturing process creates local surface roughness modifications leading to variation in cell adhesion on multifaceted TiAl6V4 samples, Bioprinting. 16 (2019).
[19] B. Lethaus, L. Poort, R. Böckmann, R. Smeets, R. Tolba, P. Kessler, Additive manufacturing for microvascular reconstruction of the mandible in 20 patients, J. Cranio-Maxillofacial Surg. 40 (2012) 43–46.
[20] C. Cosma, N. Balc, M. Moldovan, L. Morovic, P. Gogola, C. Borzan, Post-processing of customized implants made by laser beam melting from pure Titanium, Optoelectron. Adv. Mater. 19 (2017) 738–747.
[21] A.K. Srivastavaa, X. Zhangb, T. Bellc, S. Cadiganaand, Investigations on turning Ti-6Al-4V titanium alloy using super-finished tool edge geometry generated by micro-machining process (MMP), CIRP Ann. Manuf. Technol. (2011).
[22] K. Monroy, J. Delgado, J. Ciurana, Study of the pore formation on CoCrMo alloys by selective laser melting manufacturing process, Procedia Eng. 63 (2013) 361–369.
[23] S. Tammas-Williams, P.J. Withers, I. Todd, P.B. Prangnell, The Effectiveness of Hot Isostatic Pressing for Closing Porosity in Titanium Parts Manufactured by Selective Electron Beam Melting, Metall. Mater. Trans. A. 47 (2016) 1939–1946.
[24] Z.M. Taib, W. Harun, W. Sharuzi, S. Anwar, C. Ghani, R. Mohd Fadzil Faisae ab, O. Modh asnawi, R. Hazlen, Dimensional accuracy study of open cellular structure CoCrMo alloy fabricated by selective laser melting process, Adv. Mater. Res. 1133 (2016) 280–284.
[25] I. Drstvensek, N. Hren, T. Strojnik, T. Brajlih, B. Valentan, V. Podacar, T.. Hartner, Applications of rapid prototyping in cranio-maxilofacial surgery procedures, Int J Biol MBiomed Eng. 1 (2008) 29–38.
[26] M. Yu, Y. Zhang, Y. Li, D. Zhang, Adaptive sampling method for inspection planning on CMM for free-form surfaces, Int. J. Adv. Manuf. Technol. 67 (2013) 1967–1975.

## 3. Intermediate conclusion

In this chapter, we have demonstrated the feasability to produce complex-shape articular implant with additive manufacturing and diverse post treatments that comply standard specifications regarding the surface texture. The superfinishing used in this work was found to be suitable. Therefore, this study provides a reference for the design, the manufacture by selective laser melting and the post-treatment of articular medical implants made of chromium-cobalt-molybdenum.

The evolution of the deviation along the implant manufacturing chain was determined. Pores were the main defects of the specimens along with local geometrical deviations. Both concerns came from the selective laser melting process.

Different strategies exist to optimize parts quality. A first way is to modify SLM parameters to increase the energy density and also to put additional support structures. A second way is to post-process the specimens. Thermal treatment enables the release of internal stresses while hot isostatic pressing enables the closure of internal pores.

The following chapter will focus on the impact of additive manufactured surfaces on the wear behavior and the biocompatibility. It will particularly be focused on the effect of the residual porosity on the wear of polyethylene under lubricated conditions.

# CHAPTER 5:

# Impact of an additive manufactured surface on articular implant specifications: Wear behavior and biocompatibility

*Ce chapitre aborde l'impact de la fabrication additive métallique sur les spécifications des implants articulaires, tout particulièrement la résistance à l'usure et la biocompatibilité.*

*Nous avons montré dans un premier temps ; qu'il est possible de produire une tige métacarpienne en Ti6Al4V par fusion sélective par laser tout en préservant les propriétés non cytotoxiques. Ce procédé permet d'obtenir une texture de surface unique basée sur des poudres partiellement fondues et des traces créées par des pistes laser. Les résultats ont montré que les cellules ostéoblastiques adhéraient de façon inégale dans l'échantillon. Cette variation d'adhérence est directement corrélée aux variations de texturation de surface. La source des hétérogénéités de texture de surface induites par le procédé peut être contrôlée par l'inclinaison des surfaces pour promouvoir les caractéristiques nécessaires des implants à interface osseuse.*

*Nous avons étudié également les performances tribologiques entre un alliage de cobalt-chrome réalisé par fabrication additive et du polyéthylène haute-densité. Nous avons montré que la porosité inhérente du procédé de fusion sélective par laser a un impact significatif sur l'usure du polymère. L'optimisation des paramètres d'impression est donc essentielle pour réduire ce type de défaut et augmenter la durée de vie de l'implant.*

## 1. General context

The developed implant consists of two parts: a trapezium part known as a trapezium bone replacement and a metacarpal part composed of a stem anchored in the medullar canal of the 1st metacarpal bone and a polymer insert. In this chapter, the idea is to study the characteristics of the selected biomaterials in a simulated anatomical environment. In this context, metacarpal rods were produced by additive manufacture in Ti6Al4V. The idea is to understand whether the unique surface texturing resulting from additive powder bed manufacturing provides sufficient support for cell adhesion, allowing us to avoid potentially costly post-treatment. This work proposes an approach to understand and therefore control the heterogeneities of surface texturing that have a direct impact on the cellular adhesion of an osteoblastic line. In the previous chapter, advanced prototypes of the replacement trapezium bone were made of chromium-cobalt alloy by additive manufacturing on a powder bed followed by a superfinishing process. These prototypes with complex morphology do not allow us to easily simulate the biotribological environment. However, it has been demonstrated that additive manufacturing in the selected parameters induces a geometric deviation in some areas correlated with an increasing number of open pores. Simpler samples were then produced using the same process. The idea is to understand the impact of this porosity on polymer wear by simulating friction with a lubricant similar to synovial fluid. This study was conducted with cobalt-chromium-based alloy samples. By understanding the origin of wear variations, optimization solutions can be more easily understood by modifying manufacturing parameters or post-treatments such as hot isostatic compression or heat treatments.

## 2. Scientific article

- Lerebours, A., Vigneron, P., Bouvier, S., Rassineux, A., Bigerelle, M. and Egles, C., 2019. Additive manufacturing process creates local surface roughness modifications leading to variation in cell adhesion on multifaceted TiAl6V4 samples. *Bioprinting*, p.e00054.

- Lerebours, A., Demangel, C., Dembinski, L., Bouvier, S., Rassineux, A., and Egles, C., Effect of the residual porosity of selective laser melted CrCoMo parts on the wear of polyethylene under lubricated conditions. *Submitted in Biotribology*

# Article 5:

Bioprinting 16 (2019) e00054

Contents lists available at ScienceDirect

Bioprinting

journal homepage: www.elsevier.com/locate/bprint

## Additive manufacturing process creates local surface roughness modifications leading to variation in cell adhesion on multifaceted TiAl6V4 samples

Augustin Lerebours [a,*], Pascale Vigneron [b], Salima Bouvier [a], Alain Rassineux [a], Maxence Bigerelle [c], Christophe Egles [b]

[a] Alliance Sorbonne Université, Université de Technologie de Compiègne, CNRS, FRE-2012 Roberval, Centre de Recherche Royallieu, CS 60 319, 60 203, Compiègne Cedex, France

[b] Alliance Sorbonne Université, Université de Technologie de Compiègne, CNRS, UMR 7338 BioMécanique et BioIngénierie (BMBI), Centre de Recherche Royallieu, CS 60 319, 60 203, Compiègne Cedex, France

[c] LAMIH Laboratory, UMR CNRS 8201, University of Valenciennes, Valenciennes, 59313, France

ARTICLE INFO

*Keywords:*
Additive manufacturing
Selective laser melting
Inclination angle
Cell attachment
Biomedical implant
Multifaceted geometric specimen

ABSTRACT

This work looks at the effect of the surface texture variability on cell adhesion and cell morphology of an osteoblastic linage (MC3T3) using a multifaceted TiAl6V4 (stem-like) specimen produced by selective laser melting.

We produced a Ti6Al4V anchoring component presenting de facto surfaces with different inclinations with respect to the build plate. Surfaces had different complex surface textures composed of submicroscale groove tracks induced by the laser beam, and partially melted particles varying with the inclination of the surface in the SLM chamber. We measured the adhesion of cells on the specimen, having previously tested any cytotoxic effect of the material on a fibroblastic linage. Our multifaceted geometric specimens made it possible to compare potential effects of different surface textures on the same specimen. We found that cell attachment increased on surfaces with microscale grooves, and that partially melted powders were the least appreciated zones for adhesion (26-fold increase in the number of cells from a zone containing 1192 particles/mm$^2$ compared to 188,3 particles/mm$^2$). The ratio of the number of submicroscale grooves to the number of partially melted particles can be controlled by the inclination of the surface with respect to the build plate. Surfaces with a lower inclination (upskin surfaces) had fewer partially melted particles than downskin surfaces (200 particles/mm$^2$ at 35° compared to 1200 particles/mm$^2$ at 125°).

Based on our results, we propose an approach to better understand and therefore control the inherent heterogeneities of AM-based implants in order to reduce potentially costly post-processing for osseous interface implant.

## 1. Introduction

An ageing population creates a need for new material suitable for biomedical applications. For instance, it has been estimated that there are more than 2.5 million people with a hip implant in the US [1], and this is expected to have grown by 27% by 2030 [2]. Similarly, the number of knee arthroplasty procedures is expected to have grown by 32% by 2030, with 600 000 procedures forecasted annually [2]. Many of these procedures are revision surgery, due to the short lifespan of the current orthopedic implants and the increasing life expectancy of patients, together

*Abbreviations:* **AM**, additive manufacturing; **SLM**, selective laser melting; **3D**, three-Dimensional; **HAp**, hydroxyapatite; **TPS**, titanium plasma spraying; **CaP**, Calcium Phosphate; **SEM**, Scanning Electron Microscope; **EBSD**, Electron backscatter diffraction; **CPO**, crystallographic preferred inclination; **DMEM**, Dulbecco's Modified Eagle Medium; **FBS**, foetal bovine serum; **α-MEM**, α-Minimum Essential Medium; **UV**, ultraviolet; **PCA**, principal component analysis; **CHO**, Chinese hamster ovarian.

* Corresponding author. Sorbonne Universités, Université de technologie de Compiègne, CNRS, FRE-2012 Roberval, Centre de recherche Royallieu, CS 60 319, 60 203, Compiègne cedex, France.

*E-mail addresses:* augustin.lerebours@utc.fr (A. Lerebours), pascale.vigneron@utc.fr (P. Vigneron), salima.bouvier@utc.fr (S. Bouvier), alain.rassineux@utc.fr (A. Rassineux), maxence.bigerelle@uphf.fr (M. Bigerelle), christophe.egles@utc.fr (C. Egles).

https://doi.org/10.1016/j.bprint.2019.e00054
Received 6 December 2018; Received in revised form 7 June 2019; Accepted 24 June 2019

with an increased use of orthopedic implants for younger patients [2]. One of the main complications observed is the loosening between the implant and the surrounding bone [3]. The development of new technologies such as additive manufacturing has created a trend towards complex, customized implants more adapted to the pathology of the patient, meaning that more and more biomedical implants are niched.

Among the material available, the TiAl6V ELI alloy (ISO 5832-3 standard) is the most widely used material for biomedical implants due to its excellent biocompatibility, strength-to-weight ratio, corrosion resistance, toughness, and bio-inert oxide surface [4]. It has been well-established that the success rate of osseous anchored implants such as femoral stem, knee implants and dental implants, depends on the osseointegration, osteoconduction, and osteoinduction properties at the interface with the bone tissue. These complex biological processes are influenced to a certain extent by the topography, chemistry, and surface energy properties of the implant [5]. A number of research groups have proposed modifications of these surfaces for enhancing osseous integration at the interface, including grit-blasting, hydroxyapatite (HAp) coating [6,7], titanium plasma spraying (TPS) [8,9], and nanostructured Calcium Phosphate (CaP) coating [10].

Additive manufacturing (AM), also known as rapid-prototyping, is a layer-by-layer manufacturing process which allows the creation of implants with a more complex structure (internal and external), when compared to traditional manufacturing processes such as milling and turning that are more suited to mass production [11,12]. However, by its very nature the AM process creates heterogeneity in the specimen that can be seen in the topography of the surface ("stair stepping" effect) and the inner characteristics of the material used (anisotropic mechanical properties due to interlayer bonding deficiencies) [11,12]. One of the main advantages of AM is being able to adapt the implant to the patient in relation to manufacturing parameters such as porosity, shape, and surface texture. In metal AM, selective laser melting (SLM) is a technology that uses a laser to melt and fuse metallic powders together [13], as shown in Fig. 1. Some metal AM prostheses have already been designed and tested, including total knee arthroplasty [14], the femoral component of total hip replacement [15], and dental implants [16]. The drawback is that costly post-processing (HAp and TPS coating) is often required.

Some studies have looked at lattice structures in metal AM Ti6Al4V implants as a means of enhancing bone ingrowth by mimicking the trabecular osseous aspect [17,18]. These studies found that pore size and pore interconnectivity are essential for enhancing (i) osteoinduction (stimulation of progenitor cell linage to cause differentiation into osteo-blastic cells), (ii) osteoconduction (allows bone growth on the surface), and (iii) osseointegration (stable anchorage of the material by surrounding it with bony tissue) [19]. These lattice structures allow a well-fixed interconnected interface as well as HA coating. However, they have a disadvantage for revision surgery, because removing a well-fixed implant involves a technically complicated, destructive procedure [6,20,21]. The bone tissue around the implant often needs to be cut away, leaving insufficient bone stock for a new medical device to be implanted. With patients living longer and placing higher demands on their revision prostheses, an easy removal of the implant for revision is becoming a more important consideration.

The bone anchoring process (osteoinduction, osteoconduction, osseointegration) is linked to first-instant osteoblastic cell adhesion. The relation of surface roughness to cell adhesion has already been studied. Anselme et al. c [22] found that the smoother the Ti6Al4V surface, the more MC3T3 osteoblasts are able to adhere, proliferate and appear spread out on the specimens. This finding has been confirmed by other research groups [23,24]. However, melting the powder using a laser beam as part of the SLM process may create a complex surface structure, depending on the inclination, which may modify the behavior of osteoblast-like cells.

This work investigates the possibility of using an anchoring component without a porous structure, therefore avoiding any costly additional post-processing before implantation. We examined changes in cell adhesion and cell morphology of osteoblastic MC3T3 on a multifaceted TiAl6V4 specimen produced by SLM, with respect to roughness parameters and inclination.

Here, the specimen was inspired by the design of typical carpometacarpal stem component that fits into the metacarpal bone [25].

Our aim was to fully understand heterogeneities arising inherently from the AM process and the effects of these heterogeneities on osteoblastic cell adhesion for orthopedic implants. Being able to control these heterogeneities via the AM parameters is potentially of great benefit in reducing the need for costly post-processing.

## 2. Material and methods

### 2.1. Specimens

Test specimens were Ti6Al4V discs of 20 mm in diameter and 2 mm thick, and multifaceted pieces of 20 mm in height, as shown in Fig. 2 B. Both specimens were designed using CATIA V5 CAD (computer-assisted-design) software. The digital CAD file for the specimens was converted to the stereolithography (STL) file format required by the additive manufacturing technology. The specimens were produced by powder-based 3D-printing technology, namely selective laser melting (the SLM SOLUTIONS SLM125HL system). The multifaceted specimens have surfaces with different inclinations to the build plate Fig. 2 A. The parameters are described in Table 1. The multifaceted specimens were built in an Ar environment with a residual oxygen content of 0.5%. A stripe hatching style was used with a different angular variation for each layer (n→ n+1) in order to obtain a low temperature gradient in the bulk volume. The raw material was atomized Ti6Al4V powder supplied by TLS Technik, with nominal chemical composition by Energy-dispersive X-ray spectroscopy (EDX), as reported in Table 2. The powder grains were spherical, as shown in Fig. 2C. A dry granulometry of the powder indicated a size in the range 15.87–55.83 µm (respectively d(0.1) and d(0.9)) (Fig. 2 D), and the powder was steamed at 45° for 48 h before the production was done. The chemical composition of the surface (a few microns) after the additive manufacturing by energy-dispersive X-ray spectroscopy (EDX) is also reported in Table 2, with significant differences in the Al, Ti, Fe and V contents.

Prior to any analysis and *in vitro* experimentation, specimens were cleaned each time successively with 30 min of ultrasound treatment in a sodium dodecyl sulfate solution at the critical micelle concentration (0.1728–0.2304% w/v), 70% alcohol and in distilled water.Finally they were sterilized in an autoclave.

### 2.2. Material characteristics

Defects in the SLM specimens in the longitudinal and transversal directions were identified using an optical microscope after the surfaces had been polished.

For microstructural investigation, small samples of each of the two types of specimen were mounted in epoxy pucks for polishing, and in order to obtain a mirror-like surface finish they were polished using grit paper from grade 350 to 4000 and a 1 µm diamond suspension. A final chemical-mechanical polishing was carried using an OP-S colloidal silica solution (Struers). The microstructural-crystallographic characterization was done using a Scanning Electron Microscope (SEM) equipped with an Electron backscatter diffraction (EBSD).

The density of the SLM specimens was calculated as the ratio between pores and materials, using 10 sets of optical microscope images and the *ImageJ* program's *AnalyseParticle* plugin.

### 2.3. Surface structure analysis

Surface structure measurement of the different surfaces was done using a confocal microscope laser (Sensofar) on three multifaceted

specimens (Fig. 2) using a 1746 × 1313 µm zone and a form removal via a polynomial filter of degree 6 to remove the 3-dimensional aspect of the specimens. For each specimen, 3 measures were done per surface texture (zone 1 to 4) to extract roughness parameters:

- height parameters (peaks and valleys) including *arithmetical mean height* (Sa), *root mean square height* (Sq), *maximum height* (Sz), *skewness* (Ssk) and *kurtosis* (Sku)
- hybrid parameters including *root mean square gradient* (Sdq), *developed interfacial area ratio* (Sdr)
- functional parameters including *core roughness depth* (Sk), *reduced peak height* (SpK), *reduced valley depth* (Svk).

Skewness (Ssk) represents the degree of symmetry of the surface heights about the mean plane, while kurtosis (Sku) indicates the randomness of heights and sharpness of the structures comprising the surface.

Surface structure measurements were also performed on the grooves created by the laser track and on the surface of partly melted powders.

Specimens were also examined by SEM and optical microscopy to have complementary results. SEM images were done at an accelerating voltage of 20 kV. The unmelted particles on the surface were counted using a 3 zones of 1000 × 1000 µm from the SEM images of each different surfaces (*ImageJ*).

### 2.4. Cell culture

All culture products were obtained from Gibco™ | ThermoFisher Scientific. Mouse fibroblasts L929 cell line (ATCC CCL-1) were used to determine the cytotoxicity of the powder (raw material) and the as-SLM disc specimens. Cells were grown in DMEM (Dulbecco's Modified Eagle Medium) supplemented with 10% FBS (fetal bovine serum), 2 mM L-glutamine, 100 U/mL penicillin, and 100 µg/mL streptomycin at 37 °C in a 5% $CO_2$ humidified environment.

Mouse preosteoblasts MC3T3-E1 subclone 4 (ATCC –CRL-2593) derived from mouse calvarium tissue were used to assess the adhesion by measuring the cell covering rate and the cell nuclei count after 72 h on the SLM specimens. The cells were grown in an α-MEM medium (Minimum Essential Medium) supplemented with 10% FBS, 2 mM L-glutamin, 100 U/mL penicillin, and 100 µg/mL streptomycin at 37 °C in a 5% $CO_2$ humidified environment.

#### 2.4.1. Indirect cytotoxicity

A cytotoxicity test was performed using the indirect method according to EN ISO10993-5 "Biological evaluation of medical device-Part 5: Tests for *in vitro* cytotoxicity". L929 mouse fibroblasts are recommended by international standards for the testing of medical devices. The test results reflect the cell metabolic level when cultured with an extract of the specimen and thus, to a certain extent, the number of cells. Specimen extracts were prepared in the medium used for cell culture (DMEM) as suggested by ISO 10993–12:2009 "Biological evaluation of medical devices-Part 12: Specimen preparation and reference materials". Extracts from as-SLM disks were obtained by incubating 1 mL of medium for 3 $cm^2$ of disk surface at 37 °C, 5% $CO_2$ in air for 24 h and those from the powder were obtained by incubating 1 ml of medium with 0.2 g/mL at 37 °C, 5% $CO_2$ in air for 24 h. Extracts were then diluted at 0%, 25%, 50%, 75% in DMEM. 1 × $10^4$ L929 cells were seeded per well of a 96-well cell culture plate and incubated at 37 °C, 5% $CO_2$ in air for 24 h, before the culture medium was removed from the wells then replaced by 100 µL of test extracts and incubated for an additional 24 h at 37 °C. Control wells consisted in untreated cell cultures. 20 µL of MTS reagent (Promega, France) was added to each well and they were kept in a dark environment for 3 h at 37 °C. Subsequently, the absorbance at 490 nm was measured using a UV–visible spectrophotometer (Biorad, France). MTS assays were repeated in three separate experiments. Negative control consists in elutes of latex at 3 $cm^2$/mL and positive control consists in culture medium only.

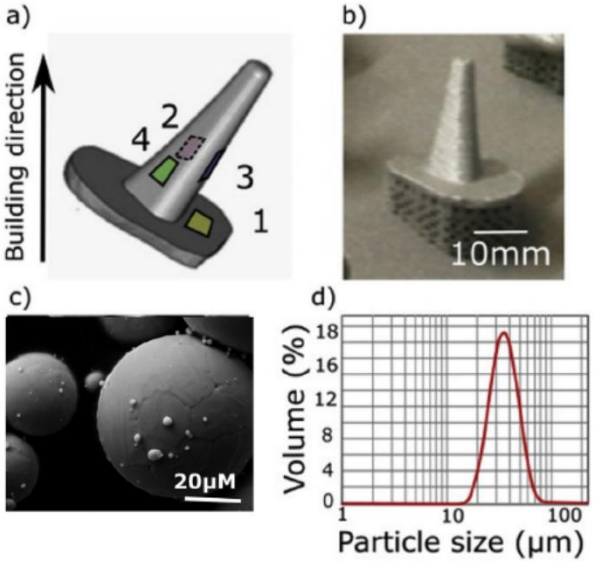


Fig. 2. a) Multifaceted stem-like specimen and inclination in the SLM manufacturing chamber with 4 distinctive surfaces defined by an angle with the AM build plate: 1) 35.7°; 2) 78.45°; 3)124.2°; 4) 53.92°; b) Multifaceted specimen created by selective laser melting (SLM); c) Morphology of the Ti6Al4Vpowder (SEM image); d) granulometry of the Ti6Al4V powder.

#### 2.4.2. Cell covering rate and nuclei count

MC3T3-E1 subclone 4 were used for cell covering was assessment 3

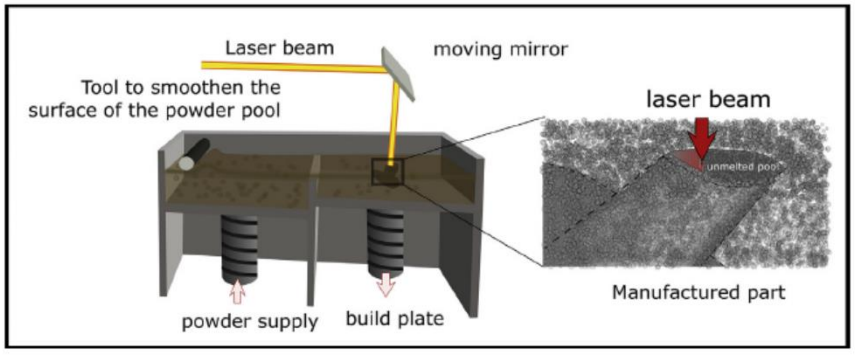


Fig. 1. Typical Selective Laser Melting (SLM) layout.

**Table 1**
Comparison between the chemical composition of Ti64 samples-as-SLM and Ti64 powders.

| Composition of Ti64-ELI powders | | | | | | | | | |
|---|---|---|---|---|---|---|---|---|---|
| Al | C | Fe | H | N | O | Ti | V | Others | All Others |
| 6.2 | 0.01 | 0.14 | 0.002 | 0.01 | 0.07 | Bal | 4.1 | <0.1 | <0.01 |
| **Composition of Ti64-ELI samples-as SLM in the surface** | | | | | | | | | |
| **Al** | **C** | **Fe** | **H** | **N** | **O** | **Ti** | **V** | **Others** | **All Others** |
| 4,97 ± 0,26 | - | 0,19 ± 0,38 | - | - | - | 91,64 ± 1,26 | 2,74 ± 0,20 | – | – |

**Table 2**
Manufacturing parameters and stripes hatching strategy.

| | Puissance | Vitesse | Gaz de protection | Argon |
|---|---|---|---|---|
| Bulk filling | 175 W | 775 mm/s | Pattern type | stripes |
| Contour filling | 100 W | 525 mm/s | Hatch vector | 120 µm |
| Border | 100 W | 525 mm/s | Distance inter ext. border/center | 60 µm |
| | | | Layer width | 30 µm |
| Stripes hatching strategy | 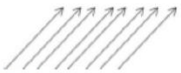 Couche n | | 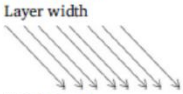 Couche n+1 | |

days post-seeding. Cells were cultivated on the different surfaces of each multifaceted specimens in a non-adhesive polystyrene tube with a gentle orbital agitation to ensure that cells would be in suspension during the entire duration of the experiment and therefore would adhere to every surface of the alloy (326 $mm^2$: CAD model prior manufacturing). $1.4.10^6$ cells contained in 20 mL of culture medium were seeded in each specimen and incubated at 37 °C in a 5% $CO_2$ atmosphere. After 72 h, that is to say enough time to allow complete adhesion and proliferation, cells were fixed in a 4% paraformaldehyde solution for 30 min and images from backscattered electrons were acquired using a Jeol SEM at 5 kV accelerating voltage to highlight cells (black) against the material (white). The cell covering rate was calculated from the picture using ImageJ software by applying an adapted thresholding with the same magnification characteristic and by subtracting the percentage obtained with the untreated specimen.

The experimental design is shown in Fig. 3.

For the cell nuclei count, the MC3T3-E1 were incubated, after a 4% paraformaldehyde fixation for 30 min in a staining solution containing fluorescein isothiocyanate 1 mg/mL in PBS (Sigma Aldrich, France, whole cells in green) and DAPI 1 µg/mL (Sigma Aldrich, France; nuclei in blue) for 5 min at room temperature. Cells were then observed with an inverted Leica DMI6000B fluorescence microscope and images were acquired. The nuclei count was estimated using the *ImageJ* program's *Cell Counter* plugin.

### 2.5. Cell morphology

MC3T3-E1 morphology was assessed after a 2-day culture by SEM. Cells grown on the different surfaces of each multifaceted specimens are fixed with 2.5% Glutaraldehyde in 0.1 M Phosphate Buffer, pH 7 for 30 min at room temperature. After dehydration in graded ethanol (70%–100%), cells were coated with gold to a thickness of approximately 100 nm and examined in a Quanta Fey 250 (FEI) SEM at an accelerating voltage of 10 kV.

### 2.6. Principal component analysis

A principal component analysis (PCA) [26] was realized on the variables (roughness parameters, inclination) and observations (zone 1 to 4 of specimen 1 to 3). The results regarding cell attachment (cell covering and cell counting) were added as supplementary variables. These variables therefore do not participate in the orthogonal basis of the PCA. PCA is a statistical procedure that uses an orthogonal transformation to convert a set of observations of possibly correlated variables into a set of values of linearly uncorrelated variables known as principal components. PCA organize the dataset in orthogonal basis-set that maximize the variance between observations and between variables. This reorganization means that the variables and observations are shown in a reduced dimension and therefore gives a global view of any potential correlation between roughness parameters, inclination and cell adhesion. As PCA is sensitive to the relative scaling of the original variables, the variables were therefore all centered and reduced.

## 3. Results

### 3.1. Material characterization

First, we concentrated on the inner characteristic properties of the material.

As shown in Fig. 4 A, the defects of the TiAl6V-as SLM consisted in pores of 1–30 µm. The pores are homogenously distributed in both longitudinal and transversal directions. A density of 99.72% was measured using the *ImageJ* program's *AnalyseParticle* plugin.

When considering the microstructure of the TiAl6V-as SLM, we had a homogeneous martensitic microstructure as shown in Fig. 4 B. It is a fully entangled martensitic hcp α' lathes microstructure inside the prior-β grains. A semi-manual method using Matlab [28] was applied. The thickness of the lathes has a mean value of 0.3 µm. The presence of prior β-grains was assessed in Fig. 4C via a semi-manual method using Matlab. Fusion layers are not observed in the crystallographic microstructure. This microstructure can be explained by the temperature history during

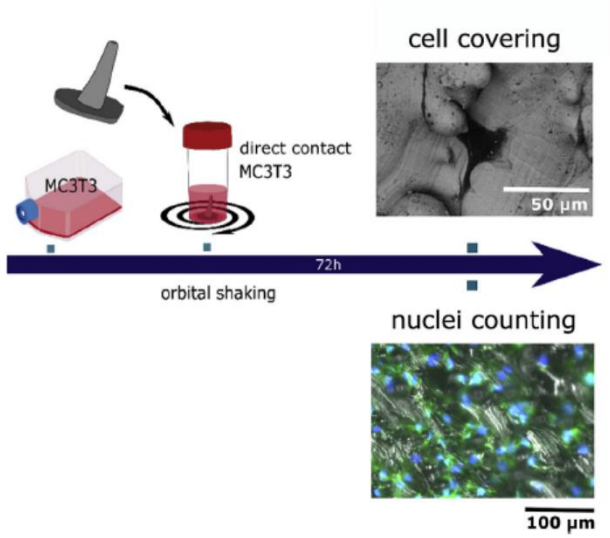


Fig. 3. Cell covering rate (backscatter electron SEM) and nuclei counting (epifluorescence microscope) experimental design.

the SLM process, as the laser beam goes around a defined point several times in a single layer and between successive layers. The peculiar morphology of the β prior grains suggests that they originated in single powder, with a circular grain shape above, and a melted grain shape below. No crystallographic preferred inclinations (CPO) were observed when comparing the inclination of grains from different $\beta$ prior grains. This isotropic characteristic is believed to be induced by the stripes hatching strategy adopted for the build, by inducing a rotation of the scanning direction for each new layer. The layers of the additive manufacturing process are not directly observed and large prior β grains indicate a good parametrization of the process.

### 3.2. Surface structure analysis

In order to test the potential heterogeneity of the surface texture between the 4 selected areas, we did an optical profilometry analysis, as shown in Fig. 5 (see also Vid S5.1, Vid S5.2, Vid S5.3, Vid S5.4). Two types of topology can be distinguished in the partly melted powder and grooves, as shown in Fig. 6 (see also Vid S6.A, Vid S6.B). The proportion of these topologies varies for each selected area. We observed that zone 1 had the lowest number of particles, with around 200 per $mm^2$, and thus the highest proportion of grooves. Zone 3 had just under 2.5 times the number of particles in zone 1, and zone 3 twice the number. Zone 4 was totally covered in particles, almost 1200 in number, with no visible grooves. We remarked that the upskin surfaces (zones 1, 2, and 3) i.e. surfaces facing upwards during the manufacturing process (Fig. 2 A) contain grooves, while the downskin surface (zone 4) does not.

Supplementary video related to this article can be found at https://doi.org/10.1016/j.bprint.2019.e00054.

The roughness parameters vary between the different areas, and appear to be linked to the quantity of partially melted powder, as shown in Table 3. The surfaces had Sa (*i.e. arithmetical mean height*) values ranging between $8.7 \pm 0.6$ µm (zone 1) and $19.2 \pm 1.12$ µm (zone 4) (Table 3), while the grooves had an Sa of $0.11 \pm 0.03$ µm. Sq varied in a similar fashion. With the exception of Sku, the grooves had negligible (submicroscale) roughness values in comparison to the other surfaces (Table 3), but they influenced the anisotropy of the surface texture, as shown in the polar spectrum of Fig. 6 and Table 3. The main texture direction of the upskin surfaces (zones 1, 2, and 3) corresponds to the direction of the grooves. Sku, that is to say *kurtosis*, is a coefficient of the sharpness of the 3D profile. It is to be expected that the particle's spherical shape will negatively affect kurtosis values, and that the grooves will affect them positively (Table 3). Ssk, that is to say *skewness*, is the degree of symmetry of the surface heights about the mean plane. A predominance of peaks is indicated by negative values, and inversely for valley structures. Upskin surfaces had more peaks than valleys, in contrast to the downskin surfaces, which had a normal distribution of peaks.

The parameters Spk, Sk, and Svk are parameters determined from the Areal Material Ratio curve, according to the ISO 13565–2:1996 standard. Spk represents the mean height of peaks above the core surface, and so is a good indicator of the amount of partially melted powder above the core surface. This is why Spk has similar values for all the distinctive areas around 19 µm. Conversely, Svk is the measure of the valley depths below the core roughness and may be related to the depth of the groove. However, SvK values considerably exceeded the depth of the grooves (Fig. 6) suggesting that SvK is related to a valley topography at a higher scale. Sk is the roughness of the surface without predominant valleys and peaks, and so the larger particles were removed, which explains why the Sk values of the different zones vary similarly to the Sa values.

Finally, the 3D profile of the surface of the partially melted particle shown in Fig. 6 had a smoother surface (<0.2 µm) than the grooves (>0.7 µm), as the figure clearly shows.

### 3.3. Indirect cytotoxicity

All the implants are intended to interact with tissue and cells. For this reason, we tested any potential toxicity induced by the SLM process.

The results of the cytotoxicity of as-SLM discs and raw material (powders) are summarized in Fig. 7. The MTS cytotoxicity test revealed no indirect cytotoxicity in either the powder or the disks, values being similar to the negative control (100%). In accordance with EN ISO10993-5, specimens are judged to be non-cytotoxic, given that the viability results exceed 70% viability. In fact, viability was significantly lower with the positive control.

### 3.4. Cell covering rate and nuclei count

Recognition of the implant implies cell adhesion. We therefore tested cell covering with an osteoblastic linage.

The SEM images of the cell covering of the different surfaces are shown in Fig. 8.

MC3T3 showed a good adhesion on the specimen, with no cells observed in the supernatant. Cell distribution is not homogeneous on the specimen. Cells showed a good adhesion on the topological texture induced by the laser track i.e. the microscale groove (Zone 1: $92.5 \pm 3.8\%$) but almost no cells grew on the partially melted powders (Zone 4: $10.7 \pm 3.8\%$). Average covering rates were observed for zone 3 and zone 2 (zone 3: $54.2 \pm 24.3\%$; zone 2: $66.6 \pm 23.6\%$). Furthermore, the microgrooves tend to promote a slight contact guidance of the osteoblastic cells along a narrow range of angles.

During the experiment, there were 5 different possibilities for any given cell: (i) zone 1: high percentage of submicroscale grooves and few partially melted powders; (ii) (iii) zone 2 and 3: average percentage of submicroscale grooves and partially melted powder; (iv) zone 4: saturated number of partially melted powder with no submicroscale grooves

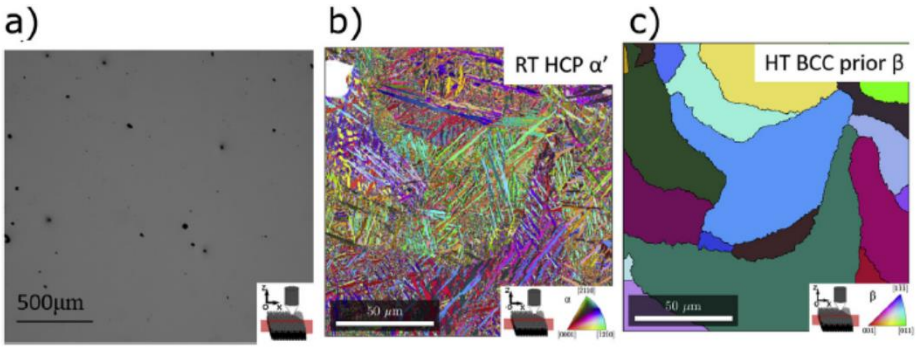


Fig. 4. Material characteristic of the Ti64-specimens-as-SLM: a) porosity (optical microscope), b) fully entangled martensitic hcp α′ lathes microstructure inside the prior-β grains (EBSD) C prior-β grains (semi-manual method in MATLAB).

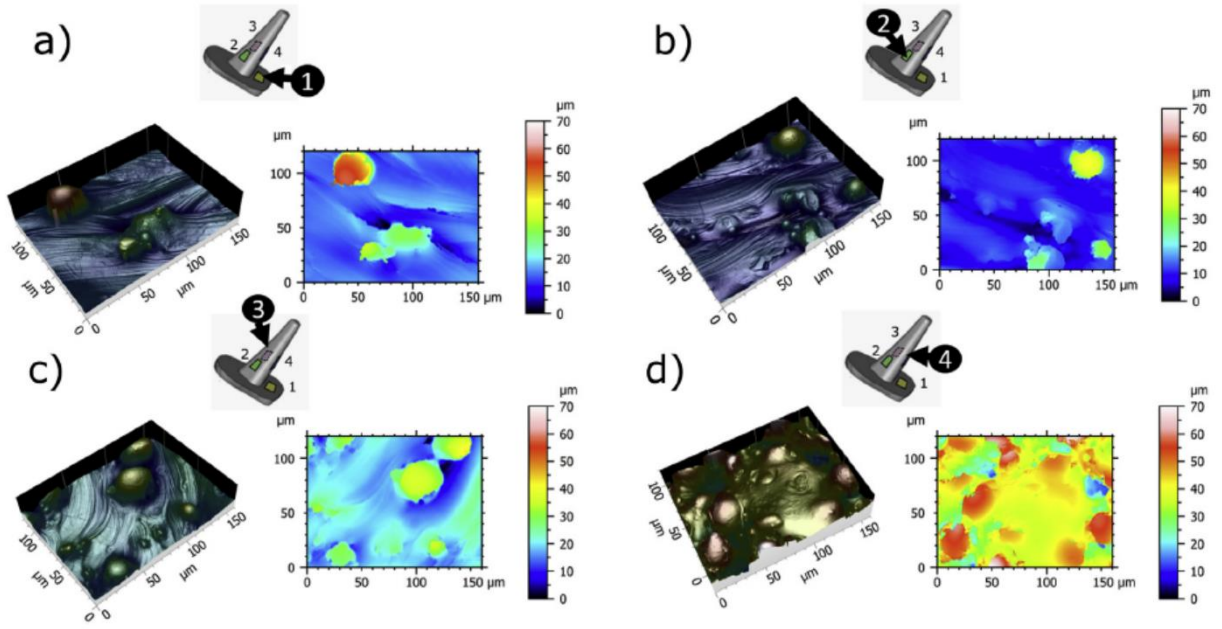


Fig. 5. Observation of the surface texture of each distinctive surface (optic profilometer); a) zone 1; b) zone 2; c) zone 3; d) zone 4.

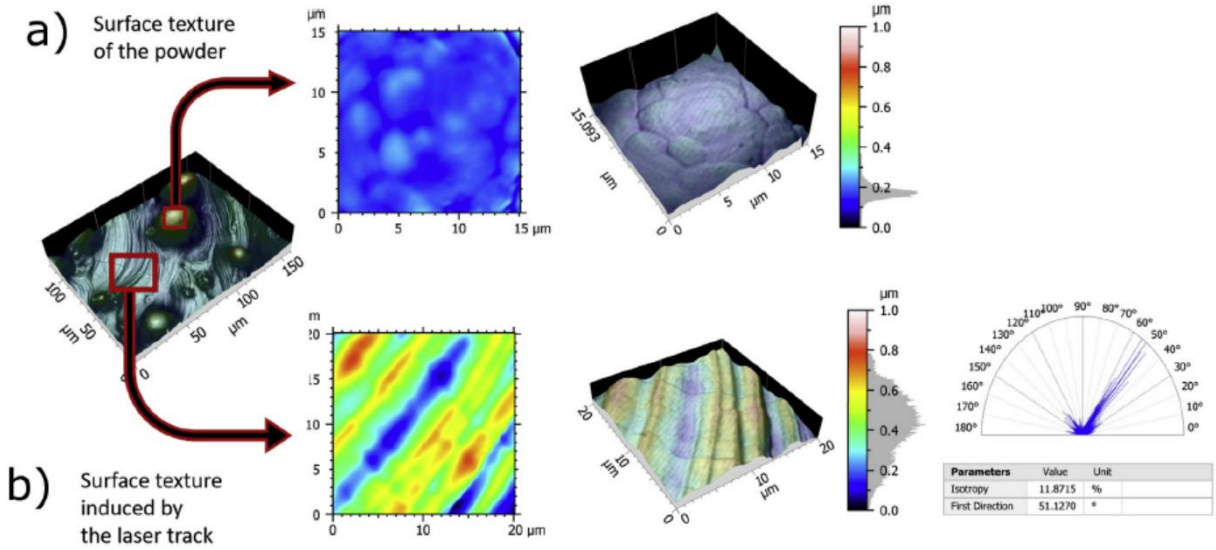


Fig. 6. Observation of the surface texture of a) the powder and b) the submicroscale grooves induce by the laser track (optic profilometer).

and (v) spheroid formation in the medium. The fact that zone 1 has a noticeably higher covering rate than zone 4 indicates that a microscale groove texture gives adhesion sites that attract more osteoblastic cells than sites with partially melted powders.

In order to quantify the attachment of the cells on the specific areas, we used fluorescence microscope images of MC3T3 cell nucleus stained with DAPI on the different surfaces, as shown in Fig. 8. Zone 4 had the lowest number of cells (Zone 4: $96 \pm 59$ cells/mm$^2$) and zone 1 had the highest (Zone 1: $2645 \pm 221$ cells/mm$^2$). Zones 2 and 3 had slightly (but nevertheless significantly) higher numbers of cells (Zone 3: $1735 \pm 337$ cells/mm$^2$; Zone 2: $2237 \pm 110$ cells/mm$^2$). This suggests that in some zones, cells may overlap.

### 3.5. Cell morphology

In order to observe cell strategy when colonizing the part of the implant, we did a morphology study using an SEM.

Cell morphology was assessed by SEM, and the results are shown in Fig. 9. The morphology of MC3T3 varied depending on the surface. In zone 1 MC3T3 had a thin (<1 µm), spread-out aspect. The entire surface, even the fine powders (<15 µm), were entirely covered by cells, making it difficult to distinguish edges. In zone 4 the cells were thicker and tended to have a globular shape. Cells were more likely to be found on partially melted powder because of the local roughness. Once attached to a powder, some cells formed bridges between surrounding partially melted powders with their cytoplasmic extensions. This suggests that the

Table 3
Measured roughness parameters on the different surfaces of the complex Ti6Al4V.

| | Zone 1 | Zone 2 | Zone 3 | Zone 4 | Laser grooves |
|---|---|---|---|---|---|
| **Number of partially melted powder/mm²** | 188,3 ± 35.9 | 412.7 ± 89.7 | 500.9 ± 81.0 | 1192.1 ± 89.4 | NA |
| Average height: **Sa (µm)** | 8,7 ± 0.6 | 9,9 ± 1.1 | 10,5 ± 0.2 | 19.2 ± 1.2 | 0.11 ± 0.03 |
| Maximum height : **Sz (µm)** | 125,8 ± 15.1 | 138,07 ± 6.8 | 161,3 ± 4.9 | 230.4 ± 2.5 | 0.87 ± 0.42 |
| Root mean square : **Sq (µm)** | 11,8 ± 0.6 | 12,8 ± 1.4 | 13,8 ± 0.6 | 24,1 ± 1.8 | 0.13 ± 0.3 |
| core roughness depth : **Sk (µm)** | 25,16 ± 3.7 | 29,48 ± 4.6 | 31,58 ± 1.6 | 61.8 ± 2.9 | 0.22 ± 0.3 |
| reduced peak height : **SpK (µm)** | 21,0 ± 0.7 | 18,2 ± 1.3 | 19,7 ± 2.9 | 18,2 ± 1.0 | 0,1 ± 0.01 |
| reduced valley depth : **SvK (µm)** | 8,2 ± 1.6 | 9,1 ± 0.8 | 10,2 ± 0.2 | 27,4 ± 5.2 | 0.11 ± 0.11 |
| kurtosis : **Sku (no unit)** | 6,1 ± 1.1 | 4,7 ± 0.8 | 5,4 ± 1.7 | 3,2 ± 0.3 | 2.73 ± 0.51 |
| skewness : **SsK (no unit)** | 1,2 ± 0.2 | 0,8 ± 0.1 | 0,8 ± 0.4 | 0,3 ± 0.1 | −0.07 ± 0.4 |
| developed interfacial area ratio : **Sdr (%)** | 79,15 ± 20.6 | 79,3 ± 23.7 | 139,1 ± 38.3 | 351.3 ± 58.7 | 3.06 ± 3.18 |
| root mean square gradient : **Sdq (no unit)** | 1,9 ± 0.3 | 1,8 ± 0.3 | 2,5 ± 0.4 | 4,3 ± 0.3 | 0.28 ± 0.21 |
| **Polar spectrum** Texture direction: **Std (°)** | 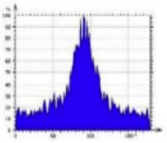 | 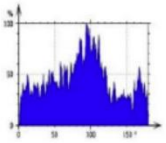 | 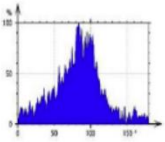 | 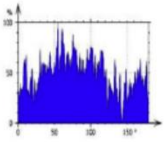 | |

roughness of the surface is not suitable for cell adhesion. Cells in zones 2 and 3 also had a thin, spread-out aspect but the greater quantity of partially melted powder often stopped the spreading. In zone 2, some cells covered less fine powders (1–20 µm). Cytoplasmic extensions of cells between nearby partially melted powders were also observed in zone 2.

### 3.6. Correlation between roughness parameters, inclination and cell adhesion

So as to have a global understanding of the variability of the areas and the interdependence of the variables, we carried out a principal component analysis (PCA).

PCA analysis (Fig. 10 A B) is a useful way to display the variables, since the two dimensions of the orthogonal basis represent 94.8% of the variability. For the purposes of understanding the overall variability, the third axis (mode) can therefore be omitted. The analysis showed that more than half of the roughness parameters are interdependent, given their close proximity in the PCA. These include SvK, Sq, Sdq, Sa, Sk, Sz, and Sdr. The number of partially melted powders on the surface is closely correlated to the inclination of the surface, and to a lesser extent to the roughness parameters described above. The first axis of the orthogonal basis-set has the same direction as the number of partially melted powders. The second axis represent the variability of the parameters, as suggested by the PCA of the observations.

The number of cells and cell covering variables are logically close and inversely correlated to the inclination and the number of partially melted particles. The two variables skewness (SsK) and kurtosis (Sku) related to the submicron-grooves are also closed variables. The quantity of partially melted powder related to SpK was the most independent variable. The PCA allows each measurement to be visualized separately. The measurements of a single surface (colored circles) are close in relation to the 1st dimension but vary more widely in relation to the 2nd dimension. The graphs in Fig. 10C D E F G H show the main correlation between surface texture, inclination and cell adhesion. Downskin surfaces (>90°) are entirely covered by partially melted powder given that the powder bed partly supports the melt pool. These surfaces have a highly isotropic surface texture, as the surface is entirely covered by powders with no significant variation in the roughness parameters. This clearly indicates that the correlation between inclination, cell attachment and partially melted powders found in our work will change for downskin surfaces (>90°).

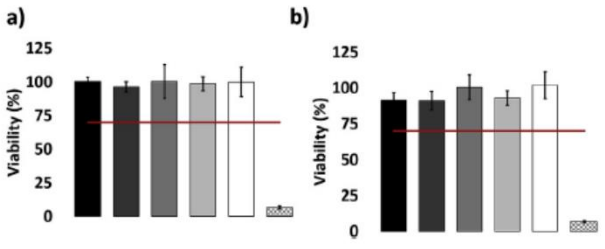


Fig. 7. Cytotoxicity results on L929 cells a) TA6V powder extracts b) TA6V-disk extracts; medium is the negative control and latex elute is the positive control.

## 4. Discussion

The study concerns the effect of the heterogeneity that is inherent AM process heterogeneity on cell adhesion and cell morphology of an osteoblastic linage, particularly in relation to the surface texture of stem-like Ti6Al4V specimens produced by SLM technology.

A multifaceted geometry was chosen to better mimic the design of stem components currently used in prostheses including total hip joint prostheses and total shoulder joint prostheses. A carpometacarpal prosthesis stem component of typical size (~20 mm × 10 mm x 10 mm) was produced in order to test the biological response of cells in contact with all the various areas at once, taking into account the potential effect of surface textures on each other, compared with specimens defined with a single inclination [28].

In our approach, heterogeneity of the surface texture has several sources: (i) a Gaussian distribution of the granular diameter of the powder used for the SLM process, (ii) laser beam track pattern and power (iii) inclination of the specimen in the manufacturing chamber because of the "stair stepping" effect and the powder bed. These different parameters act in conjunction, creating a greater heterogeneity of the surface texture over the whole specimen. However, the roughness parameters (Sa, Sz,Sq, …) do not represent the submicron roughness created by the laser track, but the quantity of partially melted powder on the surface, as shown in Table 3 and confirmed by the literature [29,30]. Our results show that the inclination of a surface regarding the build plate is mainly correlated to the number of partially melted powders and thus creating a unique surface topography with specific roughness parameters. Cabanettes et al. [30] performed topographic measurements of Ti6Al4V specimens manufactured by SLM with inclination from 0° to 90° upskin and 90°–50° downskin. They found that welded tracks are clearly visible up to an inclination angle of 40° then diminish continuously due to the increasing number of partially melted powders with the inclination, which confirms our findings. The values of their roughness parameters (Sa, Sz, Sq, …) vary similarly with inclination, although they are slightly higher. This can be explained by the use of a polynomial filter to remove the 3-dimensional aspect in our multifaceted specimen. Although, we

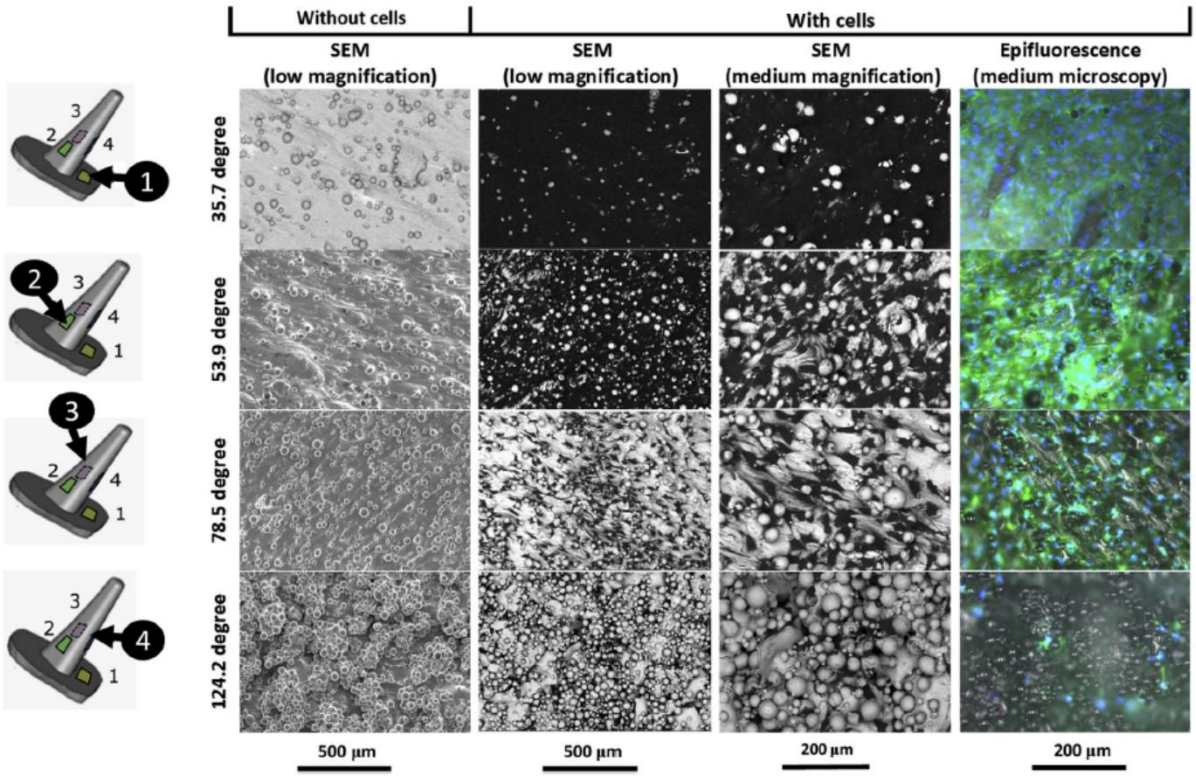


Fig. 8. Observation of the distinctive zones with and without cultivated cells (72 h) (MC3T3).

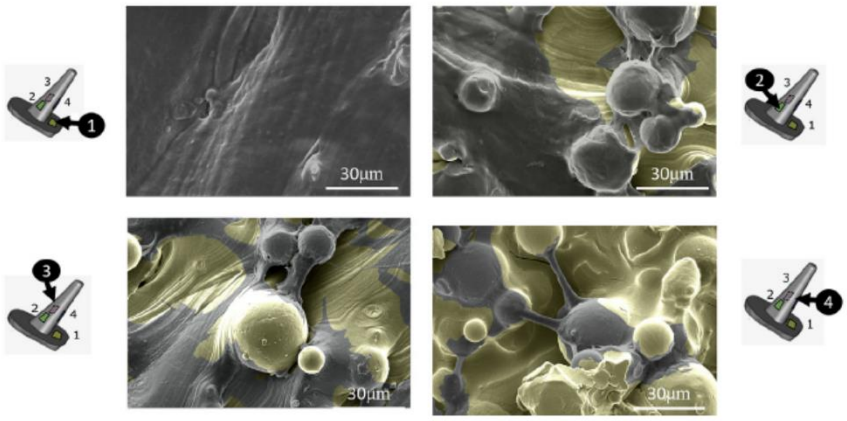


Fig. 9. Observation of the morphology of MC3T3 cells on each distinctive surface (SEM).

have only one such surface at an inclination of 124.2°, cell adhesion of MC3T3 was expected to be poor and homogeneous for all downskin surfaces, as the surface was already covered by particles [13,30].

Sarker et al. also found a link between inclination in the as-SLM specimen and cell adhesion, resulting in an increase the quantity of partially melted powder. However, they report a positive correlation of the inclination with cell attachment for upskin surfaces using Chinese hamster ovarian cells (CHO). Here we use a pre-osteoblastic MC3T3-E1 cell line as a model to test the first cell adhesion process. These cells are widely used to test cell adhesion on a material intended to be an anchoring component [31,32] because adhesion of osteoblasts is a pre-requisite for functions such as the deposition of calcium. The size of an osteoblast varies from 20 to 25 µm, while our powder diameters are about 24.17–53.51 µm, meaning that cellular mechanosensors would perceive the surface as smooth. The welding track, however, has grooves that are less than 1 µm wide, which can be detected by the osteoblastic linage. This confirms the findings of Wu et al. [33], who detected a lower proliferation rate of MC3T3 with a roughness above 1.00 µm, and a positive response of cells with a roughness in a narrower range from 0.50 to 1.00 µm. In general, submicron scale surface topography has generally been considered to positively affect the adhesion, growth and maturation of cells [34], but the effect of a roughness of between 1 and 100 µm is still controversial [34]. The difference of correlation between angle and cell adhesion in our results corresponds to other results in the literature in relation to the increased presence of submicron topography [33,35] at lower downskin inclinations as compared to CHO.

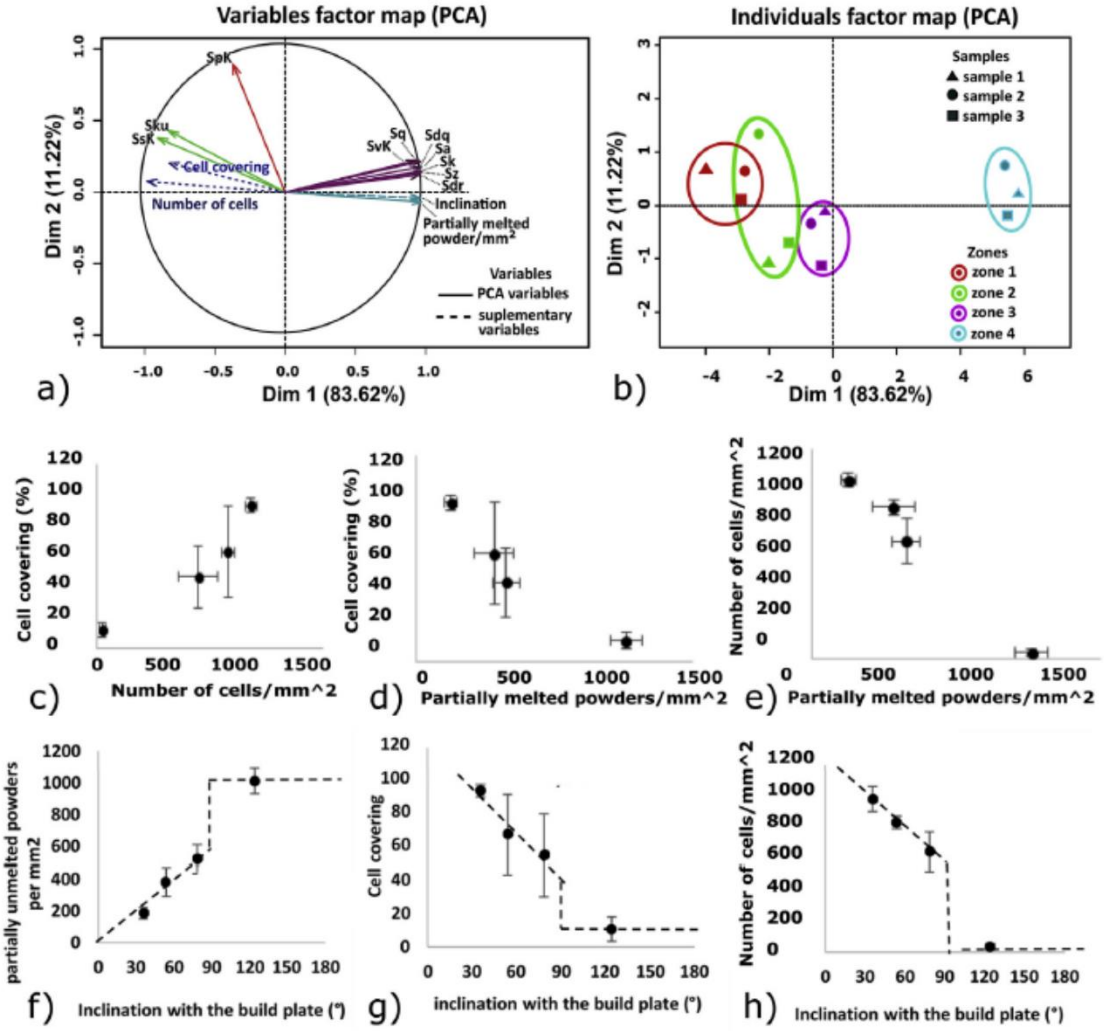


**Fig. 10.** Principal correlation between cells adhesion, surface characteristic and inclination in the SLM chamber: **a)** Principal components analysis (PCA) of the variables; **b)** Principal components analysis (PCA) of the individuals; **c)** evolution of the cell covering with the number of cells; **d)** influence of the number of partially melted powders in the cell covering; **e)** influence of the number of partially melted powders in the number of cells; **f)** influence of the inclination of a surface of the specimen with the number of partially melted powder, **g)** influence of the inclination of the surface in the cell covering, **h)** influence of the inclination of the surface in the number of cells attached.

Matouskova et al. [36] compared the effect of post-treatment after SLM on cell adhesion with a MG-63 cell linage. It was observed that cells proliferated to a greater extent on the non-treated specimens (Ra: 13.3 μm) than on the glass-blasted specimens (Ra = 3.4 μm). It confirms the benefit of surface texture induced by the AM process, particularly the submicron roughness induced by the laser beam on cell adhesion.

Although we have demonstrated a heterogeneity of surface texture in the as-SLM specimens, a heterogeneity that could affect cell adhesion, this heterogeneity is not representative of the inner properties of the material. The porosity was found to be homogeneously distributed over the whole specimen. And a fully martensitic texture-phase transition in the as-SLM Ti–6Al–4V specimen was found. This microstructure is a direct consequence of the SLM process, which implies a complete re-melting of the powder and a rapid direct solidification of the melt [13]. The material faces an *in situ* thermal cycling due to repeatable passage of the laser nearby. These findings are in agreement with other works studying the effect of SLM process in the Ti6Al4V microstructure [37,38].

Therefore, from an implant design perspective, we suggest orienting the implants so that the surfaces with osseous contact (i) are in a narrow range of inclinations so as to promote a homogeneous surface texture, and (ii) have the smallest possible inclination with respect to the build plate so as to promote cell attachment.

It is important to note that although this study has demonstrated increased osteoblast adhesion, further studies are required to confirm these results and particularly the benefit of the as-SLM specimen's low inclination for long-term bone anchoring.

This finding could benefit the implant manufacturing process by reducing the cost additional post-processing currently performed to enhance cell attachment in anchoring biomedical component surfaces.

Further studies are needed in order to clarify the effect of common post-treatments such as heating and sterilization (plasma, radiation, ethylene oxides). The effect after heat treatment is an important point as the process is commonly used after selective laser melting to reduce the

residual constraints and lower the hardness of the material [39]. It also creates oxides (TiO2) on the surface. Furthermore, Wang et al. [40] have shown that heat treatment induces a more hydrophilic and more homogeneous surface.

## 5. Conclusion

Our work describes the *in vitro* biological testing of the surface texture variation of Ti6Al4V multifaceted shape specimens produced using SLM technology. Following a comparison of the topography of each surface having a different inclination with the build plate, it was determined that MC3T3-E1 osteoblastic cells' preferred sites for adhesion are upskin surface with a small inclination (that exhibited a lower number of partially melted particles), rather than downskin surfaces (that were entirely covered by particles).

The study concludes that:

(i) TA6V powder and as-SLM specimen showed no sign of indirect cytotoxicity.
(ii) in an SLM specimen the SLM process induces a complex surface texture composed of submicroscale groove tracks induced by the laser beam and of partially melted particles, whose quantity varies with the inclination of the surface in the SLM chamber
(iii) the quantity of partially melted powder on the surface is closely correlated to around half of the measured roughness variables including Sz, Sa, Sk, Sdr, Sdq, Svk, and Sq, and varies linearly with the inclination for upskin surfaces only.
(iv) Osteoblastic cells grew inhomogeneously on the specimen. Cell attachment increased on surface with microscale grooves (measured using the Ssk and Sku parameters), in contrast to partially melted powders which were the least appreciated zones for attachment.

The source of process-induced surface texture heterogeneities therefore needs first be understood and then manipulated by controlling the AM process in order to reduce potentially costly post-processing for osseous interface implants. In relation to bio-anchoring, particular care is required while orientating the specimen to manufacture by SLM.

## Funding source

The work was supported by the "Agence National de la Recherche" (ANR-11-IDEX-0004-02 under Idex "Sorbonne Universités" by a IUIS project for the promotion of healthcare innovation.

## Conflicts of interests

The authors have no conflicts to declare.

## Acknowledgements

We thank Raphael DELTOMB of the LAMIH laboratory at the University of Valenciennes for his technical assistance in performing surface texture measurements. We also acknowledge Dr Dorick DURAND for his Matlab code for treating EBSD data, and Frederic Nadaud of the *Service d'Analyse Physico-Chimique* (SAPC) at UTC (Université de technologie de Compiègne) for sharing with us his considerable expertise in SEM acquisition.

## References

[1] N. Lemme, A. Boulos, "Total Hip Arthroplasty," in *Essential Orthopedic Review*, Springer International Publishing, Cham, 2018, pp. 141–143.
[2] S. Kurtz, K. Ong, E. Lau, F. Mowat, M. Halpern, Projections of primary and revision hip and knee arthroplasty in the United States from 2005 to 2030, JBJS 89 (4) (2007) 780–785.
[3] D. Apostu, O. Lucaciu, C. Berce, D. Lucaciu, D. Cosma, Current methods of preventing aseptic loosening and improving osseointegration of titanium implants in cementless total hip arthroplasty: a review, J. Int. Med. Res. 46 (6) (2018) 2104–2119.
[4] M. Textor, C. Sittig, V. Frauchiger, S. Tosatti, D.M. Brunette, Properties and biological significance of natural oxide films on titanium and its alloys, in: Titanium In Medicine, Springer, Heidelberg, 2001, pp. 171–230.
[5] K. Anselme, Osteoblast adhesion on biomaterials, Biomaterials 21 (7) (2000) 667–681.
[6] Stephen J. Kelly, Stephen J. Incavo, Bruce Beynnon, The use of a hydroxyapatite-coated primary stem in revision total hip arthroplasty, J. Arthroplast. 21 (1) (2006) 64–71.
[7] S. Saber-Samandari, S. Baradaran, B. Nasiri-Tabrizi, K. Alamara, W.J. Basirun, Microstructural evolution and micromechanical properties of thermally sprayed hydroxyapatite coating, Adv. Appl. Ceram. 117 (8) (2018) 452–460.
[8] V. Koshuro, A. Fomin, I. Rodionov, Composition, structure and mechanical properties of metal oxide coatings produced on titanium using plasma spraying and modified by micro-arc oxidation, Ceram. Int. 44 (11) (2018) 12593–12599.
[9] J. Lombardi, A. Manocchio, K. Berend, M. Morris, J. Adams, Early experience with a short, tapered titanium porous plasma sprayed stem with updated design, Surg. Technol. Int. 31 (2018).
[10] K. Park, et al., Fabrication and biological properties of calcium phosphate/chitosan composite coating on titanium in modified SBF, Mater. Sci. Eng. C 90 (2018) 113–118.
[11] A.L. Jardini, et al., Customised titanium implant fabricated in additive manufacturing for craniomaxillofacial surgery, Virtual Phys. Prototyp. 9 (2) (2014) 115–125.
[12] F. Trevisan, et al., Additive manufacturing of titanium alloys in the biomedical field: processes, properties and applications, J. Appl. Biomater. Funct. Mater. 16 (2) (2018) 57–67.
[13] B. Vandenbroucke, J.P. Kruth, Selective laser melting of biocompatible metals for rapid manufacturing of medical parts, Rapid Prototyp. J. 13 (4) (2007) 196–203.
[14] L. Murr, S. Gaytan, E. Martinez, R.B. Wicker, F. Medina, Next generation orthopaedic implants by additive manufacturing using electron beam melting, Int. J. Biom. 2012 (2012) 1–14, 2012.
[15] C. Song, Y. Yang, Y. Wang, D. Wang, J. Yu, Research on rapid manufacturing of CoCrMo alloy femoral component based on selective laser melting, Int. J. Adv. Manuf. Technol. 75 (1–4) (2014) 445–453.
[16] R. Van Noort, The future of dental devices is digital, Dent. Mater. 28 (1) (2012) 3–12.
[17] S. Arabnejad, et al., High-strength porous biomaterials for bone replacement: a strategy to assess the interplay between cell morphology, mechanical properties, bone ingrowth and manufacturing constraints, Acta Biomater. 30 (2016) 345–356.
[18] N. Taniguchi, et al., Effect of pore size on bone ingrowth into porous titanium implants fabricated by additive manufacturing: an in vivo experiment, Mater. Sci. Eng. C 59 (2016) 690–701.
[19] J.P. Li, J.R. de Wijn, C.A. van Blitterswijk, K. de Groot, The effect of scaffold architecture on properties of direct 3D fiber deposition of porous Ti6Al4V for orthopedic implants, J. Biomed. Mater. Res. A 92A (1) (2010) 33–42.
[20] R. Barrack, M. Jasty, C. Bragdon, T. Haire, W. Harris, Thigh pain despite bone ingrowth into uncemented femoral stems, J. Bone Joint Surg. Br. 74-B (4) (Jul. 1992) 507–510.
[21] A.L. Malkani, D.G. Lewallen, M.E. Cabanela, S.L. Wallrichs, Femoral component revision using an uncemented, proximally coated, long-stem prosthesis, J. Arthroplast. 11 (4) (1996) 411–418.
[22] K. Anselme, et al., Qualitative and quantitative study of human osteoblast adhesion on materials with various surface roughnesses, J. Biomed. Mater. Res. 49 (2) (2000) 155–166.
[23] A. Naji, M. Harmand, Study of the effect of the surface state on the cytocompatibility of a Co-Cr alloy using human osteoblasts and fibroblasts, J. Biomed. Mater. Res. 24 (7) (1990) 861–871.
[24] K. Kieswetter, et al., Surface roughness modulates the local production of growth factors and cytokines by osteoblast-like MG-63 cells, J. Biomed. Mater. Res. 32 (1) (1996) 55–63.
[25] K. Huang, N. Hollevoet, G. Giddins, Thumb carpometacarpal joint total arthroplasty: a systematic review, J. Hand Surg. European 40 (4) (2015) 338–350.
[26] I. Jolliffe, "Principal component analysis," in *in*, in: M. Lovric (Ed.), International Encyclopedia of Statistical Science, Springer Berlin Heidelberg, 2011.
[28] A. Sarker, et al., Angle defines attachment: switching the biological response to titanium interfaces by modifying the inclination angle during selective laser melting, Mater. Des. 154 (2018) 326–339.
[29] I. Yadroitsev, I. Smurov, Surface morphology in selective laser melting of metal powders, Phys. Procedia 12 (2011) 264–270.
[30] F. Cabanettes, et al., Topography of as built surfaces generated in metal additive manufacturing: a multi scale analysis from form to roughness, Precis. Eng. 52 (2018) 249–265.
[31] P. Linez-Bataillon, F. Monchau, M. Bigerelle, H.F. Hildebrand, In vitro MC3T3 osteoblast adhesion with respect to surface roughness of Ti6Al4V substrates, Biomol. Eng. 19 (2–6) (2002) 133–141.
[32] L. Cerroni, R. Filocamo, M. Fabbri, C. Piconi, S. Caropreso, S.G. Condo, Growth of osteoblast-like cells on porous hydroxyapatite ceramics: an in vitro study, Biomol. Eng. 19 (2–6) (2002) 119–124.
[33] C. Wu, M. Chen, T. Zheng, X. Yang, Effect of surface roughness on the initial response of MC3T3-E1 cells cultured on polished titanium alloy, Bio Med. Mater. Eng. 26 (1) (2015) S155–S164.

[34] L. Bacakova, E. Filova, M. Parizek, T. Ruml, V. Svorcik, Modulation of cell adhesion, proliferation and differentiation on materials designed for body implants, Biotechnol. Adv. 29 (6) (2011) 739–767.
[35] K. Anselme, et al., The relative influence of the topography and chemistry of TiAl6V4 surfaces on osteoblastic cell behaviour, Biomaterials 21 (15) (2000) 1567–1577.
[36] L. Matouskova, M. Ackermann, J. Horakova, L. Capek, P. Henys, J. Safka, How does the surface treatment change the cytocompatibility of implants made by selective laser melting? Expert Rev. Med. Devices 15 (4) (2018) 313–321.
[37] N. Kazantseva, et al., Texture and twinning in selective laser melting Ti-6Al-4V alloys, World Acad. Sci. Eng. Technol. Int. J. Chem. Mol. Nucl. Mater. Metall. Eng. 11 (11) (2017) 745–748.
[38] L. Thijs, F. Verhaeghe, T. Craeghs, J. Van Humbeeck, J.P. Kruth, "A study of the microstructural evolution during selective laser melting of Ti–6Al–4V, Acta Mater. 58 (9) (2010) 3303–3312.
[39] A. Khorasani, I. Gibson, M. Goldberg, G. Littlefair, On the role of different annealing heat treatments on mechanical properties and microstructure of selective laser melted and conventional wrought Ti-6Al-4V, Rapid Prototyp. J. 23 (2) (2017) 295–304.
[40] N. Kaz Wang, Y. M.Wu, S. Lu, T. Chen, Y. Zhao, H. Chen, Z. Tang, Fabrication and characterization of selective laser melting printed Ti–6Al–4V alloys subjected to heat treatment for customized implants design", Prog. Nat. Sci.: Materials International 26 (6) (2016) 671–677.

# Article 6:
# Effect of the residual porosity of selective laser melted CoCrMo parts on wear of polyethylene under lubricated conditions

Augustin LEREBOURS[1*], Clemence DEMANGEL[2], Lucas DEMBINSKI[3], Salima BOUVIER[1], Alain RASSINEUX[1], Christophe EGLES[4].

[1] Alliance Sorbonne Université, Université de technologie de Compiègne, CNRS, FRE 2012 Roberval, Centre de recherche Royallieu, CS 60 319, 60 203 Compiègne cedex, France ; augustin.lerebours@utc.fr, salima.bouvier@utc.fr, alain.rassineux@utc.fr

[2] CRITT-MDTS, 3 bd Jean Delautre F-08000 Charleville-Mézières, France, c.demangel@critt-mdts.com

[3] LERMPS, ICB UMR 6303, CNRS, Univ. Bourgogne Franche-Comté, UTBM, F-90010 Belfort, France

[4] Alliance Sorbonne Université, Université de technologie de Compiègne, CNRS, UMR 7338 BioMécanique et BioIngénierie (BMBI), Centre de recherche Royallieu, CS 60 319, 60 203 Compiègne cedex, France ; christophe.egles@utc.fr.

***Corresponding author :** Augustin LEREBOURS, Alliance Sorbonne Université, Université de technologie de Compiègne, CNRS, FRE-2012 Roberval, Centre de recherche Royallieu, CS 60 319, 60 203 Compiègne cedex, France ; phone number: +33 6 58 01 99 46, Email : augustin.lerebours@utc.fr,

# Abstract

Cobalt based alloy are commonly used materials for articular implants coupled with ultra-high molecular weight polyethylene. The manufacturing of complex parts made of cobalt based alloys is possible thanks to metal additive manufacturing such as Selective Laser Melting technology. We produce selective laser melting samples to highlight the effect of cavities in the surface. Parts were then superfinished. The wear behavior of UHMWPE pin against selective laser melting CoCrMo disc was studied with a multidirectional pin-on-disc machine in diluted bovine serum lubricant at 37°. It allows the estimation of the life expectancy of implants in biomechanical and physiological conditions. All configurations were in accordance with the ASTM F732 standard acceptance criteria. The results demonstrate a strong correlation between mass loss of UHMWPE and the total surface porosity in SLM-CoCrMo-discs. Reducing the surface porosity is beneficial for improving the wear resistance of UHMWPE. Two wear mechanisms were identified: (i) adhesion wear and (ii) abrasion wear. Adhesion wear was essentially found in the configuration of nearly full-dense discs (0,4% volume) shown by the transfer of polyethylene on the metallic surface. Abrasion wear was found on all configurations. Abrasion was enhanced because of sharp pore edges on the surface and metallic third body particles trapped between the surfaces. Interestingly the pores also limit the abrasive effect of a third body particles by acting as debris collector. This work underlines the necessity to precisely adjust the powder-based additive manufacturing parameters to obtain parts with the lowest porosity in order to enhance the biotribological performance.



**Keywords**

Additive manufacturing, Selective laser melting, wear behavior, Cobalt-chromium-molybdenum alloy, polyethylene, porosity


**Abbreviations**

**AM**, additive manufacturing; **SLM**, selective laser melting; **3D**, three-Dimensional; **CoCrMo**, Cobalt-chromium-molybdenum alloy; **UHMWPE**, ultra-high molecular weight polyethylene; **SEM**, Scanning Electron, **EBSD**, Electron backscatter diffraction.

# Introduction

Additive manufacturing (AM) allows the creation of parts with complex internal and external geometry by adding material layer by layer directly from a computer-assisted-design model according to ASTM standard F2792-10 and ISO 17296. Among the AM technologies, Selective Laser Melting (SLM) is capable of producing metal parts using a high-power laser that progressively and locally fuses a metal powder in a controlled atmosphere (Ar, $N_2$, $H_2$).

The manufacturing process itself is complex as it possesses many parameters which all play a role in producing fully dense parts with minimum internal stress. These parameters includes (i) the laser parameters (power, scanning speed, beam diameter, etc), (ii) the system parameters (thickness of the powder layer, the treated powder surface, hatch space, the scanning strategies, etc), (iii) the environmental parameters (preheating temperature, the atmosphere and gas pressures) and (iv) the powders characteristics (morphology, size, distribution) [1].

Metal additive manufacturing offers many advantages: (i) freedom of design in relation to subtractive processes, (ii) lighter structures possible either by lattice structures or by the design of parts where the material is only where it is needed without further constraints, (iii) new functions such as complex internal channels, (iv) net shape process leading to less raw material consumption and reducing the number of assembly operations and tools needed, (v) short production cycle time for complex parts.

SLM creates unique material characteristics which thereby might modify the mechanical, biological and physico-chemical properties. The process consists of melting and solidifying a small surface of metallic powders with a laser beam of high energy. The thermal history due to the rapid melting and solidification of the material leads to fine microstructural propertie. Most of the materials made by SLM are found to be anisotropic. An anisotropy in the Z direction is due to the superposition of layers while an anisotropy in X-Y directions is related to the scanning strategy [2]. Typical defects can be observed including partially melted particles, lack of fusion, pores, cracks and inclusions [2]. Such defects defects can be linked to poor process parameters optimization, construction strategy, part orientation or inadequate powder quality.

Once the parts have been manufactured, surfaces usually have to be polished to achieve mirror or extremely smooth finishes to meet articular implant specifications [3].

Pores in the parts created by SLM can significantly affect their mechanical behavior and therefore their performance [4]. Thus, in many applications, the objective is to obtain full dense parts without any porosity. Parameters optimization may be a challenge for some materials that poorly accommodate high internal stress during the fabrication process [5]. The development of metal additive manufacturing especially selective laser melting has enabled the production of cobalt-chromium-molybdenum (CoCrMo) parts with complex geometries [6,7]. CoCrMo alloy is a biocompatible material which has been widely used for orthopedic implant [8]. It is a particularly good candidate for articular parts because of its hardness along with good corrosion properties, tensile and fatigue properties.

In this work, SLM was applied on a CoCrMo powder to study the effect of pores on the sliding wear of polyethylene under biology-like lubricated conditions in order to control the performance of the parts for further artificial joint implant applications. We focus on the contact couple CoCrMo/Ultra-High Molecular-Weight-Polyethylene (UHMWPE) because it is a commonly used material couple for articular implants such as knee and hip replacement implants [9]. This work is particularly important regarding the development of complex geometric AM-based implant. In an attempt to be as close as possible to the application, we used a superfinishing process on our specimens based on a physico-catalytic method that can also be applied for such complex geometric parts.
This is the first study to highlight the need to fine-tune the manufacturing parameters of powder-based additive manufacturing to obtain parts with the lowest porosity in order to optimize biotribological performance with polyethylene.

# Material and methods

### 1. Specimens

Cylindrical discs of a 20mm radius and 5mm thickness were manufactured by SLM in CoCrMo. Cylindrical UHMWPE pins were machined from an extruded UHMWPE bar (GUR 415). They were not irradiated. Each pins was of a 7mm radius and 30mm length.
The manufacturing process of the CoCrMo discs includes (i) SLM of the disc from CoCrMo powder, (ii) removal of the SLM supports, (iii) cleaning of the specimens by a sandblasting process (iv) superfinishing of the specimens by micromachining process and (v) removal of the micromachining supports.
Three CoCrMo-discs were produced with a gradient of defects in order to understand their impact on the wear behavior of UHMWPE. The characteristics of the surface and their defects is described in the results.

### 1.1. CoCrMo powder

The CoCrMo powder was gas atomized under Ar and has a spherical shape (Fig.1.(i)). The average particle diameter was measured as 33.53 µm by a granulometer (Fig.1.(ii)). They had a chemical composition similar to the ASTM F75 alloy as seen in Fig.1.(iii).

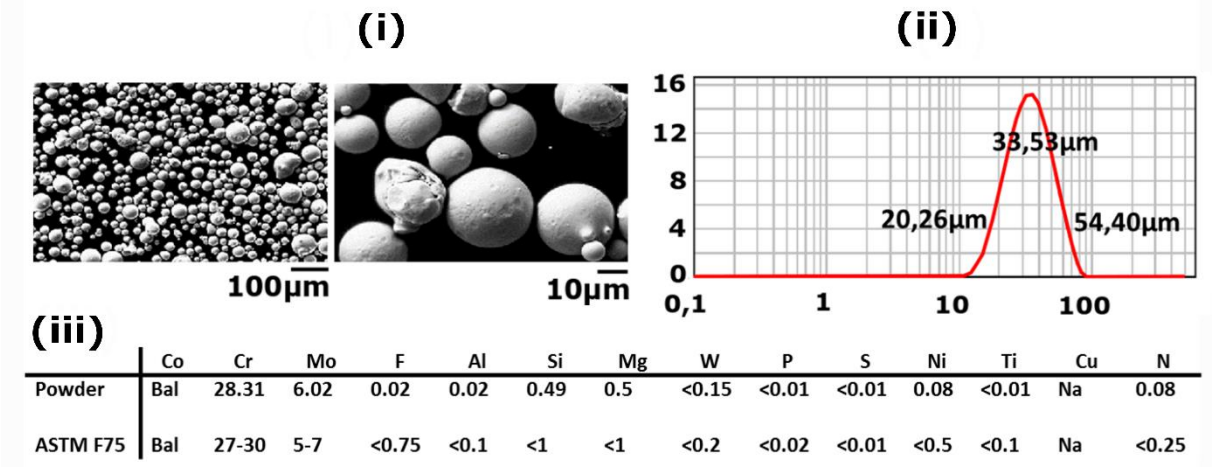


(iii)

| | Co | Cr | Mo | F | Al | Si | Mg | W | P | S | Ni | Ti | Cu | N |
|---|---|---|---|---|---|---|---|---|---|---|---|---|---|---|
| Powder | Bal | 28.31 | 6.02 | 0.02 | 0.02 | 0.49 | 0.5 | <0.15 | <0.01 | <0.01 | 0.08 | <0.01 | Na | 0.08 |
| ASTM F75 | Bal | 27-30 | 5-7 | <0.75 | <0.1 | <1 | <1 | <0.2 | <0.02 | <0.01 | <0.5 | <0.1 | Na | <0.25 |

**Figure 1**: CoCrMo Powder analysis : (i) morphology of the powder observed by SEM imaging, (ii) dry granulometry of the powder and (iii) chemical composition of the powder by EDX and comparison to the ASTM F75 standard

### 1.2. Selective laser melting

Selective laser melting (SLM) principle and the parameters used for this study is shown in Fig.2.

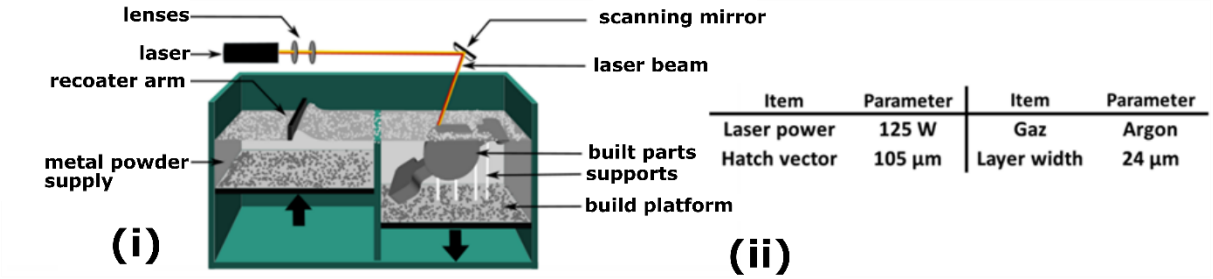


| Item | Parameter | Item | Parameter |
|---|---|---|---|
| Laser power | 125 W | Gaz | Argon |
| Hatch vector | 105 µm | Layer width | 24 µm |

**Figure 2:** Selective laser melting (SML) process: (i) SLM principle, (ii) Manufacturing parameters strategy used in this study.

### 1.3. Superfinishing by micromachining process

Specimens were superfinished by a micromachining method. It is a physico-catalyst surface treatment applied to specimens inside a liquid environment. The media used is unique and developed by the company BESTinCLASS. The advantage of the process is a uniform removal and a smooth surface mirror-like finish below 0.1µm. Our approach was to mirror-like polish our specimen using a more reproducible and automatic method [10] which might be used for complex additive manufactured implants. The test configuration

is more representative of the AM-based implant reality. This is an additional element compared to literature.

Before testing, specimens were cleaned in an ultrasonic bath with, consecutively, sodium dodecyl sulfate at the critical micelle concentration 8.2 mM, acetone, ethanol, and pure water for 15min each followed by a drying of the specimens.

## 2. Multidirectional Pin-On-Disk Testing

A multidirectional pin-on-disc machine was used to perform wear tests representative of those endured by articular implant devices as seen in Fig.3. The pin-on-disc machine is able to apply cross shear through several changes of direction during each cycle. In the literature, it has been demonstrated that wear on polyethylene is more relevant (and debris size and shape also) when shear forces are added to motion. More specifically, the wear rate is directly correlated to the shear rate [11,12] when nearly no mass loss is detected with unidirectional motions [13]. Indeed, the alignment of polymeric molecular chains at material surface follows the principal direction of sliding. As a consequence, multidirectional motion is necessary to generate realistic wear rates [13,14]. The standard also suggests running the test at 37 ± 2 °C to reflect body temperature. At higher test temperatures, a degradation of the protein content in the lubricant might occur creating artefacts in the results.

Physiological contact pressure is applied on 7mm diameter pins taking also into account the surface states. The lubricant was made with bovine serum diluted in demineralized water with an antibiotic (Proclin 300). The total protein concentration in the mixture is 30g/L which is a clinically relevant concentration. It is filtered before use and heated at 37°C. An individual silicon gaiter ensures the sealing and avoids evaporation or cooling of the lubricant. The tests conditions were inspired by the ASTM F 732-17 Annex 2: « Wear testing of polymeric materials used in total joint prostheses », as seen in Fig.3.

Reported wear rates are about 10mg/million cycles for a standard UHMWPE [13], and 3-4 mg/million cycles for a cross-linked polyethylene [14] where the wear rate decreases with the rise of PE crosslinking rate [11].

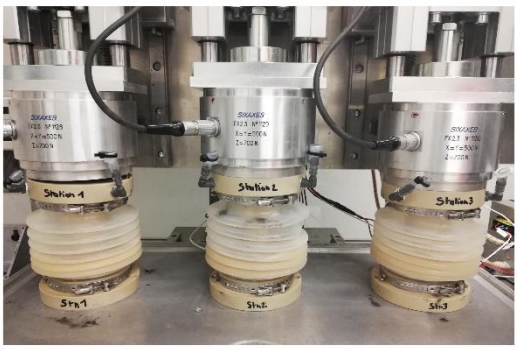


| Test protocol | Parameter |
|---|---|
| Load | 150 N (i.e. 3,9 MPa) |
| Kinematics | Triangular (6 mm for the base) |
| Sliding speed | Between 30-35 mm/s |
| Number of cycles | 840 000 |
| Distance per cycle | 19,4 mm |
| Lubricant | Bovine serum (diluted at 30g/L), 37°C |

(i) (ii)

**Figure 3**: Pin-on-disc wear test: (i) photograph of the test running, (ii) test conditions used in this work.

### 3. Gravimetric measurements

Gravimetric weight loss per pin was determined every 0.12, 0.24, 0.34, 0.48 and 0.84 million cycles (SARTORIUS ME 235S® with 0.2 mg of accuracy).

### 4. Surface texture measurements

Surface texture measurements were carried out using a confocal microscope laser (Sensofar®) on the specimens before wear testing. Roughness parameters were measured in order to characterize the surface of the discs at 2 different scales:

- the entire discs (assembling of zones), reflecting the geometrical deviation induce by the SLM process,
- zone of 132, 10µm x 177,44µm with an applied form removal filter (polynomial order 6). It reflects the superfinishing results of the physico-catalytic process.

Surface texture measurements were also done on the wear grooves of the CoCrMo surface and on the worn out pin. The wear grooves o the CoCrMo surface were also examined by SEM and optical microscopy to have complementary results. The accelerating voltage used was 20kV.

### 5. Microstructure analysis

To investigate the microstructure of SLM-CoCrMo, the specimens were mounted in epoxy pucks and polished up to 4000 grit paper, and finally chemical-mechanical polished with an OP-S colloidal silica solution (Struers). The microstructural-crystallographic characterization was carried out with an Electron backscatter diffraction (EBSD).

### 6. Hardness measurements

The hardness of the material was measured prior the tests using a microdurometer (ZWICK ZHV-μs(H115)) in accordance to ISO-6507 and ASTM E384.

### 7. Defects analysis in the sliding path

Images of the defects were taken using an optical microscope (Keyence®, VHX-6000) and the defects present in the sliding path of the UHMWPE were extracted using the integrated software (measure of grains). Parameters including area, diameter and circularity were measured for each defects.

## Results and discussion

### 1. Specimens Characteristics

This work focused on the tribological performance of polyethylene against superfinished SLM samples. The characteristics of the sliding surface of SLM-CoCrMo discs as well as the UHMWPE pins are detailed here.

Figure 4. (i) shows an SEM micrograph taken from the superfinished sliding surface of an SLM-CoCrMo discs. The superfinished surfaces appear to be highly polished with brilliant mirror-like finished surface. The superfinishing process has also revealed pores on the surface specific to SLM materials. It indicates that the SLM samples were not fully dense. The pores have various sizes from a few microns to 1500μm. Two type of pores were revealed: (i) small and round shaped pores which are due to gas entrapment and (ii) irregular shaped pores which are the result of incomplete fusion, and/or incomplete adhesion between two successive layers, and/or a collapse of parts structure due to either a lack of support material or poor orientation.

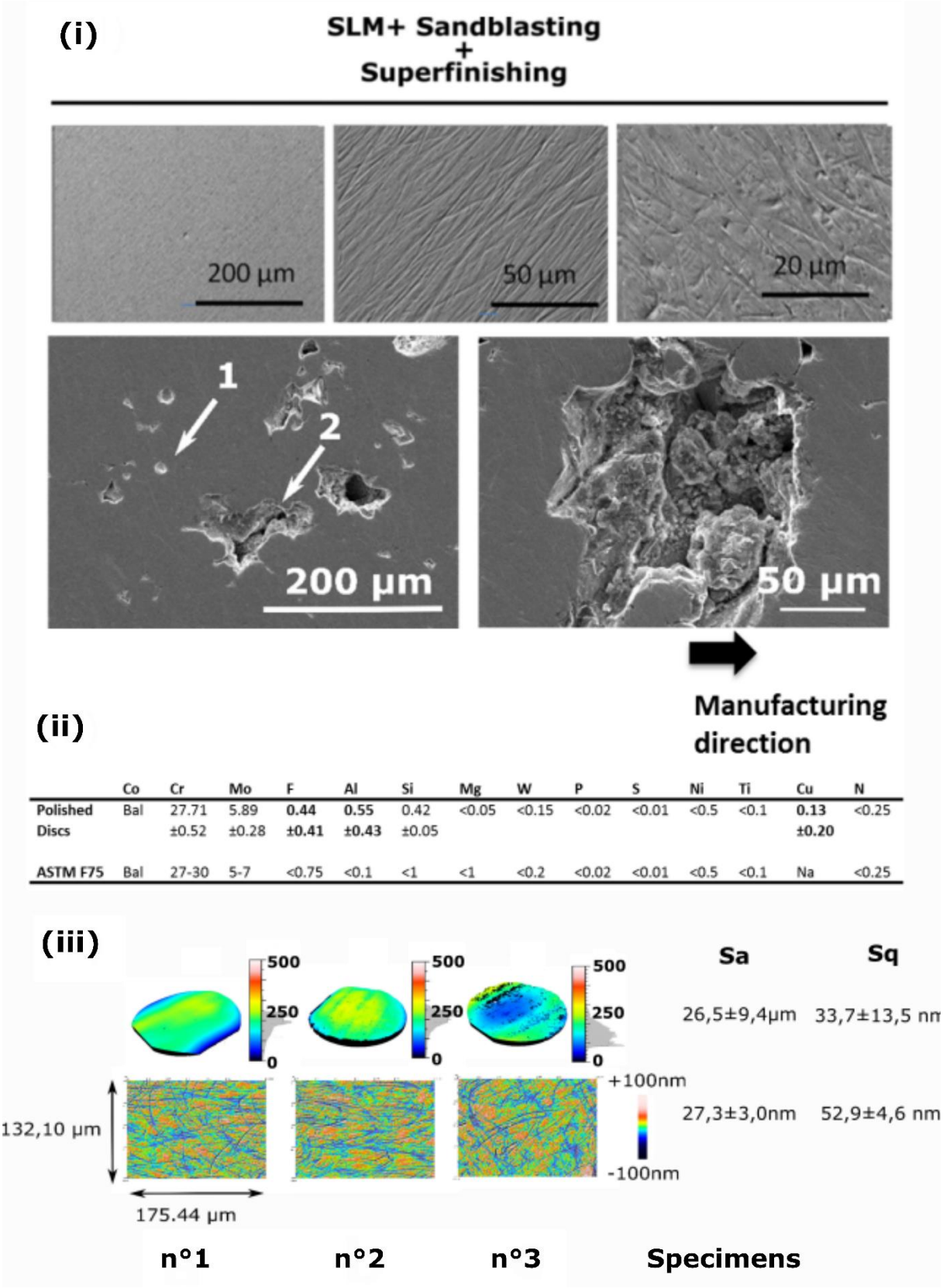


| | Co | Cr | Mo | F | Al | Si | Mg | W | P | S | Ni | Ti | Cu | N |
|---|---|---|---|---|---|---|---|---|---|---|---|---|---|---|
| Polished Discs | Bal | 27.71 ±0.52 | 5.89 ±0.28 | **0.44 ±0.41** | **0.55 ±0.43** | 0.42 ±0.05 | <0.05 | <0.15 | <0.02 | <0.01 | <0.5 | <0.1 | **0.13 ±0.20** | <0.25 |
| ASTM F75 | Bal | 27-30 | 5-7 | <0.75 | <0.1 | <1 | <1 | <0.2 | <0.02 | <0.01 | <0.5 | <0.1 | Na | <0.25 |

**Figure 4** : Superfinished surface : (i) SEM images showing the surface of the discs after superfinishing and the type of pores small and round pores (1) due to gas entrapment and irregular pores (2) due to sintering process, (ii) Chemical composition of the surface by EDX analysis, (iii) Surface texture measurements

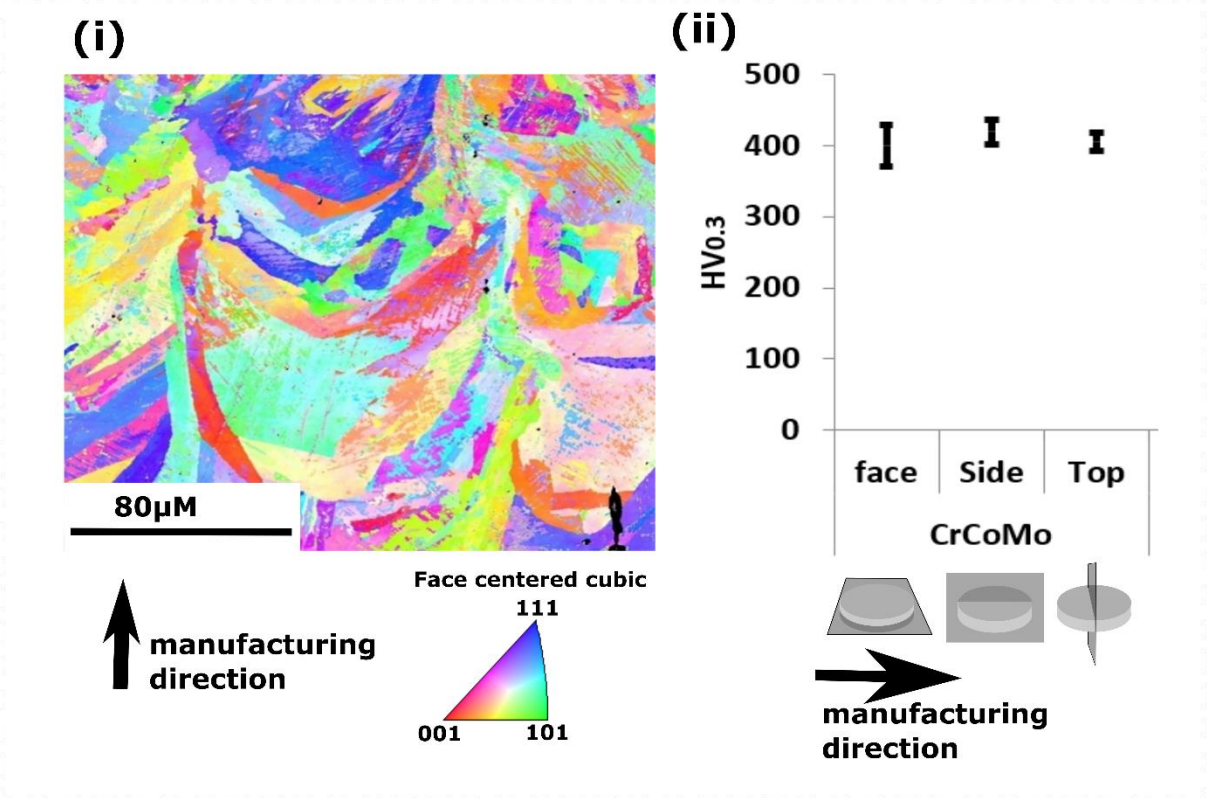


**Figure 5:** (i) Microstructure revealed by EBSD analysis of the core material and (ii) impacted hardness along the different directions (HV)

The chemical composition of the superfinished surface revealed an increase in the Iron, Copper and Aluminum content compared to ASTM F75 alloy standard and the chemical composition of the CoCrMo powder (Fig.4. (ii)). It might be a contamination of the superfinishing process that was not removed by the cleaning step.

The surface is textured with submicron grooves as seen in Fig.4. (iii) with an average height roughness (Sa) of 27, 3 ±3,0nm. The obtained roughness is in the specification recommended by the ISO 21534:2007 standard: "Non-active surgical implants — Joint replacement implants — Particular requirements" which indicate a Ra maximum of 0,100nm for the metallic part against UHMWPE, and a maximum of 50nm when the surface is convex. This surface texturation (Fig.4. (iii)) is due to the mechanical part of the superfinishing process, a flux is composed of aggregated particles of microtools created "in situ" by means of the catalyst. The average roughness parameter on the entire surfaces of all three discs was 26.5±9.4 µm (Fig.4. (iii)). It reflects the geometrical deviations that occur during the SLM process

The microstructural features of the SLM-CoCrMo discs are presented in Fig.5.(i). The laser molten pools can be seen with an average size of 90µm (Fig.5.(i)). It is explained by the thermal history of the process. During SLM, materials experience fast local melting along

the tracks of a high energy laser followed by rapid solidification. Due to severe temperature gradients, this material microstructure tend to be far from equilibrium conditions [15]. The matrix is face center cubic (fcc) (Fig.5.(i)) with precipitates at the joints of dendritic-shaped grains. The resulted surface hardness (Fig.5.(ii)) was found to be at 400 $HV_{0,3}$ with a slight increase of 20 $HV_{0,3}$ in the direction of the building direction but not significant. Comparatively, the microstructure of the cast alloy features dendrite-like structural pattern with a larger grain size [6,16]. Cast alloys also contain blocks of carbides of about 50 µm homogeneously spread into the fcc matrix. They are known to reduce the wear rate because of their very high hardness [17].

The defects extraction and the analysis of the measured parameters is shown in fig.6.(i) and (ii)-(vii) respectively. The 3 specimens feature a gradient of porosity, 0.14%, 9,0% and 17,4% respectively for specimen n°1, n°2 and n°3, in the sliding area as seen in fig.6.(i) and (iv). Most of the pores are small as 75% of the pores have an area inferior to 3500$\mu m^2$ (fig.6.(ii)). These pores are due to gas entrapment during the process as seen in fig.4 (i). Logically, the analysis of the perimeter of each pore features the same tendency because of the spherical nature of these defects (fig.6.(iii)). The small number of large and irregular pores is the discriminating factor which leads to a difference in the ratio (%) of the overall porosity between the specimens (fig.6.(ii-iv-vi). Specimens n°2 and n°3 have a similar number of pores (≈1500) and a similar number of pores presenting similar size distribution. The main difference results in the number of pores that are superior to $10^5$ $\mu m^2$ in term of area. Specimen n°1 has significantly less pores (<500). All its pores are smaller than $10^4 \mu m^2$. Analysis of the overall porosity perimeter shows a gradient between specimens which is equivalent to that of the area (fig.6.(v)).

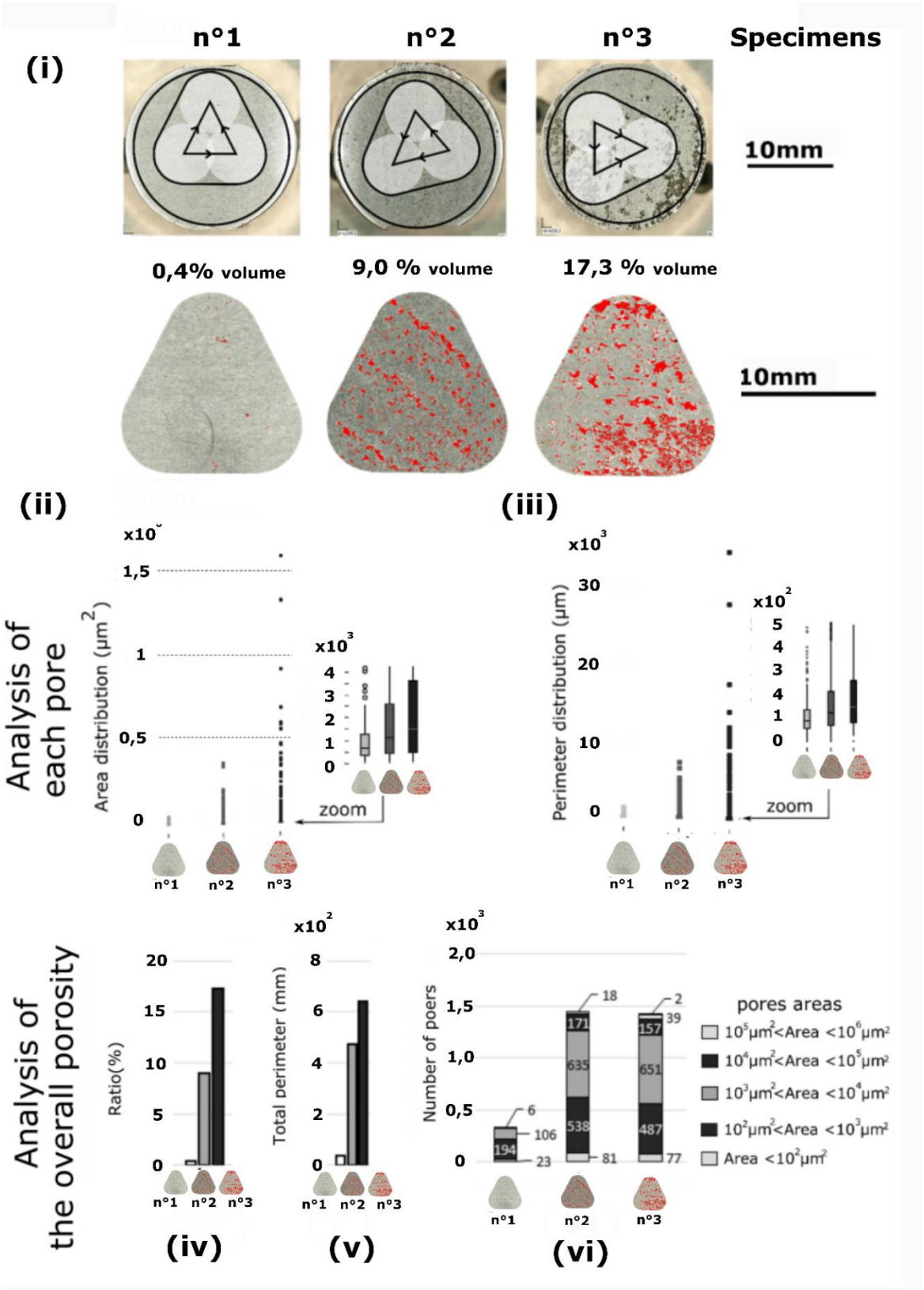


**Figure 6**: Pores analysis: (i) Optical microscope images showing the path of the UHMWPE pin on the CoCrMo discs and the porosity distribution on the sliding area, (ii) area distribution of the pores, (iii) perimeter distribution of the pores, (iv) Total ratio (%) of the pores areas compared to the sliding area, (v) total perimeter and (vi) number of pores regarding the pores size.

## 2. Polyethylene Wear behavior against SLM-CoCrMo

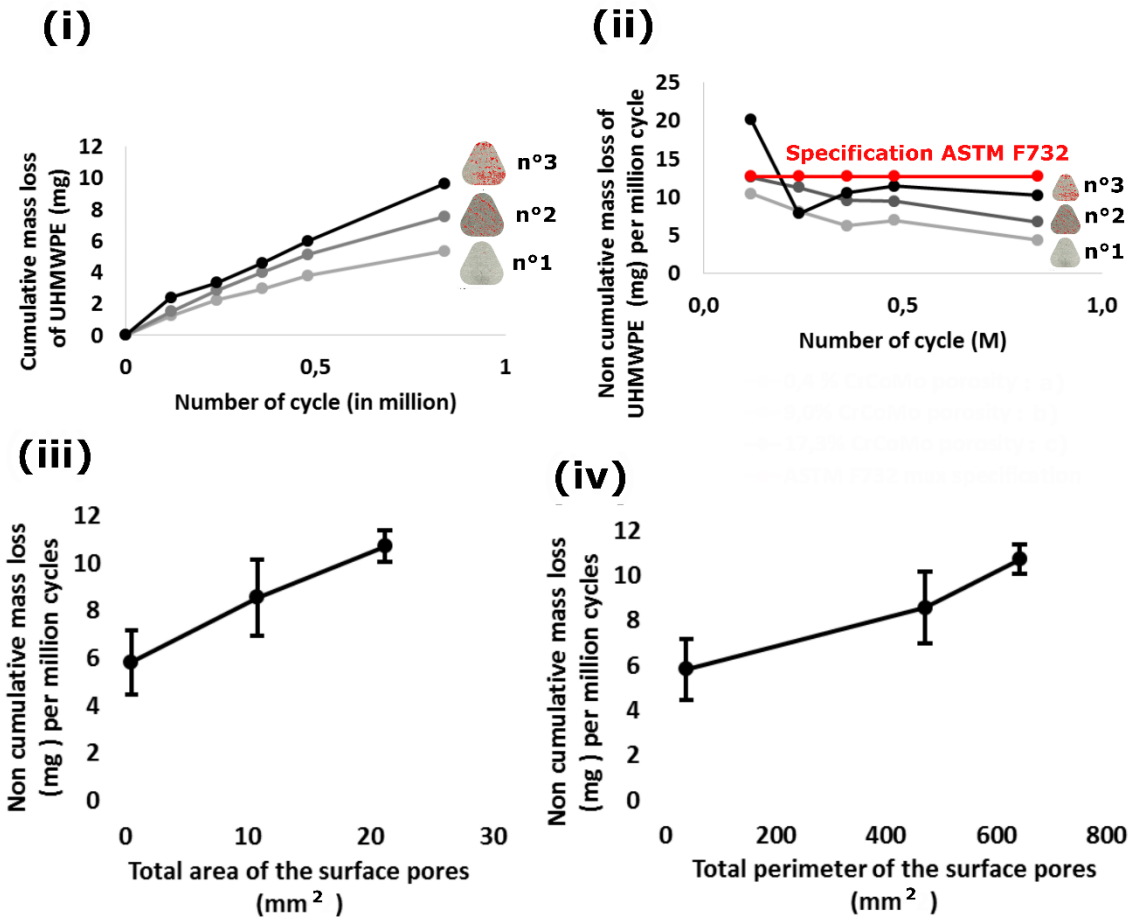


**Figure 7:** Polyethylene wear against SLM-CoCrMo discs characterized by a gradient of pores: (i) cumulative mass loss of the UHMWPE pins, (ii) evolution of the non-cumulative mass loss per million cycle during the test, (iii) evolution non-cumulative mass loss results per million cycle regarding the total area of the pores, (iv) evolution of the non-cumulative mass loss results per million cycle regarding the total perimeter of the pores.

The results of UHMWPE mass loss of against SLM-CoCrMo discs featuring a gradient of defects are shown in Fig.7. Throughout the test, the cumulative mass loss of the UHMWPE is higher when sliding against specimen n°3 than specimen n°2 followed by specimen n°1. The non-cumulative mass loss per million cycle shown in Fig 7.(ii) demonstrates an initial high wear which decreases in the first 240 000 cycles. The mass loss values of the UHMWPE per million cycles are within the specifications recommended by the ASTM F732 standard after 240 000 cycles for all the specimens. The mass loss values of the UHMWPE per million cycles seemed linearly and positively correlated to the total area of porosity (Fig.7 (iii)) and the total perimeter of the pores (Fig.7 (iv)). Therefore, an increase of 0,213mg of polyethylene mass loss per $mm^2$ of pores' area is estimated.

Similarly, an increase of 0,007mg of polyethylene mass loss per mm of pores' perimeter is estimated. According to Fig.7 (iii), a polyethylene mass loss of 5,5mg/million cycles is expected against a full dense SLM-CoCrMo disc. The data of Fig.7.(iv) gives an estimate of 5,1mg/million cycles. Sun *et al.* [18] performed pin-on-dics tribological test on SLM-316L against spherical stainless steel pin under dry conditions. They found that the wear rate of SLM 316L is positively correlated to the porosity percentage in terms of volume. Although the tests were performed with a different couple of materials and different tribological parameters (e.g. unlubricated condition, rotating sliding motion), the results confirms the deteriorating effect of the porosity on the wear performance of SLM parts. It is therefore essential that SLM components are properly manufactured with the least porosity.

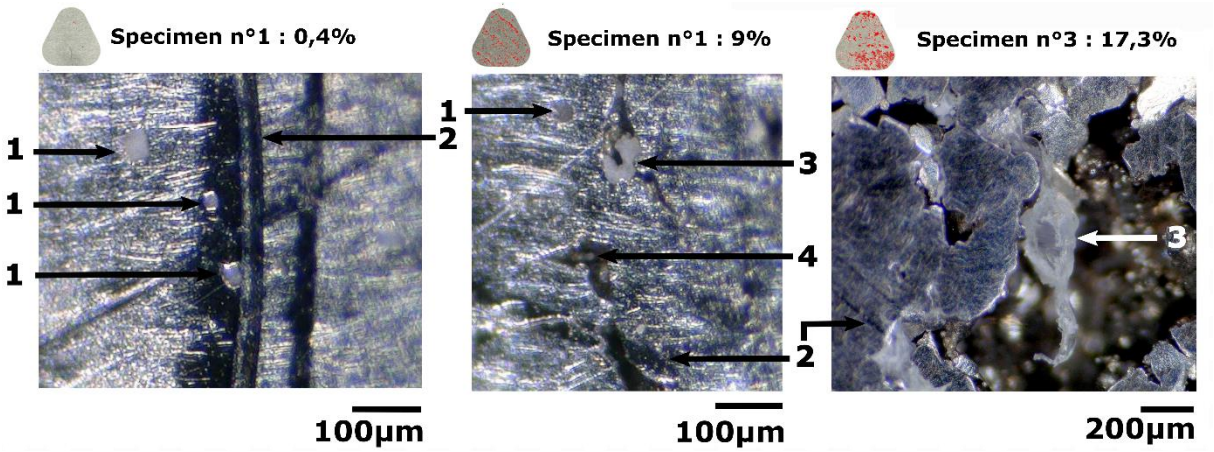


**Figure 8:** UHMWPE material on the SLM-CoCrMo discs after the test; observation at the optical microscope. 1 : entirelly filled pore with polyethylene; 2: trace of burnt polyethylene; 3 : large flake-like polyethylen debris on a pore edge; 4 : round and small (10-15µm) debris of polyethylen inside a large pore; 5.

Some UHMWPE wear debris were embedded in the SLM-CoCrMo discs after the test as seen in Fig.8. In the case of specimens n°1 and n°2, the polyethylene debris filled the pores which are mostly small and circular. In the case of specimen n°3, the polyethylene debris have also filled the small circular pores but are additionally seen at the edge of the irregular pores (Fig.8.n°3). In this last configuration, the debris are much larger (Fig.8.n°3) and some have a flake shape. Specimen n°2 has the same polyethylene debris type than specimen n°3 but in a lower content and smaller debris size (Fig.8.n°2).

All the polyethylene pins' surfaces featured triangular scratching (Fig. 9) as can be explained by the kinematics of the test. The increase in pin roughness (Sa) coincides with the increase in porosity. This confirms the abrasive behavior of the pore edge (Fig.9).

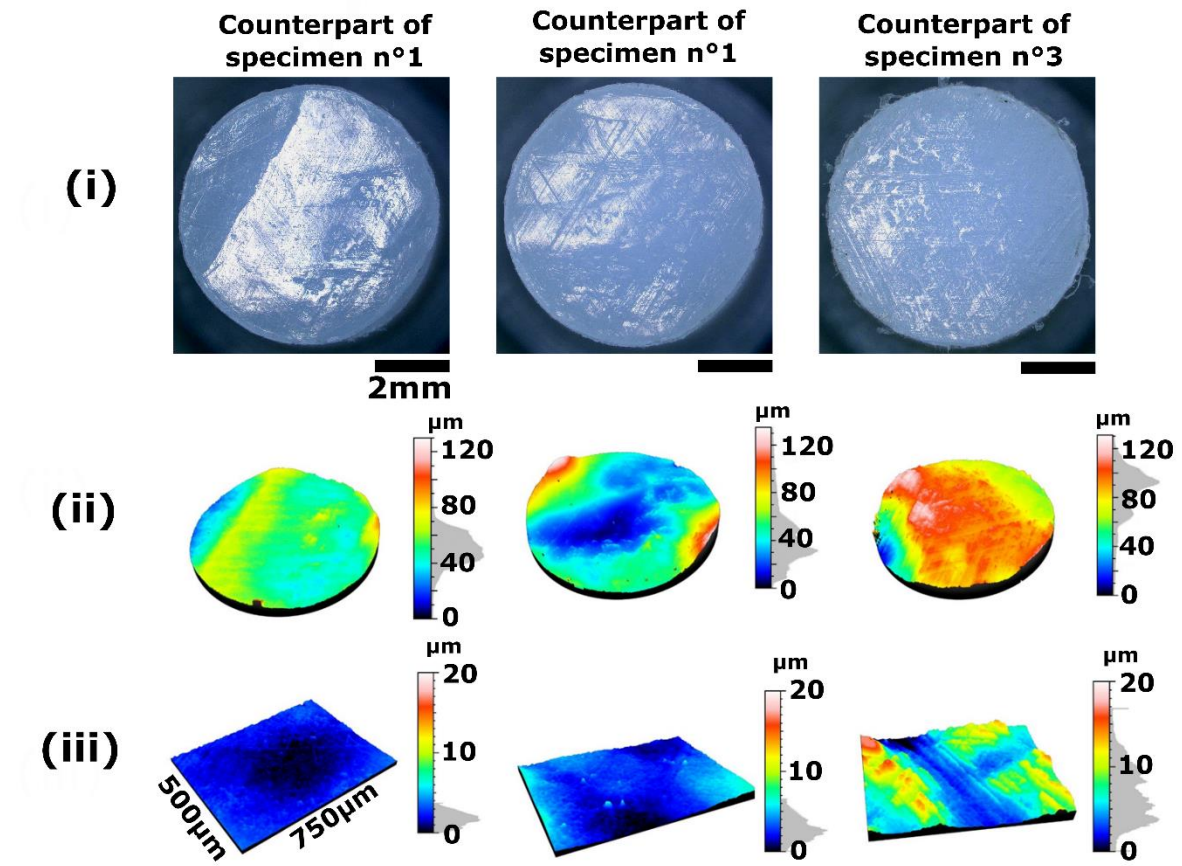


| | | | |
|---|---|---|---|
| **Sa(µm)** | 0,71 | 1,49 | 2,01 |
| **Sq(µm)** | 0,87 | 1,87 | 2,54 |

**Figure 9:** Surface texturation of the UHMWPE pins after the wear test : (i) optical microscope, (ii) Non-contact 3D optical profiler of the entire surface, (iii) Non-contact 3D optical profiler of the entire surface of a zone of 500x700µm

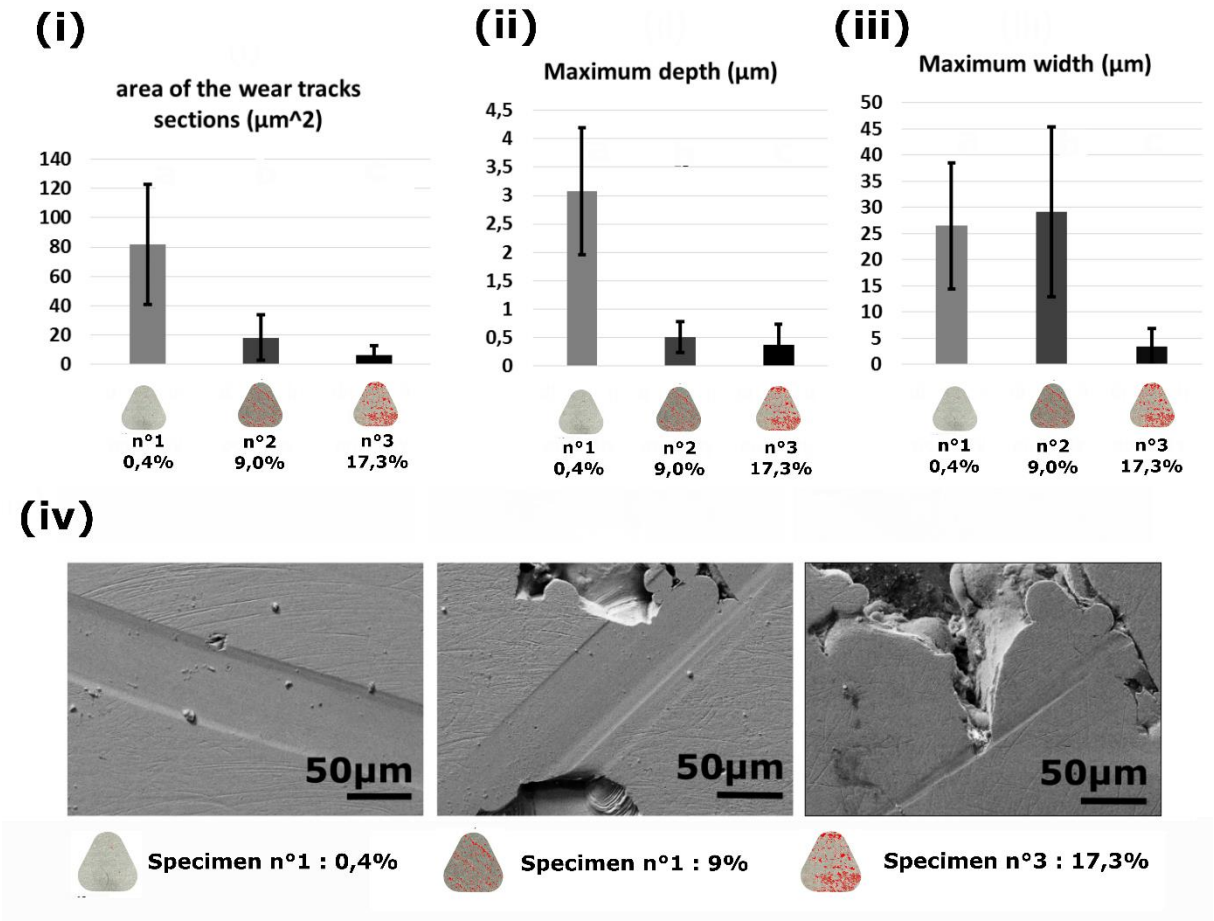


**Figure 10:** Profile analysis of the wear tracks located on the CrCoMo discs after the wear test : (i) area of the wear tracks, (ii) maximum depth, (iii) maximum width and (iv) SEM images

Similarly, there were scratches visible on all the CoCrMo discs (Fig.10). Traces of burnt polyethylene were also seen at the surface of all the discs (Fig.8). Many traces are visible on the specimen n°1 compared to specimens n°2 and n°3. These traces are typical of polymer adhesion mechanisms.

The wear tracks visible onto the surface of the disc suggest that metallic third-body particles were created during the tests. Specimen n°1 had larger and deeper wear tracks compared to specimen n°3. Specimen n°2 had wear tracks as wide as specimen n°1, but less deep. The width of the wear tracks can be explained by the morphology of the 3rd body that was formed during the test. The wear tracks of specimens n°1 and n°2 might reflects flat and wide debris while the wear tracks of specimen n°3 might reflects small debris. The fact that specimen n°3 had more irregular pores which might release metallic particles with time tends to confirm this hypothesis. The depth of the wear tracks might be explained by the potential effect of the large pores to collect debris. Indeed, these 3rd bodies tend to slide over a shorter period of time as in the presence of large pores, leading

to reduced superficial wear tracks. A total absence of debris will not ever be possible. There will always be wear and tear. However, by reducing the abrasiveness of pore edges, it would be possible to exploit their debris trapping characteristic.

Abrasion wear was therefore found on all configuration of tests resulting from two different mechanisms: (i) abrasion from the sharp pore edges on the surface and (ii) abrasion from the metallic third-body particles trapped between the surfaces.

# Conclusion

The microstructure and the defects of additive manufactured CoCrMo by selective laser melting was investigated and the wear behavior of UHMWPE against SLM CoCrMo was evaluated with multidirectional pin-on-disc experiments in synovial fluid-like lubricant at 37°. The testing conditions were set to simulate the wear of a total joint arthroplasty implant which is composed of a metallic part made of CoCrMo by SLM and UHMWPE. We produce SLM samples to highlight the effect of the pores in the surface; the specimens have a volume of porosity ranging from 0,4 to 19,7%. The paper allows the following conclusions to be drawn:

- Under the present testing conditions, the SLM samples exhibit wear rates in accordance with the ASTM F732 standard acceptance criteria
- There is a strong correlation between wear rate of UHMWPE and the total area of the porosity in SLM CoCrMo discs. Reducing porosity is beneficial for improving the wear resistance of UHMWPE.
- The edges of irregular pores in SLM samples are abrasive, which leads to increased numbers if polyethylene debris and an accelerated UHMWPE mass loss during the lubricated sliding process.
- Adhesion wear was identified particularly in the nearly full-dense disc configuration. It was generated by the transfer of polyethylene material on the metallic surface.
- Abrasion wear was identified on all configuration of tests because of (i) sharp edges asperities on the surface and (ii) third -body particles trapped between the surfaces.
- The pores also limit the abrasive effect of the third body particles by acting as debris collectors.

## Acknowledgements

We thank CRITT MDTS for their excellent expertise in biotribology and for the use of their cutting-edge equipment and machines.

## Funding source

The work was supported by the “Agence National de la Recherche” (ANR-11-IDEX-0004-02 under Idex “Sorbonne Universités” by an IUIS project for the promotion of healthcare innovation. Augustin Lerebours was recipient of a Ph.D. fellowship from the French Ministry of Science and Technology.

## Conflicts of interests

The authors have no conflicts to declare.

## References

[1] D. Joguet, S. Costil, H. Liao, Y. Danlos, Porosity content control of CoCrMo and titanium parts by Taguchi method applied to selective laser melting process parameter, Rapid Prototyp. J. 22 (2016) 20–30.

[2] W.E. Frazier, Metal Additive Manufacturing: A Review, J. Mater. Eng. Perform. 23 (2014) 1917–1928.

[3] ISO 21536: Non-active surgical implants – Joint replacement implants – Specific requirements for knee-joint implants, (2007) 5.

[4] S. Dadbakhsh, L. Hao, N. Sewell, Effect of selective laser melting layout on the quality of stainless steel parts, Rapid Prototyp. J. 18 (2012) 241–249.

[5] P. Gokuldoss, S. Kolla, J. Eckert, Additive manufacturing processes: Selective laser melting, electron beam melting and binder jetting—Selection guidelines, Mater. . 10 (2017) 672.

[6] Y.S. Hedberg, B. Qian, Z. Shen, S. Virtanen, I. Odnevall Wallinder, In vitro biocompatibility of CoCrMo dental alloys fabricated by selective laser melting, Dent. Mater. (2014) 525–534. doi:10.1016/J.DENTAL.2014.02.008.

[7] A. Lerebours, P. Vigneron, S. Bouvier, A. Rassineux, M. Bigerelle, C. Egles, Additive manufacturing process creates local surface roughness modifications leading to variation in cell adhesion on multifaceted TiAl6V4 samples, Bioprinting. 16 (2019).

[8] M. Nasab, M. Hassan, B. Sahari, Metallic biomaterials of knee and hip-a review, Trends Biomater. Artif. Organs. 24 (2010) 69–82.

[9] V.P. Mantripragada, B. Lecka-Czernik, N.A. Ebraheim, A.C. Jayasuriya, An overview of recent advances in designing orthopedic and craniofacial implants, J. Biomed. Mater. Res. Part A. (2012) 3349–3364. doi:10.1002/jbm.a.34605.

[10] F. Bordonado, Traitement sélectif de la rugosité des surfaces. Applications industrielles, Matériaux Tech. 88 (2000) 82–88.

[11] A. Wang, A unified theory of wear for ultra-high molecular weight polyethylene in multi-directional sliding, Wear. 248 (2001) 38–47.

[12] E.W. Patten, D. Van Citters, M.D. Ries, L.A. Pruitt, Quantifying cross-shear under translation, rolling, and rotation, and its effect on UHMWPE wear, Wear. 313 (2014) 125–134.

[13] C.R. Bragdon, D.O. O'Connor, J.D. Lowenstein, M. Jasty, S.. Biggs, W.H. Harris, A new pin-on-disk wear testing method for simulating wear of polyethylene on cobalt-chrome alloy in total hip arthroplasty, J. Arthroplasty. 16 (2001) 658–665.

[14] V. Saikko, A Hip Wear Simulator with 100 Test Stations, Proc. Inst. Mech. Eng. Part H J. Eng. Med. 219 (2005) 309–318.

[15] X. Zhou, K. Li, D. Zhang, X. Liu, J. Ma, W. Liu, Z. Shen, Textures formed in a CoCrMo alloy by selective laser melting, J. Alloys Compd. 631 (2015) 153–164. doi:10.1016/j.jallcom.2015.01.096.

[16] X. Xin, J. Chen, N. Xiang, B. Wei, Surface Properties and Corrosion Behavior of Co–Cr Alloy Fabricated with Selective Laser Melting Technique, Cell Biochem. Biophys. 67 (2013) 983–990.

[17] Y. Liao, E. Hoffman, M. Wimmer, A. Fischer, J. Jacobs, L. Marks, CoCrMo metal-on-metal hip replacements., Phys. Chem. Chem. Phys. 15 (2013) 746–56.

[18] Y. Sun, A. Moroz, K. Alrbaey, Sliding Wear Characteristics and Corrosion Behaviour of Selective Laser Melted 316L Stainless Steel, J. Mater. Eng. Perform. 23 (2014) 518–526.

## 3. Intermediate conclusion

The different parts that constitute the trapezo-metacarpal implant are undergoing different stresses. The metacarpal stem, an anchor element with bone material, must have essential biocompatibility properties to avoid loosening of the stem after implantation. While the polymer insert and the trapezium bone replacement are in movement with one another in order to offer the range of mobility of the trapezo-metacarpal joint. The fatigue strength of these two components is more related to the wear resistance property. In this chapter, we have analyzed the selected biomaterials, Ti6Al4V, CoCrMo, 316L and UHMWPE in relation to the function to be fulfilled according to the medical device standards. The work showed that it is possible to produce a metacarpal stem in Ti6Al4V by selective laser fusion on a powder bed while preserving the non-cytoxicity properties. It has been shown that the process results in a unique surface texturing based on partially melted powders and traces created by laser tracks. The results showed that the osteoblastic cells adhered unevenly into the sample. This variation in adhesion is directly correlated with variations in surface texture induced by the inclination of the surface during the additive manufacturing process. In fact, cell attachment has been improved on the surface with microscopic grooves compared to partially molten powders. Therefore, the source of process-induced surface texture heterogeneities can be controlled to promote the necessary characteristics of bone interface implants. The work also showed that the porosity of chromium-cobalt-based samples induced by the laser powder-bed fusion process significantly impacts the wear of the Pehd. Optimization of the printing parameters is therefore essential in order to reduce this type of defect and increase the life expectancy of the implant.

# CHAPTER 6:

# Philosophical research on prehension and a further prehension loss due to arthrosis at the carpometacarpal joint

*Dans ce chapitre, est étudié le point de vue du patient souffrant d'arthrose trapézo-métacarpienne. En comprenant les frustrations induites par la pathologie, nous avons acquis une meilleure compréhension de la valeur perçue des solutions thérapeutiques et particulièrement de l'arthroplastie prothétique personnalisée.*

## 1. General context

Trapeziometacarpal osteoarthritis is common in later life. It affects 10-20% of post-menopausal women and reaches 66% after 80 years of age while 23% of men are affected [1]. At this stage of prevalence, it can be assumed that this is an inevitable development at old age that is felt to be "normal". Indeed, only a limited percentage of patients with trapeziometacarpal osteoarthritis at a very advanced stage consult a doctor and an even smaller cohort choose to opt for an implant. In this context, it would be useful to know to what extent patients perceive the pathology and the therapeutic solutions.

This investigation also analyses the impact of the pathology on the patient's identity, daily life and the frustrations and tensions that it causes.

## 2. Introduction

Studied by medicine, ethnology, cognitive sciences and many other disciplines, the role of the hand is central to the human species. In order to understand the psychological impact of loss of grip, it is essential to question the importance of this essential part of the body in our daily lives, from the simplest to the most technical gestures. Our hands are essential for us to eat, write, communicate, work... We have appropriated them so much during our lives that their importance is rendered invisible and it is only when we lose their functionality that we can measure the extent of their impact on our lives. We therefore focused on the study of the functions of the hand for the human being, from both an individual and species perspective. Through an in-depth literature review, we were able to identify them. The problem we have raised is therefore the following: In what way are hands essential for man and why? The aim of our study is to understand the requirements and experiences of patients in the most extreme cases of osteoarthritis where the patient gradually loses the mobility of the thumb impacting the grip of the hand. This first bibliographic section allows us to identify the central role of the hands for each human being in order to better understand the consequences of loss of strength, motor skills and/or grip, from a psychological and social point of view, on patients suffering from this pathology. In order to design the implant as well as possible, it is essential to question the impact of the gesture of gripping on the human body and the importance for patients to recover the gripping.

### 2.1. An impact on human as a species and society

In The Hand [2], Frank R. Wilson's objective is to show the impact of the hand on human as an individual as well as a species and society. Indeed, morphologically, essentially and evolutionarily, his hands characterize Man as a species and sentimentally and psychologically, as an individual. The author, a neurologist and writer, is interested in the subject of the hand following personal experiences in the world of music and piano in particular. Indeed, many musicians suffer from focal dystonia of the hand, which generally manifests itself as a painless loss of muscle control when performing high level movements. He then questions himself about the deep roles of the hand and how it has defined Man and the society in which he lives. The importance of hands to any individual stems directly from their interdependence with the brain. "Bodily movement and brain activity are functionally interdependent, and their synergy is so powerfully formulated that no single science or discipline can independently explain human skill or behavior".

Thus, our relationship with hands is so deeply rooted and automatic, from a neuromotor point of view, that it is difficult to take a step back from their essential roles for humans as long as our hands are functional. Wilson cites the three main roles of the hands:

1) anthropological and evolutionary: the hand determines the emergence of human-specific behaviours and movements essential to survival and that lead to brain development;
2) biomechanical and physiological: hands are structured to allow the control of objects (tools). The structure and function are in complete agreement;
3) neurobehavioral and developmental: interactions between the hand and the brain determine the behaviours specific to humans to think, communicate by speech and create (creativity).

We are here in the presence of a transduction between human behaviour and structure. The concept of transduction was proposed by Gilbert Simondon [3] and can be defined as follows: a mechanism of co-constitution and then permanent co-evolution by reciprocal feedback between two (or more) elements that form a system, that co-produce each other. Here, structure and behaviour define each other over the course of evolution, with behaviours modifying brain structures by creating new neural connections, for example, which in turn allow new behaviours. "The modern human brain (structure) might have evolved as a consequence of the increase in tool use (behaviour)" according to Sherwood Washburn [4]. "Behavior and structure form an interacting complex, with each change in one affect the other". In particular, the transition from quadruped to biped (structure) contributes to the determination of Man as a species (Homo Sapiens), freeing the hand and speech (behaviour). The opposable thumb also allows better precision in the handling of small objects in addition to larger objects: "this small modification would have greatly enlarged the functional potential of the hand at both ends of the existing behavioral repertoire, opening the possibility for both a more combative and a more digitally dexterous individual". The thumb therefore allows freedom of movement and generates new neurological abilities that can control more precise and new movements. In the course of evolution, we therefore see the specific characteristics of Man such as language, the use of tools, reason and self-awareness appear. All these features derive from the "long process of brain enlargement that began with the expansion of novel and inventive tool use by Homo Habilis", often permitted by hand. Finally, Peter C. Reynolds [5] suggests that complex tools, such as knives or axes, may have been produced by groups of humans working together. This involves the formation of communities and thus forms of

communication that have then been translated into languages until the emergence of cultures and social organizations. The hand would therefore be an essential element in the organization of Man in society, which is also a determining feature of our species.

## 2.2. An impact on Man as an individual

### 2.2.1. Build your identity on a daily basis

Frank R. Wilson realizes how much this affects musician patients for whom the use of hands to play is not only professionally but also personally essential. For them, music is "the essential physical instrument for realization of they own ideas or the communication of closely held feelings. [...] Musicians love to work and are miserable when they cannot." This shows that hands allow musicians to communicate and be. Music being the means of expressing oneself, of communicating, of feeling oneself, it is possible to see that the hand is essential to Man to build his identity and to express himself and communicate, but not only. The example of musicians is very representative, but the use of hands is essential for any individual. Think of the people doing manual work or our everyday actions. Thus, hands seem essential for daily living, eating, washing, dressing, opening a door or shaking hands. All these gestures depend on our hands and the ability to grasp them. But we can also think of the impact that the use of hands has on our social status and our life in society: to clap on the computer, to write, to drive, to greet... We use this part of the body to work and communicate with others. Hands are generally essential for interaction with the outside world and with others. Finally, we use it for leisure activities such as a sport, a passion (music, art...) or a hobby (knitting, cooking...). All these actions allow us to build our personal identity and live within society.

### 2.2.2. The hand, a constitutive role of our experience

Our hands are a contact surface between us and the world around us, which allows us to have "emotional feedbacks": in other words, stimuli emitted by what constitutes our environment (people, objects, etc.). These stimuli allow us to anchor ourselves directly in the space around us and therefore allow us to orient ourselves. A distinction is made between "direct" touch, which is everything that is physical contact, and "indirect" touch, which corresponds to drawing the caller's attention to a single object through the gaze or gesture of the hand. But why choose the hand over other organs such as the eyes or ears? We get involved sensory with our hands: this is what makes it so special. Being able to touch, move, grab what surrounds us therefore allows us to anchor ourselves in space because we actively act on what surrounds us. Gripping strength, touch and mobility

therefore play a key role. "We are inventive creatures, we conceive the world instrumentally" [6] : unlike other species, we want to interfere with nature in order to serve our own interests and the hand is the first tool that allowed us to do this: the example of tools cut from flint or wood is quite representative. We do not only have a visual or auditory concept of the things around us: we also have a manual idea of them. We can learn manually and therefore we have a manual memory. Moreover, the hand has allowed Man to develop a first form of language: sign language. The hand also includes a significant number of nerve endings compared to the rest of the body: the sensory homunculus (see below), corresponding to a silhouette representative of the different parts of the human body according to the way they are projected in the cerebral cortex. This diagram shows us the impact of the hand on the brain and on our proprioception.

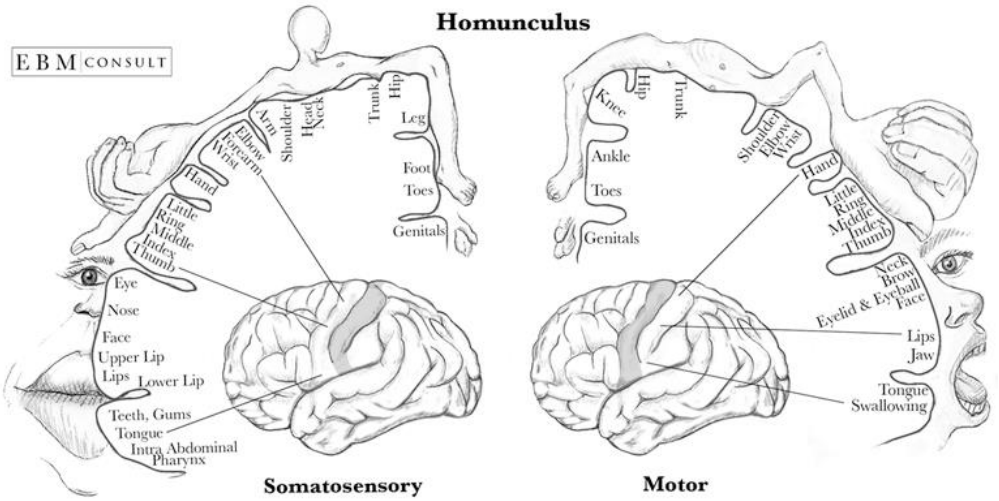


**Figure 1**: Homonculus sensitif (source : https://www.ebmconsult.com/)

Proprioception can be defined as the perception we have of our own movements: a peripersonal space encompassing us and the field of reality with which we interact. When we take an object, for example, we enlarge this space, which is called peripersonal space. This is made possible by the hand which can be considered as an intelligent tool [6]. "It is with, and only with, my body that I am able to exist in relation to things in the world, and it is with my hands that I am able to directly manipulate and bring about change in my world" [7]. By touching and being touched, we experience the world both as a subject and as an object. The hand allows us to act on the world because it allows us to include it within our peripersonal space. Things are then put within our reach: that is how we conceive the world, with our hands as a reference. S.A.J Stuart explains that Kant defends the fact that by building our peripersonal space through this contact surface we are building our "subjective world". Kant is indeed a pioneer of the idealistic current: although

an absolute and objective reality exists, we never fully reach it. We each have a so-called subjective reality. We can notice that there is a kind of co-evolution between our personal construction and the construction of our subjective world. We define ourselves in terms of how we perceive the world when we live in it. It is indeed our reality: it defines us as much as we define it.

### 2.2.3. The FAST: diagram of the functions of the hand

The bibliographical study allowed us to draw up a FAST (Function Analysis System Technics) schematizing the main functions of the hand for Man. The FAST is a diagram used in value analysis to create a functional representation of the object under study, networking the goals (left) and concrete solutions (right).
The result obtained is presented in figure 2.
We were therefore able to identify the five main functions of the hands, which allow us:

- to perceive the world;
- to express, communicate and interact;
- to build our identity;
- to have the characteristics of our species;
- to be organized in society.

By developing each function, we were able to identify the "questioning perimeter", i.e. the roles that can be impacted by a loss of strength, motor skills and/or grip. Functions with a black outline will not be covered in this study. Indeed, functions that are made possible by the sense of touch or by neurophysiological mechanisms (which allow us, for example, to recognize symmetrical shapes) do not fall within our field of action because we are only interested in the loss of strength, motor skills and/or grip in order to understand the experiences of the patients in our study. In addition, we have excluded the function: "the hand allows Man to be as a species" (essence of Man). Although the hand has a predominant role in the evolution of Man, it is not a characteristic that alone defines our species: a person without hands at birth is still a human being.

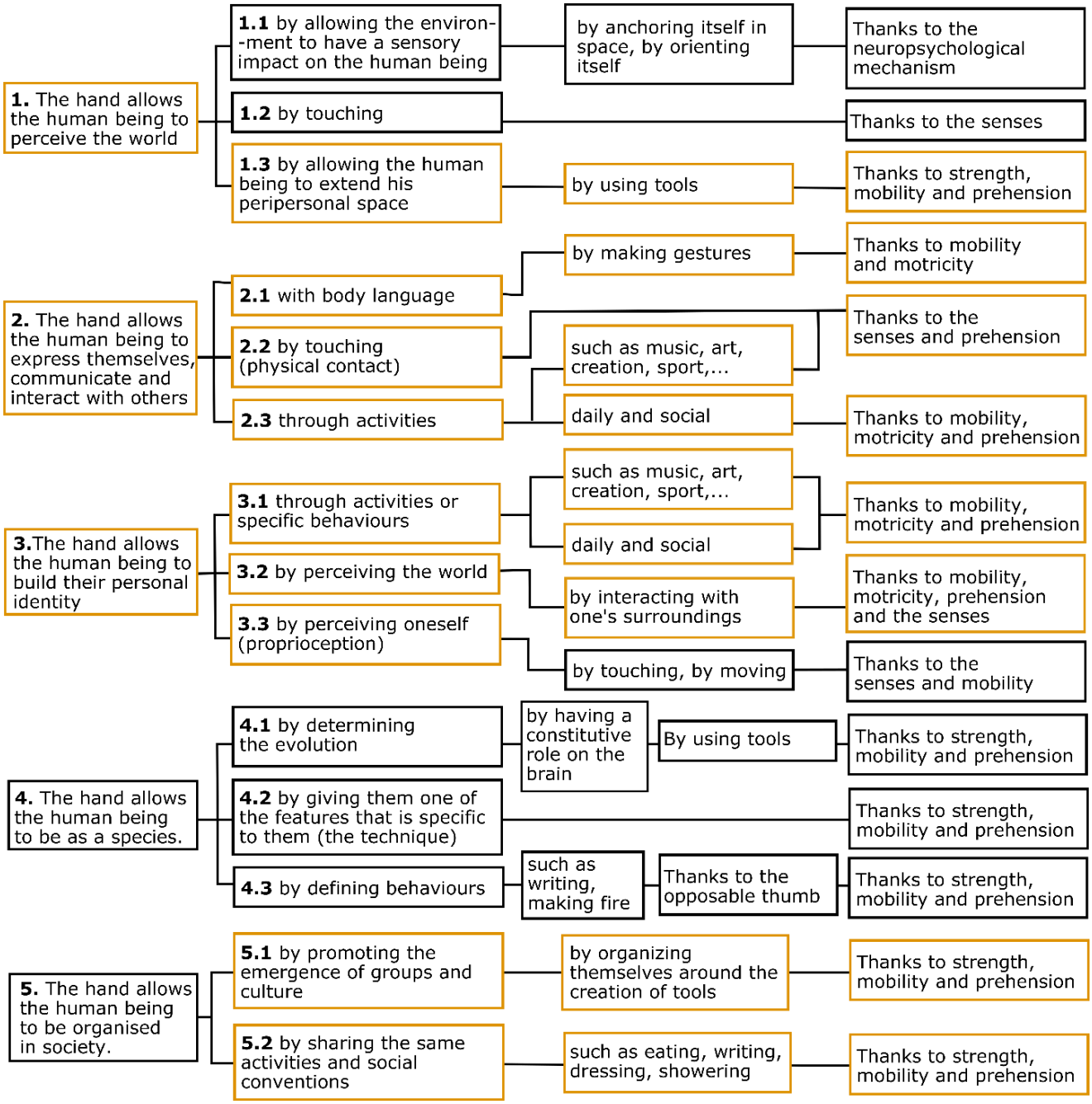


**Figure 2**: FAST of hand functions

First, we will look at the importance of hands in perceiving the world by acting on it (1.1). Indeed, the grip, strength and motor skills of our hands allow us to grasp and build tools, such as microscopes or telescopes, for example that help us to perceive the world around us. But the use of tools with hands also involves an extension of our peripersonal space, as shown in Figure 3: "Using a tool modifies the representation of the body, regardless of the task to be performed afterwards, and will correlatively modify objects perceived as being attainable [8].

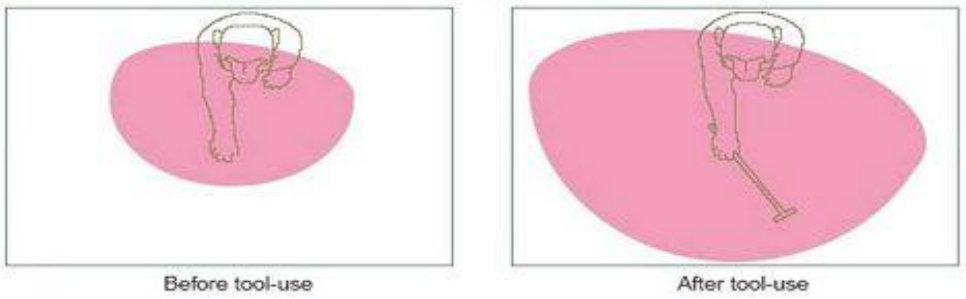


**Figure 3** : Increasing peripersonal space through the use of a tool

We can therefore affirm that the hand allows us to perceive a larger part of the world and to extend our power of action over it. Second, hands allow us to express ourselves and interact with others. For example, our body language (2.1) is essential in communicating with others and in physical contact (2.2): a handshake, a caress, a gesture, etc. In addition, certain activities (2.3) allowed by the hands, such as music, art or writing, are essential for us to express ourselves and interact. Third, we use our hands to build our personal identity. For example, the activities (3.1) that each individual performs and that characterize him or her are carried out through the use of this part of the body. In particular, the job carried out defines the social status of the individual, and therefore his or her identity in relation to others: "Work is, after the family, one of the essential components of identity" [9]. But our inner world (3.2) is also created by our interaction with the outer world, as Kant explains. Thus, perceiving and interacting with the environment helps us to build our own world. Our identity also depends on how we perceive ourselves (3.3), by perceiving our own bodies through touch and movement we create our own proprioception (self-perception). Finally, the evolution of the anatomy of the hand (opposable thumb) has allowed the creation of tools. The use of these has led to the emergence of neural connections that in turn promote the complexity of the tools and the society in which they are embedded. It is therefore possible that our organization as a society may depend in part on the hand. Indeed, as we said earlier, it is perhaps around the manufacture of tools that groups of individuals have formed and developed into cultures and societies (4.1). In addition, each culture and society shares the same activities and conventions (4.2), such as dressing or eating with cutlery. Most of these activities depend on hands. Once again, we want to highlight the role of work which, in addition to constituting a large part of our identity, is essential for our integration into society and our relations with others.

The hand plays an essential role for the human being. Bibliographic studies have allowed us to take a step back and analyze the functions of the hand from a practical but also a

more conceptual point of view. This helped us to ask ourselves the right questions about the consequences of a loss of grip strength. While some functions do not seem to be consistent for the rest of our study, others seem central to identifying patients' needs and feelings. In particular, we retain the importance of hands for the identity of the individual, for communication and expression with others, for interaction with the world and for his place in society. These aspects will be studied by interviewing patients to better understand the issues of loss of grip and/or hand mobility. Finally, the evolution of the anatomy of the hand (opposable thumb) has allowed the creation of tools. The use of these has led to the emergence of neural connections that in turn promote the complexity of the tools and the society in which they are embedded. It is therefore possible that our organization as a society may depend in part on the hand. Indeed, as we said earlier, it is perhaps around the manufacture of tools that groups of individuals have formed and developed into cultures and societies (4.1). In addition, each culture and society shares the same activities and conventions (4.2), such as dressing or eating with cutlery. Most of these activities depend on hands. Once again, we want to highlight the role of work which, in addition to constituting a large part of our identity, is essential for our integration into society and our relations with others.

## 3. Methods

Four interviews were conducted with people suffering from osteoarthrosis. These were semi-directive interviews in which the questions asked guided the interlocutors to address several points that emerged from our literature search.

No medical data were collected during the interviews, the following information is an analysis of the feelings and experiences of the patients that we have transcribed and interpreted. A functional analysis tools was used to complete this work.

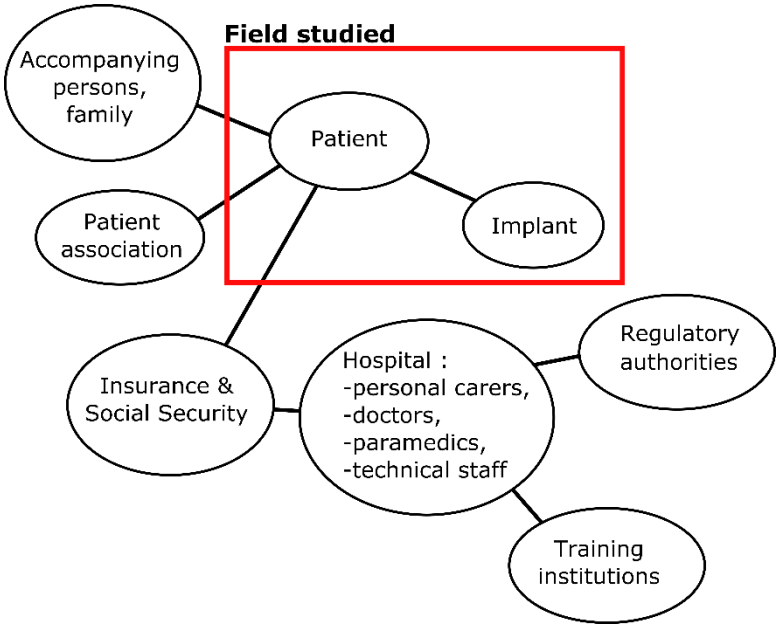


**Figure 4** : Graphical form of the socio-technical system

## 4. Results

### 4.1. The pathology

The four interviewees belong to an age group between 45 and 60 years, including four women. All of them have a job in which the use of the hand is essential and in which many tasks require its use: writing on the board, typing on the computer, holding a pen... Indeed, these people work in the administrative, academic or maintenance sector.

For all of them, the pathology of osteoarthritis has been diagnosed by a rheumatologist, but some have a more advanced stage than others. Thus, continuous pain with peaks of intensity is observed when the hand is stimulated by movements or pain is only present when specific movements are performed. A person also has pain attacks that manifest themselves as electrical shocks and are relieved only (and not systematically) by wearing an orthosis.

All patients experience a loss of:

- gripping;
- force;
- mobility;
- precision

Thus, many gestures become difficult to perform and many tools become difficult to handle, even impossible. For example, in the kitchen, the use of vegetable peels, opening jars and bottles, opening preserves becomes complicated. Vacuuming or ironing become

impossible tasks and making your shoelaces, buttoning up, putting on tights or socks, massaging your hair during shampooing are everyday gestures that make it difficult. In the workplace, holding a pen, signing, writing more than 10 lines, typing and grabbing the mouse are difficult and often painful actions.

### 4.2. Rehabilitation of the daily routine

This impossibility of using tools leads to a rehabilitation of the procedure performed by the patient. Indeed, all interviewees talk about a change in movement made for certain actions in order to reduce the pain felt or to overcome the loss of grip. Some have also equipped themselves with adapted solutions such as ergonomic objects or gadgets (mice, keyboards, can openers) designed to help them. In addition to the physical change in the gesture and environment surrounding the person (new objects), there is a psychological change in the patient. The interviewees talk about a reflection before the gesture to adapt it to their condition, no movement is made completely naturally. Sometimes, apprehension arises because of the fear of pain or failure to perform a task. The relationship to the objects that surround the osteoarthritis is therefore modified by the pathology: some take new tools, others think longer about their actions and all adapt their movements to have the least pain possible when performing a task. The rehabilitation of the interviewees is also observed in their activities: some of them have not stopped the activities they had previously carried out. Nevertheless, they often seem to force themselves to perform the same activities to maintain their lifestyle, even if it causes them pain. Generally, they have adapted their activities (knitting more slowly, cooking less often...). Others have embarked on new activities to surpass themselves and gain agility. Their daily relationship has thus changed, up to a more intense level for one of the patients who has stopped many activities, including sports (archery, tennis, table tennis...). The relationship with family and friends also seems to have been modified by the pathology. Most of the interviewees explained that a redistribution of tasks has been imposed on their homes: it is often the spouse who performs the household tasks that are problematic, such as peeling vegetables, vacuuming or opening pots. For patients living alone, rehabilitation is done on objects that substitute their hands. In addition, a more discreet reorganization of roles with the less close family and friends seems to have taken place for at least one of the interviewees. Indeed, when she cannot perform a task in a professional or associative context, for example, she explains that she succeeds in delegating this activity in particular to focus on another. More concretely, she will offer to serve food to the other person (holding the ladle is an activity that causes him pain) while

she hands the plate, for example. The people we were able to interview told us about their frustration and the gravity of the disease. Loss of autonomy and persistent pain lead to fatigue and irritability: each action requires effort and time. It's annoying, frustrating and burdensome, but patients deal with it and endure it. Despite this, some reported that their close family and friends noticed their increased irritability, which can impact their human relationships. Unlike the others, one of the patients seems to have fully integrated the pathology into her lifestyle and identity. She started new activities, met new people and surrounded herself with new objects. She has been involved in community life and has started water activities (rowing). From a professional point of view, we can say that an adaptation has taken place. The subjects found solutions to avoid being constrained in their work: changing the pace, delegating tasks, changing the medium (digital instead of paper), new gestures and new objects (ergonomic mice). Only one of these people is unable to perform all the tasks of his or her job, which is a source of frustration and concern.

### 4.3. The perception of a solution

Currently, the interviewees have or have not been treated. All have an orthosis that they use during pain attacks or to immobilize the wrist during the night. Other treatments used by some of the patients are neuromoding, i.e. the use of electrical currents to reduce pain, pain relief, pain relief, anti-inflammatory drugs and infiltration. This last practice is very painful but can relieve pain for a month or more. The person who has undergone this treatment is frightened at the thought of a new injection even though he or she recognizes the benefits of it. Drugs such as painkillers and anti-inflammatory drugs also have side effects and constraints (inability to drive, drowsiness...). The reflection that seems to emerge from the interviews is that pain is a bearable factor, while the loss of autonomy due to the impossibility or difficulty of performing certain gestures is insurmountable and extremely constraining. It is the loss of autonomy that is largely responsible for the frustration and pain experienced by patients with osteoarthritis. Thus pain causes fatigue but seems bearable to patients: the problem is not that it hurts all the time, but rather that it hurts so much at certain times that they are unable to perform a movement. The ideal solution for patients would then be a device to eliminate pain and restore pre-disease grip and mobility abilities. To choose, this last property is to be preferred according to the interviewees. Two of the subjects do not wish to receive an implant. Indeed, the pathology does not provide them with enough pain to come to such a "drastic" solution. In addition, one of the people has already suffered from algodystrophies and does not want to resort

to surgery and has completely redefined his identity around the pathology. In others, youth and/or difficulties encountered due to the disease lead to an interest in an implant as a solution. Nevertheless, it must meet certain conditions:

- First of all, if it is not possible to regain the autonomy before the pathology arrives, the implant must at least guarantee that it will not induce an additional loss of grip and mobility capacity;
- The implant must not degenerate over time or have side effects that could harm the person;
- The patient may have to eliminate the pain.

In general, a fear of the unknown is observed, it would be necessary to have guarantees on the effectiveness of the implant to make it attractive. The implant is therefore at the heart of both human and technical challenges: it constitutes what we call a socio-technical device. Indeed, this system is composed of both human and technical aspects. The objective of value creation lies in the relationship between patients and the implant.

## 5. Discussion

Following the synthesis of the interviews, we examined the analysis of certain points that emerged during the interviews and which seemed interesting to us to deal with. We therefore do not claim to cover all the avenues of analysis.

### 5.1. An identity process

Depending on the level of acceptance of the pathology, we observed two types of reactions in the people we interviewed. The first is to adapt your daily life, to talk about the disease with your family and friends so that the disease is an integral part of the subject's identity, who sees himself reinvented with his pathology (getting devices, relegating tasks, re-organizing his day, starting new activities...). The second is to deal with the disease, but not in an intrinsic way. The subject does not integrate the disease into his or her daily life, it is not part of his or her identity. He forces himself to continue his daily life despite the arrival of the disease, unlike the subject who has built his new daily life around it. This reaction of acceptance without true integration of the disease is the one we have observed most with our patients, the integration reaction being an exception. The reconstruction of one's identity following the emergence of a pathology is specific to many incurable diseases. Even more so in patients with serious illnesses, the diagnosis often marks a break in the identity of the patient who is being reconstructed. Marie-Hélène Boucand explains in "L'identité en errance" [10] that "the patient, upset by the diagnosis and

prognosis of the disease he is carrying, needs to work on himself in order to "recognize" himself in this new phase of his life. He must continue to assume his "self-preservation", even if his capacities and horizons are limited. He is caught in the dialectic between an identical self (it is not because he is sick that he is no longer the same) and a self in change as a result of the effects of the disease. Sociologists also use the term "disease trajectory" or "life course" to refer to the fact that the patient's experience is the result of the evolution of the pathology, and of all the activities, medical and non-medical, that modify its course. Also observed in patients with renal insufficiency, the dialysis they are confronted with represents an "identity process" in which the patient acquires skills about his situation and the machine but also redefines himself as a person. It is a construction of the patient's identity around the machine, the group of patients and the group of caregivers at the center. In particular, in the case of dialysis, it is the technique itself (machine) that represents the rupture of its identity. In the case of osteoarthrosis, the onset of the disease is much less severe. Nevertheless, the more or less pronounced loss of hand use implies a redefinition of self on the part of patients. The latter do not feel overwhelmed overnight by the pathology, but are readjusted, change the environment around them and sometimes even modify their activities and social relationships. We can see here that this is, if we cannot strictly speaking rebuild identity, at least readapt everyday life. We can therefore say that the onset of the disease causes a misalignment of the relationship with the patient's environment and daily life.

### 5.2. An adjustment of the daily routine due to the pathology

The notion of misadjustment comes from our history of technology courses: we speak of technical misadjustment when a new technology comes into society and societal mores are not yet "up to date": there is misadjustment of habits and customs by the technology in question until the new technology generates new mores. When a pathology enters a person's life, the person's daily life is not adjusted by the onset of the disease. Readjustment, i.e. the adaptation and creation of new behaviours, can be done at 100% (i.e. the integration reaction) but in most cases, the disease is part of the patient but is not an integral part of his identity. This level of readjustment is different depending on how long the patient has been living with the condition and also depending on its severity. An example of technical misalignment is represented by the story of the smile. Indeed, the appearance of dental techniques in the 18th century transformed the smile that was formerly considered coarse. It thus becomes a symbol of wealth: the progress of dentistry allows the appearance of a social gesture as widespread as a smile. It is therefore a

misalignment of society through the emergence of a technique. Parallelism is made here between this technical misalignment and the misalignment of patients' daily lives through the appearance and evolution of the pathology. This means that a time of adaptation is needed and new gestures appear. This daily rehabilitation applies to movements that were generally natural and become reflected, to the objects of daily life the patient, to the people around him and to leisure and professional activities.

### 5.3. Loss of autonomy and increased frustration

We also noted that most of the people we interviewed are not particularly interested in an implant, the orthosis and infiltrations sufficient to maintain the rhythm of life without too much pain. In addition, they have put in place solutions to deal with the disease. However, one of the subjects we interviewed has a profile that may be of interest to people working on an implant. The implant becomes necessary when pain is permanently present and when repeated movements during the day necessarily cause seizures and prevent the person from working. Leisure activities can always be changed and others can even be created (adapted sports, joining associations, etc...). The nature of the work and the impossibility of changing it in the case of our subject plays a major role in the need for an implant. As seen above, it is the loss of autonomy that generates the greatest frustration in the subjects: the pain being so great that certain actions can no longer be performed. People often talk about "seizures" or having their joints "blocked". Some people can avoid performing seizure-causing movements with the orthoses that block them, but when you need to perform these movements and you cannot wear orthoses on a daily basis, the implant becomes a possible solution. Age also plays an important role in the need for the implant: an operation may seem like a heavy intervention when you are close to retirement (you can then totally adapt your activities and no longer do the gestures that cause pain) and you prefer less invasive solutions.

### 5.4. Tensions

The analysis of the interviews led us to note the presence of several tensions carried by the pathology of osteoarthrosis and by the technical solution that is an implant.

#### 5.4.1. Tension : autonomy vs pain

The first tension identified is related to the daily life of patients suffering from the disease. Indeed, the actions performed provide them with pain, which leads to a loss of autonomy. All interviewees stressed that they force themselves to maintain as much autonomy and daily life as possible, which leads to constant pain.

To represent this we used the tensions tool below:

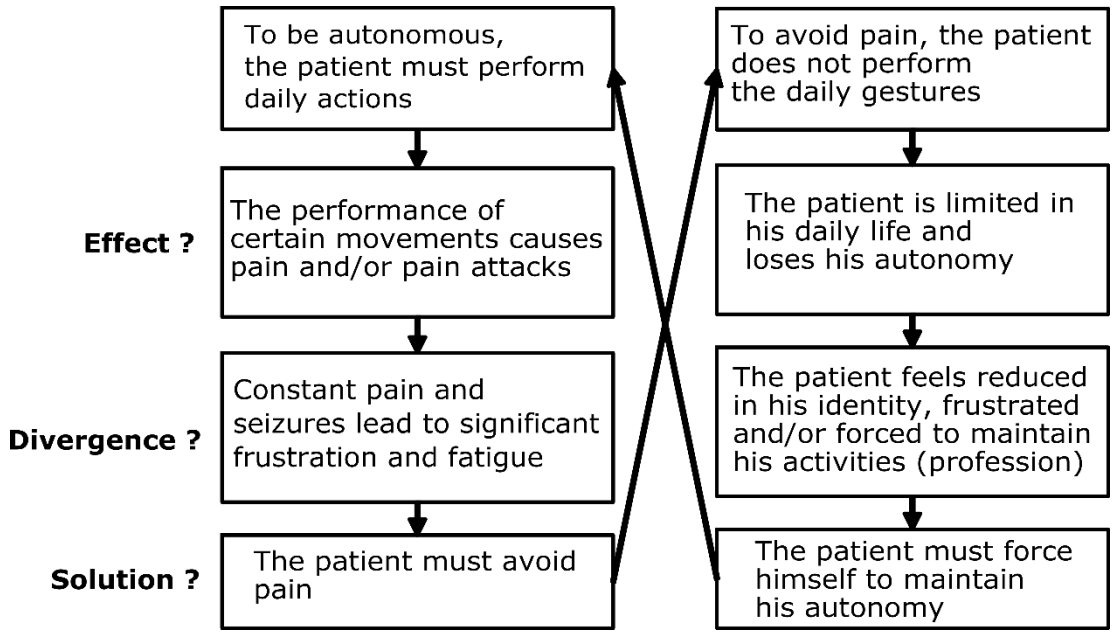


**Figure 5**: Tension: autonomy vs pain

We have identified a partial loophole developed by patients: modifying movements to reduce pain. This adaptation in turn leads to the following tension.

1.1. Tension: adapting activities vs. maintaining one's daily life

This tension has been observed in some patients. Indeed, patients who have fully integrated the disease into their daily lives and identities are not affected by this tension. On the contrary, those who "force" themselves to keep the same pace of life are subject to these difficulties of constant adaptation to the new environment.

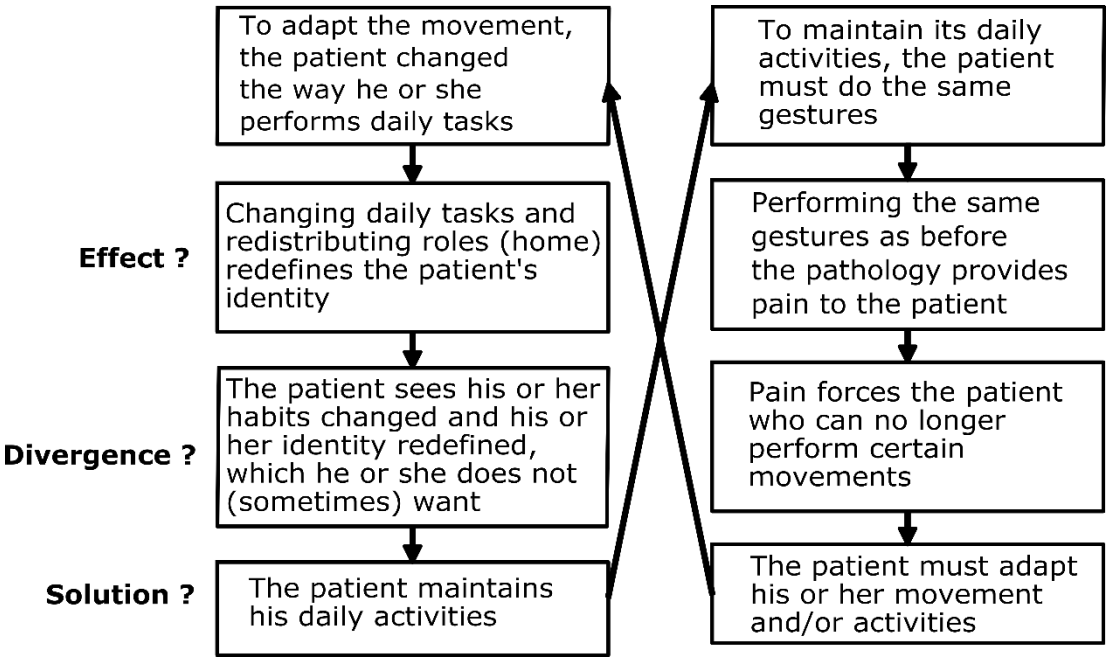


**Figure 6**: Tension: adaptation of activities vs. maintaining one's daily life

To avoid this tension, we can assume that the solution is to fully integrate the disease into one's daily life and identity: do new adapted activities, surround oneself with ergonomic objects and people with knowledge of the disease. If this tension is resolved, the implant could "shake up" the patient's new habits and identity. In the case of one the interviewees who had fully integrated the disease, an implant did not even seem to be of particular interest.

### 5.4.2. A better alternative to current solutions

Throughout this work, we were able to observe the diversity of patients' experiences, their relationship to the disease and their expectations. Some have made the disease an integral part of their life and identity, others have difficulty dealing with it; some have chronic pain with seizures sometimes, others feel pain only by making certain movements; some would like an implant, others would not. Osteoarthrosis affects up to 20% of women and less than 5% of men, at different levels of damage and severity. Following a basic treatment that has become ineffective (anti-inflammatory, infiltrations, rest orthoses, and sometimes physiotherapy), surgical intervention is generally proposed. There are several options available whose main objective is to relieve pain, by improving thumb function, but no solution can claim to make the thumb mobile, stable and strong. "In general, the pain gradually subsides after the surgery. Since the gain in mobility is facilitated by active mobilization, rehabilitation is often useful to improve the function of the operated hand, and a restriction of certain manual activities is sometimes necessary to preserve the result of the technique used." "Like any surgical procedure, there are risks of complications. The scar may take time to become painless or even infected. Ligament repair can heal slowly, or stretch gradually over time. Nervous branches under the skin can be irritated by the scar, causing unpleasant sensations in a specific area. Post-operative edema requires daily mobilization of the fingers, elevated hand or sling. The persistence of edema with pain and stiffness suggests that algodystrophy may occur. The prosthesis can wear out prematurely, dislocate, become infected, or weaken the bone in which it is implanted, up to the fracture. Post-operative hematoma is sometimes important."

The primary purpose of current implants is therefore to reduce or eliminate pain. However, the patients we were able to interview would seem to favour the restoration of autonomy above all. This work also shows the patients' apprehension for the operation and placement of an implant. The risk that "it's worse than before" frightens them. Indeed,

since the pathology is considered "bearable" by the patient, it would be a failure for him to be in a worse condition than before following the operation. The implant must therefore provide a better condition than the one before the procedure. Finally, medical follow-up generates a risk of loss of autonomy following the acquisition of autonomy by the operation, which represents a contradiction, a tension. Will patients have to return to hospital very often, which would only shift the problem of lack of autonomy caused by the disease? Indeed, if the patient wishes to have an implant placed, it is to be able to gain autonomy and be less dependent on those around him; but if he becomes dependent on a hospital department, the problem remains in another form. The patient would then have to readapt to the new constraints imposed on him, which has already required a lot of effort since the diagnosis of the pathology (cf. tension, adaptation of activities and maintenance of daily life). Medical follow-up should therefore be less but complete enough to take into account the patient's personal rehabilitation (helping him regain his autonomy, Current implants do not require particularly intense medical follow-up and rehabilitation can be done by independent patients by performing specific movements for 5 to 10 minutes every day.

## 6. Conclusion

This work shows the central place of the hand for mankind. It plays a role in communication, social life, activities and daily life. All this forges our identity as individuals. The loss of hand use for functions such as grip and pain caused by osteoarthrosis thus have a significant impact on the patient. In order to design the implant as well as possible, the study allowed us to understand the human issues surrounding grip and the expectations an implant must meet. In particular, it is important to focus on recovering autonomy rather than reducing pain; it is essential to ensure that the patient's condition improves after the operation and that medical follow-up is not intrusive. In conclusion, implants seems to provide added value to some patients who may regain some of their grip capacity and therefore autonomy. They will thus be able to resume certain activities and return to their daily lives before the pathology. It may be interesting to continue this work by interviewing patients from different backgrounds to refine our analysis.

## 7. References list


[1] S. Sodha, D. Ring, D. Zurakowski, J. Jupiter, Prevalence of osteoarthrosis of the trapeziometacarpal joint, JBJS. 87 (n.d.) 2614–8.

[2] F. Wilson, The hand: How its use shapes the brain, language, and human culture, 1999.

[3] G. Simondon, being and technology, Edinburgh University Press, 2012.

[4] S.L. Washburn, P. Dolhinow, H. Rinehart, A. Winston, Perspectives on Human Evolution, 1972.

[5] P.C. Reynolds, On the evolution of human behavior : the argument from animals to man, University of California Press, 1981.

[6] C. McGinn, Prehension : the hand and the emergence of humanity, 2015.

[7] S.A.J. Stuart, Privileging exploratory hands: prehension, apprehension, comprehension . In: Radman, Z. (ed.) The Hand, an Organ of the Mind: What the Manual Tells the Mental., MIT Press : Cambridge, MA, 2013.

[8] J. Bourgeois, Représentations motrices et perception de l'espace péripersonnel". Jérémy Bourgeois. Psychologie. Université Charles de Gaulle - Lille III, 2012. Français. - Google Search, Université Charles de Gaulle - Lille III, 2012. doi:T : 2012LIL30039. tel-00844106.

[9] H. Garner, D. Méda, La place du travail dans l'identité des personnes, Données Soc. (2006).

[10] M.-H. Boucand, L'identité en errance, in: Une Approch. Éthique Des Mal. Rares Génétiques Enjeux Reconnaiss. Compétence, 2018: pp. 225–242.

## 8. Intermediate conclusion

In this study, we studied the point of view of the patient suffering from trapeziometacarpal osteoarthritis.

By understanding the frustrations induced by the pathology, we have gained a better understanding of the perceived value of therapeutic solutions and particularly customized prosthetic arthroplasty, according to the patient's needs.

It is nevertheless necessary to continue this analysis with the various stakeholders, in particular orthopaedic hand surgeons, regulatory and reimbursement authorities. The first step is to analyse the "gold standard" in the management of osteoarthritis, then to study the perception of the offer and data to convince people of the value of innovation and finally to cross-reference the needs and recommendations of the stakeholders, particularly the patient-surgeon couple, in order to develop a maturation plan for valorization by the industry.

# CHAPTER 7:

# Conclusion and perspectives

*Ce chapitre propose une discussion générale soulignant la contribution de recherche originale des résultats de cette thèse pour la réalisation d'implants personnalisés par fabrication additive. Des perspectives sont également proposées pour la continuité du projet.*

# 1. Conclusion

Arthroplasty implants *i.e* the replacement of a human joint with a mechanical system are now widely marketed. This development began in the 1970s, particularly for the installation of total hip replacements based on Charnley's design concept. Arthoplasty implants is one of the therapeutic solutions commonly used in the case of osteoarthritis, which is the destruction or degeneration of joint surfaces. Currently, arthroplasty is performed by replacing joint surfaces with metal, high-density polyethylene, ceramic or pyrocarbon elements that are intended to mimic the morpho-functional geometric characteristics of the joint. In the particular case of the hand, it is the interphalian, metacarpal-phalangeal joints and for the thumb the trapezo-metacarpal joint that are exposed to osteoarthritis and therefore potentially subject to arthroplasty. However, failure rates are 8 to 21% for the hand or with limited functional recovery resulting in a loss of quality of life for the patient and 10-year replacement rates of 25% for some models. Thus it appears that the design of the prosthesis influences the functional performance of the joint.

In this context, failure analysis to improve the design of arthroplasty is a major issue in biomechanical research. Thus, on the basis of numerical models, it was recognized that each individual had joint mechanical characteristics that are specific to him in terms of kinematics (amplitude of motion, instantaneous axes of rotation,...) and dynamics (contact forces, distribution of contact pressure,...) due to the person's musculoskeletal specificities through bone geometry, location of muscle insertions, physiological components. As a result, the personalization and identification of subject- or patient-specific parameters have become relevant also for the analysis and design of prostheses and arthroplasty procedures. In the case of the hand, this problem is all the more exacerbated by the very large anatomical and size variations. Nevertheless, the implementation of customized designs of joint replacements, although technically feasible, has not been very much applied in routine due to the inadequacy of traditional manufacturing processes based on the standardization of sizes and geometric shapes of replacements. Implants have always been designed in a standard way, with a limited number of sizes and shapes.

As a result, surgeons may make compromises that can harm patients.

It is precisely on this point that additive manufacturing, also known as 3D printing, can play an important role thanks to the manufacture of customized prostheses. It has

completely changed the paradigms. The implant adapts to the patient rather than the opposite.

However, additive manufacturing technologies in the field of medical devices face a number of challenges:

- Validation of the mechanical and biological properties of existing materials and AM technologies. Unlike so-called substrative technologies such as milling and turning, parts made by additive manufacturing do not behave in the same way in all directions.

Development and characterization of new materials for AM. Alloys such as 316L stainless steel, titanium alloys, cobalt, chromium, etc. are already being processed. Nevertheless, research in this field is relatively recent and a standardization of processes has not yet been put in place in order to ensure sufficient and reproducible part quality.

The development of an implant raises the following issues:

- How the implant will simulate the action of the replaced part (biomechanics, ergonomics);
- How the body will react to this implant considered as a foreign body in relation to the degradation phenomenon
    - chemical degradation of the material in the human body (by corrosion),
    - mechanical wear, and in particular fretting (wear under low travel, with accumulation of wear products on the contact surface),
- How to modulate a primary (anchor screws, spikes) and secondary (osseointegration) stability of the implant?
- How to evaluate the geometric tolerance of a customized implant to the variability of the manufacturing process?

This thesis work is in line with this approach, by proposing a joint implant geometrically adapted to the patient and produced by metal additive manufacturing that would complete the arsenal of therapeutic solutions for the osteoarthritis of the trapezometacarpal joint. The objectives are to develop, analyze and validate the steps involved in the production of a complex-shaped implant processed by additive manufacturing.

The work carried out in the 2nd chapter of this manuscript first demonstrates the necessity to integrate the clinical aspect, in particular the surgical approach, in order to better understand the geometric specifications of the implant. The osteoarticular environment of the trapezium bone composed of four articulation with neighboring bones

combined with a complex geometric concavo-convex pattern, allows the prehension mobility of the hand as it is used in a daily-routine. Therefore, it appeared that an implant aimed to replace the trapezium must possesses the specific healthy shape's characteristics of the bone in order to minimize non-physiological movements, and complications related to wear and lack of stability. The 2nd chapter demonstrated the feasibility of implanting such a prosthesis described in the patent presented in Annex 2. It intended to replace entirely the former diseased bone and was firmly fixed on the trapezoid by a screw a spikes. This fusion was not seen to affect the different wrist motion in the performed cadaveric tests.

This work presents some limitations. The implant design was based on replica of two healthy trapezium bones. However it does not consider the high variability of morphology of the trapezium bones inter-subject (Halilaj et al., 2014; Loisel, F. et al., 2015; Xu et al., 1998) which could therefore affect the stability of the implant. The strategy to base the design on the contralateral bone is not a good option as osteoarthritis of the trapezometacarpal joint often morphologically deforms both bones although at a lower degree. The complication found in the performed cadaver experiments suggested to pursue the optimization of the good positioning of the implant and its stabilization. It appeared clearly that the production of patient-specific implants based on the patient's trapezium bone would significantly improve both implantation concerns and therefore the implant performance.

Taking into account the actual implantation conditions during the development of the trapezo-metacarpal implant has allowed us, among other things, to acquire a better understanding of the geometric specifications of the implant and therefore ensure its stability and good positioning.

The implantation trials resulted in the need for a trapezium bone replacement model that can geometrically match the patient's osteoarticular environment. However osteoarthritis at the base of the thumb irreversibly deforms this bone, causing pain, loss of mobility and reduced strength.

In this 3rd chapter, we have developed a method to "rejuvenate" numerically highly deformed bones in order to obtain a patient-specific implant adapted to additive manufacturing. The proposed numerical procedure is based on a reduced configuration based on an independent functional design of distinct regions and a voxel-based process. The main advantage of the configurable model is its ability to compensate for a lack of

information in raw medical imaging data or a deformed morphology due to a disease such as osteoarthritis. The voxel-based approach allows to transform the distinct regions into a single structure what enables additional topological operations. Combined with a simple smoothing process, it results in a homogeneous triangulated model, free of printability errors and makes the configurable model more anatomically realistic. The approach was applied on trapezium bones deeply affected by osteoarthritis. Configurable parameters have been set up to restore the pre-arthrosis morphology while preserving the specificities not affected by the pathology. The concavo-convex radius of curvature characteristics of the rejuvenated models appear to be robust. Indeed, the sets of values of healthy patients integrated in the arthritic models give close results (surface, radius of curvature). Additionally, this "rejuvenation" procedure makes it possible to know the areas of deformations due to osteoarthritis specific to each patient, which can be useful for clinical examination and the choice of an optimal treatment (total prosthetic arthroplasty, hemiarthroplasty, intervention, etc.)

After having designed and assessed the numerical model, it is necessary to ensure the feasibility to manufacture these complex-shaped parts with traditional biomaterials with the required surface texture for articular implant.
A major problem in the manufacture of metal additives on powder beds is the post-treatment of complex surfaces. Polishing machines are often allows us to finish implants with standard geometry which is not adapted to the morphology variability of our implant. The solution we found was to use a physico-catalytic process that polish homogeneously samples in a tank. It is therefore necessary to ensure if this process is adequate for customized implants made by selective laser melting regarding the different standard and to understanding the evolution of the deviation of the articular implant specifications along the manufacturing chain.

In the 4$^{th}$ chapter of this manuscript, we have demonstrated the feasability to produce complex-shape articular implant with additive manufacturing and diverse post treatments that comply standard specifications regarding the surface texture. The superfinishing used was a physico-catalytic process and was found to be suitable. Therefore, this study provides a reference for the design, the manufacture by selective laser melting and the post-treatment of articular medical implants made of chromium-cobalt-molybdenum.

The innovative potential of metal additive manufacturing also introduces geometrical variability which has been characterized for each manufacturing phase. It was found that pores are the main defects of the specimens along with local geometrical deviations. Both concerns came from the selective laser melting process rather than the superfinishing treatment.

Different strategies exists to optimize parts quality. A first way is to modify SLM parameters to increase the energy density and also to put additional support structures. A second way is to post-process the specimens. Thermal treatment enables the release of internal stresses while hot isostatic pressing enables the closure of internal pores.

Due to cytotoxic Co-release by CrCoMo implants, we also studied the process with another material which is 316L stainless steel presented in the annex 4 a). The specimens were found to have less pores and lower geometrical deviations. However 316L stainless steel is known to have a lower wear resistance than CrCoMo. Preliminary tests have also been perform to understand the feasibility to cover 316L and CrCoMo parts produce by SLM with a biocompatible ceramic material. The results were promising but necessitate adjustment to make the process more geometrically accurate. These data are only presented in the annex 4 b) to make the thesis manuscript focused on CrCoMo and Ti6Al4V.

Regarding the characteristic of the surfaces produced by powder-based additive manufacturing and the post-treatment process, the goal was to understand the influence of these deviations in a system that simulates the biological and mechanical environment.

In the 5th chapter of this manuscript, the influence of the surface texture was studied for both main parts of the prosthesis: the trapezium part known as a trapezium bone replacement and a metacarpal stem. The surface texture of the stem was studied directly after the selective laser melting process in Ti-6Al-4V. The idea was to understand whether the unique surface texturing resulting from additive powder bed manufacturing provides sufficient support for cell adhesion, allowing us to avoid potentially costly post-treatment. The results demonstrated a direct impact of the surface texture variability on the cellular adhesion of an osteoblastic line. We found that the positioning of the parts in the manufacturing chamber allow us to control the heterogeneities of surface textures and therefor the cell adhesion.

The surface texture of the trapezium was studied after the selective laser melting process followed by the physico-catalytic superfinishing process. These prototypes with complex morphology do not allow us to easily simulate the biotribological environment. However, it has been demonstrated that additive manufacturing in the selected parameters induces a geometric deviation in some areas correlated with an increasing number of open pores. Simpler samples were then produced using the same process. The idea was to understand the impact of this porosity on polymer wear by simulating friction with a lubricant similar to synovial fluid. The work also showed that the porosity of chromium-cobalt-based samples induced by the laser powder-bed fusion process significantly impacts the wear of the UHMWPE. Optimization of the printing parameters is therefore essential in order to reduce this type of defect and increase the life expectancy of the implant. In addition, a study was also conducted to compare the SLM process to casting with both 316L and CrCoMo. Cast-CrCoMo parts showed an increase in wear of the UHMWPE with the chromium-cobalt alloy made by SLM compared to its cast version (ISO-F75). This difference seems to have its source in the microstructure of the material. This is due to the thermal history of the material during the SLM process, which induces a unique microstructure different from its standard equivalent. The 316L stainless steel produced by SLM has a similar impact on UHMWPE wear compared to its cast version. The microstructure of the two samples is also similar, which seems to confirm the proposed hypothesis. These data were only presented in this manuscript because we decided to focus the results on CrCoMo to make the manuscript clearer for the readers. By understanding the origin of wear variations, optimization solutions can be more easily found by modifying manufacturing parameters for instance or by doing specific heat-treatments to the specimens.

All the work that have been previously discussed are mostly scientific and technical, although it is necessary to remember that trapeziometacarpal osteoarthritis affect people, mostly women. The innovation developed in this thesis is aimed to these people. In this context, to what extent patients perceive the pathology and the therapeutic solutions. Do they need this specific solution? How the pathology affect their lives in their daily-routine?

The 6$^{th}$ chapter investigates the impact of the pathology on the patient's identity, daily life and the frustrations and tensions that it causes. The results confirms the obvious: that a loss of hand functions such as gripping and handling objects as well as pain caused

by osteoarthrosis have a significant impact on the patient. Thus, the study allowed us to understand the human issues surrounding grip and the sociological expectations an implant must meet. Regarding the design development of the implant, this work suggests us to focus on recovering autonomy rather than reducing pain; it is essential to ensure that the patient's ability to realize simple gestures improves after the operation and that medical follow-up is not intrusive. They will thus be able to resume certain activities and return to their daily lives before the pathology.

## 2. Perspective

This thesis work focused on the pathology of osteoarthritis in the trapezo-metacarpal joint that irreversibly deforms the trapezium bone. This application has allowed us to develop a horizontal working approach on the contribution of manufacturing techniques for the design of customized implants. Several research axes conducted have particularly interesting challenges and perspectives for the scientific community and the biomedical industry. These axes are:

- The numerical " bone rejuvenation" process in the design of a customized implant and its integration into the design chain from imaging to additive manufacturing by taking into account clinical and anatomical considerations;
- The future of additive manufacturing parts and their various post-treatments necessary to achieve biomedical implant specifications;
- The performance and behavior of metal additive manufacturing parts in tribology;

This first point is a particularly interesting issue because it can integrate all pathologies leading to bone deformities leading to a loss of anatomical functions. Many pathologies deform bones irreversibly affecting associated functions such as bone structure stability, mobility, and stress transmission. Osteoporosis, for example, is a disease that causes a loss of bone mass by making it more fragile. It is common for vertebrae to collapse due to osteoporosis due to an imbalance in compressive forces. Bone tumors also irreversibly deform bone. Another example is Paget's disease of bone, a chronic skeletal disease. Some areas of bone tissue are subject to pathological remodelling. This results in hypertrophy and weakening of the bone.

The entire study conducted on the design of an implant manufactured by metal additive manufacturing to compensate for osteoartrosis of the trapezometacarpal joint can be extrapolated to other pathologies affecting the geometric integrity of bones as mentioned

above. However, it is necessary to carry out a study on the bone in healthy and pathological conditions in order to determine the geometric operations to be carried out for the numerical "rejuvenation" procedure as described in the 2nd article of the 3rd chapter. It is also important to take into account the clinical aspect in order to develop the approach to implanting the prosthesis. It would be interesting to design the "rejuvenated" prosthesis and test its implantability and performance on the same corpse. The difficulty is that this step results in the fact that imaging equipment is not juxtaposed with surgical schools. In addition, it is legally difficult to move a corpse to perform this type of test. This would further ensure the value of a customized implant compared to standard shapes and sizes and confirm the value of the prosthetic anchorage elements in this configuration. Once this configuration has been confirmed, it would be worth carrying out mobility tests with motion capture measurements. This would provide clear quantitative data on the contribution of implant range of motion. In addition, in order to enrich these data, it would be possible to integrate pressure sensors between each joint surface surrounding the prosthesis by applying a known force at the end of the osteoarticular column, i.e. at the distal phalanx of the thumb. While these data would be subject to uncertainty due to rigor mortis and the application of forces in an unnatural manner, this would provide information on the distribution of stresses in the different carp bones in the configuration of a trapezoid-trapezium fusion. It would give the assurance of the legitimacy of this fusion as an anchoring strategy in the design of trapezometacarpal implants.

In addition, the data collected by the pressure sensors may be useful in order to carry out wear simulations even closer to the reality of this joint and implant configuration. However, the difficulty will probably lie in managing the electrical threads so that they do not interfere with movement during the cadaver tests.

To finish with the implant design, it would be wise to lighten the implant component of the prosthesis, as it is relatively heavy when printed in 316L or CrCoMo compared to a human bone. A way would be to integrate lattice structures into it. Pressure sensor data may be useful to position these structures optimally for better stress distribution in carpal bones. The mesh quality of models obtained with the voxel technique allow us to perform finite element simulations. It is also one of the main asset of this methodology compared to STL files. Therefore, topological optimization based on FEM analysis could be an interesting solution to overcome this problem. The lattice structures in this context will not serve as supports for bone regeneration but only to lighten the structure.

We have also seen that the orientation of the parts has an impact on their functional performance due to the anisotropic nature of the additive layer-by-layer manufacturing process, both on the cellular adhesion properties on TI6AL4V rods and on the geometrical deviations and porosities of CrCoMo prosthetic trapezium. We were able to highlight the clear influence of the irregular pores of CrCoMo on the tribological performance of high density polyethylene. It would be interesting to produce CrCoMo parts with optimized parameters regarding the density to see if the anisotropy at the microstructure level also has an influence. Tests with cast-parts have also been carried out but are not presented in this manuscript. It appeared that the pores do not explain all the differences in the tribological performance. The hypothesis would be that the microstructure induced by the additive process also implies an increase in the mass loss but at a smaller scale than porosity.

In addition, the high-density polyethylene insert is not currently feasible by additive manufacturing. However, other polymers used in orthopaedic implants exist such as PEEK. The shaping of this material is possible by additive way. It would be interesting to further study the tribological performance with this type of material as well.

In the study related to cell adhesion and surface texture induced by additive manufacturing, we were able to observe the cell bridge format between powders partially melted into surfaces. It would be interesting to understand how such a structure is formed and what material and surface texture properties promote the emergence of biological behavior. In order to enrich the biological data, assays of the irritation factors such as Il-6 and TNF-α should be performed to provide an indication of the precocious inflammatory response. An implantation test on nude mice would complete the data on the response of the primary immune system. Finally, in order to get even closer to the anatomical and biological reality of a joint, it would be possible to make a replacement prosthesis for a rabbit bone using the same procedure. This would help to understand the effect of in-vivo wear of this type of prosthesis on the behavior of surrounding biological tissues.

Finally, we conducted a study on the impact of trapezometacarpal osteoarthritis on the quotidian and patients' feelings. It would be useful to continue this study with a larger number of cases in order to understand the possible differences in needs according to age, gender and socio-professional categories.

Moreover, there is no technical solution without first contacting patients and practitioners to find out their real needs and expectations.

# ANNEXES

**Annex n°1:** Functional specifications

**Annex n°2:** Patent FR3066382 A1, « Method of making a trapezo-metacarpal prosthesis and prosthesis obtained » (2018)

**Annex n°3:** Patent N°1851657 « Method of manufacturing a complex substitution object from the real object»

**Annex n°4 a):** Implant in stainless steel 316L produce by SLM

**Annex n°4 b):** Implant in CoCrMo and stainless steel 316L produce by SLM and ceramic covered

**Annex n°5:** Biological assessment

**Annex n°6 a):** Comparison of the biotribological performance of UHMWPE against 316L and CoCrMo made by metal additive manufacturing and their cast-version

**Annex n°6 b):** Study of the biotribological performance of UHMWPE against a leucite glass-ceramic coating

# Annex n°1: Functional specifications

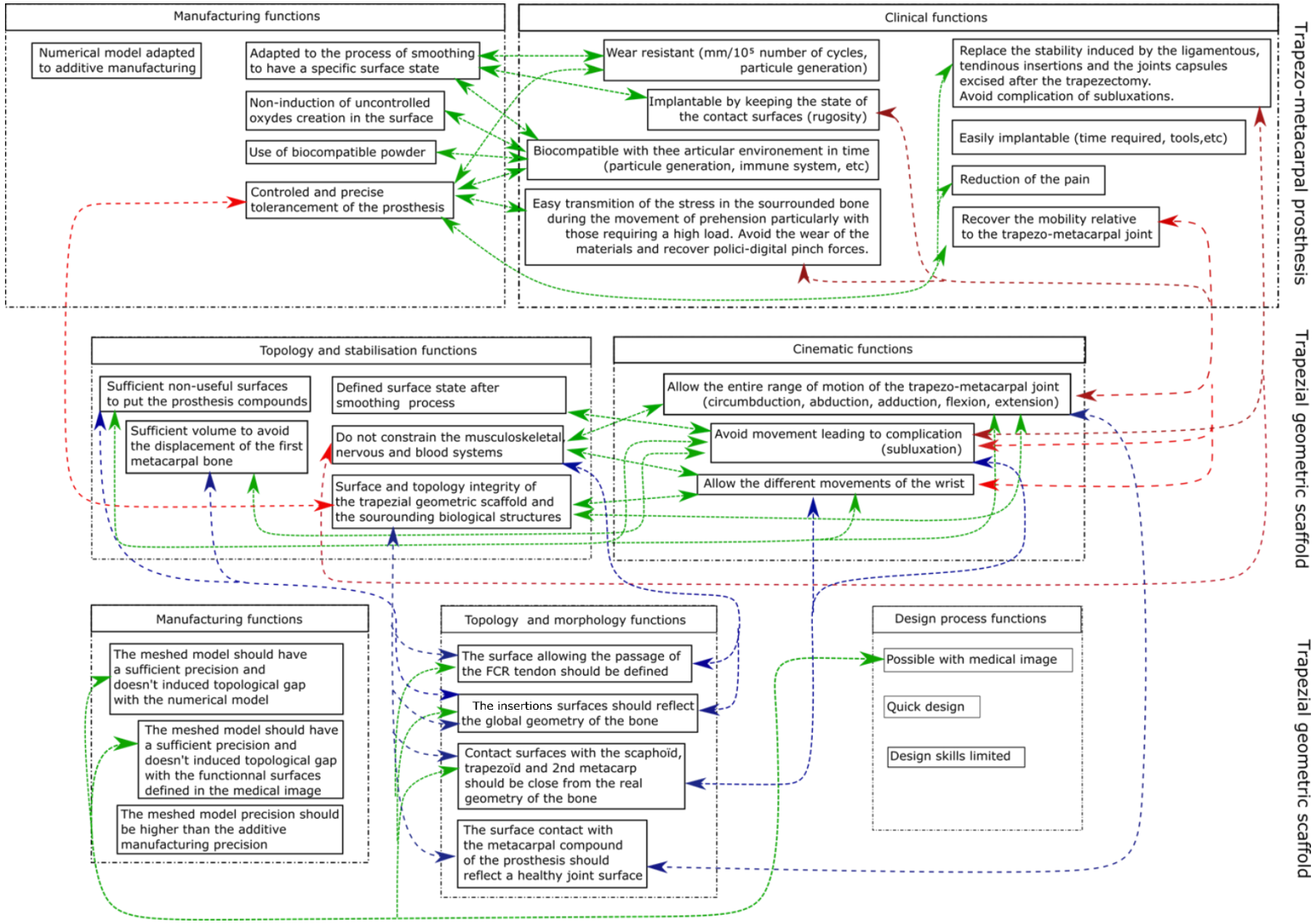

Annex n°2: Patent WO2018210953, « Method of making a trapezo-metacarpal prosthesis and prosthesis obtained » (2018)

(19) RÉPUBLIQUE FRANÇAISE

INSTITUT NATIONAL
DE LA PROPRIÉTÉ INDUSTRIELLE

COURBEVOIE

(11) N° de publication : **3 066 382**
(à n'utiliser que pour les commandes de reproduction)

(21) N° d'enregistrement national : **17 54288**

(51) Int Cl[8] : *A 61 F 2/42 (2017.01)*

# (12) DEMANDE DE BREVET D'INVENTION A1

(22) **Date de dépôt :** 16.05.17.

(30) **Priorité :**

(43) **Date de mise à la disposition du public de la demande :** 23.11.18 Bulletin 18/47.

(56) **Liste des documents cités dans le rapport de recherche préliminaire :** *Se reporter à la fin du présent fascicule*

(60) **Références à d'autres documents nationaux apparentés :**

◯ **Demande(s) d'extension :**

(71) **Demandeur(s) :** *UNIVERSITE DE TECHNOLOGIE DE COMPIEGNE Etablissement public* — FR, *CENTRE NATIONAL DE LA RECHERCHE SCIENTIFIQUE Etablissement public* — FR, *UNIVERSITE PIERRE ET MARIE CURIE Etablissement public* — FR et *ASSISTANCE PUBLIQUE - HOPITAUX DE PARIS Etablissement public* — FR.

(72) **Inventeur(s) :** MASQUELET ALAIN-CHARLES, JIHAZ NASSIM, BOUVIER SALIMA, MARIN FREDERIC, EGLES CHRISTOPHE et LEREBOURS AUGUSTIN.

(73) **Titulaire(s) :** UNIVERSITE DE TECHNOLOGIE DE COMPIEGNE,CENTRE NATIONAL DE LA RECHERCHE SCIENTIFIQUE,UNIVERSITE PIERRE ET MARIE CURIE, ASSISTANCE PUBLIQUE - HOPITAUX DE PARIS.

(74) **Mandataire(s) :** NOVAGRAAF TECHNOLOGIES.

## (54) PROCEDE DE REALISATION D'UNE PROTHESE TRAPEZO-METACARPIENNE ET PROTHESE OBTENUE.

(57) Le procédé de réalisation (100) d'une prothèse trapézo-métacarpienne comprenant un trapèze prothétique, le procédé comportant des étapes successives de :

a. Acquisition (110) d'une série d'images médicales d'une articulation trapézo-métacarpienne d'un patient à traiter ;

b. Reconstruction (120) tridimensionnelle de l'os trapèze de l'articulation trapézo-métacarpienne en un modèle tridimensionnel numérique à partir de la série d'images médicales précédemment acquises ;

c. Réalisation (130) dans le modèle tridimensionnel ainsi obtenu de moyens de réception d'un moyen d'ancrage ; et,

d. Impression (140) tridimensionnelle du trapèze prothétique à partir du modèle tridimensionnel issu de l'étape précédente.

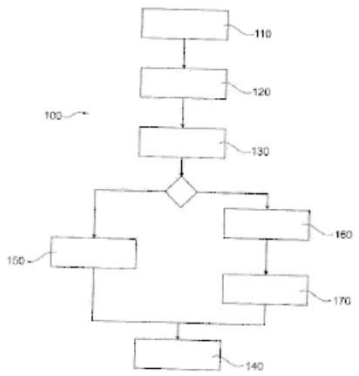


FR 3 066 382 - A1

# PROCÉDÉ DE RÉALISATION D'UNE PROTHÈSE TRAPÉZO-MÉTACARPIENNE ET PROTHÈSE OBTENUE

L'invention concerne un procédé de réalisation d'une prothèse trapézo-métacarpienne destinée à être implanté dans la main d'un patient au niveau de l'articulation trapézo-métacarpienne.

L'arthroplastie prothétique est le remplacement d'une articulation humaine par un système mécanique. Celle-ci est une des solutions thérapeutiques pratiquées couramment dans le cas de l'arthrose qui est une destruction ou une dégénérescence des surfaces articulaires. Actuellement l'arthroplastie se pratique par remplacement des surfaces articulaires endommagées par des éléments métalliques, en polyéthylène haute densité, en céramique ou encore en pyrocarbone sensé mimer les caractéristiques géométriques morpho-fonctionnelles de l'articulation ainsi traitée.

Ainsi il apparaît que le design de la prothèse influe sur la performance fonctionnelle de l'articulation. Dans le cas de la main, sont exposées à l'arthrose et donc potentiellement sujettes à une arthroplastie les articulations interphalangiennes et métacarpo-phalangiennes des doigts longs. Pour le pouce, l'articulation trapézo-métacarpienne est sujette à la rhizarthrose qui est l'arthrose de la base de la colonne du pouce.

Il a été constaté que les taux d'échec sont, pour la main, de 8 à 21% ou bien avec des reprises fonctionnelles limitées entraînant une perte de qualité de vie du patient et des

taux de remplacement à dix ans de 25% pour certains modèles de prothèses.

Or, il a été montré que chaque patient avait des caractéristiques mécaniques articulaires qui lui étaient propres en termes de cinématique (amplitude de mouvement, axes instantanés de rotation, …) et de dynamique (force de contact, répartition de la pression de contact, …) du fait des spécificités musculo-squelettiques du patient par la géométrie des os, la localisation des insertions musculaires, et les composantes physiologiques. En conséquence, la personnalisation et l'identification de paramètres spécifiques du sujet ou du patient sont devenues pertinentes pour l'analyse et la conception de prothèse. Au niveau de la main, cette problématique est d'autant plus réelle qu'il y a des variations anatomiques très importantes. Ainsi, l'arthroplastie de l'articulation trapézo-métacarpienne est contrainte par sa complexité morphologique, sa petitesse et la géométrie spécifique au patient.

A ce jour, les traitements proposés visent à éliminer la douleur, rétablir la fonction, la stabilité et la force du pouce (partiellement ou totalement) détruites par la rhizarthrose. Plusieurs options thérapeutiques existent sans qu'aucune ne fasse la preuve de sa supériorité sur le plan anatomique et/ou fonctionnel (e. g. perte partielle de la mobilité du pouce, diminution de la force dans le mouvement pour serrer la main). Parmi ces traitements, il y a :

- la trapézectomie qui consiste à enlever l'os trapèze. Le risque de cette solution thérapeutique porte sur le collapsus de l'espace trapézien entrainant une réduction de hauteur de la loge

trapézienne (recul du pouce) accompagnée de douleurs et d'une diminution de la force de serrage pouce/index. Pour y remédier, une cale molle ou rigide en pyrocarbone peut être implantée. Toutefois, des problèmes liés à la réponse du patient (réaction immunitaire, inflammations…) peuvent survenir, le risque de luxation ne peut pas être exclu et la restitution fonctionnelle de l'articulation est parfois incomplète ;

- l'arthroplastie totale qui consiste à implanter une prothèse trapézo-métacarpienne sur le principe d'une prothèse totale de hanche. Cette technique présente un risque un descellement de la cupule trapézienne. Par ailleurs, la taille des os concernés conduit à des fractures prématurées du fait des charges imposées au niveau de l'articulation. Des exemples de telles prothèses sont décrites dans les documents WO2008/070881 et WO 2010/080714 ;
- l'ostéotomie qui consiste à couper au niveau des os pour réorienter les surfaces de glissement de l'articulation et tenter de reconstituer l'os trapèze. Toutefois, du fait de la complexité de la morphologie de l'os trapèze, il est souvent difficile de reproduire sa géométrie ;
- l'arthrodèse qui conduit à bloquer l'articulation. Ce traitement entraine une perte de la fonction articulaire provoquant une gêne dans les mouvements de la vie quotidienne pour le patient.

Il n'existe donc à ce jour aucune thérapie totalement efficiente de la rhizarthrose. Par ailleurs, la main est un

organe qui présente une grande variation anatomique ce qui requiert d'adapter l'élaboration de chaque implant aux spécificités anatomiques du patient. Dans ce domaine, les techniques d'élaboration actuellement utilisées, ne permettent pas de satisfaire ces contraintes.

Un but de l'invention est de fournir un procédé de réalisation d'une prothèse trapézo-métacarpienne qui permette de traiter avec efficience la rhizarthrose, tout en offrant une solution pérenne au patient.

A cette fin, il est prévu, selon l'invention, un procédé de réalisation d'une prothèse trapézo-métacarpienne comprenant un trapèze prothétique, le procédé comportant des étapes successives de :

a. Acquisition d'une série d'images médicales d'une articulation trapézo-métacarpienne d'un patient à traiter ;

b. Reconstruction tridimensionnelle de l'os trapèze de l'articulation trapézo-métacarpienne en un modèle tridimensionnel numérique à partir de la série d'images médicales précédemment acquises ;

c. Réalisation dans le modèle tridimensionnel ainsi obtenu de moyens de réception d'un moyen d'ancrage ; et,

d. Impression tridimensionnelle du trapèze prothétique à partir du modèle tridimensionnel issu de l'étape précédente.

Ainsi le fait de reproduire un os du trapèze, pour réaliser une prothèse comportant des paramètres géométriques de l'os du patient permet d'intégrer les contraintes anatomiques, fonctionnelles et biologiques du patient et d'obtenir une prothèse trapézo-métacarpienne la plus optimale pour ce dernier. Une fois implantée, la prothèse ainsi obtenue offre au patient receveur un traitement efficace de la rhizarthrose.

Avantageusement, mais facultativement, le procédé selon l'invention présente au moins l'une des caractéristiques techniques supplémentaires suivantes :

- les moyens de réception comprennent un orifice traversant agencé de sorte à recevoir une vis d'ancrage ;
- il comprend une étape de réalisation dans le modèle numérique tridimensionnel ainsi obtenu d'une première surface remodelée à partir d'un modèle anthropomorphique avant l'étape d) d'impression tridimensionnelle du trapèze prothétique ;
- la prothèse trapézo-métacarpienne comportant en outre un pion métacarpien présentant une surface d'articulation, le procédé comporte une étape de réalisation dans le modèle numérique tridimensionnel ainsi obtenu d'une surface complémentaire de la surface d'articulation avant l'étape d) d'impression tridimensionnelle du trapèze prothétique ;
- la prothèse trapézo-métacarpienne comportant en outre un pion métacarpien présentant une surface d'articulation, le procédé comporte une étape de reconstruction numérique tridimensionnelle de la surface d'articulation d'une extrémité proximale du

premier métacarpien de l'articulation trapézo-métacarpienne à partir de la série d'images médicales précédemment acquises, puis intégration de cette reconstruction dans un modèle tridimensionnel numérique du pion métacarpien ;

- il effectue, lors de l'étape de reconstruction, dans le modèle numérique tridimensionnel, un remodelage de la surface d'articulation d'une extrémité proximale du premier métacarpien à partir du modèle numérique tridimensionnel du trapèze prothétique ;
- il comporte une étape supplémentaire d'impression tridimensionnelle du pion métacarpien à partir du modèle tridimensionnel dudit pion ainsi obtenu ; et,
- l'impression tridimensionnelle est réalisée à partir de poudre de matériaux biocompatibles.

Il est aussi prévu, selon l'invention, une prothèse trapézo-métacarpienne comportant un trapèze prothétique et un pion métacarpien, la prothèse étant réalisée selon un procédé présentant au moins l'une des caractéristiques techniques précédentes.

Avantageusement, la prothèse selon l'invention présente au moins l'une des caractéristiques techniques supplémentaires suivantes :

- le pion métacarpien comporte deux parties, les deux parties comprenant une base et une tête présentant la surface d'articulation avec le trapèze prothétique ;
- la base est métallique et la tête est réalisée en polymère ;

- elle comporte en outre une vis d'ancrage, formant le moyen d'ancrage, reçue dans les moyens de réception du trapèze prothétique ; et,
- la vis d'ancrage est une vis de compression.

D'autres caractéristiques et avantages selon l'invention apparaitront lors de la description ci-après d'un mode de réalisation et d'une variante. Aux dessins annexés :

- La figure 1 est une vue de dessus d'un squelette d'une main comportant une prothèse trapézo-métacarpienne selon l'invention ;
- La figure 2 est une vue de détail et de coté de la prothèse de la figure 1 ;
- La figue 3 est une vue tridimensionnelle de l'implantation de la prothèse de la figure 1, seuls le premier métacarpe et le trapézoïde du squelette de la main étant représentés ;
- La figure 4 est un diagramme illustrant les étapes d'un procédé de réalisation de la prothèse de la figure 1 selon l'invention ;
- La figure 5 est une vue de côté d'un trapèze prothétique de la prothèse de la figure 1 ;
- La figure 6 est une vue en coupe du trapèze prothétique de la figure 5 ;
- La figure 7 est une vue tridimensionnelle d'une tête d'un pion métacarpien de la prothèse de la figure 1 ;
- La figure 8 est une vue tridimensionnelle d'une base d'un pion métacarpien de la prothèse de la figure 1 ;
- La figure 9 est une vue en coupe de la base de la figure 8 ;
- La figure 10 est une vue tridimensionnelle d'une vis d'ancrage de la prothèse de la figure 1 ; et,

- La figure 11 est une vue tridimensionnelle partielle d'une variante de réalisation de la surface du trapèze prothétique venant en regard du trapézoïde du patient.

En remarque liminaire, la rhizarthrose, qui est l'arthrose de la base du pouce, est fréquente chez des patients âgés (en particulier une femme sur six à partir de la cinquantaine) et touche spécifiquement l'os trapèze et l'extrémité proximale du premier métacarpien. L'os trapèze se situe entre le premier métacarpien et le scaphoïde. Il présente des surfaces articulaires extrêmement complexes, en particulier pour l'articulation trapézo-métacarpienne, avec une morphologie sous forme de selle biconcave à deux degrés de liberté.

En référence aux figures 1 à 3, nous allons décrire une prothèse trapézo-métacarpienne selon l'invention. La prothèse trapézo-métacarpienne selon l'invention comporte ici un trapèze prothétique 1, un pion métacarpien 7 et une vis d'ancrage 3. La prothèse trapézo-métacarpienne selon l'invention est destinée à être mise en place entre le premier métacarpien 4 et le trapézoïde 2 d'un patient. Le trapèze prothétique 1 est ancré sur le trapézoïde 2 avec la vis d'ancrage 3. Dans le mode de réalisation illustré, le pion métacarpien 7 comporte deux parties, ici rapportées l'une sur l'autre : une base 5 et une tête 6.

En référence aux figures 5 et 6, nous allons décrire le trapèze prothétique 1 de la prothèse trapézo-métacarpienne selon l'invention. Le trapèze prothétique 1 présente une forme et des dimensions qui correspondent sensiblement à la

forme et aux dimensions de l'os trapèze de la main du patient à traiter.

En particulier, il présente une première surface 11 qui est sensiblement complémentaire d'une surface d'articulation de l'extrémité proximale du premier métacarpien de la main du patient à traiter car elle reproduit la surface correspondante de l'os trapèze de la main du patient à traiter. En variante de réalisation la première surface 11 est complémentaire d'une surface d'articulation du pion métacarpien 7 de la prothèse trapézo-métacarpienne selon l'invention. Dans une autre variante de réalisation, la première surface 11 est une portion de selle biconcave.

D'autre part, le trapèze prothétique 1 comporte une deuxième surface 12 située sur une face opposée à celle comprenant la première surface 11 précédemment décrite. Cette deuxième surface 12 est complémentaire sensiblement à une surface du trapézoïde de la main du patient. Cette deuxième surface 12 est destinée à s'étendre en regard de cette surface du trapézoïde de la main du patient et à venir en appui sur celle-ci lors de la mise en place du trapèze prothétique 1 puis d'un ancrage de celui-ci sur le trapézoïde. A cette fin, le trapèze prothétique 1 comporte des moyens de réception 10 d'un moyen d'ancrage. Ici, les moyens de réception 10 sont un trou débouchant 13,14 s'étendant depuis la surface médiale 17 du trapèze prothétique 1 jusqu'à la deuxième surface 12. Le trou débouchant comprend, ici, un lamage 13 de profondeur 16 situé du côté de surface médiale 17 qui se poursuit par un orifice cylindrique 14 débouchant au niveau de la deuxième surface 12 et de longueur 15.

Une telle configuration des moyens de réception 10 permet l'utilisation d'une vis d'ancrage 3 telle qu'illustrée en figure 10. Cette dernière comporte une tête 30 à une

extrémité d'un fût 31, un filetage 32 étant aménagé au niveau d'une autre extrémité du fût 31. En variante de réalisation, le filetage 32 est un filetage osseux. La tête 31 est destinée à être entièrement reçue dans le lamage 13. Elle présente une empreinte en creux pour l'insertion d'un ancillaire de mise en place. L'empreinte en creux est ici une empreinte hexagonale. Dans une variante de réalisation, la vis d'ancrage 3 est une vis dite « de compression ».

Dans une variante de réalisation, illustrée à la figure 11, la deuxième surface 12 comporte des moyens d'ancrage 121 du trapèze prothétique 1 qui permettent de sécuriser et de renforcer, lors d'une implantation, l'ancrage du trapèze prothétique 1 sur le trapézoïde du patient. Ici, les moyens d'ancrage comportent une série de picots 121 s'étendant en saillie depuis la deuxième surface 12 autour de l'orifice cylindrique 14 des moyens de réception 10. Les picots 121 sont de forme générale pyramidale à base polygonale ou curviligne. Ici, la base est circulaire. Le nombre de picots 121 présents sur la deuxième surface 12 est fonction des dimensions du trapèze prothétique 1 réalisé. Ce nombre est donc variable. Les dimensions des picots sont aussi adaptées en fonction : par exemple, la base des picots 121 s'inscrit dans un cercle de l'ordre de 1mm de diamètre, et leur hauteur est aussi de l'ordre de 1mm. Un tel ensemble de picot 121 permet un ancrage immédiat du trapèze prothétique 1 sur le trapézoïde du patient. De manière additionnelle et optionnelle, la série de picots 121 est secondée par un état de surface de la deuxième surface 12 permettant, sur le long terme, une ostéoconduction de la matière osseuse du trapézoïde du patient.

Le pion métacarpien 7, dans le mode de réalisation illustré, comporte une base 5 et une tête 6. La tête 6 comporte une surface d'articulation 62 s'étendant au-dessus d'une face inférieure 61 plane. La surface d'articulation 62 présente une forme et des dimensions qui reproduisent sensiblement les formes et dimensions de l'extrémité proximale du premier métacarpien de la main du patient à traiter, et ayant des caractéristiques non arthrosiques. Une fois la prothèse trapézo-métacarpienne selon l'invention implantée, la surface d'articulation 62 se trouve en regard de la première surface 11 du trapèze prothétique 1, et coopère avec celle-ci afin de simuler l'articulation trapézo-métacarpienne de la main du patient. La tête 6 comporte en outre un cône 60 s'étendant en saillie depuis la face inférieure 61. Ce cône forme des moyens de fixation de la tête 6 avec la base 5 du pion métacarpien 7. D'autres variantes de moyens de fixation de la tête 6 dans la base 7 sont un encliquetage cylindrique, encliquetage par crochet cylindriques ou par assemblage sphérique.

La base 5 comprend un plateau 56 présentant une face supérieure 52 plane, une face inférieure 51 plane et sensiblement parallèle à la face supérieure 52, ainsi qu'une face périphérique latérale 54. La face périphérique latérale 54 présente, ici, une forme et des dimensions sensiblement similaires aux forme et dimensions d'une portion d'une surface latérale de l'extrémité proximale du premier métacarpien de la main du patient à traiter, au niveau du site d'implantation de la base 5 sur le premier métacarpien.

S'étendant en saillie depuis la face inférieure 51, la base comporte une queue 50 formée d'une tige de type « press-fit ». Cette queue 50 est conformée de sorte à être insérée, lors d'une intervention, dans le canal médullaire du premier

métacarpien de la main du patient, et ce sans ciment. La queue 50 est ici de forme globale tronconique selon son axe longitudinal. L'orientation de l'axe longitudinale et les dimensions de la queue 50 sont déterminées à partir de paramètres morphologiques de l'extrémité proximale du premier métacarpe du patient à traiter.

Au niveau de la face supérieure 52, la base 5 comporte un trou borgne 53 de forme tronconique. Il est destiné, lors d'un assemblage du pion métacarpien 7, à recevoir, à coulissement au moins, le cône 60 de la tête 6. De préférence, les angles du cône 60 et du trou borgne 53 sont choisis de sorte à former un assemblage par cône Morse.

Dans une variante, les angles du cône 60 et du trou borgne 53 sont choisis de sorte à former un assemblage par encliquetage ou par assemblage sphérique.

En référence à la figure 2, nous allons maintenant décrire un procédé de réalisation 100 d'une prothèse trapézo-métacarpienne selon l'invention. Le procédé de réalisation comporte une première étape 110 durant laquelle est réalisée une acquisition d'une série d'images médicales telles que radiographiques par rayons X ou par imagerie IRM (pour « Imagerie par Résonnance Magnétique ») de l'articulation trapézo-métacarpienne de la main du patient à traiter comportant au moins l'os trapèze, et l'extrémité proximale du premier métacarpien. Cette acquisition est préopératoire et va permettre, d'une part, de préparer l'intervention chirurgicale, et, d'autre part, d'aider à la réalisation des différents composants de la prothèse trapézo-métacarpienne selon l'invention.

A partir de cette série d'images médicales, le procédé de réalisation 100 d'une prothèse trapézo-métacarpienne selon l'invention comprend une deuxième étape 120 de reconstruction de l'os trapèze en un modèle tridimensionnel numérique à partir de la série d'images médicales précédemment acquises. Cette étape est réalisée à l'aide de techniques de traitement d'images connues en soi, comme celle implémentée dans l'imagerie IRM qui permet de générer des fichiers numériques décrivant les modèles tridimensionnels des objets ainsi imagés.

Dans une étape suivante 130, le procédé de réalisation 100 d'une prothèse trapézo-métacarpienne selon l'invention prévoit la réalisation, dans le modèle tridimensionnel de l'os du trapèze ainsi obtenu lors de l'étape précédente, de moyens de réception 10 d'un moyen d'ancrage 3. Ici illustré, il s'agit du lamage 13 et de l'orifice cylindrique 14. En variante, le procédé de réalisation 100 d'une prothèse trapézo-métacarpienne selon l'invention prévoit la réalisation, dans le modèle tridimensionnel de l'os du trapèze ainsi obtenu lors de l'étape précédente, de moyens d'ancrage 121 s'étendant en saillie de la deuxième surface 12.

Puis, le procédé de réalisation 100 d'une prothèse trapézo-métacarpienne selon l'invention comporte une étape d'impression tridimensionnelle 140 du trapèze prothétique 1 à partir du modèle tridimensionnel ainsi obtenu à l'étape 130. Cette impression tridimensionnelle s'effectue en utilisant des poudres de matériau biocompatible comme des poudres d'alliages de titane, tels que le Ti40 ou le TA6V, ou des poudres d'acier inoxydable, comme le 316LVM. Les matériaux cités précédemment ne le sont qu'à titre d'exemple.

Selon un premier mode de réalisation, le procédé de réalisation 100 d'une prothèse trapézo-métacarpienne selon l'invention comprend, préalablement à l'étape d'impression tridimensionnelle 140, une étape de réalisation 150 dans le modèle tridimensionnel ainsi obtenu de la première surface 11. Cette étape permet d'adapter la première surface 11 brute issue de l'étape 120 de reconstruction tridimensionnelle de l'os trapèze. Dans ce mode de réalisation, cette adaptation permet de réaliser, dans le modèle numérique tridimensionnel ainsi obtenu, la surface 11 complémentaire à la surface d'articulation 62 du pion métacarpien qui peut présenter, par exemple, une surface sensiblement en forme de selle biconcave, ne reprenant pas, de ce fait, l'anatomie de l'extrémité proximale du premier métacarpien du patient à traiter. Cette adaptation permet également de réaliser, dans le modèle numérique tridimensionnel ainsi obtenu, une surface 11 remodelée à partir d'un modèle anthropomorphique de l'os du trapèze issu d'images d'os de trapèze sain. Cette adaptation permet de corriger les déformations dues à la rhizarthrose elle-même. Selon un deuxième mode de réalisation, le procédé de réalisation 100 d'une prothèse trapézo-métacarpienne selon l'invention comprend, préalablement à l'étape d'impression tridimensionnelle 140, une étape de reconstruction 160 de la surface d'articulation 62,54 d'une extrémité proximale du premier métacarpien de l'articulation trapézo-métacarpienne en un modèle numérique tridimensionnel à partir de la série d'images médicales précédemment acquises, puis d'intégration de cette reconstruction dans un modèle tridimensionnel numérique du pion métacarpien. En variante, un remodelage de la surface d'articulation 62 peut être effectué de sorte à corriger les déformations dues à la rhizarthrose elle-même. Le remodelage de la surface d'articulation 62, 54 est réalisée à partir du

modèle numérique tridimensionnel du trapèze prothétique précédemment réalisé. Puis, suit une étape d'impression tridimensionnelle 170 du pion métacarpien 7 à partir du modèle tridimensionnel dudit pion ainsi obtenu. Comme pour l'étape d'impression 140, l'étape d'impression 170 s'effectue en utilisant des poudres de matériau biocompatible comme des poudres d'alliages de titane, tels que le Ti40 ou le TA6V, ou des poudres d'acier inoxydable, comme le 316LVM, ou encore des poudres de polymères, telle que du polyéthylène ou du PEEK (pour Poly Ether Ether Kétone).

Dans une variante de réalisation, le pion métacarpien 7 est en deux parties : une tête 6 réalisée en polymère et une base réalisée en métal. Les deux parties sont ensuite assemblées l'une sur l'autre après impression tridimensionnelle, par exemple en préopératoire. En variante de réalisation, la tête et la base sont « collées » l'une à l'autre, formant un ensemble monobloc. Cela est possible en utilisant, pour l'impression tridimensionnelle du pion métacarpien, une tête d'impression multi-buses dont l'une des buses est dédiée à la poudre de matériau métallique et une autre des buses à la poudre de polymère. Dans une autre variante, la tête et la base sont encliquetées l'une dans l'autre.

Maintenant, nous allons brièvement décrire un procédé d'implantation d'une prothèse trapézo-métacarpienne selon l'invention telle que précédemment décrite. Le praticien réalise, chez le patient, une voie d'abord de l'articulation trapézo-métacarpienne qu'il doit remplacer par une prothèse trapézo-métacarpienne selon l'invention préalablement fabriquée selon le procédé de réalisation 100 décrit

précédemment. Il réalise ensuite une trapézectomie. Puis, il effectue une résection de l'extrémité proximale du premier métacarpien suivi d'une préparation du canal médullaire de ce dernier. Ensuite, il met en place la base 5 du pion métacarpien 7 en introduisant la queue 50 dans le canal médullaire préparé. La tête 6 est alors mise en place en introduisant le cône 60 de la tête 6 dans le trou borgne 53 tronconique de la base 5. Lors d'un geste suivant, le praticien met en place le trapèze prothétique 1 de sorte à ce que la deuxième surface 12 vienne en contact avec le trapézoïde. Il corrige l'orientation tridimensionnelle du trapèze prothétique 1 afin que la première surface 11 du trapèze prothétique vienne en regard de la surface d'articulation 62 du pion métacarpien 7. Dès lors, le praticien met en place la vis d'ancrage 3 à travers le trou débouchant 10. Le filetage 32 est alors inséré dans le trapézoïde pour réaliser l'ancrage du trapèze prothétique 1 avec ce dernier. Dans le cas où le trapèze prothétique 1 comporte des moyens d'ancrage 121, ces derniers pénètrent en grande partie dans le trapézoïde lors d'un serrage de la vis d'ancrage 3. De manière optionnelle, le praticien peut réaliser préalablement un avant trou dans le trapézoïde, dans le prolongement du trou débouchant 10 en introduisant une mèche à travers le trou borgne. Un tel avant trou permet d'éviter un éventuel éclatement du trapézoïde lors de la mise en place de la vis d'ancrage 3.

Enfin, le praticien referme la capsula articulaire et l'incision cutanée.

Bien entendu, il est possible d'apporter à l'invention de nombreuses modifications sans pour autant sortir du cadre de celle-ci.

# REVENDICATIONS

1. Procédé de réalisation (100) d'une prothèse trapézo-métacarpienne comprenant un trapèze prothétique (1), le procédé comportant des étapes successives de :

a. Acquisition (110) d'une série d'images médicales d'une articulation trapézo-métacarpienne d'un patient à traiter ;

b. Reconstruction (120) tridimensionnelle de l'os trapèze de l'articulation trapézo-métacarpienne en un modèle tridimensionnel numérique à partir de la série d'images médicales précédemment acquises ;

c. Réalisation (130) dans le modèle tridimensionnel ainsi obtenu de moyens de réception (10) d'un moyen d'ancrage (3) ; et,

d. Impression (140) tridimensionnelle du trapèze prothétique (1) à partir du modèle tridimensionnel issu de l'étape précédente.

2. Procédé selon la revendication 1, caractérisé en ce que les moyens de réception (10) comprennent un orifice traversant (13,14) agencé de sorte à recevoir une vis d'ancrage (3).

3. Procédé selon la revendication 1 ou 2, caractérisé en ce que, le procédé comprend une étape de réalisation (150) dans le modèle numérique tridimensionnel ainsi obtenu d'une première surface (11) remodelée à partir d'un modèle anthropomorphique avant l'étape d) d'impression (140) tridimensionnelle du trapèze prothétique (1).

4. Procédé selon l'une des revendications 1 à 3, caractérisé en ce que, la prothèse trapézo-métacarpienne comportant en outre un pion métacarpien (7) présentant une surface d'articulation (62), le procédé comporte une étape de réalisation (150) dans le modèle numérique tridimensionnel ainsi obtenu d'une surface complémentaire (11) de la surface d'articulation avant l'étape d) d'impression (140) tridimensionnelle du trapèze prothétique (1).

5. Procédé selon l'une des revendications 1 à 3, caractérisé en ce que, la prothèse trapézo-métacarpienne comportant en outre un pion métacarpien (7) présentant une surface d'articulation (62,54), le procédé comporte une étape de reconstruction (160) numérique tridimensionnelle de la surface d'articulation d'une extrémité proximale du premier métacarpien de l'articulation trapézo-métacarpienne à partir de la série d'images médicales précédemment acquises, puis intégration de cette reconstruction dans un modèle tridimensionnel numérique du pion métacarpien.

6. Procédé selon la revendication 5 caractérisé en ce que le procédé effectue, lors de l'étape de reconstruction (160), dans le modèle numérique tridimensionnel, un remodelage de la surface d'articulation d'une extrémité proximale du premier métacarpien à partir du modèle numérique tridimensionnel du trapèze prothétique.

7. Procédé selon la revendication 5 ou 6, caractérisé en ce que le procédé comporte une étape

supplémentaire d'impression tridimensionnelle (170) du pion métacarpien à partir du modèle tridimensionnel dudit pion ainsi obtenu.

8. Procédé selon l'une des revendications 1 à 7, caractérisé en ce que l'impression tridimensionnelle (140,170) est réalisée à partir de poudre de matériaux biocompatibles.

9. Prothèse trapézo-métacarpienne comportant un trapèze prothétique (1) et un pion métacarpien (7), caractérisé en ce qu'elle est réalisée selon le procédé selon les revendications 1 à 8.

10. Prothèse selon la revendication 9, caractérisée en ce que le pion métacarpien comporte deux parties (5,6), les deux parties comprenant une base (5) et une tête (6) présentant la surface d'articulation (62) avec le trapèze prothétique.

11. Prothèse selon la revendication 10, caractérisée en ce que la base est métallique et la tête est réalisée en polymère.

12. Prothèse selon l'une des revendications 9 à 11, caractérisé en ce qu'elle comporte en outre une vis d'ancrage (3), formant le moyen d'ancrage, reçue dans les moyens de réception (10) du trapèze prothétique (1).

13. Prothèse selon la revendication 12, caractérisée en ce que la vis d'ancrage est une vis de compression.

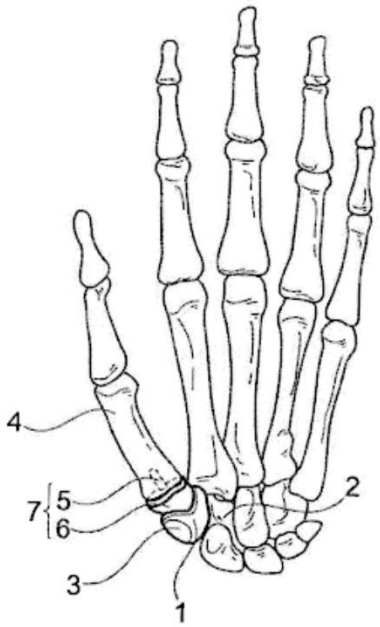


Fig. 1

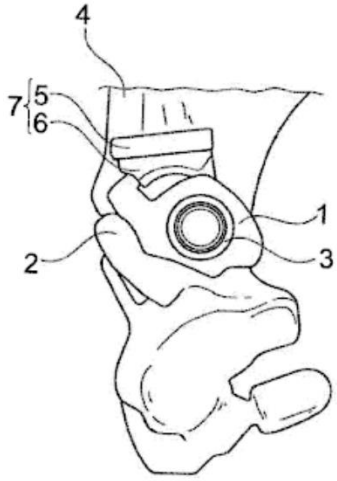


Fig. 2

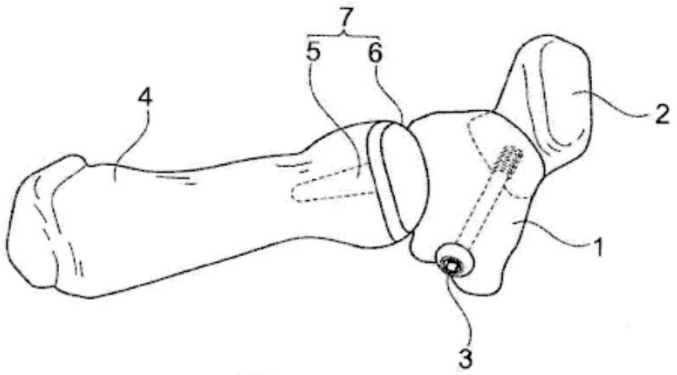


Fig. 3

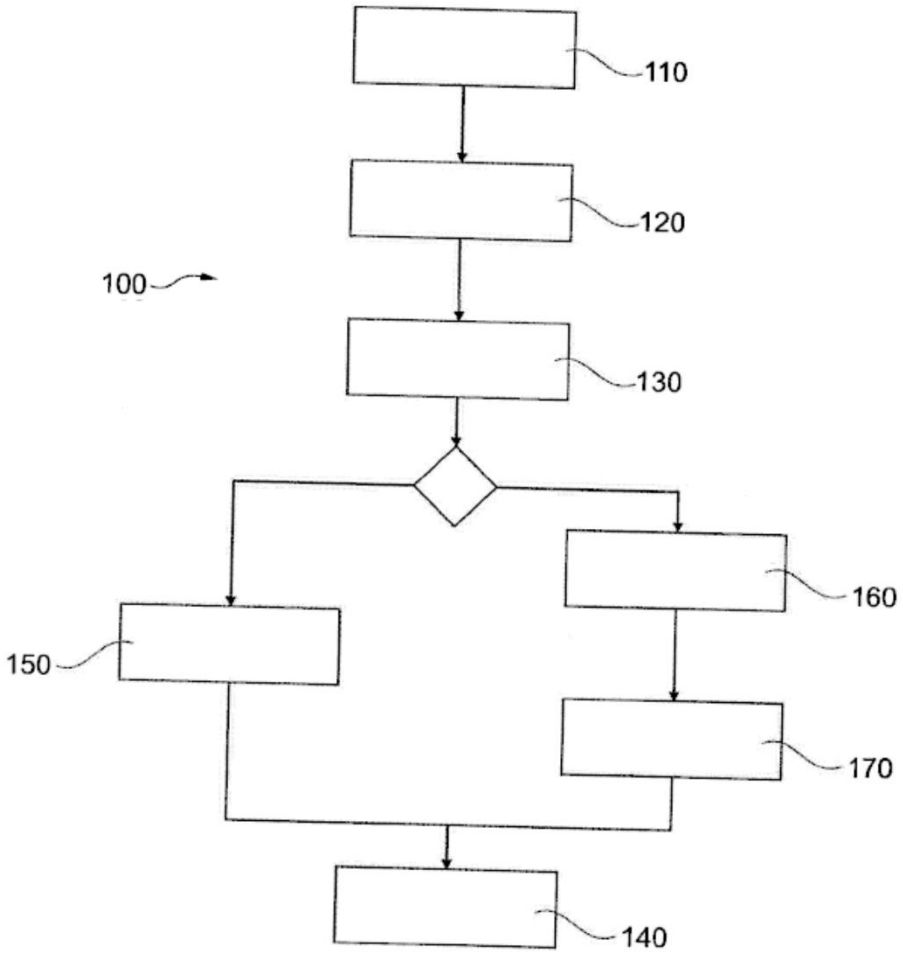


Fig. 4

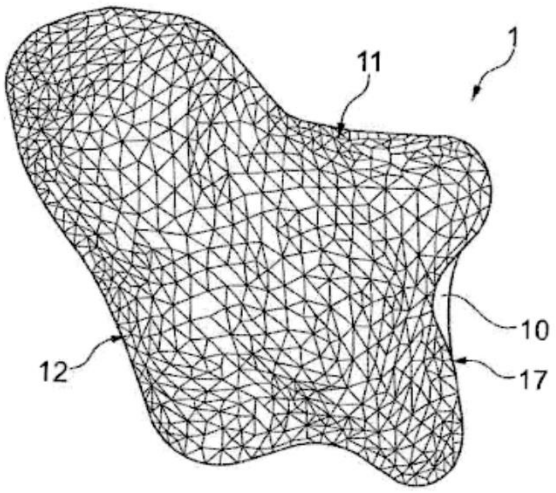


Fig. 5

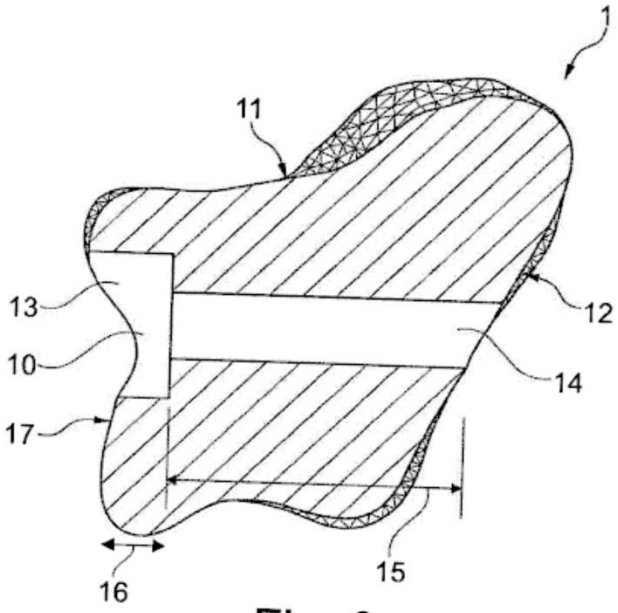


Fig. 6

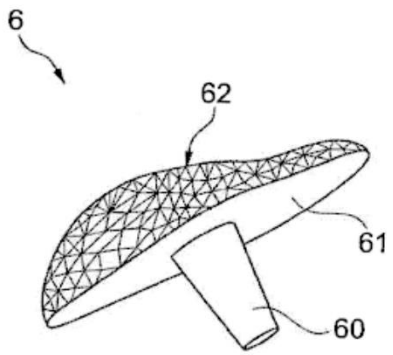


Fig. 7

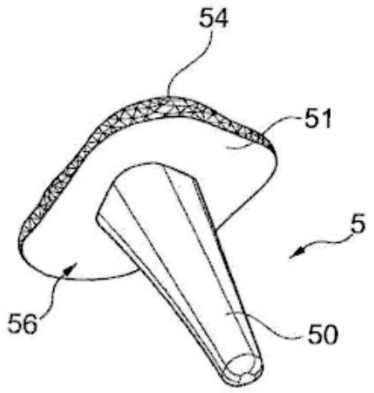


Fig. 8

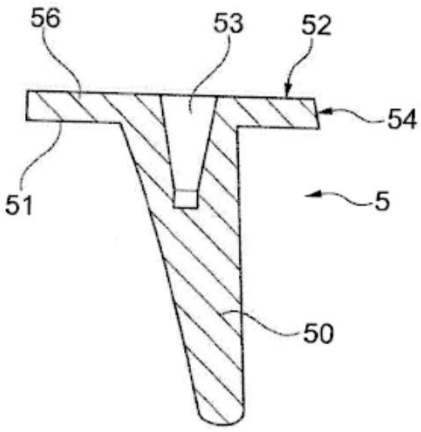


Fig. 9

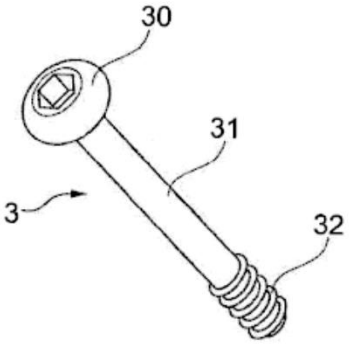


Fig. 10

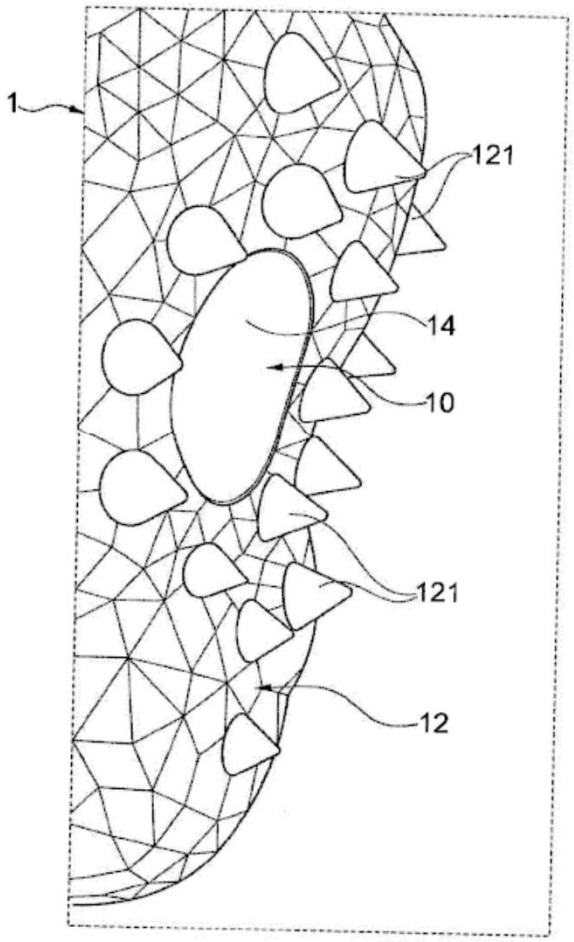


Fig. 11

Annex n°3: Patent WO2019162636A1« Method of manufacturing a complex substitution object from the real object»

(19) RÉPUBLIQUE FRANÇAISE

INSTITUT NATIONAL
DE LA PROPRIÉTÉ INDUSTRIELLE

COURBEVOIE

(11) **N° de publication :** ***3 078 418***
(à n'utiliser que pour les commandes de reproduction)

(21) **N° d'enregistrement national :** **18 51657**

(51) Int Cl[8] : ***G 06 F 17/50*** *(2018.01), A 61 F 2/42, B 33 Y 10/00, 80/00, G 06 T 19/00*

# (12) DEMANDE DE BREVET D'INVENTION A1

(22) **Date de dépôt :** 26.02.18.

(30) **Priorité :**

(43) **Date de mise à la disposition du public de la demande :** 30.08.19 Bulletin 19/35.

(56) **Liste des documents cités dans le rapport de recherche préliminaire :** *Se reporter à la fin du présent fascicule*

(60) **Références à d'autres documents nationaux apparentés :**

( ) **Demande(s) d'extension :**

(71) **Demandeur(s) :** *UNIVERSITE DE TECHNOLOGIE DE COMPIEGNE Etablissement public* — FR et *CENTRE NATIONAL DE LA RECHERCHE SCIENTIFIQUE Etablissement public* — FR.

(72) **Inventeur(s) :** BOUVIER SALIMA, LEREBOURS AUGUSTIN, RASSINEUX ALAIN et MARIN FREDERIC.

(73) **Titulaire(s) :** UNIVERSITE DE TECHNOLOGIE DE COMPIEGNE Etablissement public, CENTRE NATIONAL DE LA RECHERCHE SCIENTIFIQUE Etablissement public.

(74) **Mandataire(s) :** NOVAGRAAF TECHNOLOGIES.

## (54) PROCEDE DE FABRICATION D'UN OBJET COMPLEXE DE SUBSTITUTION A PARTIR D'UN OBJET REEL.

(57) La présente invention a pour objet un procédé de fabrication d'un objet complexe de substitution destiné à suppléer ou remplacer un objet réel dans un état donné, potentiellement endommagé, en particulier une prothèse trapézo-métacarpienne destinée remplacer l'os trapèze d'un être humain sujet à la rhizarthrose. La présente invention a également pour objet une prothèse trapézo-métacarpienne susceptible d'être obtenue par le procédé de fabrication selon l'invention.

FR 3 078 418 - A1

# PROCÉDÉ DE FABRICATION D'UN OBJET COMPLEXE DE SUBSTITUTION À PARTIR D'UN OBJET RÉEL

La présente invention concerne de manière générale la fabrication d'un objet complexe de substitution destiné à suppléer ou remplacer un objet réel dans un état donné, potentiellement endommagé, en particulier la fabrication d'une prothèse trapézo-métacarpienne pour remplacer l'os trapèze d'un être humain sujet à la rhizarthrose.

Il est difficile de réaliser un objet de substitution tel qu'une prothèse à partir de l'objet abimé, surtout s'il s'agit d'une partie d'un corps humain tel qu'un os. Néanmoins, si l'on cherche à réaliser une prothèse en se basant sur des images tridimensionnelle d'un os qui n'est pas abimé, cela ne pourra pas être celui de la personne à laquelle la prothèse est destinée. Or, cela présente l'inconvénient majeur que cette prothèse risque de ne pas lui être parfaitement adaptée. Le risque de complications post-implantation se trouve accentué du fait d'une instabilité induit par une inadéquation avec l'environnement de la prothèse. Or, si l'os est très abimé, il est généralement difficile et long, voire impossible de se baser sur des images tridimensionnelles de cet os pour réaliser un modèle de programmation du pilotage d'une machine-outil à commande numérique pour l'impression tridimensionnelle de la prothèse ou tout autre moyen de fabrication tel que l'usinage.

Afin de pallier les inconvénients précités, le demandeur a mis au point un procédé de fabrication d'un objet complexe de substitution présentant au moins une zone fonctionnelle et destiné à suppléer ou remplacer un objet réel, ledit procédé comprenant les étapes suivantes :

A. Acquisition d'une image tridimensionnelle dudit objet réel se présentant sous forme d'un nuage de

points, ladite image tridimensionnelle étant ensuite numérisée ;

B. A partir de ladite image tridimensionnelle numérisée, reconstruction à l'aide d'un logiciel de dessin ou de Conception Assistée par Ordinateur, d'un modèle tridimensionnel de l'objet réel ;

C. A partir dudit modèle tridimensionnel, programmation du pilotage d'une machine-outil à commande numérique en vue de la fabrication dudit objet complexe de substitution ;

D. fabrication additive dudit objet complexe par la machine-outil à commande numérique ;

ledit procédé étant caractérisé en ce que l'étape A est réalisée sur ledit objet réel se trouvant dans un état endommagé spécifique à une déformation donnée, et

en ce que ledit procédé comprend entre les étapes A et B, les sous-étapes suivantes :

- a'1) définition de paramètres topologiques et morphologiques invariants de l'objet réel à partir de laquelle on définit un gabarit (à l'état non endommagé);
- a'2) détermination des surfaces fonctionnelles (ou d'intérêt) et des surfaces de remplissage de l'objet réel à l'état non endommagé;
- a'3) définition des paramètres topologiques et morphologiques sensibles à la déformation de l'objet réel à l'état endommagé et identification de leurs variations au niveau de ses surfaces dites fonctionnelles ; et

en ce que l'étape B comprend en outre les sous-étapes suivantes :

b1) adaptation du gabarit sur ladite image tridimensionnelle définies à l'étape A, à

l'aide d'un logiciel de dessin ou de CAO, pour obtenir un modèle spécifique (c'est-à-dire un gabarit adapté à l'état endommagé) ;

b2) sur le modèle spécifique, reconstruction précise des surfaces fonctionnelles à l'état endommagé à partir des surfaces fonctionnelles définies à l'étape a'2), et reconstruction approximative, des surfaces de remplissage à l'état endommagé à partir des surfaces fonctionnelles définies à l'étape a'2), pour obtenir une image tridimensionnelle reconstruite à l'état endommagé ;

b3) reconstruction précise, sur l'image tridimensionnelle reconstruite à l'état endommagé, des surfaces fonctionnelles à l'état non endommagé, par modification des valeurs des paramètres topologiques et morphologiques sensibles à la déformation définis à l'étape a'3) de manière qu'ils correspondent à une absence de déformation, pour obtenir une image tridimensionnelle reconstruite à l'état non endommagé ;

b4) à partir de l'image tridimensionnelle reconstruite à l'état non endommagé, extraction d'un fichier numérique fonctionnel comprenant uniquement les zones d'intérêt et d'un fichier numérique de remplissage comprenant les zones autres que les zones d'intérêt ;

b5) Reconstruction à partir des fichiers fonctionnel et de remplissage d'un modèle volumique fermé dudit objet à reconstruire, qui est mis sous forme de fichier neutre adapté à la fabrication additive.

La première étape du procédé selon l'invention est l'étape A consistant à acquérir une image tridimensionnelle dudit objet réel qui est numérisée. Cette étape peut être réalisée de diverses manières, et notamment par numérisation tridimensionnelle (ou « *numérisation 3D* ») à l'aide d'un scanner 3D. On obtient par cette technique des images de synthèse en trois dimensions qui n'ont pas besoin d'être ensuite segmentées.

Dans le cas où l'objet réel que l'on cherche à reconstruire ou suppléer est une partie d'un corps humain ou animal, l'étape A sera plutôt réalisée en deux étapes, comprenant notamment l'acquisition des images tridimensionnelles par des techniques d'imagerie médicales telle que l'Imagerie par Résonnance Magnétique (généralement connue sous l'acronyme « IRM »), qui sont ensuite soumises à un traitement ultérieur de segmentation. Par contre, si les images sont obtenues par scan 3D, elles sont directement sous forme de nuage de points (la segmentation n'est donc pas nécessaire)

Selon un mode de réalisation de l'invention, par exemple dans le cas d'images 3D par imagerie médicale et non par scanner 3D, on réalise, au cours de l'étape A d'acquisition de l'image tridimensionnelle de l'objet réel, un formatage de l'image en un format neutre (par exemple un fichier STL) compatible avec un logiciel de dessin ou de Conception Assistée par Ordinateur.

Entre les étapes A et B, le procédé selon l'invention comprend en outre une sous-étape a'1) de définition de paramètres topologiques et morphologiques invariants de l'objet réel, à partir de laquelle on définit un gabarit.

Par paramètres topologiques et morphologiques invariants de l'objet réel, on entend, au sens de la présente invention, des paramètres qui sont constamment présents d'un objet réel à un autre, qu'il soit ou non endommagé ou non et appartenant

à la même catégorie ou type d'objet, par exemple d'un oz trapèze à l'autre.

Par gabarit, on entend, au sens de la présente invention, un modèle générique adimensionnel d'un objet non endommagé (au sens de non déformé et non abimé par un quelconque usage), qui est défini par ses paramètres topologiques et morphologiques invariants.

Les paramètres topologiques et morphologiques invariants sont placés de façon préférable sur des zones fonctionnelles.

Par zones ou surfaces fonctionnelles d'un objet donné, au sens de la présente invention des surfaces de l'objet ayant une fonction donnée, qu'elle soit d'ordre cinématique ou autre.

Le gabarit peut être défini avec des surfaces jointives ou non jointives.

Par surfaces jointives, on entend, au sens de la présente invention, des surfaces situées côte à côte et définies par une même courbe commune. Cela implique que les deux surfaces jointives sont dépendantes l'une de l'autre.

La définition du côté commun est similaire aux deux surfaces, même si elles présentent des fonctions différentes. En outre, il n'y a pas d'espace libre entre les deux surfaces.

A contrario, par surfaces jointives, on entend, au sens de la présente invention, des surfaces situées côte à côte mais qui ne s'appuient pas sur la même courbe. Cela implique que les deux surfaces sont indépendantes l'une de l'autre et il 'y a un espace libre entre les deux surfaces. Il est possible de mettre plusieurs surfaces en vis-à-vis d'une et même surface.

L'avantage de définir le gabarit par des surfaces non jointives est de permettre le raffinement des zone les plus fonctionnelles (c'est-à-dire l'augmentation du nombre de points) sans avoir la contrainte d'assurer la jonction des différentes surfaces adjacentes.

Entre les étapes A et B, le procédé selon l'invention comprend en outre, postérieurement à la sous-étape a'1), une sous-étape a'2) de détermination des surfaces fonctionnelles (ou d'intérêt) et des surfaces de remplissage (d'importance mineure, comprenant les zones autres que les zones d'intérêt) de l'objet réel à l'étape non endommagé.

Par surface de remplissage, on entend, au sens de la présente invention, toute surface qui n'est pas fonctionnelle.

Outre les sous-étapes a'1 et a'2), le procédé selon l'invention comprend une sous-étape a'3) de détermination des paramètres topologiques et morphologiques sensibles à la déformation de l'objet réel (à l'état endommagé et l'identification de leurs variations, au niveau des surfaces dites fonctionnelles. Cette étape peut être réalisée à partir d'une base de données statistiques de la géométrie réelle d'objets connus similaires audit objet réel, afin de retrouver un objet à l'état non-endommagé, particulièrement au niveau des surfaces dites fonctionnelles.

L'étape B du procédé selon l'invention consiste à reconstruire à partir de l'image tridimensionnelle éventuellement segmentée, un modèle tridimensionnel de l'objet réel à l'aide d'un logiciel de dessin ou de Conception Assistée par Ordinateur.

L'étape B du procédé selon l'invention comprend notamment une première sous-étape b1) d'adaptation du gabarit sur l'image tridimensionnelle numérisée obtenue à l'étape A, à l'aide d'un logiciel de dessin ou de CAO, pour obtenir un modèle spécifique, c'est-à-dire un gabarit adapté à l'objet endommagé.

Par ailleurs, la sous-étape b4) de reconstruction des surfaces fonctionnelles à l'état endommagé consiste à modifier, sur une image tridimensionnelle reconstruite à l'état non endommagé (obtenue à la sous-étape b3), les

paramètres morphologiques sensibles à la déformation, de manière à ce qu'ils correspondent à une absence de déformation sur la base des informations obtenues lors de la sous-étape a'3).

De manière avantageuse, l'étape B peut avantageusement comprendre, à l'issue de l'étape b5), une étape b6) de lissage global ou localisé dudit modèle volumique fermé, pouvant être réalisée par une méthode surfacique ou volumique. Cette étape est facultative mais fortement conseillée du fait du peu de nombre de points définissant le gabarit (la possibilité d'avoir des arêtes vives pouvant être nocive pour le patient *in fine*). Par ailleurs cette étape est fortement conseillée si la création du modèle volumique fermé est réalisée par voxels.

Le procédé selon l'invention est particulièrement adapté pour réaliser des objets complexes sels des semelles orthopédiques ou des prothèses dentaires, auditives, ou osseuses pour un corps humain ou animal.

Dans le cas d'une réalisation de prothèse implantable, on pourra utiliser, pour l'étape D de fabrication additive, des poudres de matériaux biocompatibles tels que des poudres de TA6V, 316L, CrCoMo, ou encore de céramique ou encore de polymère.

Dans ce cas, on entend par gabarit, au sens de la présente invention, le modèle générique adimensionnel d'une partie d'un corps humain que l'on cherche à remplacer ou suppléer (par une prothèse ou une semelle), qui est celui d'un sujet sain (personne non malade), qui n'a pas été déformé ou subi une de dégénérescence ou déformation.

En particulier, le procédé selon l'invention est particulièrement adapté à fabriquer une prothèse trapézo-métacarpienne à titre d'objet complexe de substitution d'un os trapèze d'un être humain (objet réel). Une telle prothèse est destinée à être implantée dans la main d'un patient au

niveau de l'articulation trapézo-métacarpienne. Cette implantation est réalisée lors d'une intervention chirurgicale appelée arthroplastie prothétique consistant à remplacer, en partie ou totalement, l'articulation malade par une prothèse. Il s'agit d'une solution thérapeutique couramment utilisée dans le cas de l'arthrose qui est une destruction ou une dégénérescence des surfaces articulaires.

Dans le cas de la fabrication d'une prothèse trapézo-métacarpienne à titre d'objet complexe de substitution, les zones d'intérêt de l'os trapèze seront les surfaces articulaires, c'est-à-dire la surface d'articulation avec le second métacarpe, la surface d'articulation avec le scaphoïde, la surface d'articulation avec le trapézoïde, et de façon optionnelle la surface définissant une rainure pour le passage du tendon *flexor carpi radialis*.

La présente invention a également pour objet une prothèse trapézo-métacarpienne susceptible d'être obtenue par le procédé de fabrication selon l'invention tel que défini spécifiquement pour la fabrication d'une prothèse trapézo-métacarpienne.

D'autres avantages et particularités de la présente invention résulteront de la description qui va suivre, donnée à titre d'exemple non limitatif et faite en référence aux figures annexées :

- La figure 1 est une vue de dessus d'un squelette d'une main comportant une prothèse trapézo-métacarpienne selon l'invention ;
- La figure 2 est une vue de détail et de côté de la prothèse de la figure 1 ;
- La figue 3 est une vue tridimensionnelle de l'implantation de la prothèse de la figure 1, dans lequel seuls le premier métacarpe et le trapézoïde du squelette de la main étant représentés ;

- La figue 4 montre où se situe l'articulation trapézo-métacarpienne dans la main d'un patient ;
- La figure 5 comprend deux séries d'images 3D obtenues par IRM puis segmentation de l'articulation trapézo-métacarpienne des mains de deux patients souffrant de rhizarthrose, l'une pour la main gauche des deux patients (figure 5a) et l'autre pour la main droite de ces deux patients (figure 5b) ;
- La figure 6 montre les paramètres topologiques et morphologiques constamment présent d'un os trapèze à un autre ;
- Les figures 7a à 7p montrent les variations de ces paramètres topologiques et morphologiques d'un os trapèze ;
- Les figures 8a à 8c montrent l'évolution des courbures convexes et concaves de la surface de contact avec le 1er métacarpe selon l'état arthrosique de l'articulation ;
- Les figures 9a à 9g montrent les étapes A à b6 de reconstruction numérique d'un os trapèze n'ayant pas subi de déformation liée à la rhizarthrose, conformément au procédé selon l'invention, dans laquelle l'étape b5) de reconstruction d'un modèle volumique fermé de l'objet de substitution à fabriquer est réalisée par une méthode surfacique (dite de reconstruction de Poisson : voir figure 9f) ou par une méthode volumique, dite de remplissage par *voxels* (c'est-à-dire des cubes numériques : voir figure 9g) ;
- La figure 10 montre le gabarit d'un os trapèze et l'ensemble des points et des courbes le définissant ;
- La figure 11 montre l'évolution d'un lissage du modèle volumique fermé jusqu'à obtention de la disparition des angles vifs tout en conservant

l'intégrité des paramètres d'un os trapèze sain préalablement définis ;

- La figure 12 montre les différents éléments de la prothèse trapézo-métacarpienne à ajouter (1111) ou à extraire (1111);
- La figure 13 montre les étapes C et D du procédé selon l'invention dans le cadre de la fabrication d'une prothèse trapézo-métacarpienne, depuis l'obtention du modèle volumique fermé de l'os trapèze à reconstruire jusqu'à la fabrication additive et le lissage final (respectivement étapes 13d et 13e) aboutissant à la prothèse de l'os trapèze, qui est finalement être implantée dans la main d'un patient au niveau de l'articulation trapézo-métacarpienne (13f) ;
- La figure 14 montre que les propriétés de mobilité de la main sont conservées après une opération d'arthroplastie prothétique avec la prothèse de l'os trapèze selon l'invention.

Les figures 1 à 14 sont décrites plus en détail au niveau de l'exemple qui suit, donné à titre indicatif et qui illustre l'invention sans toutefois en limiter la portée.

**EXEMPLE**

**DISPOSITIFS ET INSTRUMENTATION**

- Comparateur (appareil de mesure) : (North and Rutledge, 1983)
- Stéréophotogrammétrie (SPG) sur os de cadavres (résolution 25 µm) (Ateshian, 1992; Xu, 1998) ;
- Segmentation of Ctscan (résolution 0,625 x 0,3 x 0,3mm) (Conconi, 2014 ; Halilaj, 2014b) ;

- Scan laser 3D (LS) (Kovler, 2004; Markze, 2012) Système micro-CT sur os de cadavres (résolution 0,38µm)
- Logiciel de segmentation des images : OSIRIX, MATERIALIZE
- Logiciel de formatage des images segmentées en fichier STL : OSIRIX MATERIALIZE
- Logiciel de visualisation des fichiers STL : MESCHLAB
- Logiciel de Conception Assistée par Ordinateur : CATIA V5;

**MATÉRIAUX**

- objets réels :
  os trapèzes de deux patients masculins souffrant de rhizarthrose, âgés respectivement de 61 ans (patient 1) et de 66 ans (patient 2), dont la main malade est montrée sur les figures 5a et 5b ;
- objet à reconstruire :
  os trapèze de prothèses trapézo-métacarpiennes schématiquement représenté sur les figures 1 à 3 et montrées sur les photographies des figures 13d et 13e;
- matériau utilisé pour la fabrication additive de la prothèse : CrCoMo, TA6V.

En référence aux figures 1 à 3, nous allons décrire une prothèse trapézo-métacarpienne 1 susceptible d'être obtenu selon l'invention. Cette prothèse trapézo-métacarpienne comporte ici un trapèze prothétique 111, un pion métacarpien 117 et une vis d'ancrage 113. Elle est destinée à être mise en place entre le premier métacarpien 214 et le trapézoïde 212 d'un patient. Le trapèze prothétique 111 est ancré sur le trapézoïde 212 avec la vis d'ancrage 113. Dans le mode de réalisation illustré sur les figures 1 à 3, le pion

métacarpien 117 comporte deux parties, ici rapportées l'une sur l'autre : une base 115 et une tête 116.

**EXEMPLE 1 : Acquisition d'images tridimensionnelles segmentées des os trapèzes (étape A du procédé selon l'invention)**

La main du patient est scannée par IRM ou par tomographie puis transformée en nuages de points (format STL). Les caractéristiques techniques de l'imagerie médicale et de l'extraction en nuage de points (séquences, pondération, contraste) sont choisies de telle sorte à discrétiser la partie corticale des os (figures 5a et 5b).

Un fichier numérique STL est extrait puis les points de repères définissant le gabarit sont adaptés au modèle du patient sous un logiciel de CAO ou d'édition de maillage. Le logiciel MESHLAB, un logiciel de type « *open source* » d'édition de maillage 3D permet quant à lui de visualiser les fichiers STL.

Lorsque le modèle est très arthrosique et abimé, et que le gabarit ne peut être entièrement adapté au patient, les points de repères non adaptés sont prédits par une base de données d'os sain. Par ailleurs le gabarit permet de supprimer les protubérances et rugosités non anatomiques très présentes dans un os avec un état arthrosique avancé.

**EXEMPLE 2 : Détermination des paramètres topologiques et morphologiques constamment présents d'un objet réel à un autre pour obtenir un gabarit (étape A' du procédé selon l'invention)**

La figure 6 montre les paramètres topologiques et morphologiques constamment présents d'un os trapèze à un autre.

Sur le modèle biomécanique d'un os trapèze, on distingue trois types de points de repères :

- les points de repères anatomiques (411), définis par des experts et correspondants à des points ayant une signification biologique ;
- les pseudo-points de repères (412), qui sont construits sur un objet, sur une ligne ou entre des points de repère.

Suite à la reconstruction, des caractéristiques communes sont ressorties (illustrées sur les figures 7a à 7p) :

- présence de 4 surfaces d'articulation visibles :
  - o Trapézoïde (TPZ) 421,
  - o Métacarpe 1 (M1) 422,
  - o Métacarpe 2 (M2)423,
  - o Scaphoïde (SCP) 424 dont 2 plans (SCP et M2), et
- L'articulation M1 (422) en forme de selle de cheval.

Le choix s'est donc porté sur la mise en exergue de ces caractéristiques.

**EXEMPLE 3 : Détermination des paramètres topologiques et morphologiques variables sensibles à l'arthrose (étapes a'1 à a'3 du procédé selon l'invention)**

Les figures 7a à 7p montrent l'ensemble des mesures effectuées sur ces points de repères afin de connaitre leur variabilité en fonction de l'état arthrosique. Les paramètres relatifs à la surface de contact avec le premier métacarpe sont très sensibles à l'état arthrosique (431).

Par ailleurs, les figures 8a à 8c montrent plus spécifiquement, que les courbures concaves (441) et convexes (442) de la surface de contact avec le premier métacarpe varient en fonction de l'état arthrosique de l'articulation. Les courbures sont concaves sont très prononcées pour un

sujet sain (4411) et faiblement prononcées à l'état arthrosique (4412). Inversement les courbures convexes sont très prononcées à l'état arthrosiques (4422) et faiblement prononcées pour un sujet sain. Les courbures concaves saines (4411) décroissent le long de la ligne radio-ulnaire mais sont stables pour un sujet arthrosique (4412). Les courbures convexes saines (4421) croissent le long de la ligne radio-ulnaire mais décroissent légèrement pour un sujet arthrosique (4412).

**EXEMPLE 4 : Reconstruction à l'aide d'un logiciel de dessin, d'un modèle tridimensionnel d'os trapèze n'ayant pas subi de déformation liée à la rhizarthrose correspondant aux os trapèze des patients malades (étape B du procédé selon l'invention)**

Les figures 9a à 9f montrent les différentes étapes de reconstruction d'un modèle tridimensionnel d'un os trapèze n'ayant pas subi de déformation liée à la rhizarthrose.

Plus spécifiquement, ces figures montrent de manière détaillée :

- la mise en place (figure 9a3 : résultat de la mise en place) du gabarit (de la figure 9a2) sur le modèle numérique 3D de l'os trapèze du patient (figure 9a1),
- l'identification des valeurs des paramètres morphologiques ne concordant pas aux spécifications d'un os trapèze sain (figure 9b),
- l'identification des zones d'intérêts et de remplissage (figure 9c),
- la modification des valeurs des paramètres afin qu'elles concordent aux spécifications d'un os trapèze sain (figure 9d),

- l'extraction des zones d'intérêt et de remplissage en modèle numérique maillé avec la précision suffisante par rapport aux tolérances exigées (figure 9e),
- la reconstruction d'un modèle 3D fermé par méthode surfacique (reconstruction de poisson : figure 9f) ou méthode volumique (remplissage par voxels : figure 9g).

**EXEMPLE 5 : Obtention par impression 3D d'un os trapèze à partir du modèle tridimensionnel obtenu à l'exemple 4 (étapes C et D du procédé selon l'invention)**

La figure 14 montre que les propriétés de mobilité de la main sont conservées après une opération d'arthroplastie prothétique avec la prothèse de l'os trapèze selon l'invention. L'ensemble des mouvements relatif à l'articulation trapézo-métacarpienne ont été correctement réalisé, il s'agit des mouvements de rétropulsion (91), antépulsion (92), abduction (93), adduction (94) et circumduction selon leur étendu respective.

## REVENDICATIONS

1. Procédé de fabrication d'un objet complexe de substitution (1) présentant au moins une zone fonctionnelle et destiné à suppléer ou remplacer un objet réel (2), ledit procédé comprenant les étapes suivantes :

A. acquisition d'une image tridimensionnelle (22) dudit objet réel (2) se présentant sous forme d'un nuage de points, ladite image tridimensionnelle (22) est ensuite numérisée (23) ;

B. à partir de ladite image tridimensionnelle numérisée (23), reconstruction à l'aide d'un logiciel de dessin ou de Conception Assistée par Ordinateur, d'un modèle (3) tridimensionnel de l'objet réel (2) ;

C. à partir dudit modèle tridimensionnel (3), programmation du pilotage d'une machine-outil à commande numérique en vue de la fabrication dudit objet (1) complexe de substitution ;

D. fabrication additive dudit objet complexe par la machine-outil à commande numérique ;

ledit procédé étant caractérisé en ce que l'étape A est réalisée sur ledit objet réel (2) se trouvant dans un état endommagé spécifique à une déformation donnée, et

en ce que ledit procédé comprend entre les étapes A et B, les sous-étapes suivantes :

a'1) définition de paramètres topologiques et morphologiques invariants (4) de l'objet réel (2), à partir de laquelle on définit un gabarit (5) ;

a'2) détermination des surfaces fonctionnelles et des surfaces de remplissage de l'objet réel (2) à l'état non endommagé ;

a'3) détermination des paramètres topologiques et morphologiques sensibles à la déformation (42) de

l'objet réel (2) à l'état endommagé et identification de leurs variations, au niveau de ses surfaces dites fonctionnelles ; et

également caractérisé en ce que l'étape B comprend en outre les sous-étapes suivantes :

b1) adaptation du gabarit (5) sur ladite image tridimensionnelle (22) définie à l'étape A, à l'aide d'un logiciel de dessin ou de CAO, pour obtenir un modèle spécifique (6) ;

b2) sur ledit modèle spécifique (6), reconstruction précise des surfaces fonctionnelles à l'état endommagé (61) à partir des surfaces fonctionnelles définies à l'étape a'2) et reconstruction approximative des surfaces de remplissage à l'état endommagé (62) à partir des surfaces fonctionnelles définies à l'étape a'2), pour obtenir une image tridimensionnelle reconstruite à l'état endommagé (7);

b3) reconstruction précise, sur ladite image tridimensionnelle reconstruite à l'état endommagé (7), des surfaces fonctionnelles à l'état non endommagé (71), par modification des valeurs des paramètres topologiques et morphologiques sensibles à la déformation définis à l'étape a'3) de manière qu'ils correspondent à une absence de déformation, pour obtenir une image tridimensionnelle reconstruite à l'état non endommagé (8) ;

b4) à partir de ladite image tridimensionnelle reconstruite à l'état non endommagé (8), définition précise des zones d'intérêt de l'objet complexe (1) à reconstruire, pour en extraire un fichier numérique fonctionnel (81) comprenant uniquement lesdites zones d'intérêt et un fichier numérique de

remplissage (82) comprenant les zones autres que les zones d'intérêt ;

b5) Reconstruction à partir des fichiers fonctionnel (81) et de remplissage (82) d'un modèle volumique fermé (9) dudit objet (1) à reconstruire, qui est mis sous forme de fichier neutre (10) adapté à la fabrication additive.

2. Procédé selon la revendication 1, selon lequel l'étape B comprend en outre, à l'issue de l'étape b5), une étape b6) de lissage global ou localisé dudit modèle volumique fermé (9).

3. Procédé selon la revendication 2, selon lequel l'étape b6) est réalisée par une méthode surfacique ou volumique.

4. Procédé selon la revendication l'une quelconque des revendications 1 à 3, selon lequel on réalise, au cours de l'étape A, un formatage de ladite image tridimensionnelle (22) en un format neutre compatible avec un logiciel de dessin ou de Conception Assistée par Ordinateur.

5. Procédé selon la revendication l'une quelconque des revendications 1 à 4, selon lequel l'objet complexe (1) à fabriquer est une semelle orthopédique ou une prothèse dentaire, auditive, ou osseuse, pour un corps humain ou animal.

6. Procédé selon la revendication 5, selon lequel l'objet réel est un os trapèze, pour une fabrication d'une prothèse trapézo-métacarpienne (11).

7. Procédé selon la revendication 4, selon lequel les zones d'intérêt (26) de l'os trapèze sont les surfaces

articulaires avec le scaphoïde, le trapézoïde, le premier métacarpe, et le second métacarpe.

8. Procédé selon l'une des revendications 6 et 7, selon lequel l'étape D de fabrication additive est réalisée à partir de poudre de matériaux biocompatibles.

9. Prothèse trapézo-métacarpienne obtenue par le procédé de fabrication tel que défini selon l'une quelconque des revendications 6 à 8.

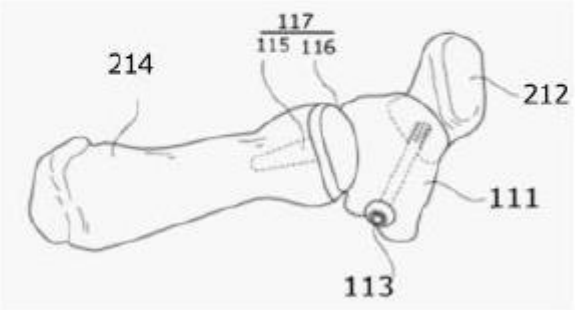


FIG. 1

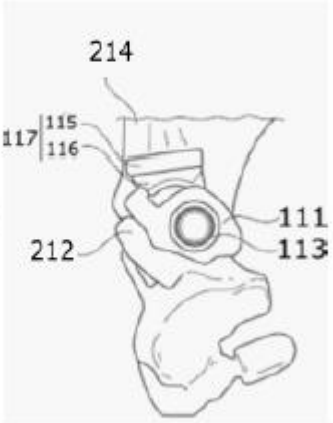


FIG. 2


FIG. 3

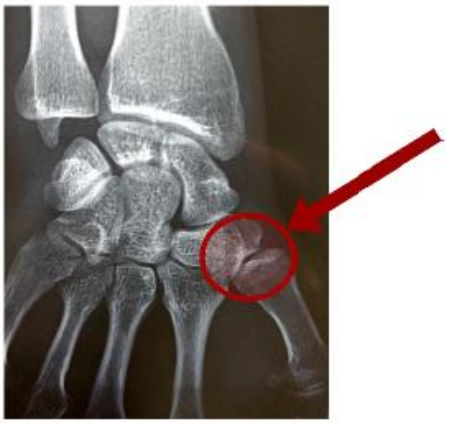

FIG. 4

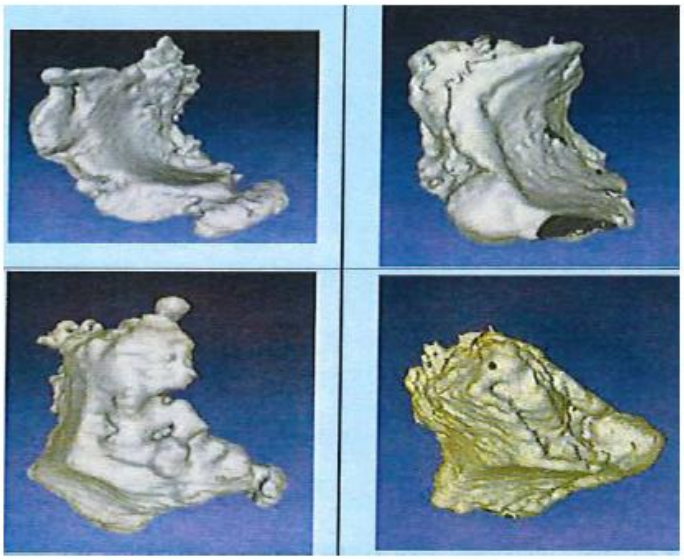

FIG. 5a

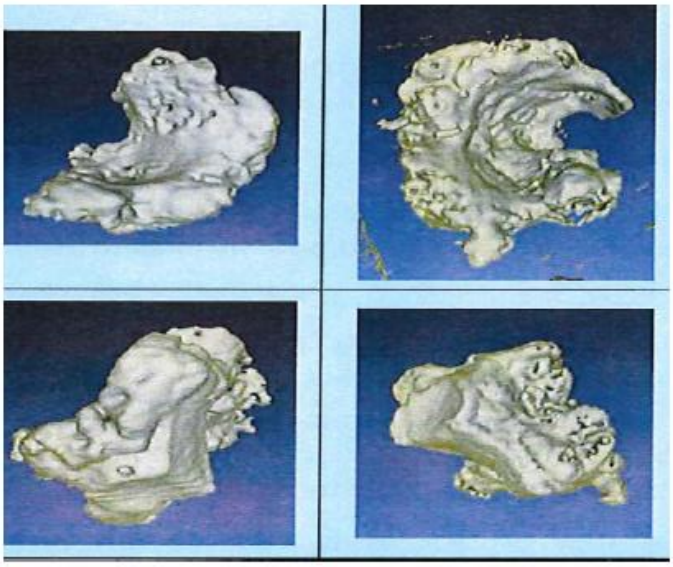

FIG. 5b

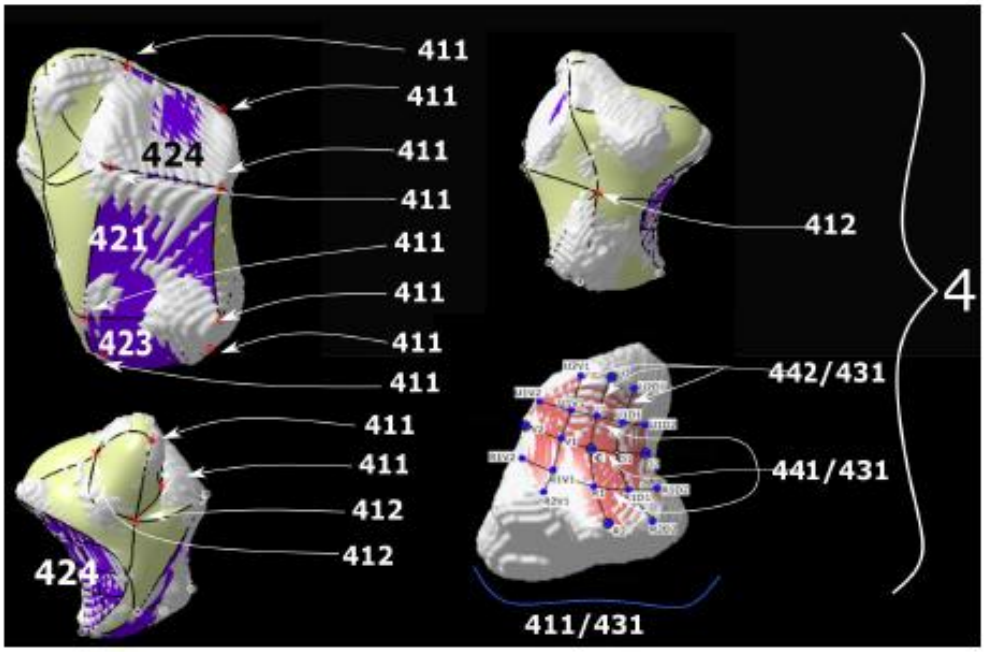


FIG. 6

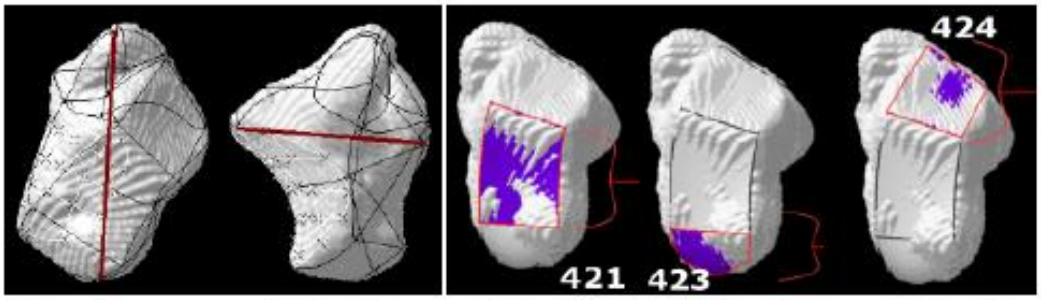


FIG. 7a FIG. 7b FIG. 7c FIG. 7d FIG. 7e

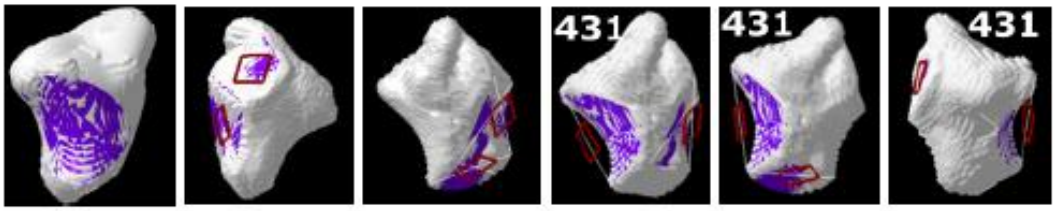


FIG. 7f FIG. 7g FIG. 7h FIG. 7i FIG. 7j FIG. 7k

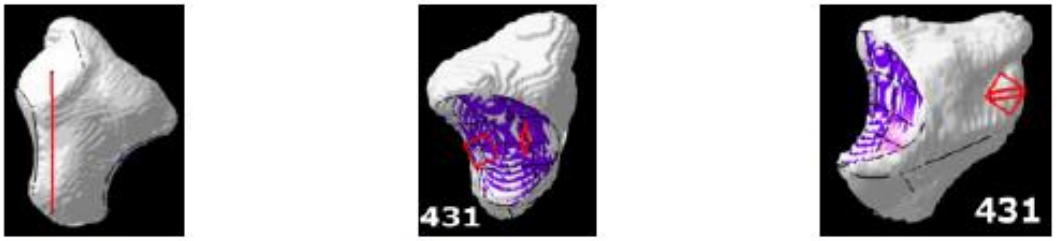


FIG. 7l FIG. 7m FIG. 7n

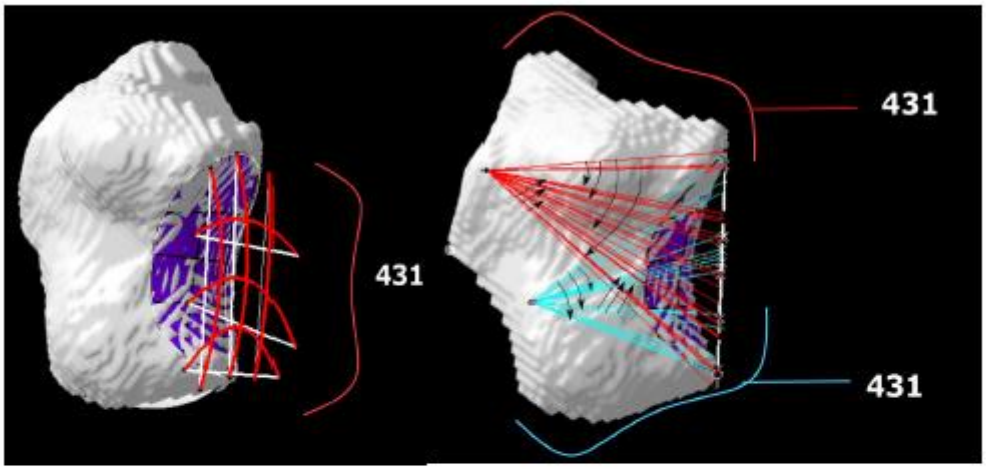


FIG. 7o

FIG. 7p

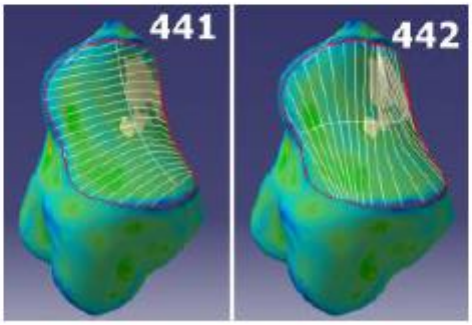


FIG. 8a

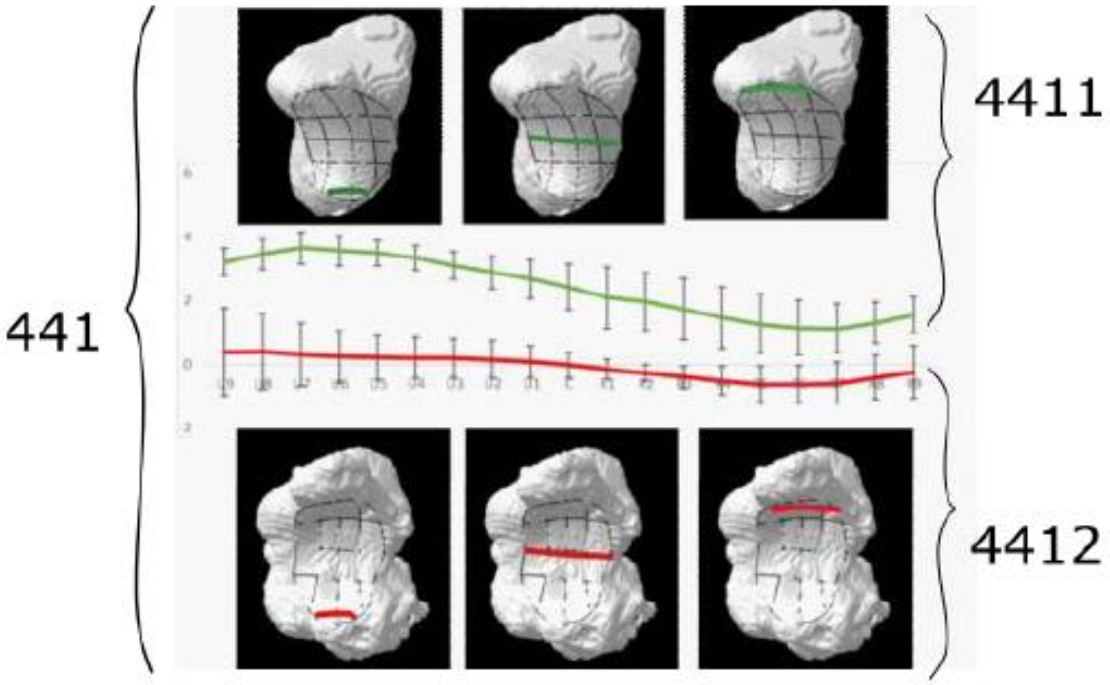


FIG. 8b

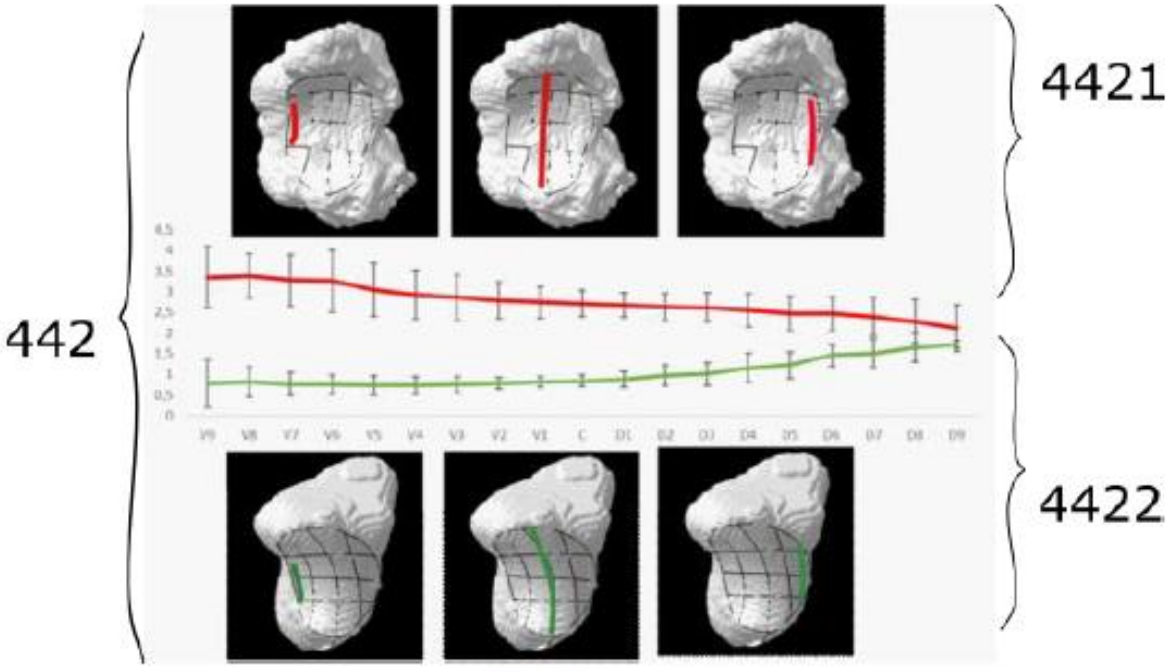


FIG. 8c

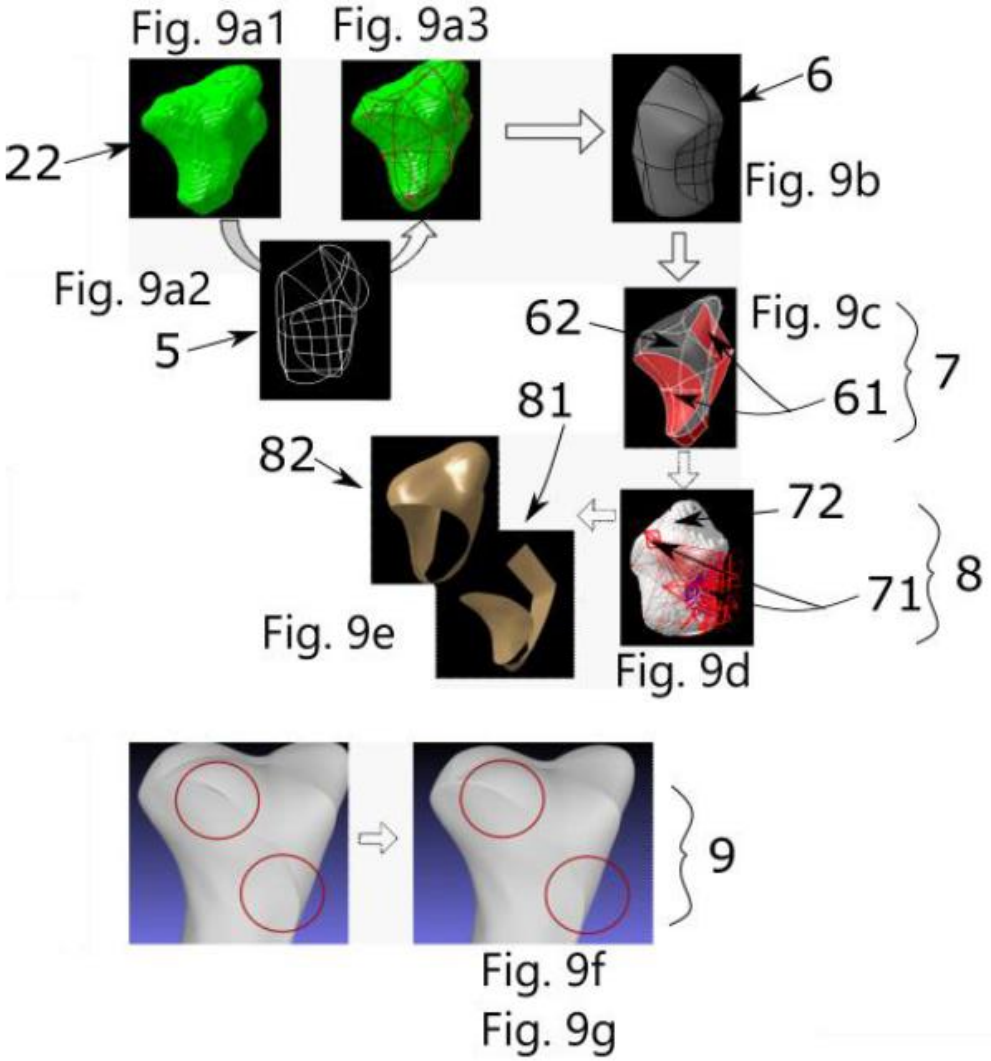


FIG. 9 Attention Fig.9f doit être à gauche

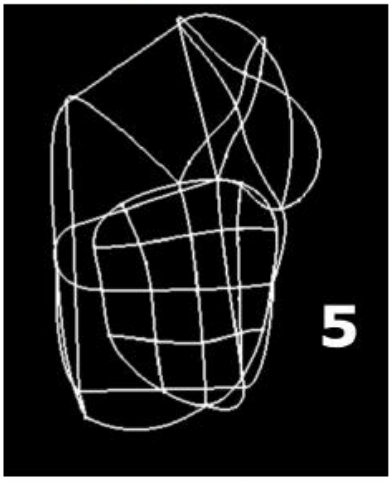


FIG. 10

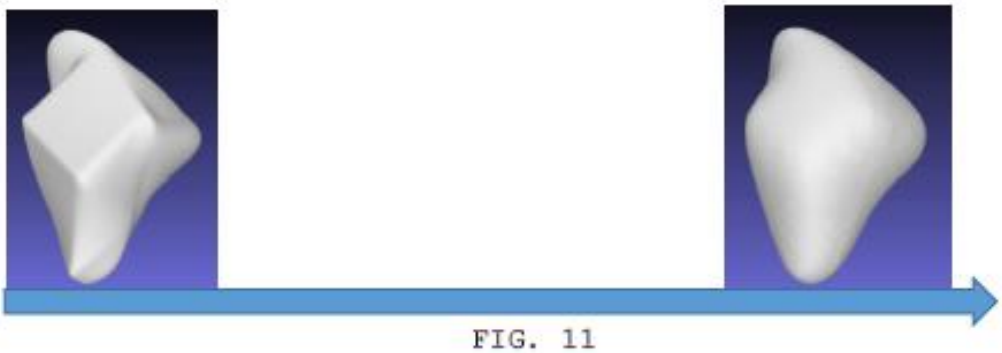

FIG. 11

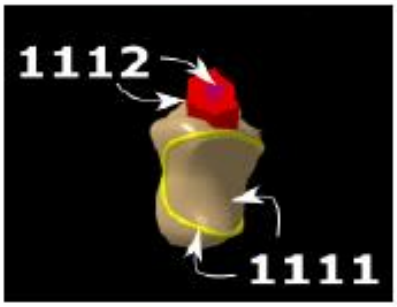


FIG. 12

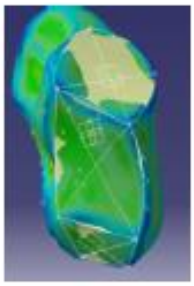

FIG. 13a

FIG. 13b

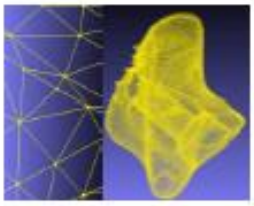

FIG. 13c

FIG. 13d

FIG. 13f

FIG. 13e


FIG. 14

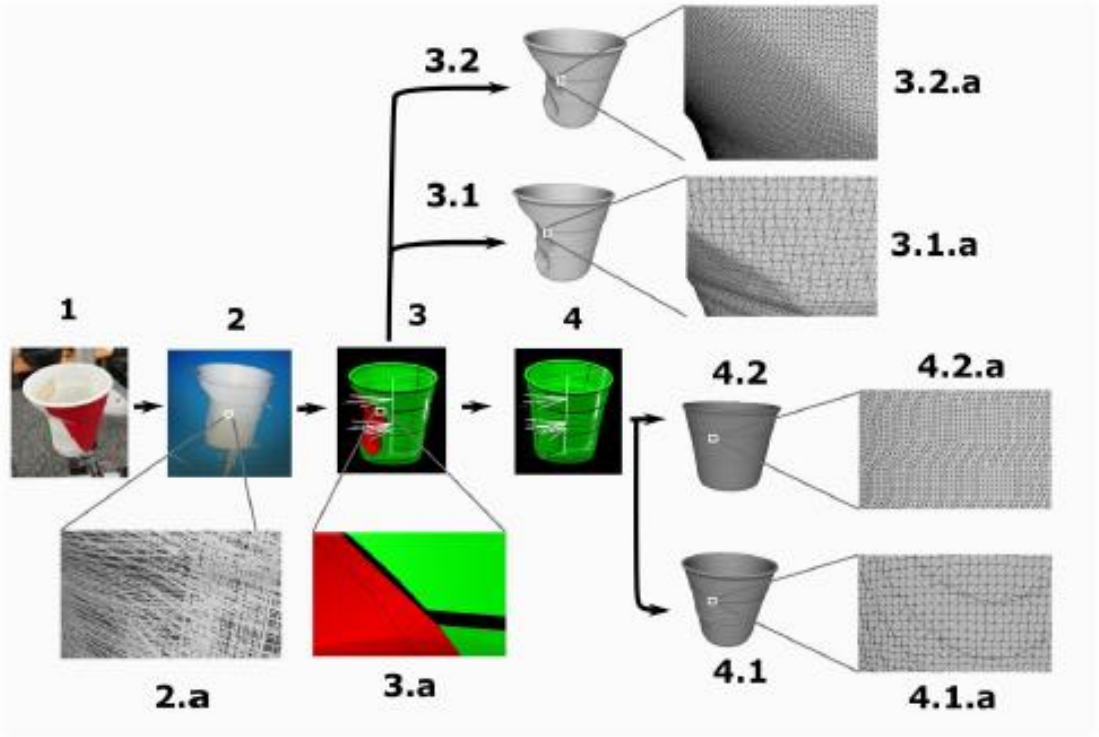


FIG. 15

Annex n°4 a): Implant in stainless steel 316L produce by SLM

## 1. Geometrical inspection

a)

b)

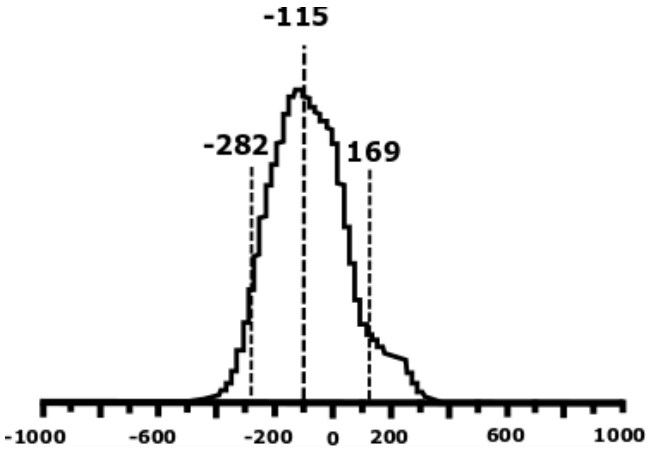


c)

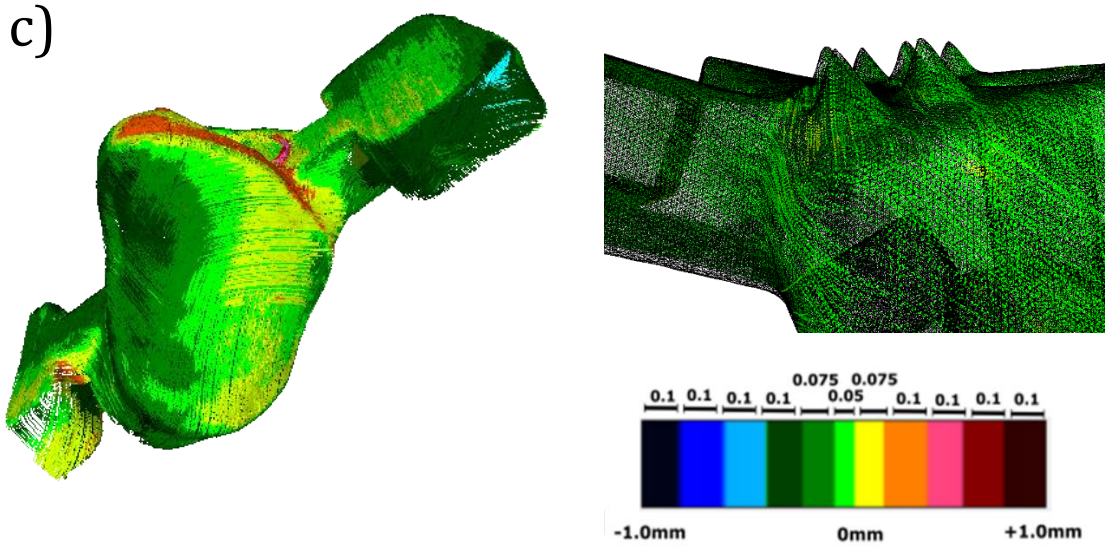


**Figure 1:** Geometrical deviation of the superfinished 316L specimen compared to the numerical model

The accuracy of the surfaces was verified by 3D scanning the version of the implants with a laser robot arm after the sandblasting and the superfinishing processes. The obtained point cloud was compared with the designed implants by the Hausdorff distance measurement. The result of each point was then gathered in a histogram as seen in fig.1.b. Following the superfinishing, the average deviation was -115µm for the 1st version. The

values containing 5% and 95% of the distances are 551µm which is far lower than the implants made in CoCrMo. It suggests that the SLM process has induced lower geometrical deviation.

The color map does not show major geometrical deviation (structure's collapse) in any of the areas of interest. The spikes located on TPZ are not bend compared to the CoCrMo version. It suggests that the part positioning was well performed, and the supports well placed.

## 2. Surface texture investigation

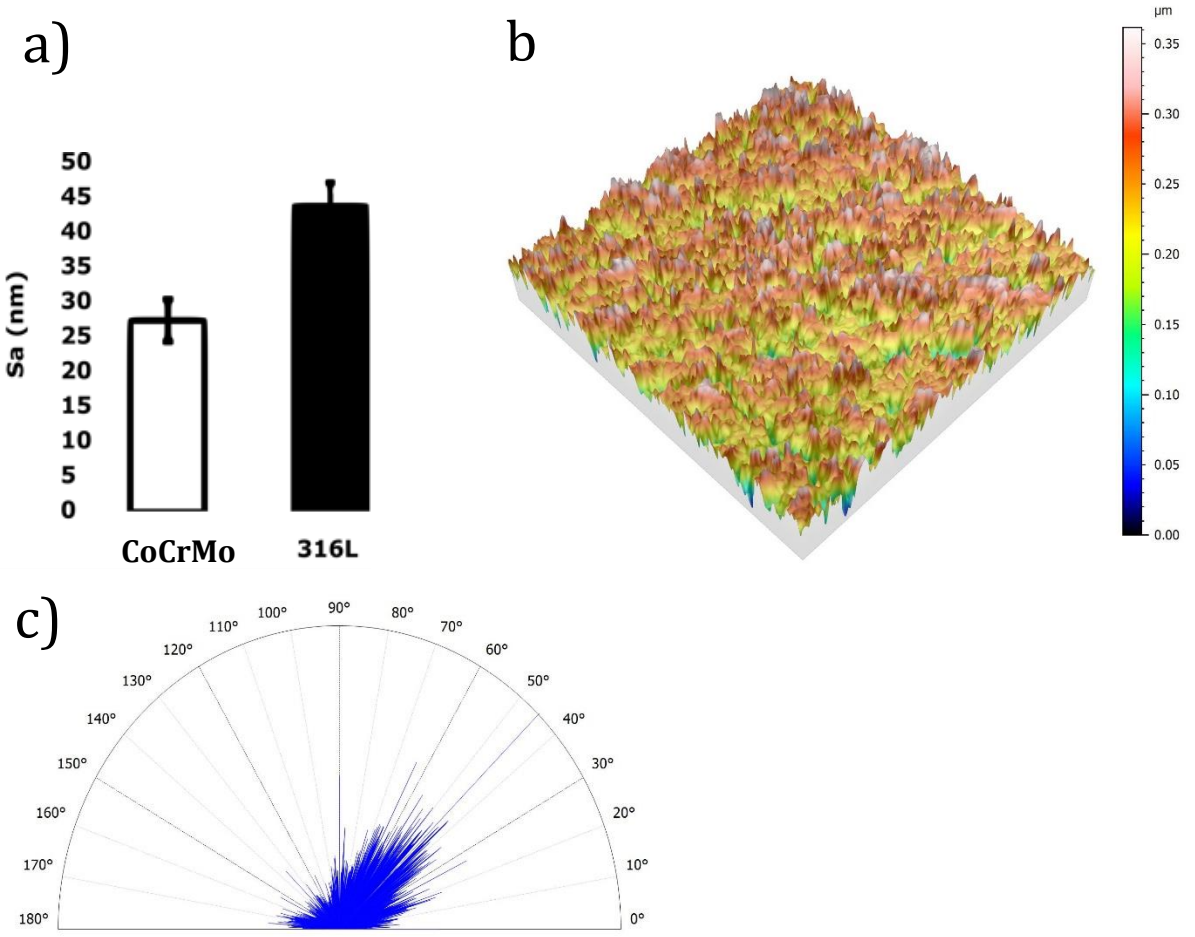


**Figure 2:** Comparison of the 316L and CoCrMo implant average roughness after the superfinishing treatment.

The final surface modification is processed by the physico-catalytic superfinishing. It results in a homogeneous surface texture with a mirror-like aspect composed of submicro-scratches that reflects the flux of the particles inside the tank (Fig.2.b &c). The Sa is reduced all around the implant to about 45nm which is slightly higher than the CoCrMo finished implants as shown in fig. 2. Both roughness values fit the specification

recommended by the standard ISO 21534 :2007 : “Non-active surgical implants — Joint replacement implants — Particular requirements”. Indeed, the standard indicates a Ra maximum of 0,100nm for the metallic part against UHMWPE, and a maximum of 50nm when the surface is convex.

## 3. Porosity investigation

Two different pores' geometries are present in the specimens similarly to the CoCrMo implants which are the small and circular pores type and large and irregular pores type. The region of interest M1 *ie* the contact surface with the 1st metacarpal has the lowest number of pores per mm2 while TPZ *ie* the contact surface with the trapezoid have the highest number of pores. The pores distribution results are similar to the CoCrMo implants.

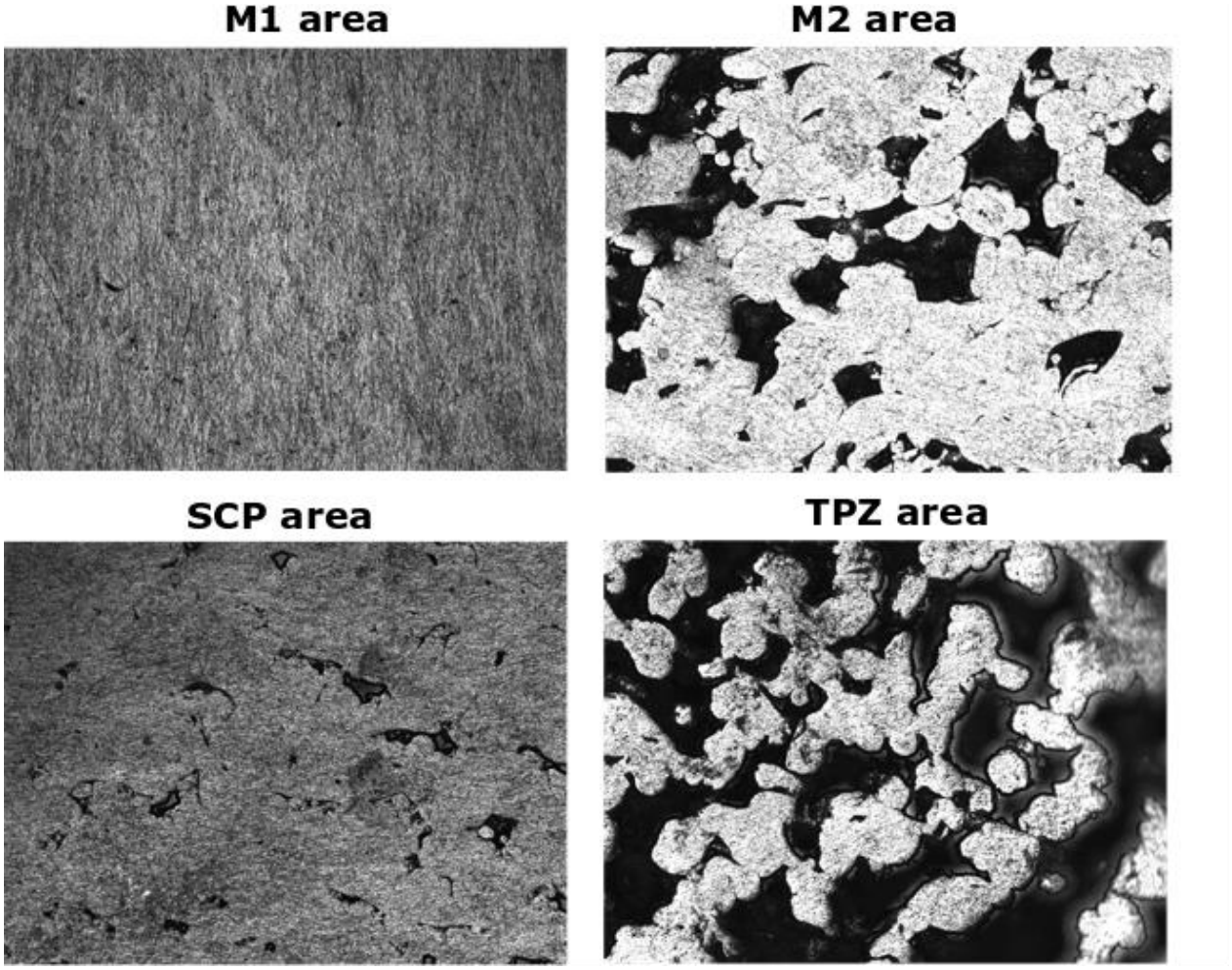


**Figure 3:** Optical microscope images of the different areas of interest composing the implant

## Annex n°4 b): Implant in CoCrMo and stainless steel 316L produce by SLM and ceramic covered

The ceramic used is composed of 35-50% of leucite KAISi2O6 which has been developed in 1995 by doctor Horn for dental restorative application. It is a glass-ceramic composed of potassium alumino-silicate. It has a tetragonal structure at room temperature which crystalizes into a cubic structure at 625° C. It is accompanied with a volume expansion of 1.2%. A Heat-pressing treatment has been performed between 1150° and 1180° C about 20 minutes. The final microstructure consists of leucite crystals, 1 to 5 µm, dispersed in a glassy matrix (yellowish color). The porosity is 9%vol. The thermal treatment has created a large amount of oxides in both metallic material 316L and CoCrMo as seen by the color of the implant. The oxides are described in Annex 5. This material has been chosen for its high hardness in order to increase the tribological performance. The initial tests show the feasibility to add a stable ceramic layer on metallic additive manufactured surface. The process should be optimized to guarantee a sufficient accuracy regarding the geometrical design.

1. **CoCrMo**

**Before** **After**

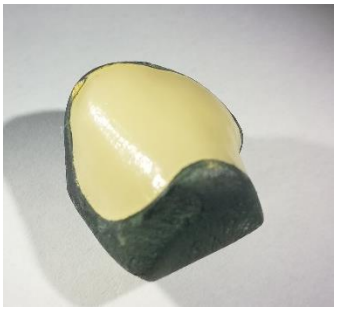

2. **316L**

**Before** **After**

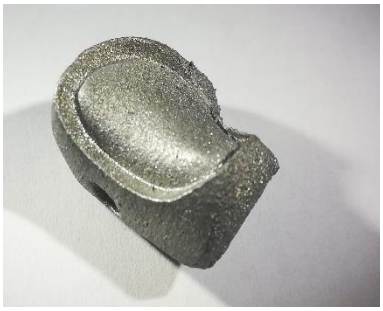

# Annex n°5 a) Comparison of the biotribological performance of UHMWPE against 316L and CoCrMo made by metal additive manufacturing and their cast-version.

## Material and methods

### 1. Specimens

Cylindrical discs of radius 20mm and 5mm thickness was manufactured in CoCrMo and in 316L by selective laser melting. Specimens were also manufacture by casting according to ASTM F75 and ASTM F138. Cylindrical Ultra High Molecular Weight PolyEthylene (UHMWPE) pins were machined from an extruded UHMWPE bar (GUR 415). They were not irradiated. Each pin was of radius 7mm and 30mm length.

The manufacturing process of the discs includes (i) SLM of the disc from powder, (ii) the removal of the SLM supports, (iii) the cleaning the specimens by a sandblasting process (iv) the superfinishing of the specimens by micromachining process and (v) the removal of the micromachining process supports.

The characteristics of the surface and their defects is described in §3.2.

#### 1.1. Powder characteristics

Both 316L and CoCrMo powder was gas atomized under Ar and has a spherical shape (Fig.1.(i)). The average particle diameter was measured as 33, 53 and 35.5 µm by a granulometer respectively for CoCrMo particles and 316L particles (Fig.1.(ii)). They had chemical composition similar to their respective standards : ASTM F75 (CoCrMo) and ASTM F153 (316L); as seen in Fig.1.(iii).

#### 1.2. Selective laser melting

Selective laser melting (SLM) principle and the parameters used for CoCrMo is described in the chapter 5 article 2 §1.2. The parameters used fo 316L has not been provided by the manufacturer.

#### 1.3. Superfinishing by micromachining process

See chapter 5 article 2 §1.3.

316L

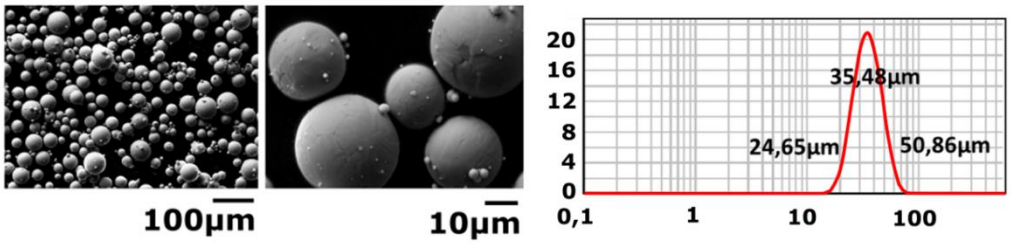


| (wt %) | Fe | Cr | Ni | Mo | Mn | Si | Cu | N | P | S | C | Al |
|---|---|---|---|---|---|---|---|---|---|---|---|---|
| **Powder** | Bal | 17.47 ±0.17 | 11.12 ±0.22 | 2.30 ±0.13 | 17.27 ±0.21 | 0.66 ±0.04 | 0.10 ±0.18 | - | - | - | - | - |
| ASTM-F 138 | Bal | 17–19 | 13–15 | 2.25–3.0 | 2.00 | 0.75 | 0.5 | 0.1 | 0.025 | 0.01 | 0.03 | Na |
| ISO 5832-1 | Bal | 17–19 | 13–15 | 2.25–3.5 | 2.00 | 1.0 | 0.5 | 0.1 | 0.025 | 0.01 | 0.03 | Na |

CoCrMo

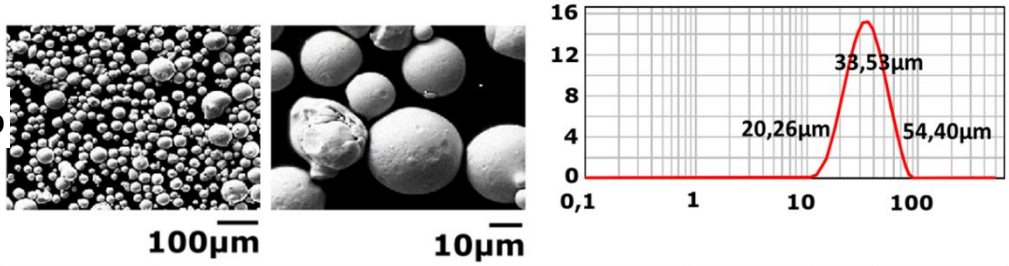


| (wt %) | Co | Cr | Mo | F | Al | Si | Mg | W | P | S | Ni | Ti | Cu | N |
|---|---|---|---|---|---|---|---|---|---|---|---|---|---|---|
| **Powder** | Bal | 28.31 ±0.48 | 6.02 ±0.20 | 0.02 ±0.05 | 0.02 ±0.05 | 0.49 ±0.06 | 0.5 ±0.03 | <0.15 | <0.01 | <0.01 | 0.08 | <0.01 | Na | 0.08 ±0.07 |
| **ASTM F75** | Bal | 27-30 | 5-7 | <0.75 | <0.1 | <1 | <1 | <0.2 | <0.02 | <0.01 | <0.5 | <0.1 | Na | <0.25 |

**Figure 9**: 316L and CoCrMo powder characteristics

## 2. Multidirectional Pin-On-Disk Testing

See chapter 5 article 2 §2.

## 3. Gravimetric measurements

See chapter 5 article 2 §3.

## 4. Surface texture measurements

Surface texture measurements were carried out using a confocal microscope laser (Sensofar®) on the specimens before wear test. Roughness parameters was measured using a zone of 132, 10µm x 177,44µm with an applied form removal filter (polynomial order 6). It reflects the superfinishing results of the physico-catalytic process. Surface texture measurements were also realized on the wear grooves on the CoCrMo surface and on the worn-out pin. The wear grooves on the CoCrMo surface were also examined by SEM and optical microscopy to have complementary results. The accelerating voltage used was 20kV.

### 5. Microstructure analysis

The microstructure of SLM-CoCrMo and 316L was investigated. The specimens were polished up to 4000 grit paper, and finally chemical-mechanical polished with an OP-S colloidal silica solution (Struers). The microstructural-crystallographic characterization was carried out with an EBSD.

### 6. Hardness measurements

The hardness of the material was measured prior the tests using a microdurometer (ZWICK ZHV-µs (H115)) in accordance to ISO-6507 and ASTM E384.

### 7. Defects analysis in the sliding path

Images of the defects were taken using an optical microscope (Keyence®, VHX-6000) and the defects present in the sliding path of the UHMWPE were extracted using the integrated software (measure of grains).

## Results and discussion

### 1. Specimens Characteristics

This work intends to understand the difference of the biotribological performance of polyethylene against superfinished selective laser manufactured samples and their cast version. The material used are 316L and CoCrMo, currently used for articular part of orthopedic application. The characteristics of the sliding surface of selective laser manufactured and casted discs as well as the UHMWPE pins are detailed here.

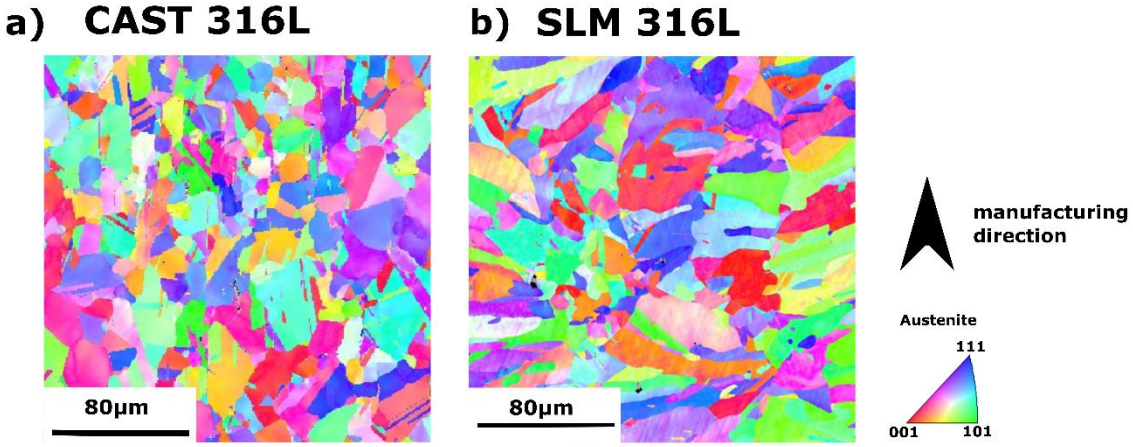


c)

| | Fe | Cr | Ni | Mo | Mn | Si | Cu | N | P | S | C | Al |
|---|---|---|---|---|---|---|---|---|---|---|---|---|
| **Ultrafinished Discs** | Bal | 17.27 ±0.21 | 11,73 ±0.08 | 2.48 ±0.12 | 0.11 ±0.19 | 0.65 ±0.05 | 0,17 ±0.09 | - | - | - | - | 0.30 ±0.06 |
| ASTM-F 138 | Bal | 17–19 | 13–15 | 2.25–3.0 | 2.00 | 0.75 | 0.5 | 0.1 | 0.025 | 0.01 | 0.03 | Na |
| ISO 5832-1 | Bal | 17–19 | 13–15 | 2.25–3.5 | 2.00 | 1.0 | 0.5 | 0.1 | 0.025 | 0.01 | 0.03 | Na |

**Figure 2**: 316L material characteristics after the SLM process and MMP process a) as-cast; b) as-SLM

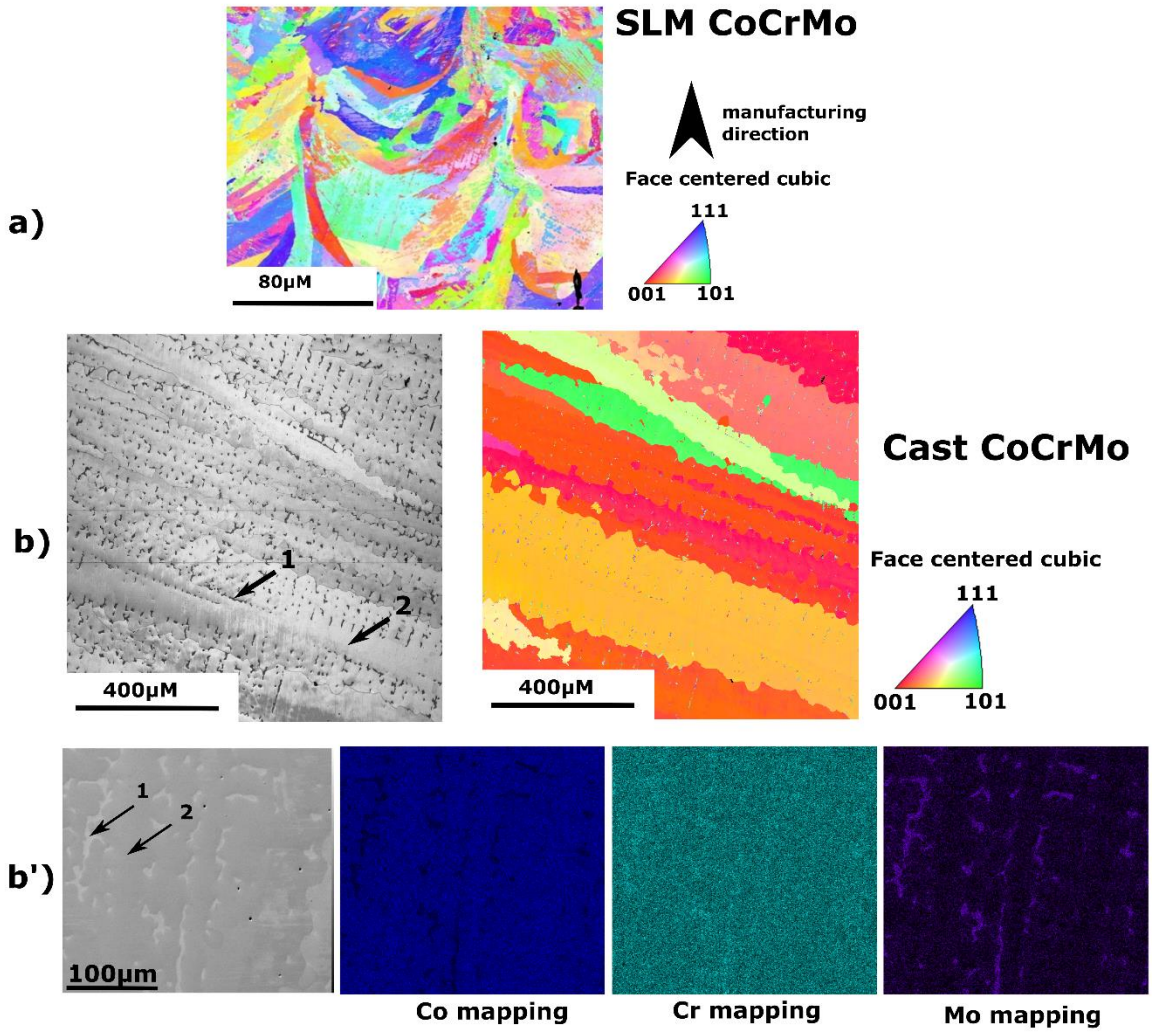


c)

| | Co | Cr | Mo | F | Al | Si | Mg | W | P | S | Ni | Ti | Cu | N |
|---|---|---|---|---|---|---|---|---|---|---|---|---|---|---|
| Ultrafinished Discs | Bal | 27.71 ±0.52 | 5.89 ±0.28 | 0.44 ±0.41 | 0.55 ±0.43 | 0.42 ±0.05 | <0.05 | <0.15 | <0.02 | <0.01 | <0.5 | <0.1 | 0.13 ±0.20 | <0.25 |
| ASTM F75 | Bal | 27-30 | 5-7 | <0.75 | <0.1 | <1 | <1 | <0.2 | <0.02 | <0.01 | <0.5 | <0.1 | Na | <0.25 |

**Figure 3**: CoCrMo material characteristics after the SLM process and MMP process

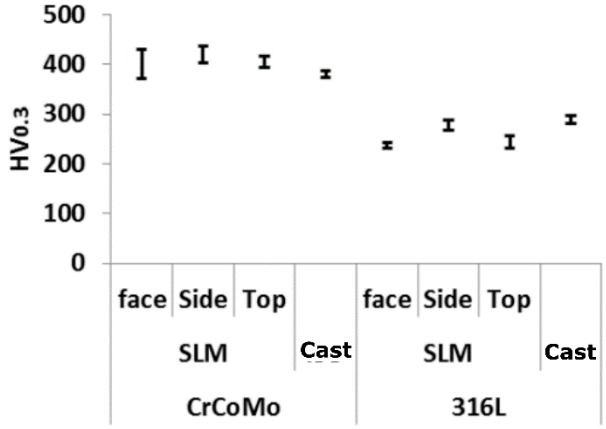


**Figure 4**: CoCrMo and 316L hardness

Figure 2. shows the microstructural features of 316L after SLM and casting. No melting pools are noticeable because of grain cross pool boundaries in the microstructure of SLM-316L. The matrix is austenitic face center cubic (fcc). It confirms that the solidification process creates new grains by epitaxial growth. The thermal history of the process induces a partial remelting, which allows the formation of nearby grains with the same crystallographic orientation. It is largely reported that SLM produce texture and preferred crystallographic orientation of grains along the building direction and that the scanning direction has an influence in the texture. However, the EBSD analysis demonstrates no preferential orientation of grains. The stripes hatching strategy adopted for the build, by inducing a rotation of the scanning direction for each new layer is believed to avoid the formation of the texture in the horizontal direction. It therefor results in a more isotropic polycrystalline material. The resulted surface hardness was found to be at 230 $HV_{0,3}$ with a slight increase of 30 $HV_{0,3}$ in the direction of the building direction but not significant (Fig.4). The hardness of the molded part is similar to the hardness of the SLM part in the direction of the building direction which is about 260 $HV_{0.3}$. The SLM parts demonstrate an equivalent microstructure than the cast version.

Comparatively, the laser molten pools can be clearly seen for the CoCrMo parts. The molten pools have an average size of 90µm. It is explained by the thermal history of the process. During SLM, materials experience fast local melting of the material along the tracks of a high energy laser and solidification far from equilibrium conditions which is driven by severe temperature gradients [14]. The matrix is face center cubic (fcc) with precipitates at the joints of fine cellular dendritic-shaped grains.No carbide were observed. The cast alloy is different as it features dendrite-like structural pattern with elongated (<1mm) and larger (100-500µm) grain size [12,15]. The main difference results in the presence of carbides. They have a large, irregular and blocky morphology, and are located within the grains and at the grain boundaries (Fig.3.b & b'). The carbides are depleted of Co and enriched of Mo (Fig.3. b'). The resulted SLM-surface hardness was found to be at 400 $HV_{0,3}$ with a slight increase of 20 $HV_{0,3}$ in the direction of the building direction but not significant (Fig. 4). The hardness of the molded part is slightly lower than that of SLM parts by about 30 $HV_{0.3}$.

The CoCrMo chemical composition of the superfinished surface revealed an increase in the Iron, Copper and Aluminum content compared to ASTM F75 alloy standard and the chemical composition of the CoCrMo powder (Fig.3). Whereas the 316L chemical composition of the superfinished surface revealed an increase in te Aluminum content

compared to ASTM F138 and ISO 5832-1 (Fig.2). These might be a contamination of the baslting and superfinishing process that have not been removed by the cleaning step.

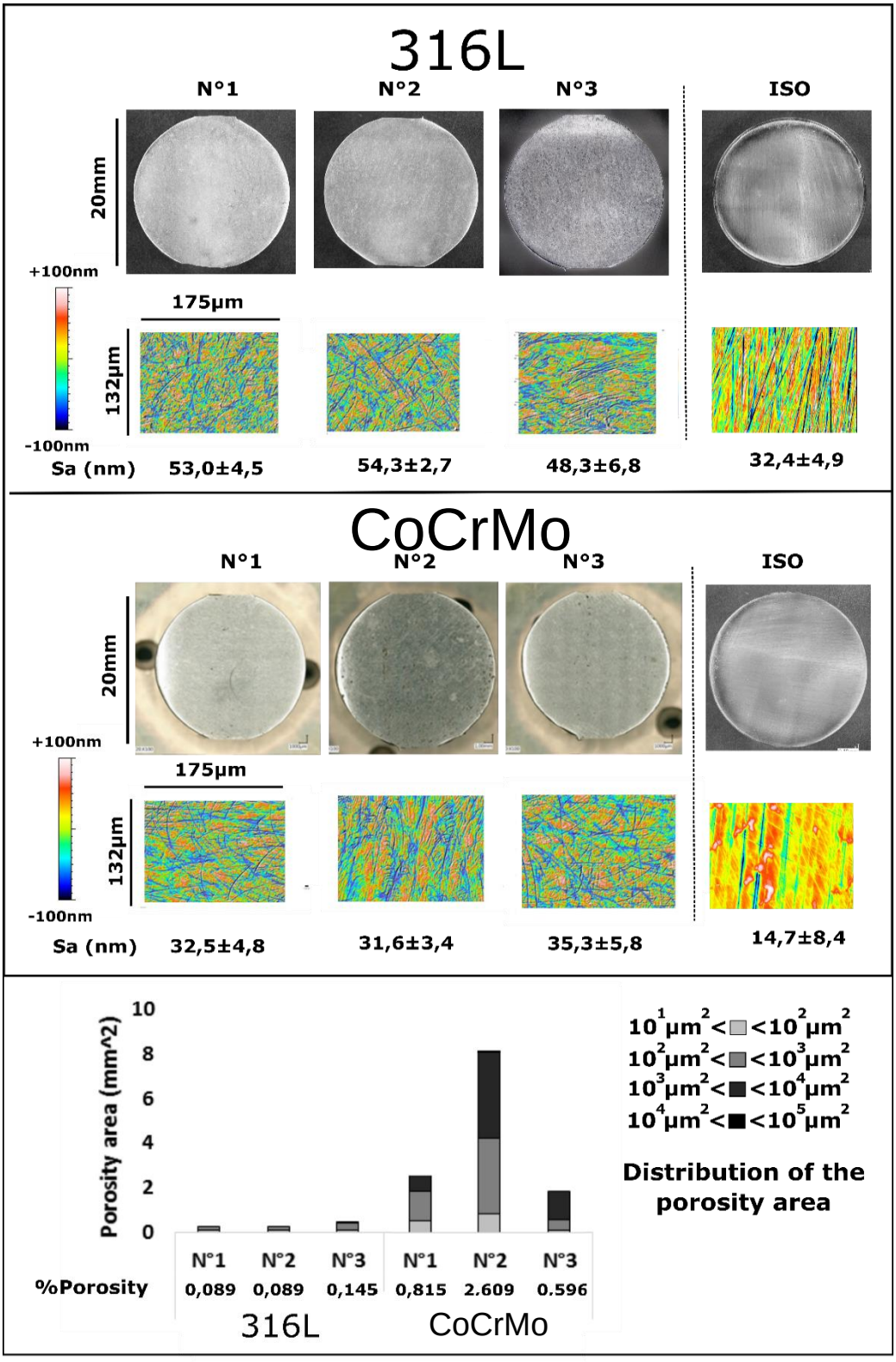


**Figure 5**: 316L and CoCrMo surface characteristics after the SLM process and MMP process

Figure 5 shows the 316L and CoCrMo specimens after the superfinishing treatment. All surfaces appear to be highly polished with brilliant mirror-like finished surface. The

superfinishing process has also revealed few pores on both CoCrMo and 316L surface. It indicates that the SLM samples were not fully dense. Porosity is the most reported defect in SLM parts [16]. The pores were small and round shaped pores due to gas entrapment. The surface is textured with submicron grooves as seen in Fig.3. with an average height roughness (Sa) of 27, 3 ±3,0nm and 51,8± respectively for CoCrMo and 316L. The obtained roughness is in the specification recommended by the standard ISO 21534: 2007: "Non-active surgical implants — Joint replacement implants — Particular requirements" which indicate a Ra maximum of 0,100nm for the metallic part against UHMWPE. This surface texturation (Fig.3) is due to the mechanical part of the superfinishing process, a flux is composed of aggregated particles of microtools created "in situ" by means of the catalyst. Liverani et al. [18] have manually polished their specimens before their tribological tests, however this process cannot be used industrially because of potential uncontrolled geometric deviation. Our approach was to mirror-like polish our specimen using a more reproducible and automatic method, a micromachining process inside a tank [20].

The porosity analysis is shown in figure 3. The 316L specimens feature an area porosity in between 0,085% and 0,150%, whereas the CoCrMo specimens have a porosity area in between 0,55% and 2.65% which is explained by the presence of pores that have an area in between $10^4$ $\mu m^2$ and $10^5$ $\mu m^2$ . Most of the pores are small and circular. These pores are due to gas entrapment during the process.

## 2. Polyethylene Wear behavior against CoCrMo and 316L made by SLM and casting (ASTM)

The results of the mass loss of the UHMWPE against the CoCrMo and 316L discs are shown in Fig.6. The cumulative mass loss of UHWMPE against SLM parts is higher than their cast version for both materials. The non-cumulative mass loss of UHMWPE against 316-as-SLM demonstrate a higher initial wear than its cast version at the first 360 000 cycles and then equalize. Whereas, the non-cumulative mass loss of UHMWPE is significantly higher against CoCrMo-as-SLM than its cast version throughout the test. All the configuration tested demonstrate mass loss values within the specifications recommended by the ASTM standard. Both SLM specimens induce similar UHMWPE mass loss although the cast version of CoCrMo induce a significantly lower UHMWPE mass loss than 316L-as-cast. The difference of mass loss induces by the SLM and cast CoCrMo specimens might partly be explained by the difference of microstructure between the two versions. One have melting pool like FCC grains while the other has carbide within a FCC matrix. The may be confirmed by similar values of mass loss induced by the 316L discs as the microstructure

of the cast and SLM version are almost similar; an isotropic polycrystalline FCC austenite material. The hardness on the contrary does not correlate with the value of mass loss.

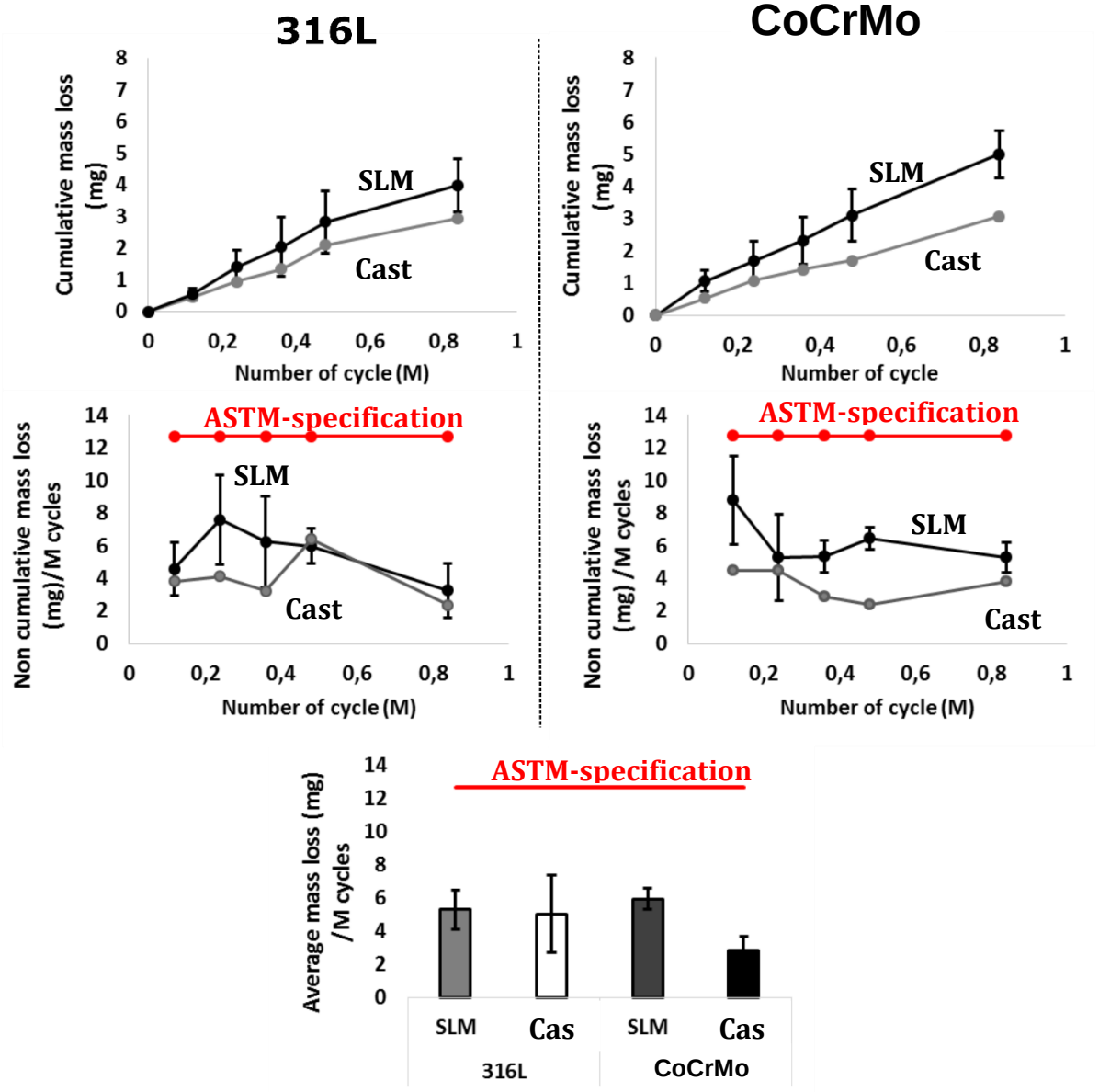


**Figure 6**: Wear behavior of UHMWPE against 316-as-SLM and CoCrMo-as-SLM compared to their respective standard: 316L-as-cast-F138 and CoCrMo-as-cast-F75; red line: ASTM specification for biomedical wear couple including UHMWPE.

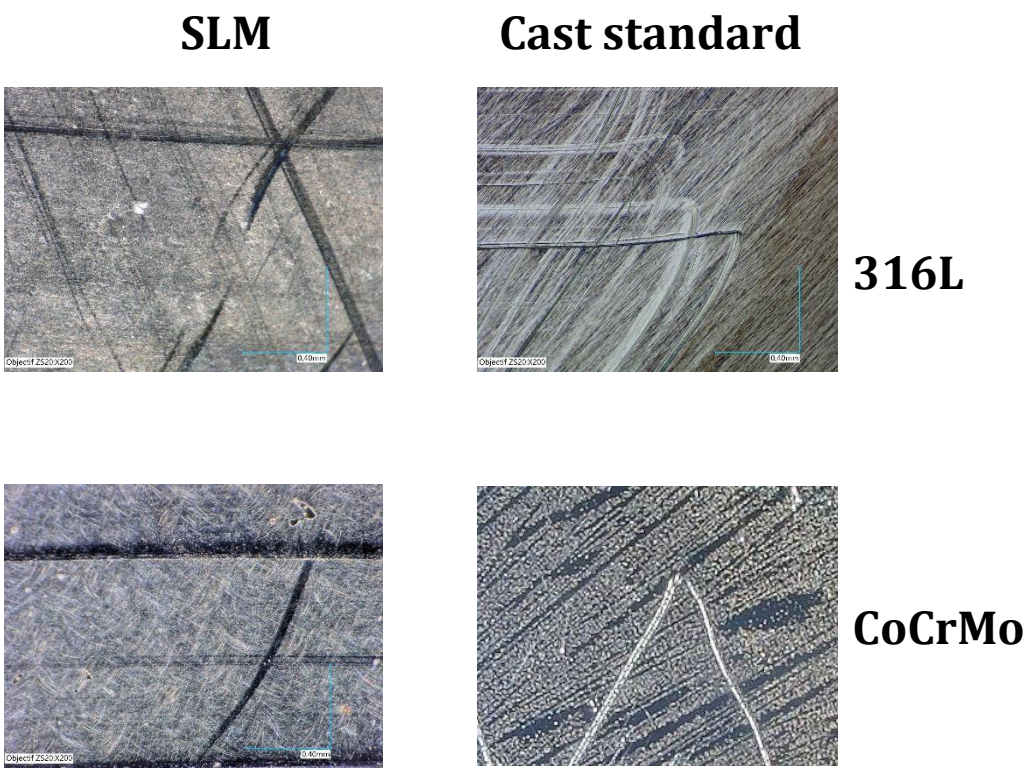


**Figure 7**: Polymer adhesion tracks on the SLM-316L discs after 840 000 sliding cycles but not present for the cast -316L.

Some UHMWPE wear debris adhered in both SLM discs (316L and CoCrMo) after the test as seen in Fig.7 from the triangular burn marks which is typical of polymer adhesion mechanism. The cast-versions, on the contrary, no burn marks were seen.

All the pins' surfaces featured triangular scratching as seen in figure 8. The difference of the average roughness of the total surface between the specimens is due to the creation of facet during the sliding and the appearance of wear blister (pin against cast-CoCrMo) as seen in figure 6. The increased of the average roughness of the pin n°2' against CoCrMo-as SLM (n°2) compared to the pin n°1 and 3 may be explained by the higher porosity of the CoCrMo disc (Fig 5). It confirms the abrasive behavior of pores. This observation may partly explain the higher mass loss induced by the CoCrMo-as-SLM compared to the cast-version. The difference of average roughness in the UHMWPE pins the 316L specimens cannot be explained by the difference of porosity.

The metallic specimens feature wear tracks after the test in addition to the burn marks. The difference of the wear tracks regarding width and depth may be explained by the nature of the 3rd body that was formed during the test. The specimens that have the deepest wear tracks might have release larger metallic particles during the test (316L-as-

cast; disc n°1 CoCrMo-as-SLM). The wear tracks of CoCrMo-as-cast might reflects flat and wide polyethylene debris.

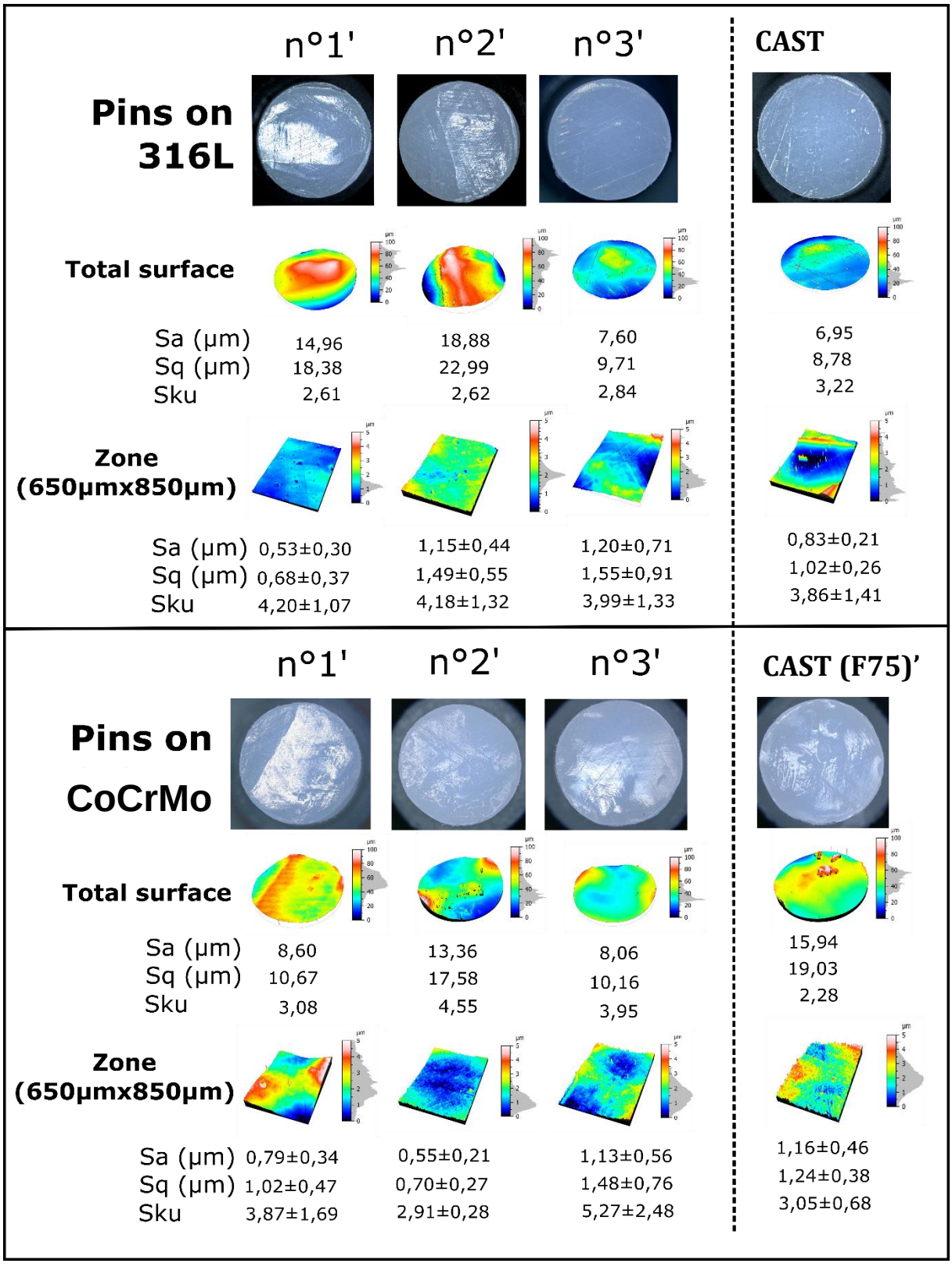


**Figure 8**: Surface characteristics of UHMWPE after 840 000 sliding cycles against 316-as-SLM, 316L-as-cast (ASTM F138), CoCrMo-as-SLM and CoCrMo-as-cast (ASTM F75)

Liverani et al. [18] performed dry sliding wear tests of SLM parts carried out on a flat-on-cylinder tribometer with a steel counterpart. Their results shown low wear rate typical of a mild-triboxidative wear regime confirmed by the presence of a compact oxide transfer layer on the worn surfaces. In comparison, our results showed a polymer abrasion and adhesion mechanisms. Adhesion mechanism was particularly seen on SLM specimens.

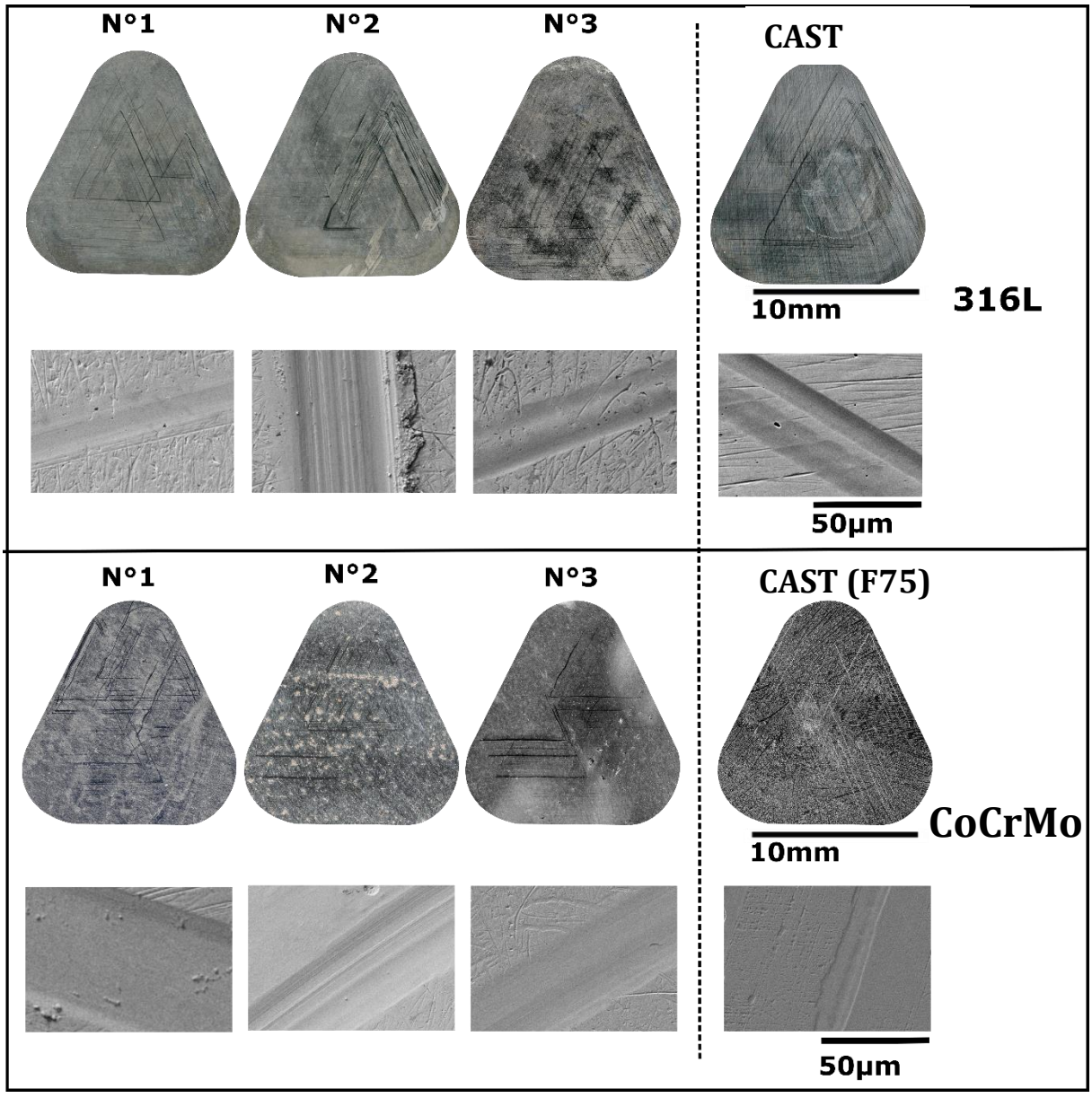


**Figure 9**: Wear tracks analysis on the 316L and CoCrMo discs after 840 000 sliding cycles

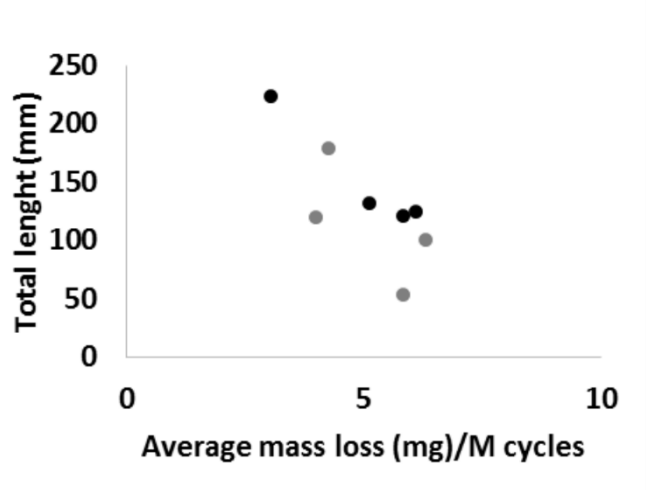


**Figure 10**: Correlation between the total length of the wear tracks and the average mass loss of UHMWPE after 840 000 sliding cycles

It seems that there is a correlation between the total length of the wear tracks and the average mass loss. The appearance of wear tracks onto the specimens during the test may exhibit a more abrasive behavior of the disc against UHMWPE and therefore inducing a greater mass loss.

# Conclusion

The influence of the microstructure of additive manufactured CoCrMo by selective laser melting was investigated on the wear behaviour of UHMWPE against SLM parts. It was evaluated in a multidirectional pin-on-disc simulation in synovial fluid-like lubrication at 37°. The testing conditions were set to simulate the wear of a total joint arthroplasty implant which is composed of a metallic part either made of CoCrMo or 316L by SLM and UHMWPE. The paper allows following conclusions to be drawn:

- Cast and SLM 316L parts induce an equivalent mass loss rate of UHMWPE which is due to a similar microstructure.
- SLM-CoCrMo parts induce higher mass loss rate of UHMWPE than cast-CoCrMo which is assimilated to a (i) different microstructure and (ii) the presence of pores.
- In the present laser-based additive manufacturing parameters, 316L and CoCrMo have an equivalent and acceptable biotribological performance according to with the standard acceptance criteria;

# Annex n°5 b): Study of the biotribological performance of UHMWPE against a leucite glass-ceramic coating

## 1. Specimens

Cylindrical discs of radius 20mm and 5mm thickness was manufactured in CoCrMo by selective laser melting. Leucite material was then affixed on the specimens and then heated. Cylindrical Ultra High Molecular Weight PolyEthylene (UHMWPE) pins were machined from an extruded UHMWPE bar (GUR 415). They were not irradiated. Each pins was of radius 7mm and 30mm length.

The specimens were manually polished up to 4000 grit prior the biotribological test.

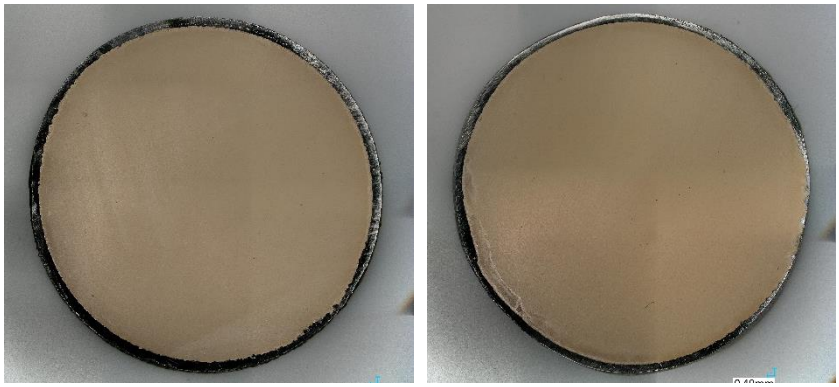

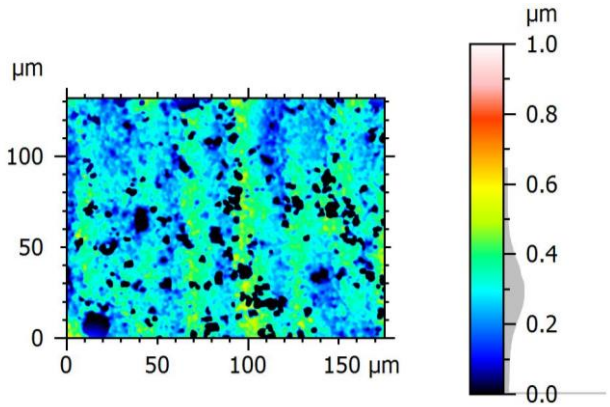


| | Sa (nm) | Sq (nm) |
|---|---|---|
| **N°1** | 80±9 | 110±9 |
| **N°2** | 87±14 | 112±19 |

**Figure 10** : Leucite on CoCrMo specimen n°1 and n°2 and resulted surface texture after the manual polishing

## 2. Polyethylene Wear behavior against leucite affixed on SLM-CoCrMo

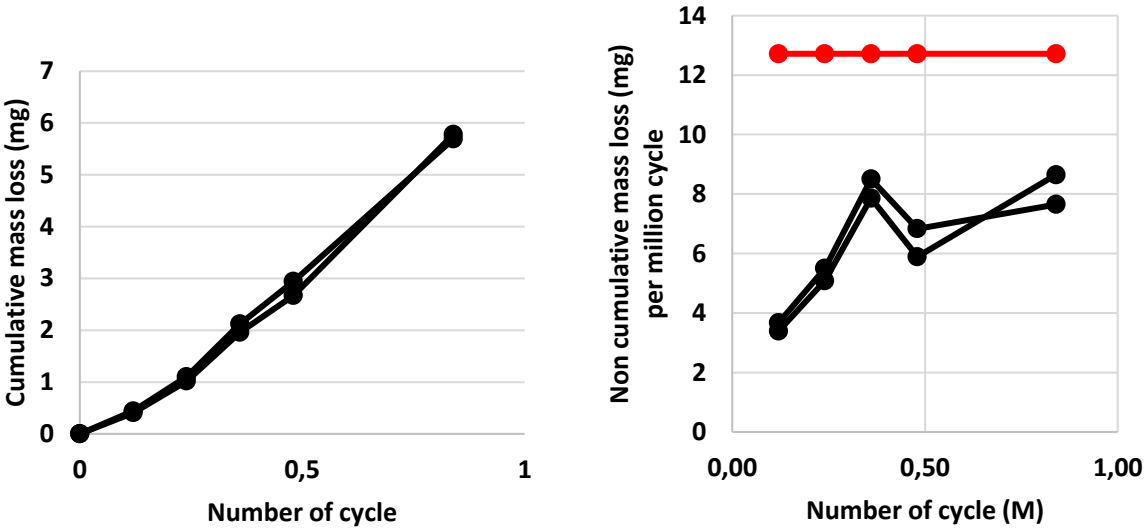


**Figure 11** : Wear behavior of UHMWPE against leucite affixed on CoCrMo specimen n°1 and n°2

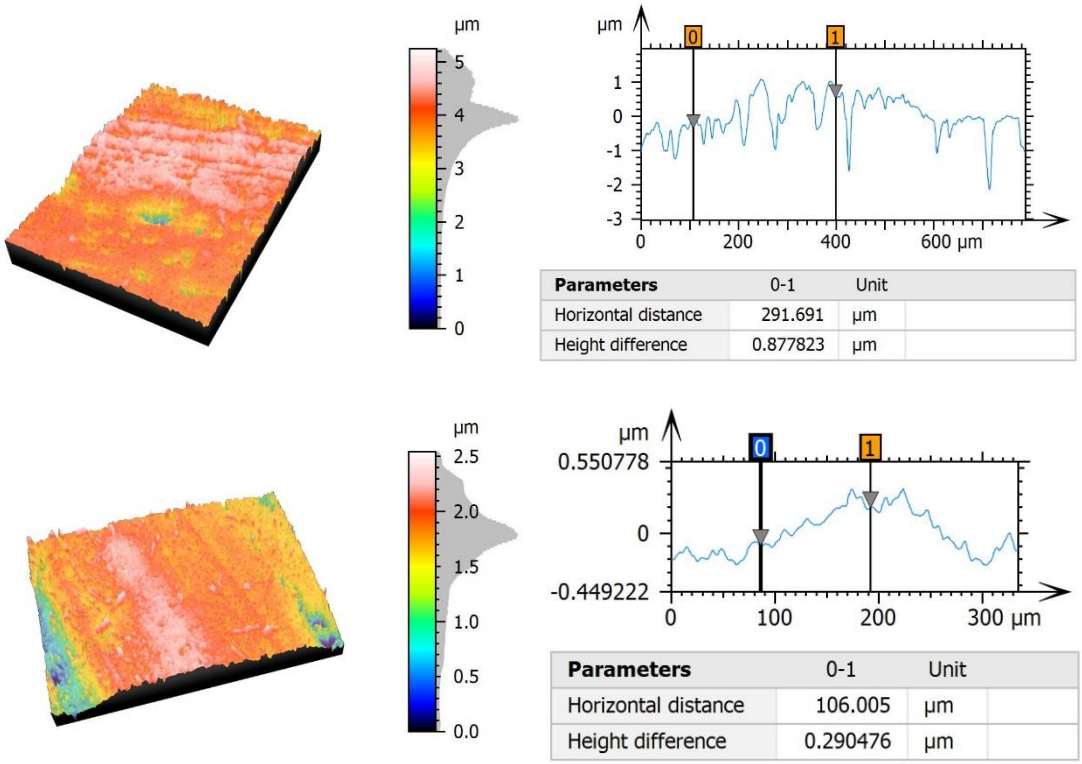


**Figure 12** : Highlight of the adhesion of UHMWPE on the leucite after the biotribological test

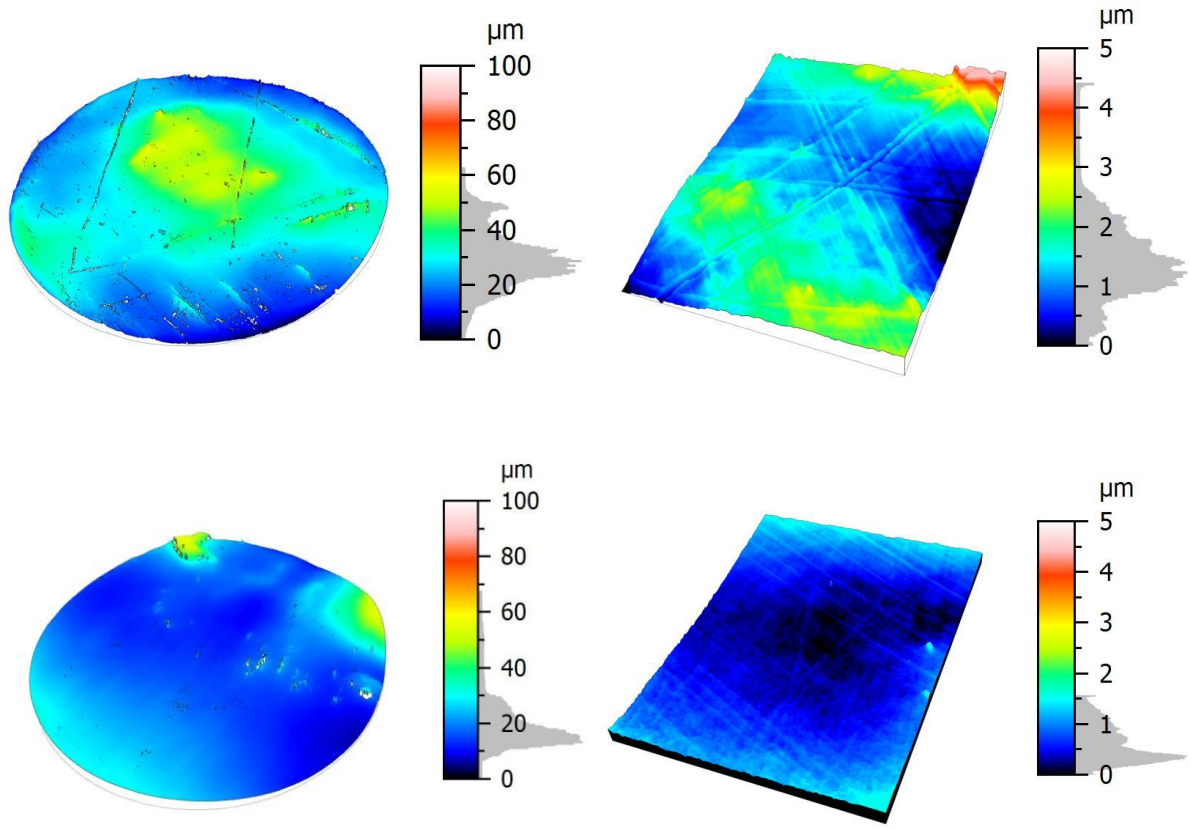


| | Sa (µm) | Sq (µm) | Sku |
|---|---|---|---|
| **Pin n°1** | 0,450 ± 0,252 | 0,564 ± 0,322 | 3,36 ± 1,01 |
| **Pin n°2** | 0,376 ± 0,350 | 20,531 ± 63,762 | 6,20 ± 6,104 |

**Figure 13** : Surface characteristics of UHMWPE after 840 000 sliding cycles against leucite

The results of the mass loss of the UHMWPE against leucite are shown in fig.8. The cumulative mass loss of UHWMPE against leucite is higher than SLM-316L and SLM-CoCrMo. The non-cumulative mass loss of UHMWPE against 316-as-SLM demonstrate a low initial wear that increase until 460 000 cycles around 7,5mg/million cycles. It as to be noted that the mass loss values are within the specifications recommended by the ASTM standard.

No wear tracks were visible on the leucite after the test. However, polymer adhesion was noticed as shown in fig.9. On the contrary, the pins after the test demonstrate visible wear tracks. We were therefore in presence of adhesion and abrasive mechanism during the biotribological test.

# Annex n°6: Biological assessment

## 1. Cytotoxic assays

We performed MTS assay which is a cytotoxicity test using the indirect method according to EN ISO10993-5. The cell used were L929 mouse fibroblasts. Extracts from as-SLM disks were obtained by incubating 1mL of medium (DMEM) for 3cm² of disk surface at 37°C, 5% $CO_2$ in air for 24 h. Extracts were then diluted at 0%, 25%, 50%, 75% in DMEM. $1x10^4$ L929 cells were seeded per well of a 96-well cell culture plate and incubated at 37°C, 5% $CO_2$ in air for 24 h, before the culture medium was removed from the wells then replaced by 100µL of test extracts and incubated for an additional 24 h at 37°C. Control wells consisted in untreated cell cultures. 20 µL of MTS reagent (Promega, France) was added to each well and they were kept in a dark environment for 3 h at 37°C. Subsequently, the absorbance at 490 nm was measured using a UV–visible spectrophotometer (Biorad, France). Negative control consists in elutes of latex at 3cm²/mL and positive control consists in culture medium only.

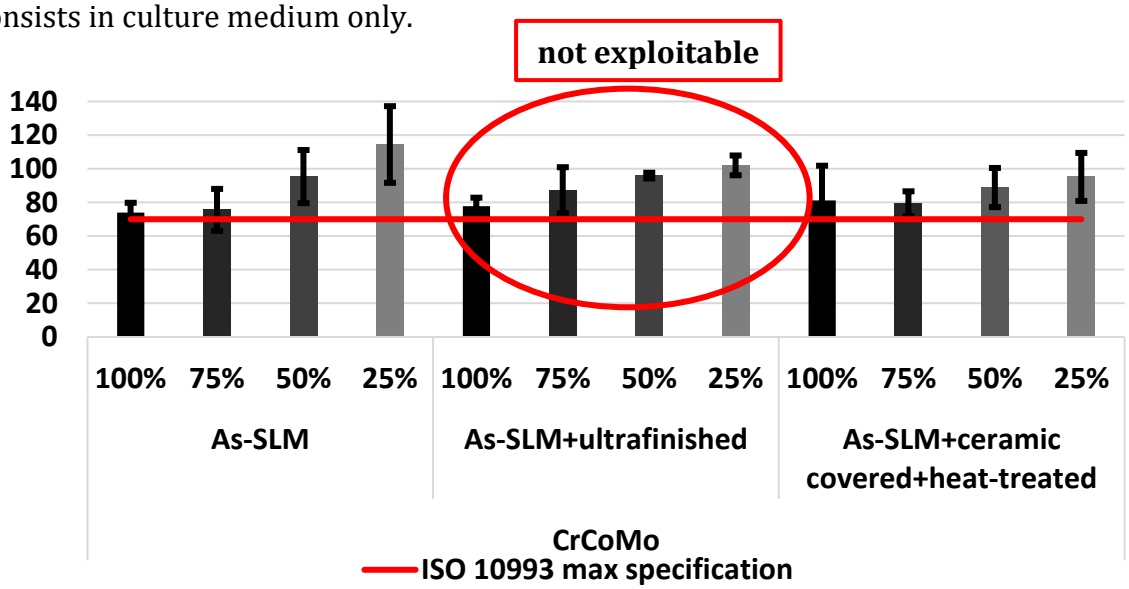


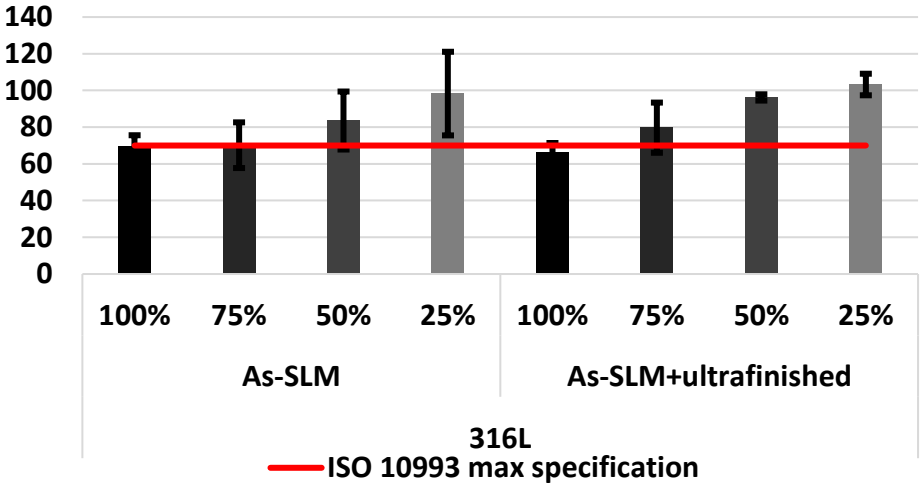

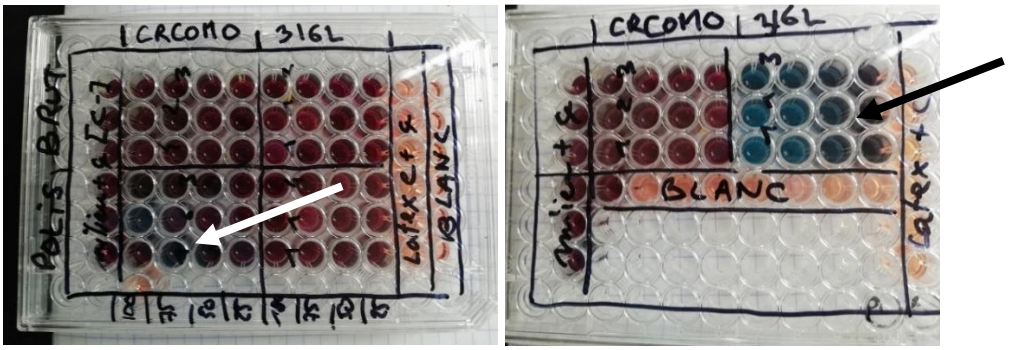


**Figure 1:** Cytotoxic essay realized by indirect MTT test; Not-exploitable: chemical interference with the enzymatic reaction

Several wells solution turned blue as seen in figure 1. It was particularly seen for the well medium that have been in contact with ceramic coated - 316L disc. The disc has been heated for the purpose of the coating resulting in a layer of oxides onto its uncoated surface. This kind of reaction has already been described in the literature. "This interference does not seem to affect the enzymatic reaction but lies rather in the insoluble nature of MTT-formazan". [1] "The MTT assay requires the formation of a water-insoluble formazan crystal which can interact with various reagents. It is possible that the water-soluble [iron oxides] nanoparticles created with the wet-transfer method interfered with the formation and growth of the formazan crystals, causing a suppression of the viability results." [2]

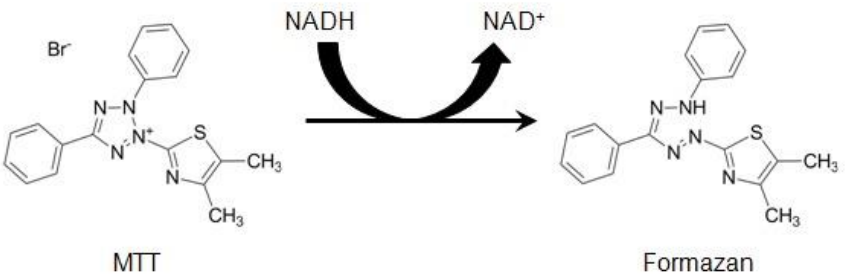


It therefore seems that the oxides produce by the heat treatment of stainless steel 316L have interfered the enzymatic reaction. It seems that some oxides present in the surperfinished CoCrMo specimens also reacted but to a lower extend. Some authors suggest that it is iron oxide that have reacted [2] which is probable due to the chemical composition of our specimens.

The RX results are presented below. The blue coloration induced by the superfinished CoCrMo specimens cannot be explained by these measurements. Further investigation is needed.

Although some chemical interference was observed in some well, it can be concluded that the specimens as-SLM (316L and CoCrMo) are not cytotoxic according to EN ISO10993-5. The superfinished 316L specimens as well as the ceramic-on-CoCrMo discs were not found to be cytotoxic.

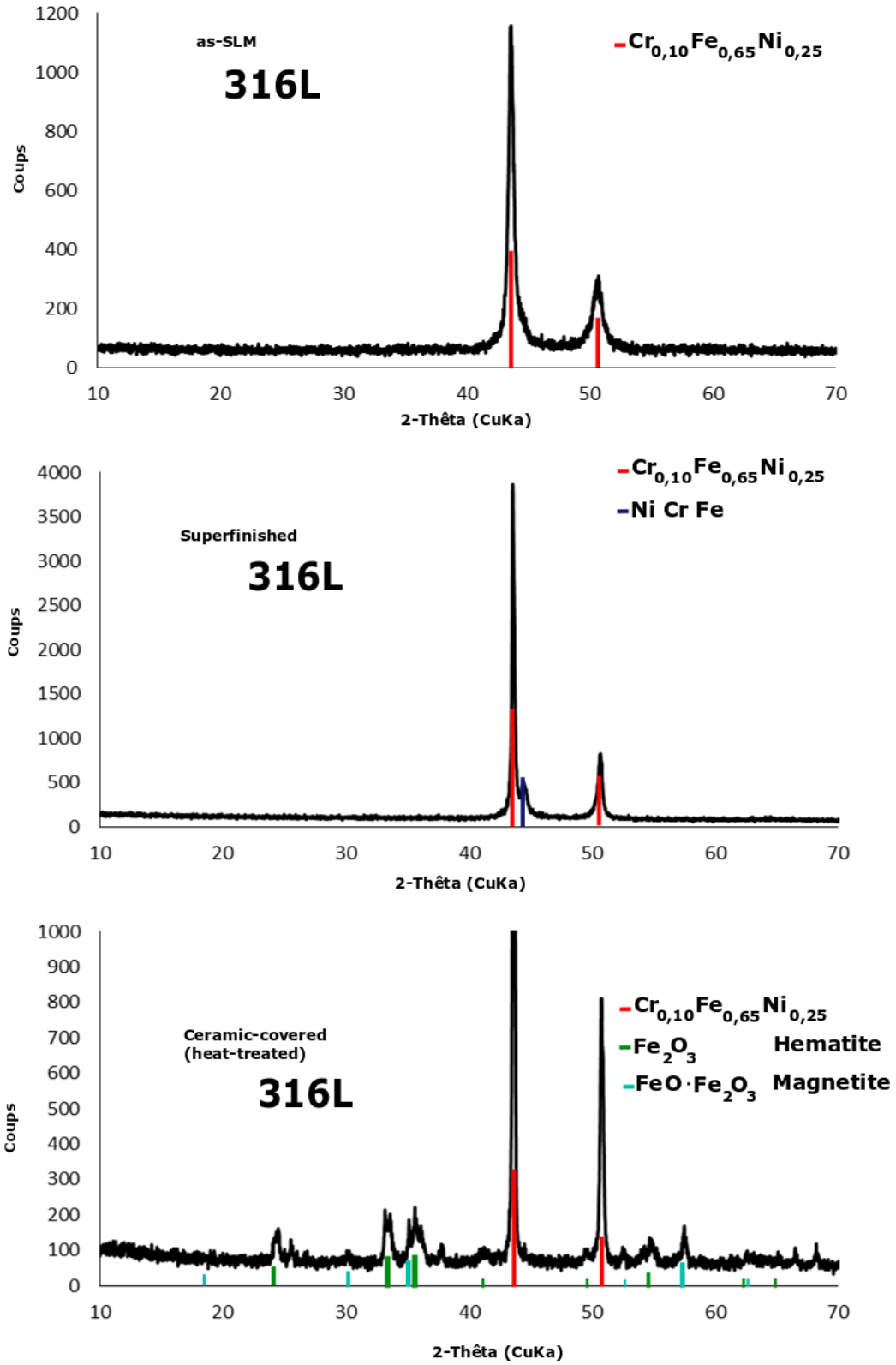


**Figure 2:** RX of the 316L stainless steel specimens

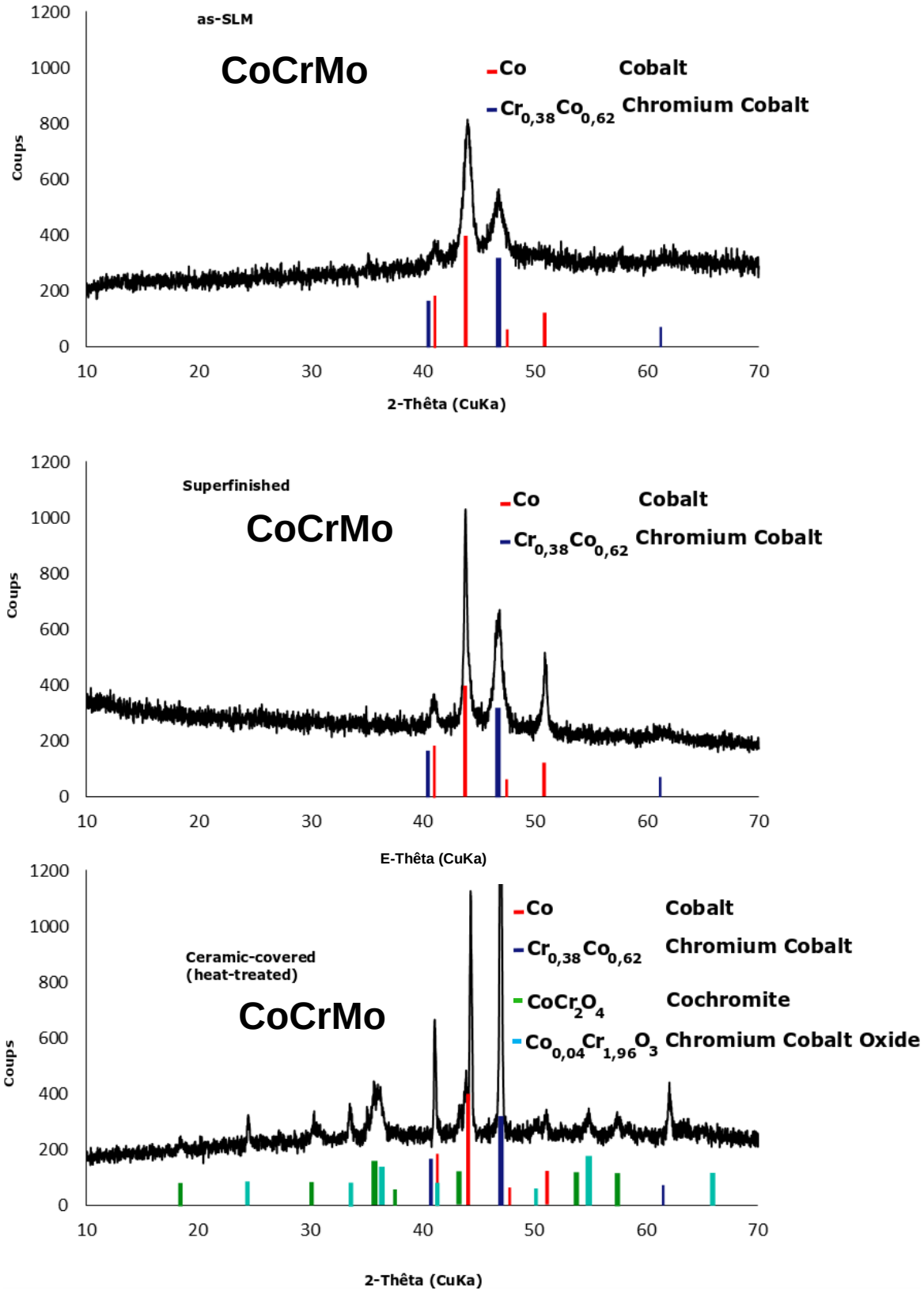


**Figure 3:** RX of the CoCrMo specimens

## 2. Cytokins dosage

We performed a semi-contact test between macrophage and discs for 24h and we realized IL-6 and TNF-α dosage with ELISA tests with the extracts as well as a cell counting (living and dead cells). The cell used were J774 mouse macrophage. We first seeded 750 000 cells in each well of 6-well-plates in 4 ml of medium (DMEM). Discs were placed in 3µm-inserts above the cells as seen in figure 4 and incubated at 37°C, 5% $CO_2$ in air for 24 h. Living cells and dead cells were counted and the culture medium was extracted to perform IL-6 and TNF-α dosages with ELISA tests. Control wells consisted in untreated cell cultures. Positive control consists in LPS and negative control consists in culture medium only.

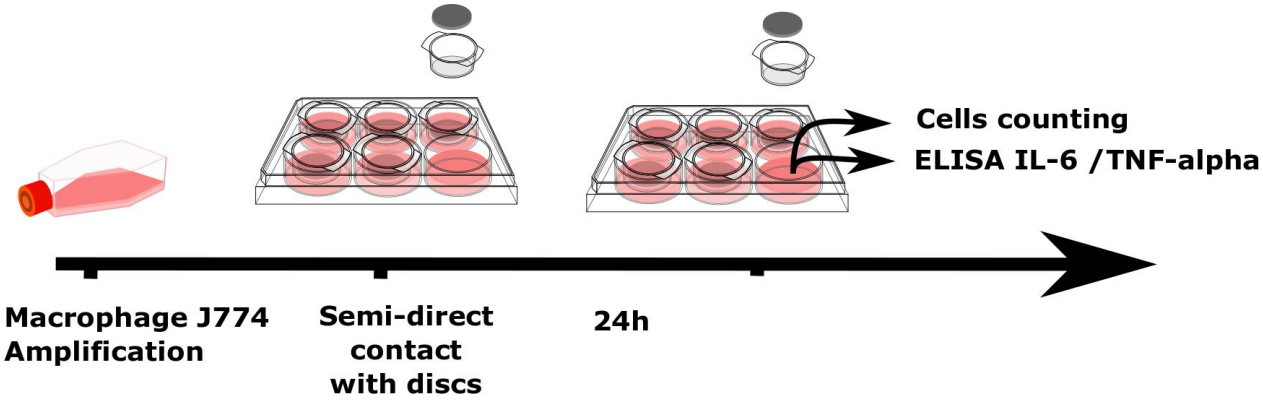


**Figure 4:** Cytokins dosage test with semi-direct contact

Although the test was performed on several specimens for certain condition, it should be done again to verify the data obtained. Up to now, we could conclude that the specimens do not induce the macrophage to produce cytokines. Some superfinished CoCrMo specimens (3/5) induce the production of TNF-α [12,12 ; 49,27 ; 292 ] pg/ml/$10^6$ cells. If we do not consider the number of living cells, all the values are similar. However, we observed for all superfinished CoCrMo specimens the induction of cell mortality, from 45% to 100% compared to the average 25% of mortality. Two CoCrMo superfinished specimens have particularly induce cell mortality [100%; 85%]. Once the test was realized, these samples showed corrosion patterns on the surface as seen in figure 5. Corrosion pits are particularly located near the open pores. We notice also crystals slightly larger than cell size at the bottom of the cell plate as seen in figure 6.a), although the specimens were separated by a 3 µm membrane. It therefore means that some compounds were released from the specimens and then reacted in the medium filled with the macrophages. The nearby macrophages seem to have absorbed some waste as seen

by their color. The chemical composition of the crystals composition could not be measured by EDX nor RX due to the small amount crystals produced. The medium that contains the crystals was also browner than the others.

**Table 1:** dosage of irritation factors IL6 and TNF-α from J774 mice macrophages in contact for 24h with different specimens produced by additive metal fabrication

| | | IL6 (pg/ml/$10^6$ cells) | TNF-α (pg/ml/$10^6$ cells) | Ratio living cells |
|---|---|---|---|---|
| | **Control -** | 0,0 ± 11,8 | 0,0 ± 16,3 | 0,86 |
| | **Control +** | 43,0 ± 35,0 | 131,2 ± 48,4 | 0,80 |
| **316L** | **ISO (n:1)** | ND | ND | 0,78 |
| | **ceramic-Coated (n:2)** | ND | 1,5 ± 4,4 | 0,99 |
| | **Superfinished (n:2)** | ND | ND | 0,54 |
| | **as-SLM (sandblasted) (n:2)** | ND | ND | 0,77 |
| **CoCrMo** | **ISO (n:1)** | 5,4 | 8,70 | 0,78 |
| | **ceramic-Coated (n:3)** | ND | ND | 0,79 |
| | **Superfinished (n:6)** | ND** | 12,5 ± 26,0**/*** | 0,48 |
| | **as-SLM (sandblasted) (n:3)** | ND | ND | 0,79 |

* ND: the value is below the control – meaning that the kit was not able to dose the cytokine
** For one specimen, all cells were dead at the end of the experiment, the dosage per living cells could not be performed
*** a value of 292pg/ml/$10^6$ cells has been measured and was considered as an outlier

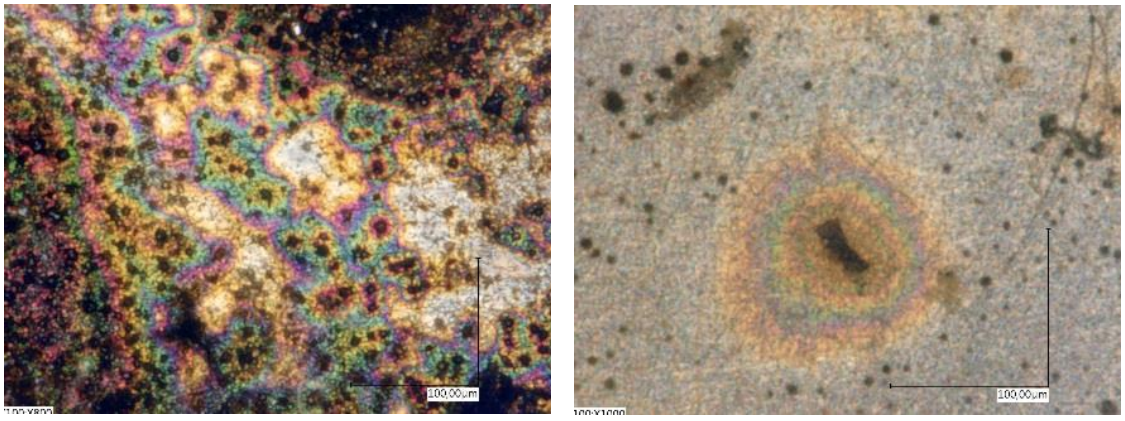

**Figure 5:** Corrosion of some superfinished CoCrMo specimens after the test

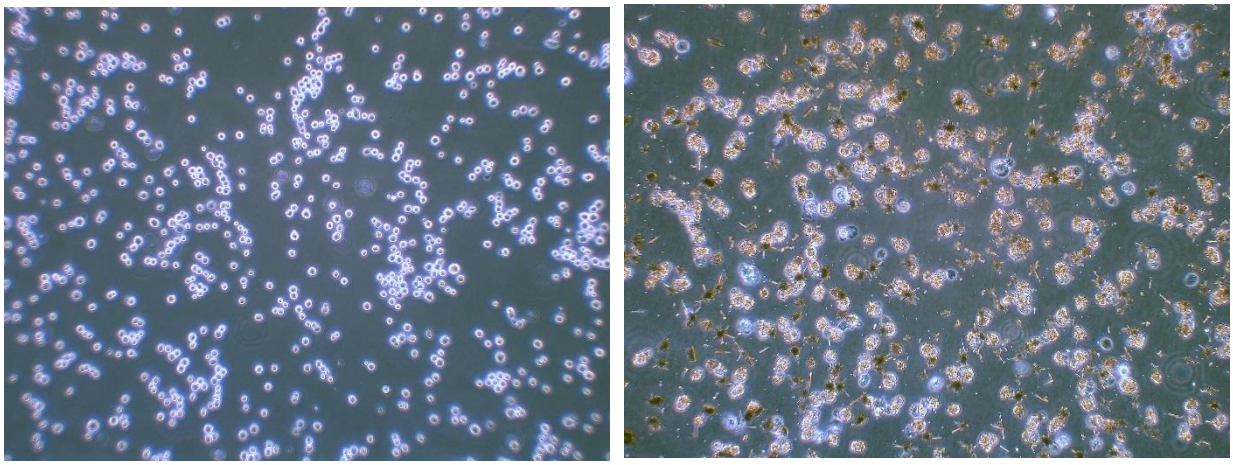

**Figure 6:** Highlight of the crystals at the bottom of the cell plate with superfinished CoCrMo specimens compared to healthy J774 (medium)

The CoCrMo specimens tested directly after SLM (sandblasted) did not demonstrate the same behavior and did not produce these crystals. The 316L specimens did not have this behavior either.

Different hypothesis could be done:

- the superfinishing treatment removed the passive oxide layer which has been formed during the SLM process and the sandblasting process and created a new one thin and homogenous. The imperfections and flaws at the surface (pores) were therefore much able to initiate corrosion particularly in the medium.
  - > Some products of the corrosion were released in the medium and reacted with some compounds of the medium or J774 cells and were found to be cytotoxic or inflammatory.
- the superfinishing treatment used cytotoxic products that were not able to be removed by the cleaning with the different bath of sonication. These products were particularly found in the open pores.
  - > Some products of these elements were released in the medium and reacted with some compounds of the medium and was found to be cytotoxic

The figure below shows the contamination induce by the superfinishing.

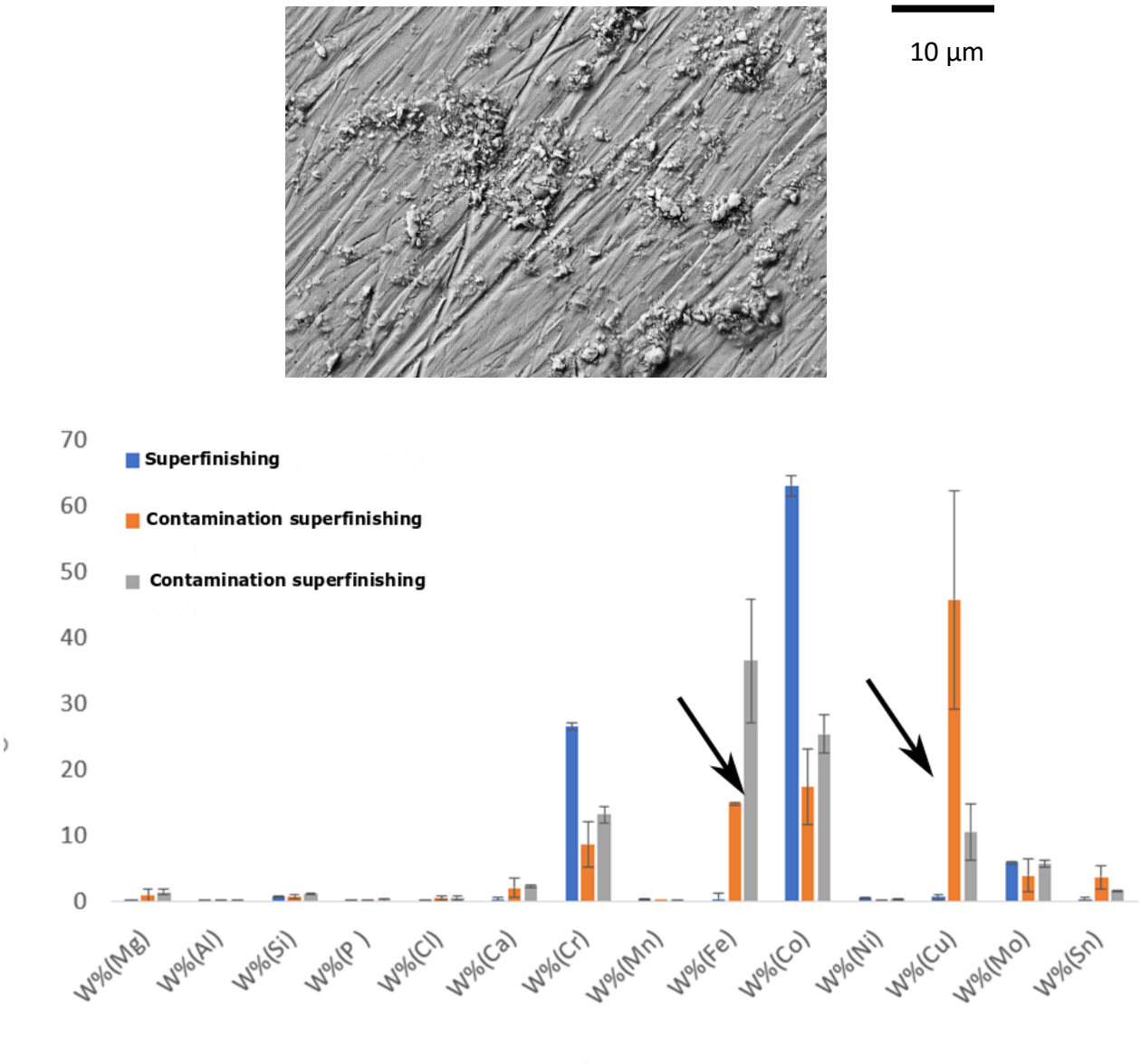


**Figure 7:** Contamination induce by the superfinishing process

References:

[1] J.M. Wörle-Knirsch, K. Pulskamp, H.F. Krug, Oops They Did It Again! Carbon Nanotubes Hoax Scientists in Viability Assays, Nano Lett. 6 (2006) 1261–1268.

[2] M. Gonzales, L.M. Mitsumori, J. V. Kushleika, M.E. Rosenfeld, K.M. Krishnan, Cytotoxicity of iron oxide nanoparticles made from the thermal decomposition of organometallics and aqueous phase transfer with Pluronic F127, Contrast Media Mol. Imaging. 5 (2010) 286–293.

Further investigation are needed to confirm these data, these tests enables us to:

- Highlight the importance to perform different test to avoid bias because of unexpected chemical reactions (§1)
- The specimens after SLM (316L and CoCrMo) are not cytotoxic according to ISO-120993
- The ceramic coating is not cytotoxic (on CoCrMo (L929/J774); on 316L ( J774))
- Superfinishing treatment releases products that react with the macrophages/medium and that are cytotoxic
    - Specimens polished differently would allow us to confirm the origin of the product released
- The specimens after SLM (316L and CoCrMo) do not induce the production of cytokins (24h) by the macrophage (according to the accuracy of the ELISA tests)
    - A test at 48h would allow to confirm the result

**Titre** : Apports des techniques de fabrication additive pour la conception d'implants personnalisés. Application à la chirurgie réparatrice de la main.

**Mots-clés** : Fabrication additive, implant articulaire, CoCrMo, Ti6Al4V, 316L, arthrose, biocompatibilité, résistance à l'usure, texturation de surface, conception numérique, implantation chirurgical, test de performance sur cadavre.

**Résumé** : L'arthrose est une pathologie entrainant la dégénération des surfaces articulaires. Dans le cas particulier de l'articulation trapézo-métacarpienne, l'arthrose déforme de façon irréversible l'os trapèze entrainant perte de la mobilité et amoindrissement de la force de préhension couplé à des douleurs à la base du pouce. Les solutions thérapeutiques ne sont cependant pas satisfaisantes avec des reprises fonctionnelles limitées entraînant une perte de qualité de vie du patient. Dans le cas de la main, la personnalisation des implants semble être pertinente du fait de la grande variabilité des caractéristiques mécaniques articulaires et des spécificités musculo-squelettiques. Ce travail de thèse porte sur la méthodologie de réalisation d'implant trapézo-métacarpien patient-spécifique, basé sur les potentialités des technologies de fabrication additive métal. Il s'agit plus globalement de développer, analyser et valider les étapes de réalisation d'un implant à géométrie complexe quelconque depuis l'imagerie médical jusqu'à l'implantation. Les travaux se concentrent dans un premier temps sur l'identification de paramètres spécifiques du patient afin de « rajeunir » numériquement son os déformé à son stade pré-pathologique pour concevoir l'implant idéal et l'adaptation du modèle à la fabrication d'additive (DfAM). La fabrication de l'implant et les post-traitements sont également étudiés d'un point de vue biologique (cytocompatibilité, réaction du système immunitaire), mécanique (microstructure, propriété de frottement) et morphologique (quantification des déviations géométriques). L'approche d'implantation chirurgicale est abordée au travers de divers tests sur des cadavres permettant de mieux intégrer les bénéfices/risques pour le patient. Une étude sur la psychologie du patient souffrant de la rhizarthrose et de ses attentes clôture ce manuscrit. Les résultats ont donné lieu aux dépôts de 2 brevets et à la rédaction de 6 articles scientifiques.

**Title:** Use of additive manufacturing techniques for the production of customized implants with complex geometry. Application to reparative hand surgery

**Keywords:** Additive manufacturing, articular implant, CoCrMo, Ti6Al4V, 316L, arthrosis, biocompatibility, wear resistance, surface texture, numerical design, surgical implantation, performance test on cadaver.

**Summary:** Osteoarthritis is a pathology that causes the degeneration of joint surfaces. In the particular case of the trapezo-metacarpal joint, osteoarthritis irreversibly deforms the trapezium bone, causing loss of mobility and reduced grip strength coupled with pain at the base of the thumb. However, therapeutic solutions are not satisfactory with limited functional recovery resulting in a loss of quality of life for the patient. In the case of the hand, the personalization of implants seems to be relevant because of the great variability of the joint mechanical characteristics and the musculoskeletal specificities. This thesis work focuses on the methodology for creating a trapezio-metacarpal implant patient-matched, based on the potentialities of additive metal manufacturing technologies. More generally, it involves developing, analyzing and validating the steps involved in the manufacture of any complex geometric implant from medical imaging to implantation. The work initially focuses on identifying specific patient parameters in order to numerically "rejuvenate" the deformed bone in its pre-pathological stage to design the ideal implant and adapt the model to additive manufacturing (DfAM). Implant manufacturing and post-treatment are also studied from a biological (cytocompatibility, immune system response), mechanical (microstructure, friction property) and morphological (quantification of geometric deviations) point of view. The surgical implantation approach is addressed through various tests on cadavers to better integrate the benefits / risks for the patient. A study on the psychology of the patient suffering from rhizarthrosis and his expectations for a therapeutic solution concludes this manuscript. The results have led to 2 patents and the writing of 6 scientific articles.